Title
Pharmacogenetics of Chemotherapy-Induced Peripheral Neuropathy

Author
Chua, Katherina Cairene

Publication Date
2020

Peer reviewed|Thesis/dissertation

Pharmacogenetics of Chemotherapy-Induced Peripheral Neuropathy

by
Katherina Chua

DISSERTATION
Submitted in partial satisfaction of the requirements for degree of
DOCTOR OF PHILOSOPHY

in

Pharmaceutical Sciences and Pharmacogenomics

in the

GRADUATE DIVISION
of the
UNIVERSITY OF CALIFORNIA, SAN FRANCISCO

Approved:

DocuSigned by:
Deanna Kroetz
0611A116B51E4AA...

Deanna Kroetz
Chair

DocuSigned by:
John S. Witte

John S. Witte

DocuSigned by:
Laura Van 'T Veer
05739E1F793F420...

Laura Van 'T Veer

Committee Members

ACKNOWLEDGEMENTS

All the work presented in this dissertation could not have been achieved without the support and guidance from friends, family, colleagues, and mentors throughout my graduate career. I only hope that I will continue to give the same level of encouragement to current and future scientists.

I would first like to thank my advisor, Deanna Kroetz, who has been such an incredible mentor through my entire PhD journey. She has continually given her full support as both my research advisor and the PSPG program director, holding my scientific training above all. I will always thank her for allowing me to foster my passions and creativity while creating a safe environment to discover and develop new skills as an independent scientist. It is a privilege to have worked alongside her at UCSF and I will always cherish these years. I also want to acknowledge some of my former mentors, Drs. Amybeth Cohen, Laura Arce, Michael Bridges, and María Soledad Ramírez, who saw my passion and interest in science at California State University, Fullerton and provided me many opportunities that led me to UCSF.

Thank you to all the collaborators that I have worked with on the completion of this dissertation; the work presented here would not have been possible without your efforts. In particular, I would like to thank Dr. Kouros Owzar, who has consistently contributed his expertise in statistical genetics. I thank him for giving Deanna and I opportunities to learn and grasp a better understanding of statistics through our comprehensive discussions. I also want to thank my dissertation committee members, Drs. John Witte and Laura van't Veer, for taking the time to give me helpful feedback and advise on all of my research projects during my graduate career.

To the former and current members of the Kroetz laboratory, I want to thank you all for the help and optimism that has led to culmination of the work herein. I want to thank Megan Li and Sulggi Lee for passing along their technical expertise on designing and analyzing genetic data. I also want to thank Aishwarya Jayagopal for constantly encouraging me through all the difficult times and always helping to keep my PhD journey in perspective during all of our coffee breaks. I want to thank Chenling Xiong for welcoming such a fruitful partnership for the completion of functional experiments. Lastly, I also want to thank Josefina Priotti and Nura El-Haj for fashioning such a wonderful lab environment in my last year. I will always value our scientific discussions and talks of reassurance that has blessed me during my final year. It has been truly a pleasure working alongside all of you.

To my fellow PSPG graduate students and other UCSF friends, I thank you all for the unbelievable experience I have shared in the last 5 years. Thank you for getting me through the toughest of times, celebrating all the small and big wins with me, and helping me become the scientist I am today. I have always dreamed to part of a community that shares a common spirit and devotion to improve and advance healthcare; I am truly honored that I have found that here amongst all of my colleagues. My journey at UCSF would not have been the same without the constant support at every stage from each and every one of you.

Lastly, I would like to thank my family for their unconditional love and support through this whole process. Thank you for believing in me and allowing me to pursue what I have been truly passionate about. There are no words to describe how much their support has meant to me these past years and I only hope to continue to make them proud.

CONTRIBUTIONS

Chapter 1 was modified and expanded from "Genetic Advances Uncover Mechanisms of Chemotherapy-Induced Peripheral Neuropathy" as it was published in the *Clinical Pharmacology and Therapeutics* in 2019. Katherina C. Chua wrote the manuscript with contributions from Deanna L. Kroetz.

Chapter 2 was modified from a manuscript in preparation "Genome-Wide Meta-Analysis in CALGB 40502 and CALGB 40101 (Alliance) Identifies a *S1PR1* Genomic Region Associated with Microtubule Targeting Agent-Induced Sensory Peripheral Neuropathy". Katherina C. Chua, Chenling Xiong, and Carol Ho contributed to study design, execution, and analyses. Katherina C. Chua wrote the manuscript with contributions from Deanna L. Kroetz.

Pharmacogenetics of Chemotherapy-Induced Peripheral Neuropathy

Katherina Cairene Chua

ABSTRACT

Anticancer therapies are commonly prescribed for breast cancer and other solid tumors. While cytotoxic agents are therapeutically efficacious in treatment of many cancers, they often lead to significant toxicities. One of the main non-hematological dose-limiting toxicities for cytotoxic chemotherapies is sensory peripheral neuropathy. Currently, there are no effective therapeutic strategies to prevent or treat chemotherapy-induced peripheral neuropathy (CIPN) due to the lack of understanding in the mechanisms underlying patient susceptibility. This dissertation presents a pharmacogenetic approach to aid in the identification of critical genetic networks that may explain the development of CIPN. With the use of genome-wide association studies conducted from clinical samples of breast cancer patients treated with microtubule-targeting agents, we highlighted the role of sphingosine lipid signaling in microtubule-targeting agent (MTA)-induced peripheral neuropathy (PN). Functional studies using human sensory neurons derived from induced pluripotent stem cells show that inhibiting such pathway attenuates paclitaxel-induced neuronal injury. Additional genes also involved in Rho GTPase signaling were further revealed from a next-generation exome sequencing study on patients treated with MTA chemotherapy. Future efforts are needed to explore how disruption in this signaling pathway develops on the molecular level and subsequently leads to manifestation of CIPN. While these studies have focused on revealing insights of the pathophysiology underlying CIPN, we also investigated the use of early patient-reported symptoms and genome-wide data for the prediction of dose-limiting neuropathy events. We show that early patient-reported outcomes can be used as a tool to predict

risk for dose-limiting toxicity events. Future studies aimed at determining whether other types of genomic and clinical information may help improve such predictions. Together, the work presented herein provide novel insights to mechanisms underlying the development of CIPN in efforts to discover novel strategies for CIPN prevention and treatment.

TABLE OF CONTENTS

LIST OF FIGURES

LIST OF TABLES

CHAPTER 1: Clinical and Mechanistic Features of Chemotherapy-Induced Peripheral Neuropathy

Cytotoxic chemotherapeutic agents, or antineoplastic agents, are a class of drugs that target and eliminate rapidly dividing cells, and are clinically efficacious as first-line treatments for various cancers. However, clinical benefit of anticancer therapies can often be limited by serious adverse toxicities that significantly impact a patient's quality of life during and after treatment. While incidence varies among therapeutic regimens, chemotherapy-induced peripheral neuropathy (CIPN) is a common dose-limiting toxicity generally experienced in 30-40% of patients undergoing treatment with certain single or combination anticancer therapies[1]. Common chemotherapeutics associated with CIPN include taxanes (*e.g.*, paclitaxel and docetaxel), vinca alkaloids (*e.g.*, vincristine and vinblastine), platinum agents (*e.g.*, oxaliplatin and cisplatin), epothilones (*i.e.* ixabepilone), proteasome inhibitors (*i.e.* bortezomib) and others (*e.g.*, eribulin and thalidomide)[2]. Treatments with taxanes and platinum agents have the highest reported rates of CIPN among these drug classes, ranging up to more than 85%[3–5] . While much is known about these drug classes and their mechanisms of action, the mechanisms by which CIPN initiates, develops, and progresses are still inadequately understood, despite decades of research. As a result, there are also no currently effective strategies for its prevention or treatment.

Clinical Characteristics and Diagnosis of CIPN

Chemotherapy-induced nerve damage is experienced in a "glove and stocking" distribution, where longest axons and most distal nerves are first affected. CIPN presents predominantly as a sensory neuropathy, manifesting in the hands and feet; motor neuropathy is less common and when present typically develops subsequent to sensory neuropathy. Variability in patient experience of CIPN presents a challenge in characterizing the severity of the toxicity, and

symptoms can vary depending on the therapy; however, typical sensory neuropathic symptoms comprise of numbness and/or tingling, abnormal touch sensations, temperature-stimulated hypersensitivity, and/or burning/painful vibrations.[5–7] Of note, oxaliplatin is known to specifically induce cold-stimulated pain and tingling in about 80% of patients[8,9], a phenotype not observed with other neurotoxic chemotherapeutics. Neurological examination of patients with CIPN often shows loss of reflexes and reduced sensory perception to external touch and vibration[2,5,10,11]. Severe CIPN symptoms can significantly interfere with daily activities such as writing, dressing, or even walking, which give rise to secondary complications[1]. CIPN symptoms can persist for years[1,7,12–14]; these symptoms can even progress or "coast" even after treatment has ceased[2,15], a commonly documented phenomenon with platinum-based therapies. In severe cases of CIPN, normal function may never completely return[16,17]. Survivors with chronic CIPN symptoms also bear significant post-treatment economic burden with higher healthcare costs and increased workloss burden[7,18,19].

Table 1.1 Reported incidence rates of CIPN and observed threshold cumulative doses for most common chemotherapy agents[2–4,11,20–22]

Drug class	Chemotherapy agent	Reported onset cumulative dose (mg/m^2)	Incidence reported
Platinum-based agents	Cisplatin	≥ 300-600	49-100%
	Carboplatin	≥ 400-600	25%
	Oxaliplatin	≥ 300-700	40-70%
Vinca alkaloid	Vincristine	> 4-20	20-60%
Taxanes	Paclitaxel	≥ 800-1400	30-100%
	Nab-paclitaxel	NR	10-51%
	Docetaxel	> 400-600	6-10%
Immunomodulatory agent	Thalidomide	20 g (total)	25-75%
Epothilone	Ixabepilone	> 40	15-71%
Proteasome inhibitor	Bortezomib	1-1.3	35-50%

NR: not reported

The onset and severity of CIPN symptoms are drug-specific (Table 1.1) but generally dependent on the dosing frequency, route of delivery, and cumulative drug exposure[2–4,11,20–22]. Treatments with taxanes and platinum-based agents have been documented to induce acute neuropathic pain as early as the first cycle[23,24], which is not typically observed with other chemotherapeutics. Clinical risk factors for developing CIPN include pre-existing neuropathy (*e.g.*, diabetic neuropathy or inherited neuropathy), diabetic status, age, abnormal creatinine clearance, prior treatment with neurotoxic agents, and high-exposure dosing regimens[1,4,25]; however, these factors do not completely account for the interindividual variation in CIPN clinically observed[6]. Recent studies have aimed at identifying genetic risk factors, including single nucleotide polymorphisms (SNPs), to understand patient susceptibility and guide treatment decisions. While currently no genetic association has shown clinical utility to predict risk of CIPN, these efforts have discovered exciting insights into the pathophysiology of CIPN and are reviewed in a later section.

A number of assessment tools are used for diagnosing, monitoring and describing the progression of CIPN, including common toxicity grading scales, neurophysiological tests, and patient reported surveys[5,11,26]. The traditional method used for evaluating CIPN is the National Cancer Institute – Common Terminology Criteria for Adverse Events (NCI-CTCAE) scale, where clinicians grade CIPN severity on a 1-5 scale (Table 1.2). Dose reductions, treatment delays, or cessation of therapy are considered when severe neuropathy is experienced, usually defined as grade 3 or higher events where sensory impairment interferes with activities of daily living[26]. Neurological quantitative sensory tests can be used to diagnose CIPN, and measure diminished neurological function characterized by reduced sensory nerve conduction velocities,

sensory nerve action potential amplitudes, and increased vibration thresholds[27,28]. However, these tests are only limited to diagnosis without any standard guidelines to implement the results into clinical practice, and have not shown consistent correlation to severity of CIPN[10,29,30]. Recently, there is increasing interest in utilization of patient reported outcomes (PRO) in clinical settings. In at least some studies, PRO shows clinical validity and reliability compared with NCI-CTCAE reporting[31–34]; however, the development of PRO-based standard protocols is critical for application into clinical decisions.

Table 1.2 Grading scale for NCI-CTCAE for peripheral sensory neuropathy

Grade 1	**Grade 2**	**Grade 3**	**Grade 4**	**Grade 5**
Asymptomatic; loss of deep tendon reflexes or paresthesia	Moderate symptoms; limiting instrumental ADL	Severe symptoms; limiting self care ADL	Life-threatening consequences; urgent intervention indicated	Death

ADL: activity of daily living

As the number of cancer survivors continues to increase, the importance of addressing CIPN to improve long-term quality of life has gained recognition. As a result, the 2014 American Society of Clinical Oncology (ASCO) clinical practice guideline[6] reviewed previously investigated prevention and treatment strategies against CIPN from clinical trial results, including use of chemoprotectants (amifostine, recombinant human leukemia inhibitory factor, nimodipine), anticonvulsants (carbamazepine, oxycarbazepine, lamotrigine, gabapentin), antidepressants (nortriptyline, amitriptyline, venlafaxine, ketamine, duloxetine), and various supplements (calcium and magnesium, vitamin E, glutathione, acetylcysteine, acetyl-L-carnitine, glutamate/glutamine, omega-3 fatty acids, goshajinkigan, retinoic acid, diethyldithiocarbamate). Despite all these efforts to identify therapeutic approaches to combat CIPN, there are currently no clinical recommendations for prevention and only a moderate recommendation for the use of duloxetine in the treatment of existing CIPN[6]. The most effective method for preventing CIPN is dose reduction and/or therapy discontinuation, which influences the decision to balance

maximum chemotherapeutic benefit that may lead to survival and long-term well-being after completion of therapy. The development of clinically effective therapies to prevent and/or treat CIPN is limited by our current understanding of the molecular basis for CIPN. Although clinical presentation of CIPN is relatively consistent among chemotherapies, genetic and functional studies collectively suggest that the predisposition and mechanisms of this neurotoxicity may be chemotherapy-specific.

Pathogenesis of CIPN

Decades of research with *in vitro* and *in vivo* models of CIPN have revealed some key morphological changes in the affected nerves that are now hallmarks of CIPN[5,35–43], including the loss of intraepidermal nerve fiber endings, preferential sensory axonal degeneration, mitochondrial vacuolation, and varying degrees of demyelination. Although the presence, severity, and mechanism of these traits vary with drug treatment, loss of nerve innervation is the most consistent morphological effect observed from patient skin biopsies[44–47] and *in vivo* models of CIPN[35,36,48–50]. This "dying back" phenotype occurs when epidermal nerve fibers on the outermost layer of the skin are depleted and/or fragmented[51] (Figure 1.1), and is mostly attributed to drug-specific damage inflicted on the dorsal root ganglion (DRG) neurons.

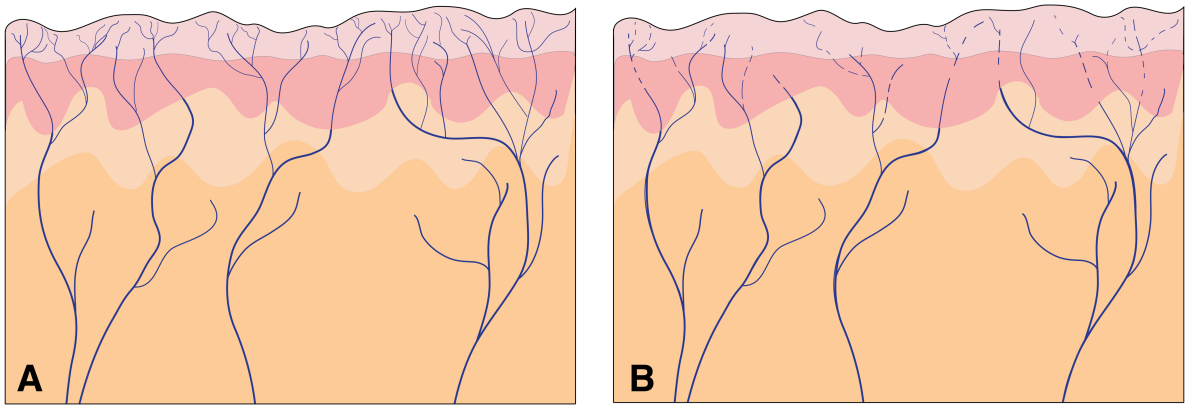

Figure 1.1 Diagram of innervation of skin in healthy individuals (A) and in those with neuropathy (B). (Adapted from Landowskia et al.[51])

Since the majority of the mechanistic studies that characterize CIPN and our clinical pharmacogenomic studies are derived from studying neuropathy induced by microtubule-targeting agents (taxanes, vinca alkaloids, eribulin, epothilones), we focus hereafter on reviewing the study findings of microtubule-targeting agent-induced neuropathy. In general, microtubule-targeting agents (MTAs) are anticancer drugs that target and disrupt microtubule dynamics, resulting in mitotic arrest and cell death. Although clinically effective for cancer cells, this antineoplastic activity also considerably impairs the elongated microtubules found in sensory neurons (Figure 1.2). Early studies in mouse dorsal root ganglion cultures and rodents show presence of paclitaxel within peripheral nerves alone cause axonal microtubule aggregation[52–54] that effectively lead to diminished axonal transport of cargo between the cell body to nerve distal ends essential for synaptic function and neural maintenance[55,56]. These initial findings were further validated in rodents that were dosed with paclitaxel systemically[57–59], observing consistent intraaxonal microtubular accumulation mainly in peripheral nerves associated with swollen degenerated axons, reduction in sensory nerve conduction velocities, impaired coordination, and altered pain perception. Studies using primary DRG, sural nerves, and other

neuronal cultures have suggested that paclitaxel-induced disruption of microtubule organization impairs axonal transport[60–63]. Disruption in axonal transport has also been implicated as the main contribution to neuropathy with other microtubule-targeting agents[64,65].

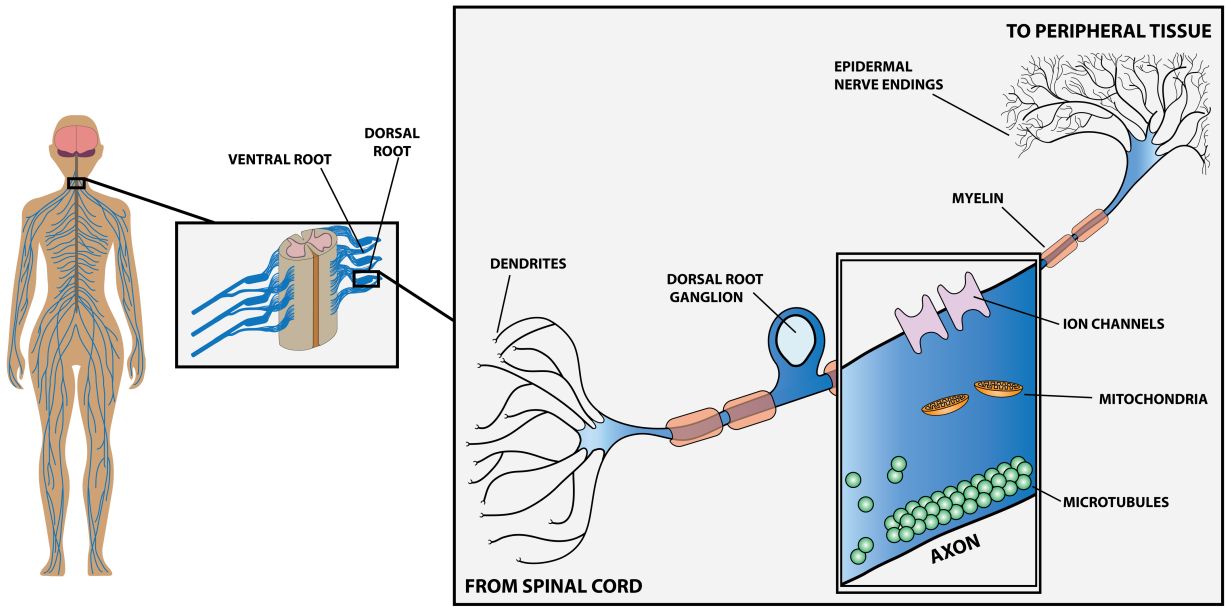

Figure 1.2 Proposed mechanisms for development of MTA-induced peripheral neuropathy include axonopathy due to distruptions in microtubule dynamics, mitochondrial function, ion channel activity, myelin sheaths, and degeneration of nerve endings.

Interestingly, key studies using the Wld^s mouse, a strain resistant to axonal degeneration, have highlighted the importance of axonal degeneration in the severity of sensory neuropathy after paclitaxel exposure. Wld^s mice were protected against impairment of sensorimotor coordination, reduction in sensory nerve action potentials and sensory nerve conduction velocities, and diminished sensory axonal density and numbers[66,67]. Vincristine exposure to DRG cultures from Wld^s mice also shown similar protective effects with axonal degeneration[67,68]. Other genetic mouse models (*e.g.* SARM1-deletion) resistant to axonal damage also demonstrate that MTA-induced peripheral neuropathy is dependent on axonal loss[69]. Additional studies in primary DRG and rodent models of CIPN have also documented that damage to the distal regions of the axon are necessary to initiate neuropathy, causing predominant sensory axonal

polyneuropathy[35,36,40,70–72] and likely result in the loss of epidermal nerve fibers observed in human biopsies[44–47] (Figure 1.2).

As damage in axonal transport can also affect cargo needed for mitochondrial function[59] (Figure 1.2), paclitaxel-induced neuropathic pain in rats also shows prominent amounts of swollen and vacuolated axonal mitochondria within sensory nerves[37,73], which is not observed in motor nerves[38]. This morphological change corresponds to compromised mitochondria respiration, which increases oxidative stress levels in rodents *in vivo*[74–77] and DRG *in vitro* models[78]. Heightened oxidative stress from paclitaxel treatment has been linked to abnormal excitability in afferent nerve fibers[79] and may explain abnormal touch/pain sensations experienced by patients. Alongside oxidative stress, paclitaxel treatment has also been shown to release calcium from mitochondria[80] in mouse pancreatic cells. Paclitaxel and vincristine treatments in rodent CIPN models and human neuroblastoma cell lines have corroborated these findings, showing abnormal cellular calcium levels can result from chemotherapy exposure[81–83] and similarly lead to mechanical hypersensitivity. A study on ixabepilone-induced neuropathy also observed abnormal mitochondria in both axons and Schwann cells from patient skin biopsies[84] similarly seen with paclitaxel therapy. Interestingly, a recent study identified differentially expressed genes in mitochondrial dysfunction-related pathways from breast cancer survivors with paclitaxel-induced neuropathy[85], and further implicates the role of mitochondrial homeostasis in microtubule-targeting agent-induced neuropathy.

Alterations in various neuronal ion channels responsible for excitability of peripheral nerves have also been suggested as a contributor to MTA-induced neuropathy (Figure 1.2). Initial studies using primary DRG neurons revealed changes in sensory action potentials and gene expression of various neuronal ion channels after taxane exposure[86,87], including sodium,

potassium, and TRP channels. Interestingly, upregulation of $Na_v1.7$ has been shown to correlate with calcitonin gene-related peptide (CGRP) release[87], a marker of nociception, in DRG neurons from rats treated with paclitaxel and patients with neuropathic pain. Another study has shown increased expression of calcium channels ($Ca_v3.2$) in rat DRG and spinal cord tissue after paclitaxel or vincristine treatments, associating with hyperexcitability[88–90]. Among the implicated ion channels, transient receptor potential (TRP) channels are the most studied due to their prominent role in pain and temperature sensations. Reductions in TRPV4 expression in sensory nerves can reduce paclitaxel-induced hyperalgesia *in vivo*[91]. Other TRP channels (i.e. TRPA1 and TRPV1) have also been linked to paclitaxel- and vincristine-induced neuropathic pain. TRPA1-deficient mice release less CGRP after paclitaxel exposure[92], resulting in reduced paclitaxel-evoked mechanical allodynia. Paclitaxel and vincristine treatments in rodents similarly increase TRPV1 expression in DRG neurons and paw skin[93,94]. Interestingly, a recent study using both DRG cultures and an *in vivo* rodent model suggests calcium entry into TRPV1 occurs after paclitaxel exposure, leading to DRG cytotoxicity and neuropathic pain[95].

Lastly, neuroinflammation and other immune responses may also be involved in the development of MTA-induced neuropathy. Initial studies observed paclitaxel or vincristine treatment in rats stimulated activation of macrophages within DRG and peripheral nerves[96–98], consequently triggering neuropathy. Later studies demonstrated that paclitaxel treatment of primary DRG cultures[99,100] and *in vivo*[100,101] increased monocyte chemoattractant protein-1 (MCP-1) and signaled the infiltration of macrophages into DRG tissue, ensuing in neuronal apoptosis, loss of intraepidermal nerve fibers and mechanical hypersensitivity. Depletion of macrophages within DRG show significant prevention in development of paclitaxel-induced neuropathic pain[100,102]. Alongisde activation of MCP-1, paclitaxel and vincristine treatments

have also consistently shown increased expression levels of IL-1β, IL-6, TNF-α, and other inflammation signals in primary DRG tissues[103–107], which are similarly associated with increased nociceptive responses such as release of pain markers (*e.g.*, substance P and CGRP), reduction in intraepidermal nerve fibers, and mechanical/thermal hypersensitivities. Intriguingly, patients with severe neuropathy after chemotherapy treatment have been shown to have higher IL-6 serum concentrations when compared with patients without neuropathy symptoms[108]. Recent studies have shown that blocking these pro-inflammatory signals (i.e. IL-1, IL-6) or introducing anti-inflammatory cytokines (IL-10) reduce global nociceptive responses in paclitaxel-treated primary cultured DRG neurons and rodent models[103,108], which offers a promising avenue for treatment of CIPN.

While disruption in axonal transport is the most widely-accepted mechanism for MTA-induced neuropathy, it is still unclear which mechanisms are the primary cause for pathogenesis and which are secondary cellular responses after onset of peripheral degeneration. However, these studies have highlighted the biological complexity underlying this drug-induced toxicity, and underscore the need for novel approaches to enhance our understanding of how chemotherapeutics stimulate peripheral nerve degeneration. In particular, human reverse translational studies and novel *in vitro* models using human sensory neurons should lead to increased understanding of the underlying mechanisms.

Genetic Association Studies Provide Clues to the Molecular Mechanisms Underlying MTA-induced Peripheral Neuropathy

Human genetic association studies are an important tool for identification of genetic networks involved in drug response or toxicity and have been increasingly applied to understand MTA-

induced peripheral neuropathy. These genomic approaches have given us more clues as to what biological processes may be important in the pathophysiology underlying MTA-induced neuropathy, with the promise that this information can be translated into improved chemotherapy selection and novel strategies for the prevention and/or treatment of this dose-limiting toxicity. Genome-wide association studies have enabled the transition from biased candidate genes studies to genome-wide studies of CIPN, which have revealed additional insights into which genetic pathways are vital to drug-induced sensory peripheral neuropathy.

The dose-dependent nature of MTA-induced neuropathy led to an initial focus in pharmacogenetic studies on candidate genes involved in drug pharmacokinetics and pharmacodynamics. Candidate gene studies on microtubule targeting agent-induced peripheral neuropathy implicated genetic polymorphisms in drug metabolizing enzymes (*CYP2C8/9*, *CYP3A4/5*)[109–117] and transporters (*ABCB1, ABCC2*)[113,118–123]. The first candidate gene studies[120,124] investigated *ABCB1* variants and its role in taxane-induced neuropathy, which have been replicated in other validation cohorts[113,119,122]. A decreased function *ABCB1* variant is consistent with increased risk of neuropathy since P-glycoprotein (encoded by *ABCB1*) effluxes toxic substances out of the nervous system back into systemic circulation. Investigation of genes involved in vincristine pharmacokinetics revealed *ABCC2* variants associated with increased neurotoxicity[121]. Other initial studies discovered susceptibility of severe neuropathy in patients harboring *CYP2C8* and *CYP3A4* polymorphisms[110,113], which is consistent with taxane dose-dependent toxicity and has been replicated in other candidate gene studies[109,111,112,125]. Variants in *CYP3A5* have been shown to be more relevant than *CYP3A4* to metabolism and neurotoxicity in patients treated with vincristine[114]. Additional candidate gene association studies have also found variants in genes related to drug targets. Polymorphisms that disrupt biological pathways

involving actin, tau, and microtubule regulation and function may alter taxane activity within sensory neurons and result in axonal degeneration. This hypothesis is emphasized by candidate gene studies discovering associations with variants in *TUBB2A, MAPT,* and *GSK3B*[126–128] to sensitivity of taxane-related neuropathy. Genes involved in interactions between the actin and microtubule cytoskeleton (*i.e.*, *ACTG1, CAPG*)[129] were further highlighted in a study on vincristine-induced neuropathy.

While these candidate genes studies provided fundamental insights on MTA-induced peripheral neuropathy, genome-wide approaches capture novel associations in an unbiased manner, interrogating both direct and indirect genetic effects on CIPN. Table 1.3 summarizes findings from genome-wide association studies on MTA-induced peripheral neuropathy to date. Although the early candidate gene association studies suggested neurotoxicity may be related to overall drug exposure, genome-wide association studies have shown that genes in nerve repair mechanisms seem to play a more important role than pharmacokinetic or pharmacodynamic genes. The first GWAS[130] on paclitaxel-induced peripheral neuropathy identified three novel genes important in neurite growth during development (*EPHA5*, *FZD3*) and in regulation of actin in filopodia/lamellipodia formation (*FGD4*), while a recent GWAS of docetaxel-induced peripheral neuropathy[131] identified a gene implicated in neurodegeneration (*VAC14*). *EPHA5*, a gene encoding for an ephrin signaling receptor that functions to guide axon growth during development, was identified and replicated in additional genetic association studies of paclitaxel-induced neuropathy[132–134]. Genetic association studies of vincristine-induced neurotoxicity have also implicated additional genes related to neuron structure, including those involved in microtubule/actin organization (*CEP72, SYNE2*)[135,136] and nerve innervation (*COCH*)[137]. Other taxane-induced neuropathy studies have further highlighted nerve regeneration (*e.g.*, *GPR177,*

SBF2)[138,139] as well as inflammatory (*RFX2, FCAMR*)[138,140] responses as important biological mechanisms of CIPN.

Of note, *FGD4* is a known gene causal to Charcot-Marie-Tooth disease, a hereditary neuropathy characterized by overall peripheral nerve damage and loss of muscle. This finding was further highlighted by the discovery of other CMT genes (*ARHGEF10* and *PRX*)[141,142] associated with taxane-induced neuropathy. In these cases, individuals with genetic variants in these genes only develop neuropathy symptoms in response to MTA exposure. It is possible that these individuals have compromised ability to repair nerve damage after MTA therapy, thus leading to a high probability of developing drug-induced neuropathy. Additionally, many of the implicated genes (*FGD4*[130], *EPHA4/5/6/8*[130], *LIMK2*[133], *ARHGEF10*[141,142], *SBF2*[139], *S1PR1* (Chapter 2)) associated with taxane-induced neuropathy from GWAS and sequencing studies converge on Rho-GTPase signaling pathways, a critical biological process that governs axonal guidance and neuronal extension (*i.e.*, formation of filopodia and lamellipodia). These findings suggest genetic perturbations that cause axonal degeneration or inhibit axonal regeneration processes may prevent the proper innervation of new epidermal layers after chemotherapy exposure, and potentially perpetuate the development of MTA-induced peripheral neuropathy.

While identification of biologically relevant genes and pathways from GWAS has given us some intriguing findings and supports ongoing functional studies in CIPN, the biggest challenge for all pharmacogenetic studies is finding appropriately sized and phenotyped populations for replication. As a result, most of these GWAS findings remain unreplicated. Nonetheless, genome-wide association studies have revealed the polygenic nature of MTA-induced peripheral neuroapthy[143], and overall, suggest a role for peripheral nerve repair pathways in determining sensitivity to chemotherapeutic agents. The discovery and replication of more

genetic associations would undoubtedly lead us closer to understanding the delicate balance between peripheral nerve damage and repair following exposure to neurotoxic chemotherapies, which may offer innovative strategies for CIPN management and for early screening of CIPN susceptibility. As genomic sequencing technologies advance and become more affordable, and standard neurotoxicity assessments become readily available, novel clinically relevant genetic associations will be uncovered and currently reported associations will be validated.

Table 1.3 Summary of genome-wide analyses on microtubule-targeting agent-induced peripheral neuropathy

Citation	Sucheston-Campbell et al. 2018[145]	Diouf et al. 2015[135]	Abaji et al. 2018[136,§]	Li et al. 2019[137]
Chemotherapy	Taxane	Vincristine	Vincristine	Vincristine
Phenotype[§]	Grade 3+ PN	Grade 2+ PN	Grade 3+ PN	Time-to-first grade 3+ PN; TNS-PV scores
No. Samples	1269 EUR; 139 AFR	321[‡]	237[‡]	1,128[‡]
Ancestry	EUR; AFR	MIXED	EUR	EUR
Gene/SNP (Effect; P)	*GNGT1*/rs1858826 (0.29[¥, Å]; 1.1E-07[Å])	*CEP72*/rs924607 (2.43[¥]$_{\text{St Jude Total XIIIB}}$, 4.1[¥]$_{\text{COG AALL0433}}$; 6.3E-09[Å])	*SYNE2*/rs2781377 (2.5[¥]; 0.01) *MRPL47*/rs10513762 (3.3[¥]; 0.01) *BAHD1*/rs3803357 (0.35[¥]; 0.007)	*COCH*/rs1045644 (-1.02[C]$_{\text{POG}}$, -2.36[C]$_{\text{ADVANCE}}$; 8.66E-06[Å]) *EYS*/rs796352/rs554669 (0.80[C]$_{\text{POG}}$, 2.16[C]$_{\text{ADVANCE}}$; 1.05E-05[Å])
Replication	No, but meta-analysis with Baldwin et al. 2012[130] (855; EUR)	No	Yes (405)	No
Biological pathway	Photoreceptor function	Microtubule organization	Actin reorganization, mitochondrial homeostasis, transcriptional regulation	Nerve innervation, photoreceptor function

LCL: lymphoblastoid cell lines; NR: not reported; EUR, European; AFR, African America; MIXED, multi-ethnic ancestry
[§] All grading are defined by NCI-CTCAE criteria. [‡] Pediatric population. [§]Genome-wide exome sequencing study. [Z]Z-score. [C]β Coefficient. [R]Relative risk. [†] Hazard ratio. [¥]Odds ratio.
[Å] Effects or *P* values of meta-analysis

Table 1.3 (cont.) Summary of genome-wide analyses on microtubule-targeting agent-induced peripheral neuropathy

Citation	Komatsu et al. 2015[144]	Schneider et al. 2015[138]	Schneider et al. 2015[138]	Schneider et al. 2016[139,§]	Hertz et al. 2016[131]
Chemotherapy	Paclitaxel	Paclitaxel	Paclitaxel	Paclitaxel	Docetaxel
Phenotype[§]	Paclitaxel-induced cytotoxicity	Grade 2+ PN	Grade 3+ PN	Grade 3+ PN	Cumulative dose to first Grade 3+ PN
No. Samples	116 LCL	213	1,357	126	623
Ancestry	ASN	AFR	EUR	AFR	EUR
Gene/SNP (Effect; P)	*AIPL1*/rs3892315 (0.207[C]; 8.72E-07) *AIPL1*/rs11651916 (0.207[C]; 8.75E-07) *AIPL1*/rs3892316 (0.206[C]; 9.23E-07)	*FCAMR*/rs1856746 (5.54[¥]; 1.57E-07)	*GPR177*/rs3125923 (1.8[¥]; 4.99E-05)	*SBF2* (4.35E-06)	*VAC14*/rs875858 (3.60[†] ; 2.12E-08)
Replication	No	Yes (2,096)	Yes (2,096)	No	No
Biological pathway	Photoreceptor function	Inflammation	Neuronal development	Axonal degeneration	Neurodegeneration

LCL: lymphoblastoid cell lines; NR: not reported; EUR, European; AFR, African America; MIXED, multi-ethnic ancestry
[§] All grading are defined by NCI-CTCAE criteria. [‡] Pediatric population. [$]Genome-wide exome sequencing study. [Z]Z-score. [C]β Coefficient. [R]Relative risk. [†] Hazard ratio. [¥]Odds ratio.
[A] Effects or *P* values of meta-analysis

Table 1.3 (cont.) Summary of genome-wide analyses on microtubule-targeting agent-induced peripheral neuropathy

Citation	Baldwin et al. 2012[130]	Leandro-García et al. 2013[133]	Wheeler et al. 2013[140]
Chemotherapy	Paclitaxel	Paclitaxel and/or carboplatin	Paclitaxel
Phenotype[§]	Cumulative dose to first grade 2+ PN (onset); ordinal grades (severity)	Cumulative dose to first grade 2+ PN	Paclitaxel-induced cytotoxicity
No. Samples	855	144	247 LCL
Ancestry	EUR	EUR	MIXED
Gene/SNP (Effect; P)	*EPHA5*/rs7349683 (1.63[†] ; 9.6E-07) *FGD4*/rs10771973 (1.57[†] ; 2.6E-06) *FZD3*/rs7001034 (0.57[¥]; 3.1E-09) *FZD3*/rs7833751 (0.58[¥]; 7.5E-09)	*EPHA4*/rs17348202 (4.85[†] ; 1.02E-06) *EPHA6*/rs301927 (2.35[†] ; 3.44E-05) *EPHA5*/rs1159057 (2.01[†] ; 6.84E-05) *EPHA5*/rs7349683 (1.83[†] ; 3.33E-04) *EPHA5*/rs7349683 (1.68[†,Å]; 1.4E-09[Å]) *XKR4*/rs4737264 (1.71[†,Å]; 3.1E-08[Å]) *LIMK2*/rs4141404 (2.41[†] ; 3.22E-06) *LIMK2*/rs5749248 (2.78[†] ; 1.98E-07)	*RFX2*/rs7254081 (3.44[Ž]; 5.9E-04)
Replication	Yes (177; AFR)	No, but meta-analysis with Baldwin et al. 2012[130] (855; EUR)	No
Biological pathway	Axonal guidance, neuronal development, actin reorganization	Axonal guidance, apoptosis, actin reorganization	Inflammation

LCL: lymphoblastoid cell lines; NR: not reported; EUR, European; AFR, African America; MIXED, multi-ethnic ancestry

[§] All grading are defined by NCI-CTCAE criteria. [‡] Pediatric population. [$]Genome-wide exome sequencing study. [Ž]Z-score. [C]β Coefficient. [R]Relative risk. [†] Hazard ratio. [¥]Odds ratio. [Å] Effects or *P* values of meta-analysis

Translation of Genetic Findings using Human Sensory Neurons

Human induced pluripotent stem cell (iPSC)-derived sensory neurons hold great promise for understanding the genes and pathways underlying drug-induced neuropathy, defining the contribution of genetic variation to the toxicity, and screening for drug targets. Recent studies have highlighted the use of human stem cell-derived neurons for modeling chemotherapy-induced sensory neuronal damage[131,135,153–156,144,146–152], where some have focused on translating the genetic findings from GWAS into molecular mechanisms that can be exploited for novel targets against CIPN. Human derived sensory nociceptors originating from fibroblasts or blood have shown sensitivity upon exposure to various anticancer drug classes that cause neuropathy[152,153,157], resulting in dose-dependent changes in neuronal morphology which include reductions of neurite length, neuron count, cell viability, and apoptosis. Other studies[146–148,155] have shown similar effects with commercially available iPSCs (iCell® neurons, Peri.4U® neurons) that are more robust for high-throughput screening of potential genetic targets.

As these iPSC-derived neurons appear to embody similar nociceptive responses to chemotherapy exposure as human sensory neurons, recent work has utilized these *in vitro* models for validation of GWAS findings, measuring changes to chemotherapy sensitivity after modulating identified genetic targets. Of note, genetically inhibiting *TUBB2A* in iCell® neurons increase paclitaxel-induced neurite retraction by ~ 20%[147]. Validation of *AIPL1* from a genome-wide association study (Table 1.3) on paclitaxel-induced neuropathy used the same *in vitro* model, with decreased *AIPL1* expression resulting in overall protection against paclitaxel-induced neurite morphological damage[144]. Similarly, Diouf et al.[135] reported support for the involvement of *CEP72* in vincristine-induced neuropathy using this *in vitro* model. Using iCell® neurons, the authors demonstrated genetically silencing *CEP72*, a representation of a loss of

function variant in the promoter of *CEP72*, displayed greater vincristine-induced neuronal damage (i.e. reduced neurite lengths and branching). While these validation studies are crucial in translating GWAS findings into molecular targets, it is also important to note that iCell® neurons are distinctly central neurons and may show differences in effect compared with peripheral neurons. Intriguingly, one study[149] using Peri.4U® neurons, iPSC-derived "peripheral-like" neurons, has shown sensitivity to MTA treatments but not platinum agents or thalidomide. Unlike iCell® neurons that are affected by all CIPN-related drugs, this result suggests human iPSC-derived sensory peripheral neurons rather than iPSC-derived central neurons are likely the most appropriate *in vitro* model to recapitulate MTA-induced axonal degeneration. One study has used Peri4.U® neurons for validation of VAC14 in docetaxel-induced neuropathy[131] (Table 1.3), revealing siVAC14 Peri.4U neurons have less neurite outgrowth and less neurite branches under paclitaxel and docetaxel exposure, respectively, compared to a nontargeting control. Further corroborating the result found in Peri.4U® neurons, the authors show that *Vac14*$^{-/-}$ mice have increased nociceptive sensitivity compared to wildtype mice following docetaxel treatment, attesting that these *in vitro* models are suitable to validate and screen potential genetic targets associated with MTA-induced peripheral neuropathy.

With the continuing implementation of iPSC-derived sensory neurons into pharmacogenetic studies, we will be able to truly isolate how patient-specific genetic variation determines CIPN predisposition and build a platform to screen potential tailored neuroprotective targets. A recent study has shown successful utilization of patient iPSC-derived sensory neurons to treat severe small fiber neuropathic pain[151], demonstrating that such models can more faithfully mimic target tissues and translate patient experience.

Gaps in Research and Focus of this Dissertation

The main limitation to develop therapeutic strategies against CIPN is the lack of knowledge in its pathophysiology across chemotherapies. With advances in genomic technologies and more robust functional models of CIPN, we have only begun to address the current gaps in our understanding of how CIPN develops. The work described herein utilizes a pharmacogenetic approach (Figure 1.3) using human-level data to investigate the underlying mechanisms contributing to MTA-induced neuropathy. Chapters 2 and 3 describe genome-wide association studies using genotyping and next-generation sequencing data, which were designed to discover novel genetic targets that are clinically relevant to MTA-induced peripheral neuropathy and directly provide insight on patient sensitivity to chemotherapy-induced peripheral nerve damage. These efforts to uncover underlying actionable markers and validate in robust model systems are the next critical steps to translate genomic targets into therapies for drug-induced neuropathy. As the importance of cancer survivors' long-term well-being continues to gain acknowledgement, there is an increasing interest in effectively monitoring and controlling patient symptoms. Chapter 4 explored how patient genetics and early symptom monitoring may aid in the prediction of dose-limiting neuropathy events. The ability to predict severe MTA-induced peripheral neuropathy events early in treatment would considerably support clinical decisions when balancing chemotherapy benefit and patient quality of life. Overall, the findings from the work herein contribute new insights into critical genetic networks responsible for this complex drug-induced toxicity, and will enable future studies to develop standardized tools to predict, manage, and treat at-risk patients genetically susceptible to MTA-induced peripheral neuropathy.

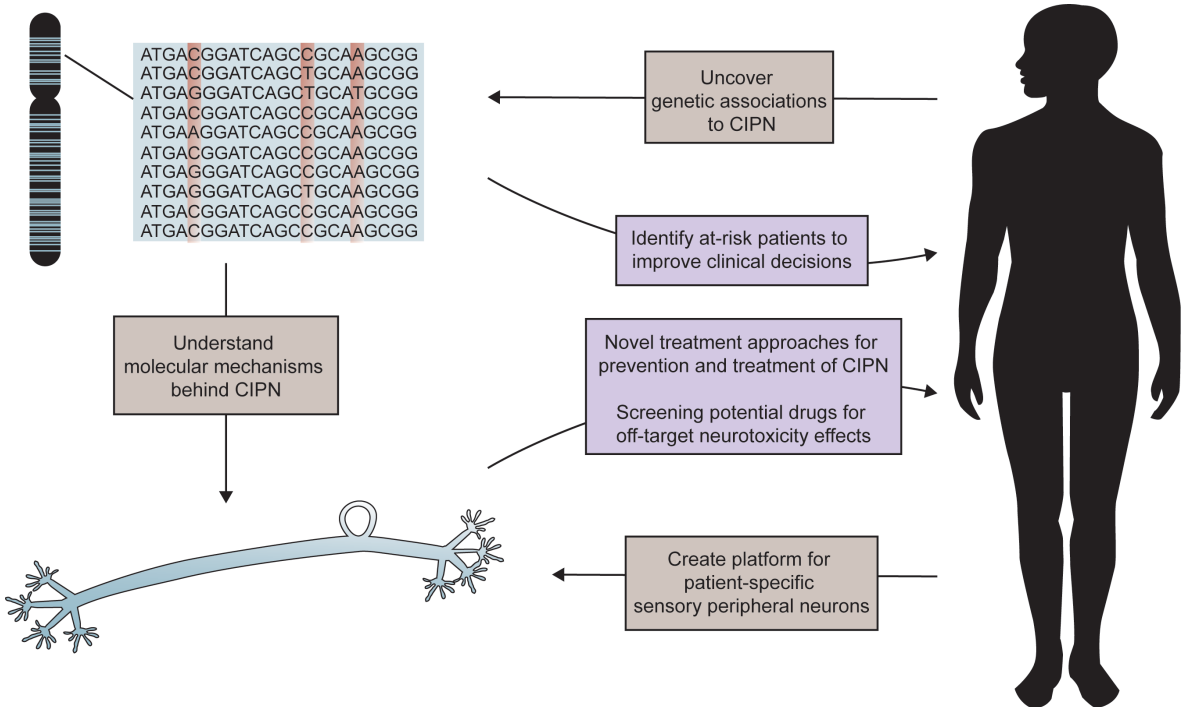

Figure 1.3 The precision medicine approach incorporates both genome-wide association studies and functional models to understand the molecular mechanisms underlying CIPN, with the goal of discovering novel strategies to prevent and treat this dose-limiting toxicity. The identification of genetic biomarkers will enable screening for CIPN risk, thereby improving clinical decisions. *In vitro* models to study CIPN have the potential to inform how patient susceptibility develops, identify novel therapeutic strategies for treatment and prevention, and test new chemical entities for liability for this toxicity.

References

1. Shah, A., Hoffman, E. M., Mauermann, M. L., Loprinzi, C. L., Klein, C. J., Staff, N. P., Clinic, M. & Clinic, M. Peripheral Neuropathy in a Population-Based Cohort. **89**, 636–641 (2018).
2. Grisold, W., Cavaletti, G. & Windebank, A. J. Peripheral neuropathies from chemotherapeutics and targeted agents: Diagnosis, treatment, and prevention. *Neuro. Oncol.* **14**, 45–54 (2012).
3. Zajaczkowską, R., Kocot-Kępska, M., Leppert, W., Wrzosek, A., Mika, J. & Wordliczek, J. Mechanisms of chemotherapy-induced peripheral neuropathy. *Int. J. Mol. Sci.* **20**, (2019).
4. Seretny, M., Currie, G. L., Sena, E. S., Ramnarine, S., Grant, R., Macleod, M. R., Colvin, L. A. & Fallon, M. Incidence, prevalence, and predictors of chemotherapy-induced peripheral neuropathy: A systematic review and meta-analysis. *Pain* **155**, 2461–2470 (2014).
5. Flatters, S. J. L., Dougherty, P. M. & Colvin, L. A. Clinical and preclinical perspectives on Chemotherapy-Induced Peripheral Neuropathy (CIPN): A narrative review. *Br. J. Anaesth.* **119**, 737–749 (2017).
6. Hershman, D. L., Lacchetti, C., Dworkin, R. H., Lavoie Smith, E. M., Bleeker, J., Cavaletti, G., Chauhan, C., Gavin, P., Lavino, A., Lustberg, M. B., Paice, J., Schneider, B., Smith, M. Lou, Smith, T., Terstriep, S., Wagner-Johnston, N., Bak, K. & Loprinzi, C. L. Prevention and management of chemotherapy-induced peripheral neuropathy in survivors of adult cancers: American society of clinical oncology clinical practice guideline. *J. Clin. Oncol.* **32**, 1941–1967 (2014).

7. Cavaletti, G., Alberti, P., Argyriou, A. A., Lustberg, M., Staff, N. P. & Tamburin, S. Chemotherapy-induced peripheral neurotoxicity: A multifaceted, still unsolved issue. *J. Peripher. Nerv. Syst.* **24**, S6–S12 (2019).

8. Argyriou, A. A., Cavaletti, G., Briani, C., Velasco, R., Bruna, J., Campagnolo, M., Alberti, P., Bergamo, F., Cortinovis, D., Cazzaniga, M., Santos, C., Papadimitriou, K. & Kalofonos, H. P. Clinical pattern and associations of oxaliplatin acute neurotoxicity: A prospective study in 170 patients with colorectal cancer. *Cancer* **119**, 438–444 (2013).

9. Attal, N., Bouhassira, D., Gautron, M., Vaillant, J. N., Mitry, E., Lepère, C., Rougier, P. & Guirimand, F. Thermal hyperalgesia as a marker of oxaliplatin neurotoxicity: A prospective quantified sensory assessment study. *Pain* **144**, 245–252 (2009).

10. Hershman, D. L., Weimer, L. H., Wang, A., Kranwinkel, G., Brafman, L., Fuentes, D., Awad, D. & Crew, K. D. Association between patient reported outcomes and quantitative sensory tests for measuring long-term neurotoxicity in breast cancer survivors treated with adjuvant paclitaxel chemotherapy. *Breast Cancer Res. Treat.* **125**, 767–774 (2011).

11. Quasthoff, S. & Hartung, H. P. Chemotherapy-induced peripheral neuropathy. *J. Neurol.* **249**, 9–17 (2002).

12. Glendenning, J. L., Barbachano, Y., Norman, A. R., Dearnaley, D. P., Horwich, A. & Huddart, R. A. Long-term neurologic and peripheral vascular toxicity after chemotherapy treatment of testicular cancer. *Cancer* **116**, 2322–2331 (2010).

13. Brouwers, E. E. M., Huitema, A. D. R., Boogerd, W., Beijnen, J. H. & Schellens, J. H. M. Persistent neuropathy after treatment with cisplatin and oxaliplatin. *Acta Oncol. (Madr).* **48**, 832–841 (2009).

14. Ewertz, M., Qvortrup, C. & Eckhoff, L. Chemotherapy-induced peripheral neuropathy in

patients treated with taxanes and platinum derivatives. *Acta Oncol. (Madr).* **54**, 587–591 (2015).

15. Cavaletti, G., Alberti, P., Frigeni, B., Piatti, M. & Susani, E. Chemotherapy-Induced Neuropathy. *Curr. Treat. Options Neurol.* **13**, 180–190 (2011).

16. Joly, F., Ahmed-Lecheheb, D., Kalbacher, E., Heutte, N., Clarisse, B., Grellard, J. M., Gernier, F., Berton-Rigaud, D., Tredan, O., Fabbro, M., Savoye, A. M., Kurtz, J. E., Alexandre, J., Follana, P., Delecroix, V., Dohollou, N., Roemer-Becuwe, C., De Rauglaudre, G., Lortholary, A., *et al.* Long-Term fatigue and quality of life among epithelial ovarian cancer survivors: A GINECO case/control VIVROVAIRE i study. *Ann. Oncol.* **30**, 845–852 (2019).

17. Ezendam, N. P. M., Pijlman, B., Bhugwandass, C., Pruijt, J. F. M., Mols, F., Vos, M. C., Pijnenborg, J. M. A. & Van De Poll-Franse, L. V. Chemotherapy-induced peripheral neuropathy and its impact on health-related quality of life among ovarian cancer survivors: Results from the population-based PROFILES registry. *Gynecol. Oncol.* **135**, 510–517 (2014).

18. Pike, C. T., Birnbaum, H. G., Muehlenbein, C. E., Pohl, G. M. & Natale, R. B. Healthcare Costs and Workloss Burden of Patients with Chemotherapy-Associated Peripheral Neuropathy in Breast, Ovarian, Head and Neck, and Nonsmall Cell Lung Cancer. *Chemother. Res. Pract.* **2012**, 1–10 (2012).

19. Calhoun, E. A. Evaluating the Total Costs of Chemotherapy-Induced Toxicity: Results from a Pilot Study with Ovarian Cancer Patients. *Oncologist* **6**, 441–445 (2001).

20. Park, S. B., Krishnan, a V, Lin, C. S.-Y., Goldstein, D., Friedlander, M. & Kiernan, M. C. Mechanisms underlying chemotherapy-induced neurotoxicity and the potential for

neuroprotective strategies. *Curr. Med. Chem.* **15**, 3081–3094 (2008).

21. Vahdat, L. T., Thomas, E. S., Roché, H. H., Hortobagyi, G. N., Sparano, J. A., Yelle, L., Fornier, M. N., Martín, M., Bunnell, C. A., Mukhopadhyay, P., Peck, R. A. & Perez, E. A. Ixabepilone-associated peripheral neuropathy: Data from across the phase II and III clinical trials. *Support. Care Cancer* **20**, 2661–2668 (2012).

22. Argyriou, A. A., Kyritsis, A. P., Makatsoris, T. & Kalofonos, H. P. Chemotherapy-induced peripheral neuropathy in adults: A comprehensive update of the literature. *Cancer Manag. Res.* **6**, 135–147 (2014).

23. Wozniak, K. M., Vornov, J. J., Wu, Y., Liu, Y., Carozzi, V. A., Rodriguez-Menendez, V., Ballarini, E., Alberti, P., Pozzi, E., Semperboni, S., Cook, B. M., Littlefield, B. A., Nomoto, K., Condon, K., Eckley, S., DesJardins, C., Wilson, L., Jordan, M. A., Feinstein, S. C., *et al.* Peripheral neuropathy induced by microtubule-targeted chemotherapies: Insights into acute injury and long-term recovery. *Cancer Res.* **78**, 817–829 (2018).

24. Wilson, R. H., Lehky, T., Thomas, R. R., Quinn, M. G., Floeter, M. K. & Grem, J. L. Acute oxaliplatin-induced peripheral nerve hyperexcitability. *J. Clin. Oncol.* **20**, 1767–1774 (2002).

25. Greenwald, M. K., Ruterbusch, J. J., Beebe-Dimmer, J. L., Simon, M. S., Albrecht, T. L. & Schwartz, A. G. Risk of incident claims for chemotherapy-induced peripheral neuropathy among women with breast cancer in a Medicare population. *Cancer* **125**, 269–277 (2019).

26. Park, S. B., Alberti, P., Kolb, N. A., Gewandter, J. S., Schenone, A. & Argyriou, A. A. Overview and critical revision of clinical assessment tools in chemotherapy-induced peripheral neurotoxicity. *J. Peripher. Nerv. Syst.* **24**, S13–S25 (2019).

27. Berger, T., Malayeri, R., Doppelbauer, A., Krajnik, G., Huber, H., Auff, E. & Pirker, R. Neurological Monitoring of Neurotoxicity Induced by Paclitaxel/Cisplatin Chemotherapy. *Eur. J. Cancer* **33**, 1393–1399 (1997).

28. Chaudhry, V., Rowinsky, E. K., Sartorius, S. E., Donehower, R. C. & Cornblath, D. R. Peripheral neuropathy from taxol and cisplatin combination chemotherapy: Clinical and electrophysiological studies. *Ann. Neurol.* **35**, 304–311 (1994).

29. Forsyth, P. A., Balmaceda, C., Peterson, K., Seidman, A. D., Brasher, P. & DeAngelis, L. M. Prospective study of paclitaxel-induced peripheral neuropathy with quantitative sensory testing. *J. Neurooncol.* **35**, 47–53 (1997).

30. Zhi, W. I., Chen, P., Kwon, A., Chen, C., Harte, S. E., Piulson, L., Li, S., Patil, S., Mao, J. J. & Bao, T. Chemotherapy-induced peripheral neuropathy (CIPN) in breast cancer survivors: a comparison of patient-reported outcomes and quantitative sensory testing. *Breast Cancer Res. Treat.* **178**, 587–595 (2019).

31. Le-Rademacher, J., Kanwar, R., Seisler, D., Pachman, D. R., Qin, R., Abyzov, A., Ruddy, K. J., Banck, M. S., Lavoie Smith, E. M., Dorsey, S. G., Aaronson, N. K., Sloan, J., Loprinzi, C. L. & Beutler, A. S. Patient-reported (EORTC QLQ-CIPN20) versus physician-reported (CTCAE) quantification of oxaliplatin- and paclitaxel/carboplatin-induced peripheral neuropathy in NCCTG/Alliance clinical trials. *Support. Care Cancer* **25**, 3537–3544 (2017).

32. Shimozuma, K., Ohashi, Y., Takeuchi, A., Aranishi, T., Morita, S., Kuroi, K., Ohsumi, S., Makino, H., Mukai, H., Katsumata, N., Sunada, Y., Watanabe, T. & Hausheer, F. H. Feasibility and validity of the Patient Neurotoxicity Questionnaire during taxane chemotherapy in a phase III randomized trial in patients with breast cancer: N-SAS BC

02. *Support. Care Cancer* **17**, 1483–1491 (2009).

33. Nyrop, K. A., Deal, A. M., Reeder-Hayes, K. E., Shachar, S. S., Reeve, B. B., Basch, E., Choi, S. K., Lee, J. T., Wood, W. A., Anders, C. K., Carey, L. A., Dees, E. C., Jolly, T. A., Kimmick, G. G., Karuturi, M. S., Reinbolt, R. E., Speca, J. E. C. & Muss, H. B. Patient-reported and clinician-reported chemotherapy-induced peripheral neuropathy in patients with early breast cancer: Current clinical practice. *Cancer* **125**, 2945–2954 (2019).

34. Cavaletti, G., Cornblath, D. R., Merkies, I. S. J., Postma, T. J., Rossi, E., Frigeni, B., Alberti, P., Bruna, J., Velasco, R., Argyriou, A. A., Kalofonos, H. P., Psimaras, D., Ricard, D., Pace, A., Galiè, E., Briani, C., Dalla Torre, C., Faber, C. G., Lalisang, R. I., *et al.* The chemotherapy-induced peripheral neuropathy outcome measures standardization study: From consensus to the first validity and reliability findings. *Ann. Oncol.* **24**, 454–462 (2013).

35. Siau, C., Xiao, W. & Bennett, G. J. Paclitaxel- and vincristine-evoked painful peripheral neuropathies: Loss of epidermal innervation and activation of Langerhans cells. *Exp. Neurol.* **201**, 507–514 (2006).

36. Boyette-Davis, J., Xin, W., Zhang, H. & Dougherty, P. M. Intraepidermal nerve fiber loss corresponds to the development of Taxol-induced hyperalgesia and can be prevented by treatment with minocycline. *Pain* **152**, 308–313 (2011).

37. Flatters, S. J. L. & Bennett, G. J. Studies of peripheral sensory nerves in paclitaxel-induced painful peripheral neuropathy: Evidence for mitochondrial dysfunction. *Pain* **122**, 245–257 (2006).

38. Xiao, W. H., Zheng, H., Zheng, F. Y., Nuydens, R., Meert, T. F. & Bennett, G. J.

Mitochondrial abnormality in sensory, but not motor, axons in paclitaxel-evoked painful peripheral neuropathy in the rat. *Neuroscience* **199**, 461–469 (2011).

39. Sahenk, Z., Barohn, R., New, P. & Mendell, J. R. Taxol neuropathy. Electrodiagnostic and sural nerve biopsy findings. *Arch Neurol* 726–729 (1994).

40. Boehmerle, W., Huehnchen, P., Peruzzaro, S., Balkaya, M. & Endres, M. Electrophysiological, behavioral and histological characterization of paclitaxel, cisplatin, vincristine and bortezomib-induced neuropathy in C57Bl/6 mice. *Sci Rep* **4**, 6370 (2014).

41. Fazio, R., Quattrini, A., Bolognesi, A., Bordogna, G., Villa, E., Previtali, S., Canal, N. & Nemni, R. Docetaxel neuropathy: A distal axonopathy. *Acta Neuropathol.* **98**, 651–653 (1999).

42. Xiao, W. H., Zheng, H. & Bennett, G. J. Characterization of oxaliplatin-induced chronic painful peripheral neuropathy in the rat and comparison with the neuropathy induced by paclitaxel. *Neuroscience* **203**, 194–206 (2012).

43. Zheng, H., Xiao, W. H. & Bennett, G. J. Mitotoxicity and bortezomib-induced chronic painful peripheral neuropathy. *Exp. Neurol.* **238**, 225–234 (2012).

44. Bechakra, M., Nieuwenhoff, M. D., van Rosmalen, J., Groeneveld, G. J., Scheltens-de Boer, M., Sonneveld, P., van Doorn, P. A., de Zeeuw, C. I. & Jongen, J. L. M. Clinical, electrophysiological, and cutaneous innervation changes in patients with bortezomib-induced peripheral neuropathy reveal insight into mechanisms of neuropathic pain. *Mol. Pain* **14**, (2018).

45. Krøigård, T., Schrøder, H. D., Qvortrup, C., Eckhoff, L., Pfeiffer, P., Gaist, D. & Sindrup, S. H. Characterization and diagnostic evaluation of chronic polyneuropathies induced by oxaliplatin and docetaxel comparing skin biopsy to quantitative sensory testing and nerve

conduction studies. *Eur. J. Neurol.* **21**, 623–629 (2014).

46. Krøigård, T., Svendsen, T. K., Wirenfeldt, M., Schrøder, H. D., Qvortrup, C., Pfeiffer, P., Gaist, D. & Sindrup, S. H. Early changes in tests of peripheral nerve function during oxaliplatin treatment and their correlation with chemotherapy-induced polyneuropathy symptoms and signs. *Eur. J. Neurol.* **27**, 68–76 (2020).

47. Koskinen, M. J., Kautio, A. L., Haanpää, M. L., Haapasalo, H. K., Kellokumpu-Lehtinen, P. L., Saarto, T. & Hietaharju, A. J. Intraepidermal nerve fibre density in cancer patients receiving adjuvant chemotherapy. *Anticancer Res.* **31**, 4413–4416 (2011).

48. Boyette-Davis, J. & Dougherty, P. M. Protection against oxaliplatin-induced mechanical hyperalgesia and intraepidermal nerve fiber loss by minocycline. *Exp. Neurol.* **229**, 353–357 (2011).

49. Singhmar, P., Huo, X. J., Li, Y., Dougherty, P. M., Mei, F., Cheng, X., Heijnen, C. J. & Kavelaars, A. Orally active Epac inhibitor reverses mechanical allodynia and loss of intraepidermal nerve fibers in a mouse model of chemotherapy-induced peripheral neuropathy. *Pain* **159**, 884–893 (2018).

50. Lauria, G., Lombardi, R., Borgna, M., Penza, P., Bianchi, R., Savino, C., Canta, A., Nicolini, G., Marmiroli, P. & Cavaletti, G. Intraepidermal nerve fiber density in rat foot pad: Neuropathologic- neurophysiologic correlation. *J. Peripher. Nerv. Syst.* **10**, 202–208 (2005).

51. Landowskia, L. M., Dyckc, P. J. B., Engelstadc, J. & Taylord, B. V. Axonopathy in peripheral neuropathies: Mechanisms and therapeutic approaches for regeneration. *J. Chem. Neuroanat.* **76**, 19–27 (2015).

52. Masurovsky, E. B., Peterson, E. R., Crain, S. M. & Horwitz, S. B. Microtubule arrays in

taxol-treated mouse dorsal root ganglion-spinal cord cultures. *Brain Res.* **217**, 392–398 (1981).

53. Roytta, M. & Raine, C. S. Taxol-induced neuropathy: chronic effects of local injection. *J. Neurocytol.* **15**, 483–496 (1986).

54. Röytta, M. & Raine, C. S. Taxol-induced neuropathy: further ultrastructural studies of nerve fibre changes in situ. *J. Neurocytol.* **14**, 157–175 (1985).

55. Komiya, Y. Changes of fast axonal transport by taxol injected subepineurally into the rat sciatic nerve. *Neurosci. Res.* **14**, 159–165 (1992).

56. Komiya, Y. & Tashiro, T. Effects of taxol on slow and fast axonal transport. *Cell Motil. Cytoskeleton* **11**, 151–156 (1988).

57. Cavaletti, G., Giovanni, T., Braga, M. & Tazzari, S. Experimental Peripheral Neuropathy Induced in Adult Rats by Repeated Intraperitoneal Administration of Taxel. *Exp. Neurol.* **133**, 64–72 (1995).

58. Cavaletti, G., Cavalletti, E., Montaguti, P., Oggioni, N., De Negri, O. & Tredici, G. Effect on the peripheral nervous system of the short-term intravenous administration of paclitaxel in the rat. *Neurotoxicology* **18**, 137–145 (1997).

59. Bobylev, I., Joshi, A. R., Barham, M., Ritter, C., Neiss, W. F., Hoke, A. & Lehmann, H. C. Paclitaxel inhibits mRNA transport in axons. *Neurobiol. Dis.* **82**, 321–331 (2015).

60. Shemesh, O. A. & Spira, M. E. Paclitaxel induces axonal microtubules polar reconfiguration and impaired organelle transport: Implications for the pathogenesis of paclitaxel-induced polyneuropathy. *Acta Neuropathol.* **119**, 235–248 (2010).

61. Bober, B. G., Gutierrez, E., Plaxe, S., Groisman, A. & Shah, S. B. Combinatorial influences of paclitaxel and strain on axonal transport. *Exp. Neurol.* **271**, 358–367 (2015).

62. Bober, B. G. & Shah, S. B. Paclitaxel alters sensory nerve biomechanical properties. *J. Biomech.* **48**, 3559–3567 (2015).

63. Theiss, C. & Meller, K. Taxol impairs anterograde axonal transport of microinjected horseradish peroxidase in dorsal root ganglia neurons in vitro. *Cell Tissue Res.* **299**, 213–224 (2000).

64. LaPointe, N. E., Morfini, G., Brady, S. T., Feinstein, S. C., Wilson, L. & Jordan, M. A. Effects of eribulin, vincristine, paclitaxel and ixabepilone on fast axonal transport and kinesin-1 driven microtubule gliding: Implications for chemotherapy-induced peripheral neuropathy. *Neurotoxicology* **37**, 231–239 (2013).

65. Topp, K. S., Tanner, K. D. & Levine, J. D. Damage to the cytoskeleton of large diameter sensory neurons and myelinated axons in vincristine-induced painful peripheral neuropathy in the rat. *J. Comp. Neurol.* **424**, 563–576 (2000).

66. Wang, M. S., Davis, A. A., Culver, D. G. & Glass, J. D. Wlds mice are resistant to paclitaxel (Taxol) neuropathy. *Ann. Neurol.* **52**, 442–447 (2002).

67. Wang, M., Wu, Y., Culver, D. G. & Glass, J. D. The gene for slow Wallerian degeneration (Wld(s)) is also protective against vincristine neuropathy. *Neurobiol. Dis.* **8**, 155–161 (2001).

68. Wang, M. S., Fang, G., Culver, D. G., Davis, A. A., Rich, M. M. & Glass, J. D. The Wlds protein protects against axonal degeneration: A model of gene therapy for peripheral neuropathy. *Ann. Neurol.* **50**, 773–779 (2001).

69. Geisler, S., Doan, R. A., Strickland, A., Huang, X., Milbrandt, J. & DiAntonio, A. Prevention of vincristine-induced peripheral neuropathy by genetic deletion of SARM1 in mice. *Brain* **139**, 3092–3108 (2016).

70. Gornstein, E. L. & Schwarz, T. L. Neurotoxic mechanisms of paclitaxel are local to the distal axon and independent of transport defects. *Exp. Neurol.* **288**, 153–166 (2017).

71. Authier, N., Gillet, J. P., Fialip, J., Eschalier, A. & Coudore, F. Description of a short-term Taxol®-induced nociceptive neuropathy in rats. *Brain Res.* **887**, 239–249 (2000).

72. Cliffer, K. D., Siuciak, J. A., Carson, S. R., Radley, H. E., Park, J. S., Lewis, D. R., Zlotchenko, E., Nguyen, T., Garcia, K., Tonra, J. R., Stambler, N., Cedarbaum, J. M., Bodine, S. C., Lindsay, R. M. & Distefano, P. S. Physiological characterization of taxol-induced large fiber sensory neuropathy in the rat. *Ann Neurol* **43**, 46–55 (1998).

73. Zheng, H., Xiao, W. H. & Bennett, G. J. Functional deficits in peripheral nerve mitochondria in rats with paclitaxel- and oxaliplatin-evoked painful peripheral neuropathy. *Exp. Neurol.* **232**, 154–161 (2011).

74. Janes, K., Doyle, T., Bryant, L., Esposito, E., Cuzzocrea, S., Ryerse, J., Bennett, G. J. & Salvemini, D. Bioenergetic deficits in peripheral nerve sensory axons during chemotherapy-induced neuropathic pain resulting from peroxynitrite-mediated post-translational nitration of mitochondrial superoxide dismutase. *Pain* **154**, 2432–2440 (2013).

75. Duggett, N. A., Griffiths, L. A., McKenna, O. E., de Santis, V., Yongsanguanchai, N., Mokori, E. B. & Flatters, S. J. L. Oxidative stress in the development, maintenance and resolution of paclitaxel-induced painful neuropathy. *Neuroscience* **333**, 13–26 (2016).

76. Griffiths, L. A. & Flatters, S. J. L. Pharmacological Modulation of the Mitochondrial Electron Transport Chain in Paclitaxel-Induced Painful Peripheral Neuropathy. *J. Pain* **16**, 981–994 (2015).

77. Joseph, E. K. & Levine, J. D. Mitochondrial electron transport in models of neuropathic

and inflammatory pain. *Pain* **121**, 105–114 (2006).

78. Duggett, N. A., Griffiths, L. A. & Flatters, S. J. L. Paclitaxel-induced painful neuropathy is associated with changes in mitochondrial bioenergetics, glycolysis, and an energy deficit in dorsal root ganglia neurons. *Pain* **158**, 1499–1508 (2017).

79. Xiao, W. H. & Bennett, G. J. Effects of mitochondrial poisons on the neuropathic pain produced by the chemotherapeutic agents, paclitaxel and oxaliplatin. *Pain* **153**, 704–709 (2012).

80. Kidd, J. F., Pilkington, M. F., Schell, M. J., Fogarty, K. E., Skepper, J. N., Taylor, C. W. & Thorn, P. Paclitaxel affects cytosolic calcium signals by opening the mitochondrial permeability transition pore. *J. Biol. Chem.* **277**, 6504–6510 (2002).

81. Siau, C. & Bennett, G. J. Dysregulation of cellular calcium homeostasis in chemotherapy-evoked painful peripheral neuropathy. *Anesth. Analg.* **102**, 1485–1490 (2006).

82. Boehmerle, W., Zhang, K., Sivula, M., Heidrich, F. M., Lee, Y., Jordt, S.-E. & Ehrlich, B. E. Chronic exposure to paclitaxel diminishes phosphoinositide signaling by calpain-mediated neuronal calcium sensor-1 degradation. *Proc. Natl. Acad. Sci. U. S. A.* **104**, 11103–8 (2007).

83. Boehmerle, W., Splittgerber, U., Lazarus, M. B., McKenzie, K. M., Johnston, D. G., Austin, D. J. & Ehrlich, B. E. Paclitaxel induces calcium oscillations via an inositol 1,4,5-trisphosphate receptor and neuronal calcium sensor 1-dependent mechanism. *Proc. Natl. Acad. Sci. U. S. A.* **103**, 18356–18361 (2006).

84. Ebenezer, G. J., Carlson, K., Donovan, D., Cobham, M., Chuang, E., Moore, A., Cigler, T., Ward, M., Lane, M. E., Ramnarain, A., Vahdat, L. T. & Polydefkis, M. Ixabepilone-induced mitochondria and sensory axon loss in breast cancer patients. *Ann. Clin. Transl.*

Neurol. **1**, 639–649 (2014).

85. Kober, K. M., Olshen, A., Conley, Y. P., Schumacher, M., Topp, K., Smoot, B., Mazor, M., Chesney, M., Hammer, M., Paul, S. M., Levine, J. D. & Miaskowski, C. Expression of mitochondrial dysfunction-related genes and pathways in paclitaxel-induced peripheral neuropathy in breast cancer survivors. *Mol. Pain* **14**, (2018).

86. Zhang, H. & Dougherty, P. M. Enhanced Excitability of Primary Sensory Neurons and Altered Gene Expression of Neuronal Ion Channels in Dorsal Root Ganglion in Paclitaxel-induced Peripheral Neuropathy. 1463–1475 (2014).

87. Li, Y., North, R. Y., Rhines, L. D., Tatsui, C. E., Rao, G., Edwards, D. D., Cassidy, R. M., Harrison, D. S., Johansson, C. A., Zhang, H. & Dougherty, P. M. Drg voltage-gated sodium channel 1.7 is upregulated in paclitaxel-induced neuropathy in rats and in humans with neuropathic pain. *J. Neurosci.* **38**, 1124–1136 (2018).

88. Li, Y., Tatsui, C. E., Rhines, L. D., North, R. Y., Harrison, D. S., Cassidy, R. M., Johansson, C. A., Kosturakis, A. K., Edwards, D. D., Zhang, H. & Dougherty, P. M. Dorsal root ganglion neurons become hyperexcitable and increase expression of voltage-gated T-type calcium channels (Cav3.2) in paclitaxel-induced peripheral neuropathy. *Pain* **158**, 417–429 (2017).

89. Flatters, S. J. L. & Bennett, G. J. Ethosuximide reverses paclitaxel- and vincristine-induced painful peripheral neuropathy. *Pain* **109**, 150–161 (2004).

90. Xiao, W., Boroujerdi, A., Bennett, G. J. & Luo, Z. D. Chemotherapy-evoked painful peripheral neuropathy: Analgesic effects of gabapentin and effects on expression of the alpha-2-delta type-1 calcium channel subunit. *Neuroscience* **144**, 714–720 (2007).

91. Alessandri-Haber, N., Dina, O. A., Yeh, J. J., Parada, C. A., Reichling, D. B. & Levine, J.

D. Transient Receptor Potential Vanilloid 4 Is Essential in Chemotherapy-Induced Neuropathic Pain in the Rat. *J. Neurosci.* **24**, 4444–4452 (2004).

92. Materazzi, S., Fusi, C., Benemei, S., Pedretti, P., Patacchini, R., Nilius, B., Prenen, J., Creminon, C., Geppetti, P. & Nassini, R. TRPA1 and TRPV4 mediate paclitaxel-induced peripheral neuropathy in mice via a glutathione-sensitive mechanism. *Eur. J. Physiol.* **463**, 561–569 (2012).

93. Hara, T., Chiba, T., Abe, K., Makabe, A., Ikeno, S., Kawakami, K., Utsunomiya, I., Hama, T. & Taguchi, K. Effect of paclitaxel on transient receptor potential vanilloid 1 in rat dorsal root ganglion. *Pain* **154**, 882–889 (2013).

94. Chiba, T., Oka, Y., Sashida, H., Kanbe, T., Abe, K., Utsunomiya, I. & Taguchi, K. Vincristine-induced peripheral neuropathic pain and expression of transient receptor potential vanilloid 1 in rat. *J. Pharmacol. Sci.* **133**, 254–260 (2017).

95. Boehmerle, W., Huehnchen, P., Lee, S. L. L., Harms, C. & Endres, M. TRPV4 inhibition prevents paclitaxel-induced neurotoxicity in preclinical models. *Exp. Neurol.* **306**, 64–75 (2018).

96. Peters, C. M., Jimenez-Andrade, J. M., Jonas, B. M., Sevcik, M. A., Koewler, N. J., Ghilardi, J. R., Wong, G. Y. & Mantyh, P. W. Intravenous paclitaxel administration in the rat induces a peripheral sensory neuropathy characterized by macrophage infiltration and injury to sensory neurons and their supporting cells. *Exp. Neurol.* **203**, 42–54 (2007).

97. Nishida, K., Kuchiiwa, S., Oiso, S., Futagawa, T., Masuda, S., Takeda, Y. & Yamada, K. Up-regulation of matrix metalloproteinase-3 in the dorsal root ganglion of rats with paclitaxel-induced neuropathy. *Cancer Sci.* **99**, 1618–1625 (2008).

98. Starobova, H., Mueller, A., Allavena, R., Lohman, R. J., Sweet, M. J. & Vetter, I.

Minocycline prevents the development of mechanical allodynia in mouse models of vincristine-induced peripheral neuropathy. *Front. Neurosci.* **13**, 1–10 (2019).

99. Zhang, H., Boyette-Davis, J. A., Kosturakis, A. K., Li, Y., Yoon, S. Y., Walters, E. T. & Dougherty, P. M. Induction of monocyte chemoattractant protein-1 (mcp-1) and its receptor ccr2 in primary sensory neurons contributes to paclitaxel-induced peripheral neuropathy. *J. Pain* **14**, 1031–1044 (2013).

100. Huang, Z. Z., Li, D., Liu, C. C., Cui, Y., Zhu, H. Q., Zhang, W. W., Li, Y. Y. & Xin, W. J. CX3CL1-mediated macrophage activation contributed to paclitaxel-induced DRG neuronal apoptosis and painful peripheral neuropathy. *Brain. Behav. Immun.* **40**, 155–165 (2014).

101. Zhang, H., Li, Y., De Carvalho-Barbosa, M., Kavelaars, A., Heijnen, C. J., Albrecht, P. J. & Dougherty, P. M. Dorsal Root Ganglion Infiltration by Macrophages Contributes to Paclitaxel Chemotherapy-Induced Peripheral Neuropathy. *J. Pain* **17**, 775–786 (2016).

102. Yu, X., Liu, H., Hamel, K. A., Morvan, M. G., Yu, S., Leff, J., Guan, Z., Braz, J. M. & Basbaum, A. I. Dorsal root ganglion macrophages contribute to both the initiation and persistence of neuropathic pain. *Nat. Commun.* **11**, 264 (2020).

103. Ledeboer, A., Jekich, B. M., Sloane, E. M., Mahoney, J. H., Langer, S. J., Milligan, E. D., Martin, D., Maier, S. F., Johnson, K. W., Leinwand, L. A., Chavez, R. A. & Watkins, L. R. Intrathecal Interleukin-10 Gene Therapy Attenuates Paclitaxel- Induced Mechanical Allodynia and Proinflammatory Cytokine Expression in Dorsal Root Ganglia in Rats. **487**, 109–113 (2007).

104. Wu, P. & Chen, Y. Evodiamine ameliorates paclitaxel-induced neuropathic pain by inhibiting inflammation and maintaining mitochondrial anti-oxidant functions. *Hum. Cell*

32, 251–259 (2019).

105. Zhang, X., Jiang, N., Li, J., Zhang, D. & Lv, X. Rapamycin alleviates proinflammatory cytokines and nociceptive behavior induced by chemotherapeutic paclitaxel. *Neurol. Res.* **41**, 52–59 (2019).

106. Al-Mazidi, S., Alotaibi, M., Nedjadi, T., Chaudhary, A., Alzoghaibi, M. & Djouhri, L. Blocking of cytokines signalling attenuates evoked and spontaneous neuropathic pain behaviours in the paclitaxel rat model of chemotherapy-induced neuropathy. *Eur. J. Pain (United Kingdom)* **22**, 810–821 (2018).

107. Xu, J., Wang, W., Zhong, X. X., Feng, Y. W., Wei, X. H. & Liu, X. G. Methylcobalamin ameliorates neuropathic pain induced by vincristine in rats: Effect on loss of peripheral nerve fibers and imbalance of cytokines in the spinal dorsal horn. *Mol. Pain* **12**, 1–14 (2016).

108. Huehnchen, P., Muenzfeld, H., Boehmerle, W. & Endres, M. Blockade of IL-6 signaling prevents paclitaxel-induced neuropathy in C57Bl/6 mice. *Cell Death Dis.* **11**, (2020).

109. Hertz, D. L., Roy, S., Motsinger-Reif, A. A., Drobish, A., Clark, L. S., McLeod, H. L., Carey, L. A. & Dees, E. C. CYP2C8*3 increases risk of neuropathy in breast cancer patients treated with paclitaxel. *Ann. Oncol.* **24**, 1472–1478 (2013).

110. Hertz, D. L., Motsinger-Reif, A. a., Drobish, A., Winham, S. J., McLeod, H. L., Carey, L. a. & Dees, E. C. CYP2C8*3 predicts benefit/risk profile in breast cancer patients receiving neoadjuvant paclitaxel. *Breast Cancer Res. Treat.* **134**, 401–410 (2012).

111. Lam, S. W., Frederiks, C. N., Van Der Straaten, T., Honkoop, A. H., Guchelaar, H. J. & Boven, E. Genotypes of CYP2C8 and FGD4 and their association with peripheral neuropathy or early dose reduction in paclitaxel-treated breast cancer patients. *Br. J.*

Cancer **115**, 1335–1342 (2016).

112. Hertz, D. L., Roy, S., Jack, J., Motsinger-Reif, A. A., Drobish, A., Clark, L. S., Carey, L. A., Dees, E. C. & McLeod, H. L. Genetic heterogeneity beyond CYP2C8*3 does not explain differential sensitivity to paclitaxel-induced neuropathy. *Breast Cancer Res. Treat.* **145**, 245–54 (2014).

113. Kus, T., Aktas, G., Kalender, M., Demiryurek, A. T., Ulasli, M., Oztuzcu, S., Sevinc, A., Kul, S. & Camci, C. Polymorphism of CYP3A4 and ABCB1 genes increase the risk of neuropathy in breast cancer patients treated with paclitaxel and docetaxel. *Onco. Targets. Ther.* **9**, 5073–5080 (2016).

114. Egbelakin, A., Ferguson, M., MacGill, E., Lehmann, A., Topletz, A., Quinney, S., Li, L., KC, M., Hall, S. & Renbarger, J. Increased risk of vincristine neurotoxicity associated with low CYP3A5 expression genotype in children with acute lymphoblastic leukemia. *Pediatr. Blood Cancer* **56**, 361–7 (2011).

115. Bosó, V., Herrero, M. J., Santaballa, A., Palomar, L., Megias, J. E., De La Cueva, H., Rojas, L., Marqués, M. R., Poveda, J. L., Montalar, J. & Aliño, S. F. SNPs and taxane toxicity in breast cancer patients. *Pharmacogenomics* **15**, 1845–1858 (2014).

116. Hu, L., Lv, Q. L., Guo, Y., Cheng, L., Wu, N. Y., Qin, C. Z. & Zhou, H. H. Genetic variation of CYP3A5 influences paclitaxel/carboplatin-induced toxicity in Chinese epithelial ovarian cancer patients. *J. Clin. Pharmacol.* **56**, 349–354 (2016).

117. Arbitrio, M., Scionti, F., Altomare, E., Di Martino, M. T., Agapito, G., Galeano, T., Staropoli, N., Iuliano, E., Grillone, F., Fabiani, F., Caracciolo, D., Cannataro, M., Arpino, G., Santini, D., Tassone, P. & Tagliaferri, P. Polymorphic Variants in NR1I3 and UGT2B7 Predict Taxane Neurotoxicity and Have Prognostic Relevance in Patients With

Breast Cancer: A Case-Control Study. *Clin. Pharmacol. Ther.* **106**, 422–431 (2019).

118. Boora, G. K., Kanwar, R., Kulkarni, A. A., Abyzov, A., Sloan, J., Ruddy, K. J., Banck, M. S., Loprinzi, C. L. & Beutler, A. S. Testing of candidate single nucleotide variants associated with paclitaxel neuropathy in the trial NCCTG N08C1 (Alliance). *Cancer Med.* n/a-n/a (2016) doi:10.1002/cam4.625.

119. Tanabe, Y., Shimizu, C., Hamada, A., Hashimoto, K., Ikeda, K., Nishizawa, D., Hasegawa, J., Shimomura, A., Ozaki, Y., Tamura, N., Yamamoto, H., Yunokawa, M., Yonemori, K., Takano, T., Kawabata, H., Tamura, K. & Fujiwara, Y. Paclitaxel-induced sensory peripheral neuropathy is associated with an ABCB1 single nucleotide polymorphism and older age in Japanese. *Cancer Chemother. Pharmacol.* **79**, 1179–1186 (2017).

120. Sissung, T. M., Baum, C. E., Deeken, J., Price, D. K., Aragon-Ching, J., Steinberg, S. M., Dahut, W., Sparreboom, A. & Figg, W. D. ABCB1 genetic variation influences the toxicity and clinical outcome of patients with androgen-independent prostate cancer treated with docetaxel. *Clin. Cancer Res.* **14**, 4543–4549 (2008).

121. Lopez-Lopez, E., Gutierrez-Camino, A., Astigarraga, I., Navajas, A., Echebarria-Barona, A., Garcia de Andoin, N., Lobo, C., Guerra-Merino, I., Martin-Guerrero, I. & Garcia-Orad, A. Vincristine pharmacokinetics pathway and neurotoxicity during early phases of. *Pharmacogenomics* **17**, 731–741 (2016).

122. Abraham, J. E., Guo, Q., Dorling, L., Tyrer, J., Ingle, S., Hardy, R., Vallier, A. L., Hiller, L., Burns, R., Jones, L., Bowden, S. J., Dunn, J. A., Poole, C. J., Caldas, C., Pharoah, P. P. D. & Earl, H. M. Replication of genetic polymorphisms reported to be associated with taxane-related sensory neuropathy in patients with early breast cancer treated with

paclitaxel. *Clin. Cancer Res.* **20**, 2466–2475 (2014).

123. Hasmats, J., Kupershmidt, I., Rodríguez-Antona, C., Su, Q. J., Khan, M. S., Jara, C., Mielgo, X., Lundeberg, J. & Green, H. Identification of candidate SNPs for drug induced toxicity from differentially expressed genes in associated tissues. *Gene* **506**, 62–68 (2012).

124. Sissung, T. M., Mross, K., Steinberg, S. M., Behringer, D., Figg, W. D., Sparreboom, A. & Mielke, S. Association of ABCB1 genotypes with paclitaxel-mediated peripheral neuropathy and neutropenia. *Eur. J. Cancer* **42**, 2893–2896 (2006).

125. Apellániz-Ruiz, M., Lee, M. Y., Sánchez-Barroso, L., Gutiérrez-Gutiérrez, G., Calvo, I., García-Estévez, L., Sereno, M., García-Donás, J., Castelo, B., Guerra, E., Leandro-García, L. J., Cascón, A., Johansson, I., Robledo, M., Ingelman-Sundberg, M. & Rodríguez-Antona, C. Whole-exome sequencing reveals defective CYP3A4 variants predictive of paclitaxel dose-limiting neuropathy. *Clin. Cancer Res.* **21**, 322–328 (2015).

126. Park, S. B., Kwok, J. B., Loy, C. T., Friedlander, M. L., Lin, C. S. Y., Krishnan, A. V., Lewis, C. R. & Kiernan, M. C. Paclitaxel-induced neuropathy: Potential association of MAPT and GSK3B genotypes. *BMC Cancer* **14**, 1–5 (2014).

127. Leandro-Garcia, L. J., Leskela, S., Jara, C., Green, H., Avall-Lundqvist, E., Wheeler, H. E., Dolan, M. E., Inglada-Perez, L., Maliszewska, A., de Cubas, A. A., Comino-Mendez, I., Mancikova, V., Cascon, A., Robledo, M. & Rodriguez-Antona, C. Regulatory Polymorphisms in -Tubulin IIa Are Associated with Paclitaxel-Induced Peripheral Neuropathy. *Clin. Cancer Res.* **18**, 4441–4448 (2012).

128. Park, S. B., Kwok, J. B., Asher, R., Lee, C. K., Beale, P., Selle, F. & Friedlander, M. Clinical and genetic predictors of paclitaxel neurotoxicity based on patient- versus clinicianreported incidence and severity of neurotoxicity in the ICON7 trial. *Ann. Oncol.*

28, 2733–2740 (2017).

129. Ceppi, F., Langlois-Pelletier, C., Gagné, V., Rousseau, J., Ciolino, C., Lorenzo, S. De, Kevin, K. M., Cijov, D., Sallan, S. E., Silverman, L. B., Neuberg, D., Kutok, J. L., Sinnett, D., Laverdière, C. & Krajinovic, M. Polymorphisms of the vincristine pathway and response to treatment in children with childhood acute lymphoblastic leukemia. *Pharmacogenomics* **15**, 1105–1116 (2014).

130. Baldwin, R. M., Owzar, K., Zembutsu, H., Chhibber, A., Kubo, M., Jiang, C., Watson, D., Eclov, R. J., Mefford, J., McLeod, H. L., Friedman, P. N., Hudis, C. A., Winer, E. P., Jorgenson, E. M., Witte, J. S., Shulman, L. N., Nakamura, Y., Ratain, M. J. & Kroetz, D. L. A genome-wide association study identifies novel loci for paclitaxel-induced sensory peripheral neuropathy in CALGB 40101. *Clin. Cancer Res.* **18**, 5099–5109 (2012).

131. Hertz, D. L., Owzar, K., Lessans, S., Wing, C., Jiang, C., Kelly, W. K., Patel, J., Halabi, S., Furukawa, Y., Wheeler, H. E., Sibley, A. B., Lassiter, C., Weisman, L., Watson, D., Krens, S. D., Mulkey, F., Renn, C. L., Small, E. J., Febbo, P. G., *et al.* Pharmacogenetic discovery in CALGB (alliance) 90401 and mechanistic validation of a VAC14 polymorphism that increases risk of docetaxel-induced neuropathy. *Clin. Cancer Res.* **22**, 4890–4900 (2016).

132. Marcath, L. A., Kidwell, K. M., Vangipuram, K., Gersch, C. L., Rae, J. M., Burness, M. L., Griggs, J. J., Van Poznak, C., Hayes, D. F., Lavoie Smith, E. M., Henry, N. L., Beutler, A. S. & Hertz, D. L. Genetic variation in EPHA contributes to sensitivity to paclitaxel-induced peripheral neuropathy . *Br. J. Clin. Pharmacol.* 0–3 (2019) doi:10.1111/bcp.14192.

133. Leandro-García, L. J., Inglada-Pérez, L., Pita, G., Hjerpe, E., Leskelä, S., Jara, C., Mielgo,

X., González-Neira, A., Robledo, M., Åvall-Lundqvist, E., Gréen, H. & Rodríguez-Antona, C. Genome-wide association study identifies ephrin type a receptors implicated in paclitaxel induced peripheral sensory neuropathy. *J. Med. Genet.* **50**, 599–605 (2013).

134. Apellaniz-Ruiz, M., Tejero, H., Inglada-Perez, L., Sanchez-Barroso, L., Gutierrez-Gutierrez, G., Calvo, I., Castelo, B., Redondo, A., García-Donas, J., Romero-Laorden, N., Sereno, M., Merino, M., Curras-Freixes, M., Montero-Conde, C., Mancikova, V., Åvall-Lundqvist, E., Green, H., Al-Shahrour, F., Cascon, A., *et al.* Targeted sequencing reveals low-frequency variants in EPHA genes as markers of paclitaxel-induced peripheral neuropathy. *Clin. Cancer Res.* **23**, 1227–1235 (2017).

135. Diouf, B., Crews, K. R., Lew, G., Pei, D., Cheng, C., Bao, J., Zheng, J. J., Yang, W., Fan, Y., Wheeler, H. E., Wing, C., Delaney, S. M., Komatsu, M., Paugh, S. W., McCorkle, J. R., Lu, X., Winick, N. J., Carroll, W. L., Loh, M. L., *et al.* Association of an Inherited Genetic Variant With Vincristine-Related Peripheral Neuropathy in Children With Acute Lymphoblastic Leukemia. *JAMA* **313**, 815 (2015).

136. Abaji, R., Ceppi, F., Patel, S., Gagné, V., Xu, C. J., Spinella, J. F., Colombini, A., Parasole, R., Buldini, B., Basso, G., Conter, V., Cazzaniga, G., Leclerc, J. M., Laverdière, C., Sinnett, D. & Krajinovic, M. Genetic risk factors for VIPN in childhood acute lymphoblastic leukemia patients identified using whole-exome sequencing. *Pharmacogenomics* **19**, 1181–1193 (2018).

137. Li, L., Sajdyk, T., Smith, E. M. L., Chang, C. W., Li, C., Ho, R. H., Hutchinson, R., Wells, E., Skiles, J. L., Winick, N., Martin, P. L. & Renbarger, J. L. Genetic Variants Associated With Vincristine-Induced Peripheral Neuropathy in Two Populations of Children With Acute Lymphoblastic Leukemia. *Clin. Pharmacol. Ther.* **105**, 1421–1428

(2019).

138. Schneider, B. P., Li, L., Radovich, M., Shen, F., Miller, K. D., Flockhart, D. A., Jiang, G., Vance, G., Gardner, L., Vatta, M., Bai, S., Lai, D., Koller, D., Zhao, F., O'Neill, A., Smith, M. Lou, Railey, E., White, C., Partridge, A., *et al.* Genome-Wide Association Studies for Taxane-Induced Peripheral Neuropathy in ECOG-5103 and ECOG-1199. *Clin. Cancer Res.* **21**, 5082–5091 (2015).

139. Schneider, B. P., Lai, D., Shen, F., Jiang, G., Radovich, M., Li, L., Gardner, L., Miller, K. D., O'Neill, A., Sparano, J. A., Xue, G., Foroud, T. & Sledge, G. W. Charcot-Marie-Tooth gene, SBF2, associated with taxaneinduced peripheral neuropathy in African Americans. *Oncotarget* **7**, 82244–82253 (2016).

140. Wheeler, H. E., Gamazon, E. R., Wing, C., Njiaju, U. O., Njoku, C., Baldwin, R. M., Owzar, K., Jiang, C., Watson, D., Shterev, I., Kubo, M., Zembutsu, H., Winer, E. P., Hudis, C. A., Shulman, L. N., Nakamura, Y., Ratain, M. J., Kroetz, D. L., Cox, N. J., *et al.* Integration of Cell Line and Clinical Trial Genome-Wide Analyses Supports a Polygenic Architecture of Paclitaxel-Induced Sensory Peripheral Neuropathy. *Clin. Cancer Res.* **19**, 491–499 (2013).

141. Beutler, A. S., Kulkarni, A. a, Kanwar, R., Klein, C. J., Therneau, T. M., Qin, R., Banck, M. S., Boora, G. K., Ruddy, K. J., Wu, Y., Smalley, R. L., Cunningham, J. M., Le-Lindqwister, N. A., Beyerlein, P., Schroth, G. P., Windebank, A. J., Züchner, S. & Loprinzi, C. L. Sequencing of Charcot-Marie-Tooth disease genes in a toxic polyneuropathy. *Ann. Neurol.* **76**, 727–37 (2014).

142. Boora, G. K., Kulkarni, A. A., Kanwar, R., Beyerlein, P., Qin, R., Banck, M. S., Ruddy, K. J., Pleticha, J., Lynch, C. A., Behrens, R. J., Züchner, S., Loprinzi, C. L. & Beutler, A.

S. Association of the Charcot-Marie-Tooth disease gene ARHGEF10 with paclitaxel induced peripheral neuropathy in NCCTG N08CA (Alliance). *J. Neurol. Sci.* **357**, 35–40 (2015).

143. Chhibber, A., Mefford, J., Stahl, E. a, Pendergrass, S. a, Baldwin, R. M., Owzar, K., Li, M., Winer, E. P., Hudis, C. a, Zembutsu, H., Kubo, M., Nakamura, Y., McLeod, H. L., Ratain, M. J., Shulman, L. N., Ritchie, M. D., Plenge, R. M., Witte, J. S. & Kroetz, D. L. Polygenic inheritance of paclitaxel-induced sensory peripheral neuropathy driven by axon outgrowth gene sets in CALGB 40101 (Alliance). *Pharmacogenomics J.* 1–7 (2014) doi:10.1038/tpj.2014.2.

144. Komatsu, M., Wheeler, H. E., Chung, S., Low, S. K., Wing, C., Delaney, S. M., Gorsic, L. K., Takahashi, A., Kubo, M., Kroetz, D. L., Zhang, W., Nakamura, Y. & Dolan, M. E. Pharmacoethnicity in paclitaxel-induced sensory peripheral neuropathy. *Clin. Cancer Res.* **21**, 4337–4346 (2015).

145. Sucheston-Campbell, L. E., Clay-Gilmour, A. I., Barlow, W. E., Budd, G. T., Stram, D. O., Haiman, C. A., Sheng, X., Yan, L., Zirpoli, G., Yao, S., Jiang, C., Owzar, K., Hershman, D., Albain, K. S., Hayes, D. F., Moore, H. C., Hobday, T. J., Stewart, J. A., Rizvi, A., *et al.* Genome-wide meta-analyses identifies novel taxane-induced peripheral neuropathy-associated loci. *Pharmacogenet. Genomics* **28**, 49–55 (2018).

146. Vojnits, K., Mahammad, S., Collins, T. J. & Bhatia, M. Chemotherapy-Induced Neuropathy and Drug Discovery Platform Using Human Sensory Neurons Converted Directly from Adult Peripheral Blood. *Stem Cells Transl. Med.* **8**, 1180–1191 (2019).

147. Morrison, G., Liu, C., Wing, C., Delaney, S. M., Zhang, W. & Dolan, M. E. Evaluation of inter-batch differences in stem-cell derived neurons. *Stem Cell Res.* **16**, 140–148 (2016).

148. Sherman, S. P. & Bang, A. G. High-throughput screen for compounds that modulate neurite growth of human induced pluripotent stem cell-derived neurons. *DMM Dis. Model. Mech.* **11**, (2018).

149. Hoelting, L., Klima, S., Karreman, C., Grinberg, M., Meisig, J., Henry, M., Rotshteyn, T., Rahnenführer, J., Blüthgen, N., Sachinidis, A., Waldmann, T. & Leist, M. Stem Cell-Derived Immature Human Dorsal Root Ganglia Neurons to Identify Peripheral Neurotoxicants. *Stem Cells Transl. Med.* **5**, 476–487 (2016).

150. Wing, C., Komatsu, M., Delaney, S. M., Krause, M., Wheeler, H. E. & Dolan, M. E. Application of stem cell derived neuronal cells to evaluate neurotoxic chemotherapy. *Stem Cell Res.* **22**, 79–88 (2017).

151. Wheeler, H. E., Wing, C., Delaney, S. M., Komatsu, M. & Dolan, M. E. Modeling chemotherapeutic neurotoxicity with human induced pluripotent stem cell-derived neuronal cells. *PLoS One* **10**, e0118020 (2015).

152. Snyder, C., Yu, L., Ngo, T., Sheinson, D., Zhu, Y., Tseng, M., Misner, D. & Staflin, K. In vitro assessment of chemotherapy-induced neuronal toxicity. *Toxicol. Vitr.* **50**, 109–123 (2018).

153. Rana, P., Luerman, G., Hess, D., Rubitski, E., Adkins, K. & Somps, C. Utilization of iPSC-derived human neurons for high-throughput drug-induced peripheral neuropathy screening. *Toxicol. In Vitro* **45**, 111–118 (2017).

154. Lee, J. H., Mitchell, R. R., McNicol, J. D., Shapovalova, Z., Laronde, S., Tanasijevic, B., Milsom, C., Casado, F., Fiebig-Comyn, A., Collins, T. J., Singh, K. K. & Bhatia, M. Single Transcription Factor Conversion of Human Blood Fate to NPCs with CNS and PNS Developmental Capacity. *Cell Reports* (2014) doi:10.1016/j.celrep.2015.04.056.

155. Namer, B., Schmidt, D., Eberhardt, E., Maroni, M., Dorfmeister, E., Kleggetveit, I. P., Kaluza, L., Meents, J., Gerlach, A., Lin, Z., Winterpacht, A., Dragicevic, E., Kohl, Z., Schüttler, J., Kurth, I., Warncke, T., Jorum, E., Winner, B. & Lampert, A. Pain relief in a neuropathy patient by lacosamide: Proof of principle of clinical translation from patient-specific iPS cell-derived nociceptors. *EBioMedicine* **39**, 401–408 (2019).

156. Wainger, B. J., Buttermore, E. D., Oliveira, J. T., Mellin, C., Lee, S., Saber, W. A., Wang, A. J., Ichida, J. K., Chiu, I. M., Barrett, L., Huebner, E. A., Bilgin, C., Tsujimoto, N., Brenneis, C., Kapur, K., Rubin, L. L., Eggan, K. & Woolf, C. J. Modeling pain in vitro using nociceptor neurons reprogrammed from fibroblasts. *Nat. Neurosci.* **18**, 17–24 (2015).

157. Lee, J. H., Mitchell, R. R., McNicol, J. D., Shapovalova, Z., Laronde, S., Tanasijevic, B., Milsom, C., Casado, F., Fiebig-Comyn, A., Collins, T. J., Singh, K. K. & Bhatia, M. Single Transcription Factor Conversion of Human Blood Fate to NPCs with CNS and PNS Developmental Capacity. *Cell Rep.* **11**, 1367–1376 (2014).

CHAPTER 2: Genome-Wide Meta-Analysis in CALGB 40502 and CALGB 40101 (Alliance) Identifies a *S1PR1* Genomic Region Associated with Microtubule Targeting Agent-Induced Sensory Peripheral Neuropathy in Breast Cancer Patients

INTRODUCTION

Microtubule-stabilizing agents such as taxanes and epothilones, are widely prescribed for treatment of various solid tumors. These tubulin inhibitors disrupt microtubule dynamics via stabilization of microtubules to primarily target and block rapidly dividing cells[1], and are effective in treating primary and metastatic breast cancer. However, a significant amount of interindividual variability exists in clinical response and adverse events[2]. The main non-hematological dose-limiting toxicity of microtubule-stabilizing agent therapy is sensory peripheral neuropathy. This nerve damage presents as distal axonal degeneration and clinically manifests as numbness or tingling, or painful sensations in a "glove and stocking" distribution[3]. Up to 50% of patients experience some degree of sensory peripheral neuropathy with as many as 30% reaching severe peripheral neuropathy (grade 3 or 4)[4,5]. These symptoms manifest as early as the first dosing cycle, and in severe cases, the symptoms persist for years after the last course of therapy[6,7]. Reported risk factors for drug-induced neuropathy include prior treatment with neurotoxic agents, frequency of chemotherapy dosing, high cumulative chemotherapy exposure, preexisting neuropathy and age[4]. However, these risk factors do not fully account for the observed incidence of chemotherapy-induced peripheral neuropathy (CIPN)[8]. There are currently no neuroprotective strategies that provide adequate clinical efficacy in preventing this toxicity and the only drug deemed at all effective for treatment of existing CIPN is duloxetine[8].

Human genetic association studies have been used as tools to identify critical genes involved in the pathophysiology of CIPN. In genetic association studies, consideration of the highest-ranking single nucleotide polymorphisms (SNPs) with respect to P-value suggested a

potential role for genes related to the regulation of neuron morphogenesis and neurodegeneration (*EPHA4/5/6*, *FGD4*, *FZD3*, *ARHGEF10*, *VAC14*) in the pathogenesis of taxane-induced peripheral neuropathy[9–12]. While most of these genetic hits did not reach genome-wide significance, candidate gene analyses in independent populations support the associations with two ephrin receptor genes[10,13], *FGD4*[14], and *ARHGEF10*[15]. The primary goal in the current study was to conduct a meta-analysis of two cohorts of breast cancer patients (CALGB 40502 and CALGB 40101) to extend these genomic findings and further elucidate this complex phenotype.

CALGB 40502 was a phase III randomized three-arm study comparing nanoparticle albumin-bound (nab) paclitaxel or ixabepilone once per week to weekly paclitaxel as first-line therapy for patients with advanced breast cancer[16]; bevacizumab was administered in all arms of the study. CALGB 40101 was a randomized trial with 2x2 factorial design to test the noninferiority of single agent paclitaxel with doxorubicin and cyclophosphamide (AC) and the superiority of six cycles of treatment over four cycles[17]. The most common grade 3 to 4 non-hematological toxicity in both studies was sensory neuropathy[16]. Findings from the pharmacogenomic association meta-analysis were functionally evaluated *in vitro* to probe the mechanistic basis of chemotherapy-induced sensory neuron damage.

MATERIALS AND METHODS

Participants

All study participants were enrolled in either CALGB 40101 or CALGB 40502. CALGB 40101 was open from May 15, 2002 to July 30, 2010, enrolling 3,873 patients. CALGB 40502 was open from October 2008 through November 2011, enrolling a total of 799 subjects. Eligibility criteria for enrollment for each clinical trial study have been previously described[16,17]. All

patients provided written informed consent for both the treatment and companion pharmacogenetic protocols that met state, federal, and institutional guidelines in both CALGB 40101 and 40502. Only subjects in CALGB 40101 receiving paclitaxel every two weeks were included in pharmacogenetic studies.

Genotype Data

Study characteristics of CALGB 40101 and CALGB 40502 are shown in Table 2.1. From the 799 patients randomized in CALGB 40502, a total of 633 consented patients with DNA samples were genotyped using the Illumina HumanOmniExpressExome-8 BeadChip, interrogating 964,055 SNPs with coverage of common variants and additional exonic content. Genotyping data were filtered using a standard quality control (QC) pipeline (Figure 2.1). All samples in CALGB 40502 were filtered for low call rate (< 0.99) or low genotyping performance; none were excluded. Non-autosomal SNPs were excluded, leaving 902,927 SNPs for use in additional sample QC. Identity-by-descent (IBD) analysis identified the presence of two closely related individuals, which were excluded and found later to be a plating error. An X chromosome heterozygosity estimation identified three genetic males that were removed, leaving 628 subjects for further analysis. Principal component analysis (PCA) was performed using directly genotyped SNPs of all 628 study subjects to determine genetic ancestry with GenABEL *R* package. A total of 485 subjects of European genetic ancestry were identified and confirmed with a second PCA using genotyped SNPs with the EIGENSTRAT method. Mean values for the first three PC vectors and eigenvectors within all patients self-declaring "White" race and "Non-Hispanic"/ "Unknown" ethnicity were determined, resulting in 478 samples (Figure 2.2). A final discovery cohort of 469 samples with phenotypic and genetic information were used in the

primary analysis. A similar process was completed for CALGB 40101[9], isolating a total of 855 individuals of European ancestry with phenotype information for further analysis. For CALGB 40502, genetic imputation was performed with 902,927 SNPs using the Michigan Imputation Server[18]. The imputation process was completed with 1000 Genomes Phase 3 v5 as reference panel and phasing using ShapeIT v2.r790. A total of 863,911 genotyped SNPs was mapped to 97.09% of the 1000G Phase 3 reference panel (Figure 2.3) and 717,432 SNPs remained after imputation server quality control. The imputation process yielded 45,933,061 SNPs and post-imputation filtering included removal of any insertions and deletions, multi-allelic sites, monoallelic sites, and those with Rsq imputation quality score < 0.3, leaving 23,210,471 imputed SNPs for association analysis.

All samples from CALGB 40101 used in the current meta-analysis were described in a prior GWAS[9]. A total of 531,729 SNPs were submitted for genetic imputation using the Michigan Imputation Server[18]. A total of 527,802 SNPs was mapped to 99.58% of the reference genome (Figure 2.3) with 527,802 SNPs remaining after imputation server quality control. A total of 47,101,766 SNPs was imputed and post-imputation filtering yielded 14,676,818 SNPs used for the meta-analysis.

Table 2.1 Study characteristics of pharmacogenetic cohorts in CALGB 40502 and CALGB 40101

	CALGB 40502	**CALGB 40101**
Consented with DNA	633	1029
Post Quality Control	628	1023
White (Non-Hispanic/Non-Latino)	478 (76%)	855 (83%)
Discovery Cohort†	469	855
Disease Stage	Locally recurrent or metastatic breast cancer	Early-stage breast cancer with 0-3 positive axillary nodes
Drug therapy	Paclitaxel (90 mg/m^2) or nab-paclitaxel (150 mg/m^2) or ixabepilone (16 mg/m^2) ± bevacizumab weekly for 3 of 4 weeks	Dose-dense paclitaxel (175 mg/m^2) biweekly for 4 or 6 cycles
Reported incidence of peripheral neuropathy‡	232 (49%)	206 (24%)
Taxane-naïve	No	Yes
Chemo-naïve	No	Yes
Informative competing risks to developing peripheral neuropathy‡	Yes	No
Genotyping array	Illumina HumanOmniExpressExome-8 BeadChip	Illumina HumanHapQuad610-Quad Genotyping BeadChip

†Self-reported White (Non-Hispanic/Non-Latino) samples with complete phenotype information
‡Within discovery cohort, where peripheral neuropathy reported as Grade 2 or higher

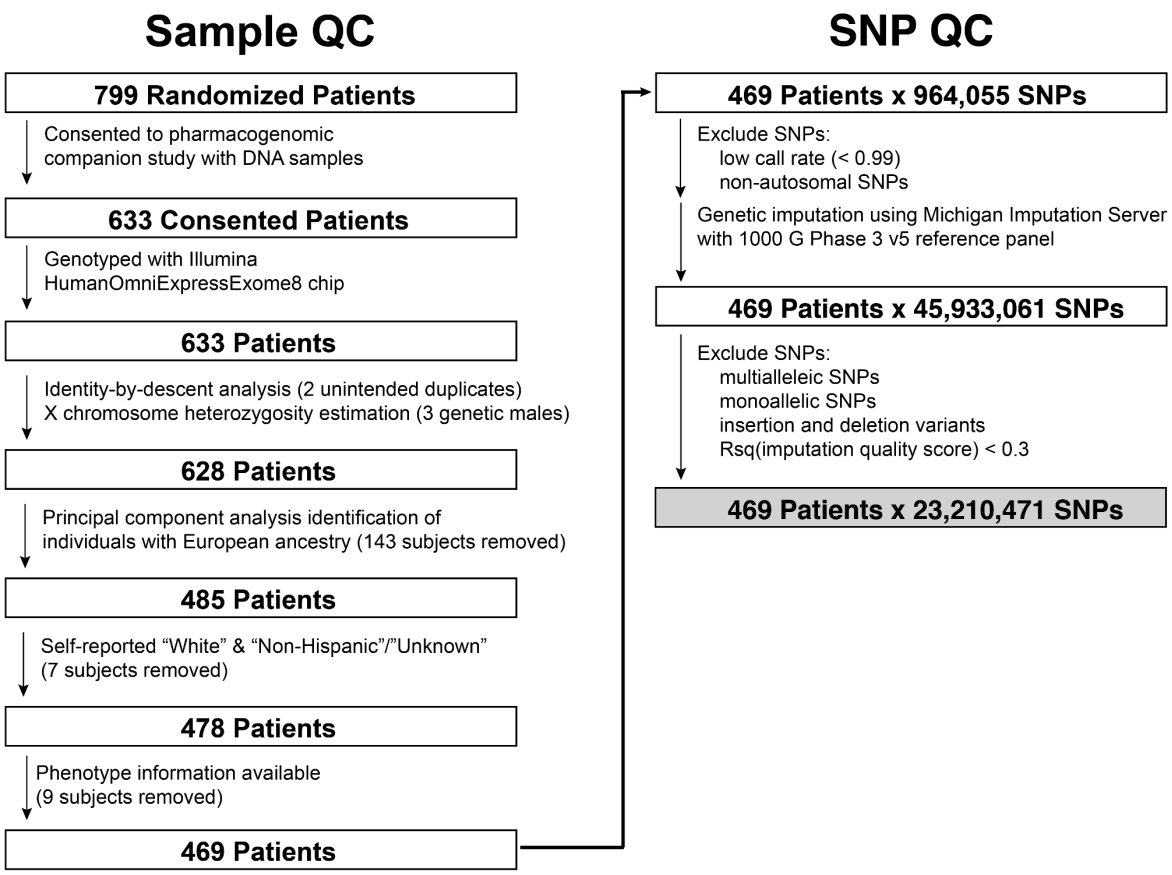

Figure 2.1 Sample and imputed genotype quality control pipeline applied to CALGB 40502.

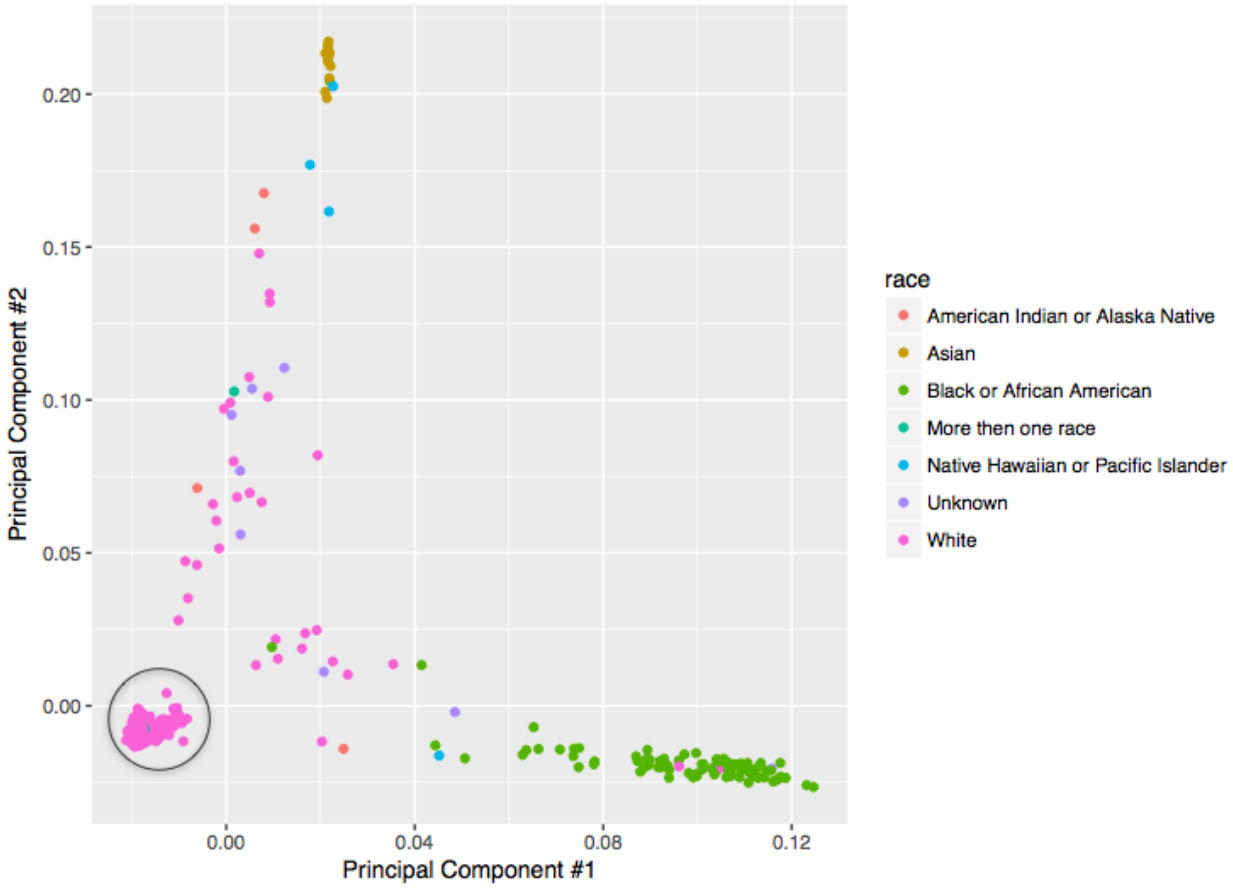

Figure 2.2 The first two principal components from the genome-wide genotype data are plotted. Each dot represents a sample from the genotyped cohort (n = 628) and each color represents a self-reported race. The pink dots within the indicated circle are defined as the "White (Non-Hispanic/Non-Latino)" discovery cohort.

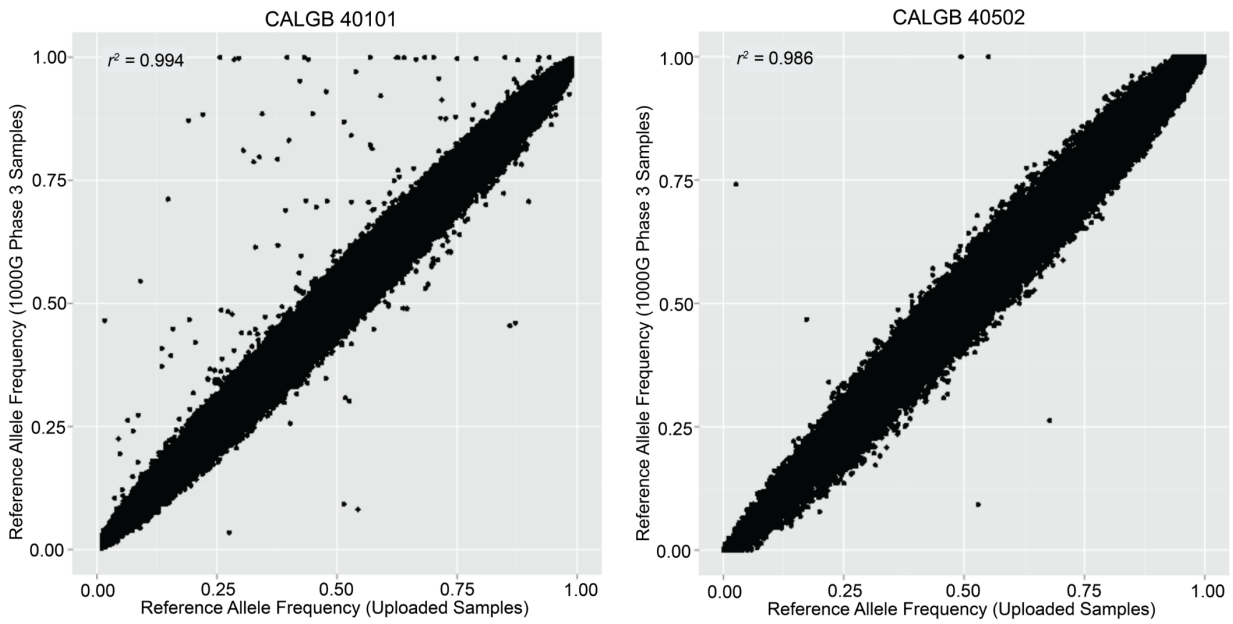

Figure 2.3 Allele-frequency correlation from imputation of CALGB 40101 and CALGB 40502 samples. The allele frequency of individual SNPs passing QC in CALGB 40101 (n = 527,8002) and CALGB 40502 (n = 717,432) were compared to the allele frequency in the 1000G Phase 3 data.

Phenotype Data

Adverse events, including chemotherapy-induced peripheral neuropathy, were graded according to the NCI Common Terminology Criteria for Adverse Events (NCI-CTCAE v3 in CALGB 40502; NCI-CTCAE v2 in CALGB 40101), defining the range of severity of neuropathy cases as Grade 0-5. Since the incidence of the toxicity is dependent on cumulative drug exposure, sensory peripheral neuropathy was assessed with a dose-to-event phenotype. An MTA-induced sensory peripheral neuropathy event was defined as the cumulative MTA dose (mg/m^2) to first instance of grade 2 or higher sensory peripheral neuropathy. Patients in CALGB 40101 for whom no neuropathy event was reported were uninformatively censored at completion of treatment (*i.e.*, four or six treatment cycles). In CALGB 40502, patients were treated until unacceptable toxicity, other complicating disease, alternative therapy, patient withdrawal, treatment completion, progression or death. Patients for whom no neuropathy event was reported were informatively censored at time of occurrence with one of the competing risks.

Statistical Analysis for Genome-wide Analysis

Genome-wide association analyses were individually completed for each CALGB cohort. In CALGB 40101, the association between genotypic variation for each SNP and hazard of neuropathy event was tested within the framework of a Cox model using the score statistic, assuming uninformative censoring. In CALGB 40502, each SNP was tested for an association with cause-specific hazard of neuropathy event within the framework of a Cox model using the Wald statistic, stratifying for treatment arm and adjusting for age. In each case, genotypic variation was inferred using imputed allele dosage for untyped SNPs and associations were tested assuming an additive genotype-phenotype effect. This analysis was conducted under the *R*

statistical environment[19] 3.3 with the GenABEL[20], survival[21], cmprsk[22], qqman[23], and ggplot2[24] packages. Per SNP summary statistics were further used to conduct an inverse-variance weighted meta-analysis using the METAL software[25]. The reported P-values and confidence interval estimates have not been adjusted to account for multiple testing or imputation error. This discovery analysis used ranking of unadjusted P-values for feature selection and prioritization for additional analyses.

In silico Functional Analysis

Selected variants associated with MTA-induced peripheral neuropathy underwent bioinformatic analysis to identify those most likely to disrupt gene function. Each variant of interest was assessed with HaploReg v4.1 (https://pubs.broadinstitute.org/mammals/haploreg/haploreg.php), GTEx v8 (https://gtexportal.org/home/), UCSC Genome Browser (https://genome.ucsc.edu/), SEdb v1.03 (http://www.licpathway.net/sedb/), and HACER (http://bioinfo.vanderbilt.edu/AE/HACER/); additional variants were further prioritized if annotated genes were linked to previous studies of chemotherapy-induced peripheral neuropathy. UCSC Genome Browser was used to visually interrogate genomic regions of interest for enrichment of regulatory elements using Open Regulatory Annotation database[26], GeneHancer database[27], brain methylation[28] and histone marks[29], and ENCODE Project[30] data, which included ChIP-seq histone modification peaks, transcription levels from RNA-seq, transcription factor ChIP-seq clusters, DNase I hypersensitivity clusters, and predicted genome segmentations (Segway, ChromHMM, and combined algorithms). HaploReg[31] was used to explore noncoding SNPs and their proxy SNPs (LD $r^2 > 0.6$) for further regulatory function using ChIP-seq, DNAse I hypersensitivity, and ChromHMM chromatin state predictions from the Roadmap

Epigenomics[32] and ENCODE Project[30]. Expression and splicing qualitative trait loci associated with these SNPs were summarized from the GTEx Portal[33]. Human super-enhancer regions were also identified from SEdb[34], a comprehensive human super-enhancer database using a collection of H3K27ac ChIP-seq data from NCBI Gene Expression Omnibus, ENCODE Project, Roadmap Epigenomics Project, and Genomics of Gene Regulation Project. These super-enhancer regions were queried for predicted enhancer-gene interactions using the HACER database[35] that incorporates FANTOM5, GTEx eQTL data, and experimentally validated interactions from 4DGenome, Hi-C, ChIA-PET, HiChIP and Capture Hi-C data.

iPSC-Induced Sensory Neuron Differentiation and Culture

Human induced pluripotent stem cell (iPSC) line WTC was previously validated and established[36]. WTC was differentiated into peripheral sensory neurons using a previously described protocol[37]. Briefly, human iPSCs were cultured in mTesR medium (STEMCELL Technologies, cat. no. 05850; Cambridge, MA) on matrigel (Corning, cat. no. 356234; Corning, NY) coated plates at a density of 50,000 cells/cm^2. Neural differentiation was initiated (days 0-5) using KSR medium and SMAD inhibitors: 100 nM LDN-193189 (Selleck, cat. no. S7507; Houston, TX) and 10 μM SB431542 (Selleck, cat. no. S1067; Houston, TX). The KSR medium consisted of 80% knockout DMEM, 20% knockout serum replacement, 2 mM GlutaMAX (100X), MEM nonessential amino acids (100X) and 0.1 nM β-mercaptoethanol (ThermoFisher, cat. nos. 10829018, 10828028, 35050061, 11140050, 21985023; Waltham, MA). Early nociceptor differentiation began on day 2 with introduction of 3 μM CHIR99021, 10 μM SU5402, and 10 μM DAPT (Selleck, cat. nos. S1263, SU5402, S2215; Houston, TX). N2 medium (ThermoFisher, cat. no. 17502048; Waltham, MA) was added in stepwise increments of

25% starting at day 4 until reaching 100% on day 10. N2 medium was composed of 50% DMEM/F12 medium with 100X N2 supplement (ThermoFisher, cat. nos. 11320033, 17502048; Waltham, MA) and 50% Neurobasal medium with 50X B27 supplement (ThermoFisher, cat. nos. 21103049, 17504044; Waltham, MA). Mature nociceptors were induced on day 12 and maintained with neuronal growth factors (10 ng/ml human β-NGF, BDNF, GDNF, and NT3; PeproTech, cat. nos. 450-01, 450-02, 450-10, 450-03; Rocky Hill, NJ). On day 12, human iPSCs were seeded at ~35,000 cells/cm^2 and cultured on 96-well plates (Greiner Bio-One, cat. no. 655090; Monroe, NC) triple coated with 15 µg/ml poly-L-ornithine hydrobromide (Sigma-Aldrich, cat. no. P3655; St. Louis, MO), 2 µg/ml laminin-1 (Cultrex R&D Systems, cat. no. 3400-010-1; Minneapolis, MN), and 2 µg/ml fibronectin (BD Biosciences, cat. no. 356008; San Jose, CA). Cells were differentiated and maintained at 37ºC and 5% CO_2. A single differentiation originating from iPSCs was considered one independent experiment.

In vitro Neurotoxicity Studies

After iPSCs were differentiated into mature nociceptors (day 35+), iPSC-SNs were treated with paclitaxel (Sigma-Aldrich, cat. no. T7402; St. Louis, MO) with or without FTY720 (Cayman Chemical; cat. no. 11975) or W146 (Cayman Chemical, cat. no. 10009109; Ann Arbor, MI), and compared to those treated with 0.2% DMSO (Sigma-Aldrich, cat. no. D2650; St. Louis, MO) as a vehicle control. After 48 hours of drug treatment, sensory neurons were fixed in 4% paraformaldehyde for 15 min at room temperature. After washing with PBS, cells were permeabilized with 0.25% Triton-X (Sigma-Aldrich; Saint Louis, MO) in PBS for 10 min at room temperature. Cells were then blocked with the addition of 10% goat serum (Jackson ImmunoResearch Laboratories, Inc.; West Grove, PA) in 1% BSA and 0.5% Tween-20 blocking

solution for 1 hour. Fixed cells were incubated overnight at 4ºC with anti-TUJ1 antibody (Covance, cat. no. MRB-435P; Princeton, NJ). Goat anti-rabbit secondary antibody (Life Technologies, cat. no. A-11008; Carlsbad, CA) was added in blocking buffer for 1 hour. After PBS washes, DAPI stain (ThermoFisher, cat. no. D1306; Waltham, MA) was added to stain for nuclei. Imaging was performed at 20X magnification using the IN Cell Analyzer 2000 (GE Healthcare Life Sciences; Pittsburgh, PA).

Imaging Data Analysis

Workflow of the imaging analysis is shown in Figure 2.4. Nine raw images were generated from each well, representing a field-of-view of 15.95 mm^2 (2048 x 2048 pixels; 47% of well area). These images were batch processed through an imaging processing software, MIPAR^{TM}, with a custom-built algorithm to analyze measurements for chemotherapy-induced neuronal damage. This algorithm generates optimized grayscale images by reducing overall noise and minimizing the amount of non-specific staining to identify and quantify the neurite networks within each field-of-view image. A subsequent segmentation algorithm was performed to estimate nuclei within each field-of-view image. After processing, each image or field-of-view yielded measurements of total neurite area and neuron count. Neurite area was defined by the total area of pixels captured within the identified TUJ1-stained network for each image. Cell counts were designated with DAPI-stained nuclei, rejecting DAPI-stained particles less than 50 pixels to exclude non-specific DAPI staining. To get a global measurement for each well, total neurite area and total cell count were generated by summing measurements across the nine field-of-view images. Processed images included further in the analysis were required to pass quality control on a per-well basis to assess the quality of the neurons and images (Figure 2.4). Per-well images

were stitched together using an in-house script to batch process all nine field-of-view images, using the Grid/Collection Stitching plugin in Fiji. Wells were only included if neurites cover ≥ 50% of the entire well, no more than 3 field-of-view images (out of 9) contained out-of-focus images, and a majority of the signal intensities captured were not from artifacts.

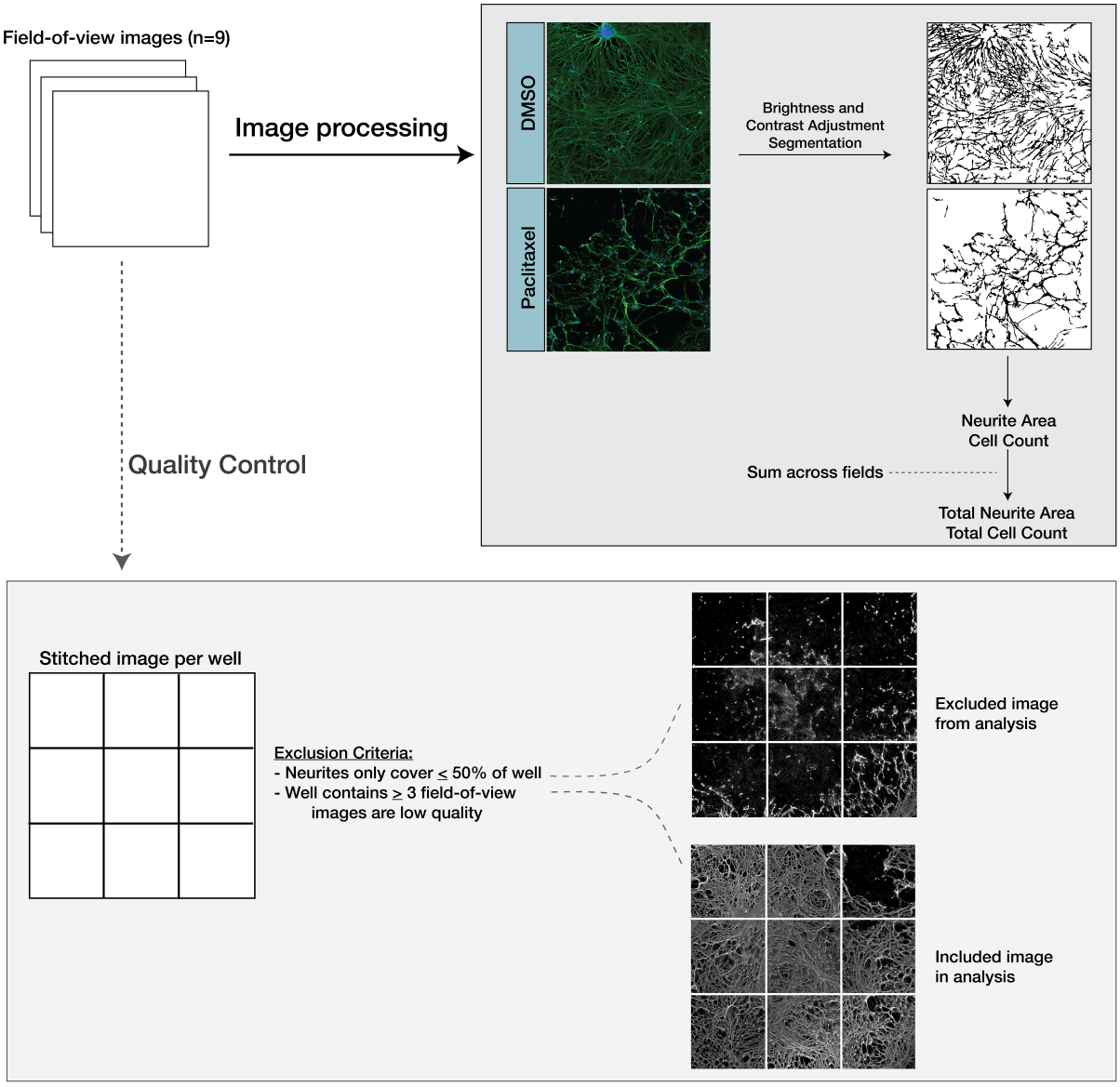

Figure 2.4 Quality control workflow of imaging analysis with field-of-view images.

Statistical Analysis for Image Analysis

For each experiment, all drug treatments were completed with 6-8 replicates on the same plate and raw neurite area measurements and cell counts from imaging data were averaged to obtain a mean total neurite area/cell count per condition. Mean total neurite areas and mean total cell counts were expressed as a ratio of drug-treated to vehicle-treated samples. Differences between relative ratios for the treatment groups were tested for significance by one-way ANOVA test using the function *aov* and subsequent post-hoc multiple comparisons using unpaired, two-sided Student's t-test with the function *t.test* in *R*[19] version 3.5.3. The effect of $S1PR_1$ modulators on paclitaxel effects were assessed by comparison to paclitaxel-treated cells. Experiments were repeated three times with independent neuron differentiations and the results represent the mean phenotype measurements from each differentiation. The reported P-values and confidence interval estimates have not been adjusted for multiple testing.

RESULTS

Of the 799 individuals randomized to the three-arm treatment in CALGB 40502, only 615 subjects were genotyped and had complete phenotype information. Patient characteristics of the CALGB 40502 subjects are listed in Table 2.2; the distribution of age, race, ethnicity, prior taxane status, and tumor subtype in the pharmacogenetics cohort was similar to the entire clinical trial cohort. Patient characteristics for the CALGB 40101 subjects were previously summarized[9], and differences in sample size, disease stage, drug therapy, and genotyping arrays between the two cohorts are described in Table 2.1. The main non-hematological toxicity in CALGB 40502 and CALGB 40101 was sensory peripheral neuropathy with reported event rates of grade 2 or higher of 49% and 24%, respectively (Table 2.1). A similar cumulative incidence of peripheral neuropathy was observed regardless of treatment arm in CALGB 40502 (Figures 2.5 and 2.6), where risk of developing peripheral neuropathy was a function of cumulative chemotherapy dose. The main competing risk for developing peripheral neuropathy in the nab-paclitaxel arm was disease progression or death while other competing risks, such as other adverse events, other complicating disease, alternative therapy, patient refusal, and treatment completion were more likely to lead to censoring for the peripheral neuropathy phenotype in the paclitaxel and ixabepilone arms.

Table 2.2 Patient demographics in CALGB 40502

		Pharmacogenetic Cohort[†] (N = 615) No. (%)	**Clinical Trial** (N = 799) No. (%)
Age (yrs)	20-49	164 (27)	218 (27)
	50-69	390 (63)	500 (63)
	70+	61 (10)	81 (10)
Race[‡]	White	501 (81)	640 (80)
	Black	81 (13)	113 (14)
	Other	23 (4)	32 (4)
	Unknown	10 (2)	14 (2)
Ethnicity[‡]	Hispanic or Latino	31 (5)	47 (6)
	Non-Hispanic	548 (89)	712 (89)
	Unknown	36 (6)	40 (5)
Taxane as adjuvant therapy	Yes	270 (44)	352 (44)
	No	345 (56)	447 (56)
Tumor subtype	ER or PgR unknown/missing	0 (0)	16 (2)
	ER or PgR positive	443 (72)	573 (72)
	ER and PgR negative	172 (28)	210 (26)

ER: estrogen receptor; PgR: progesterone receptor
[†]Genotyped samples with complete phenotype information
[‡]Self-reported race and ethnicity

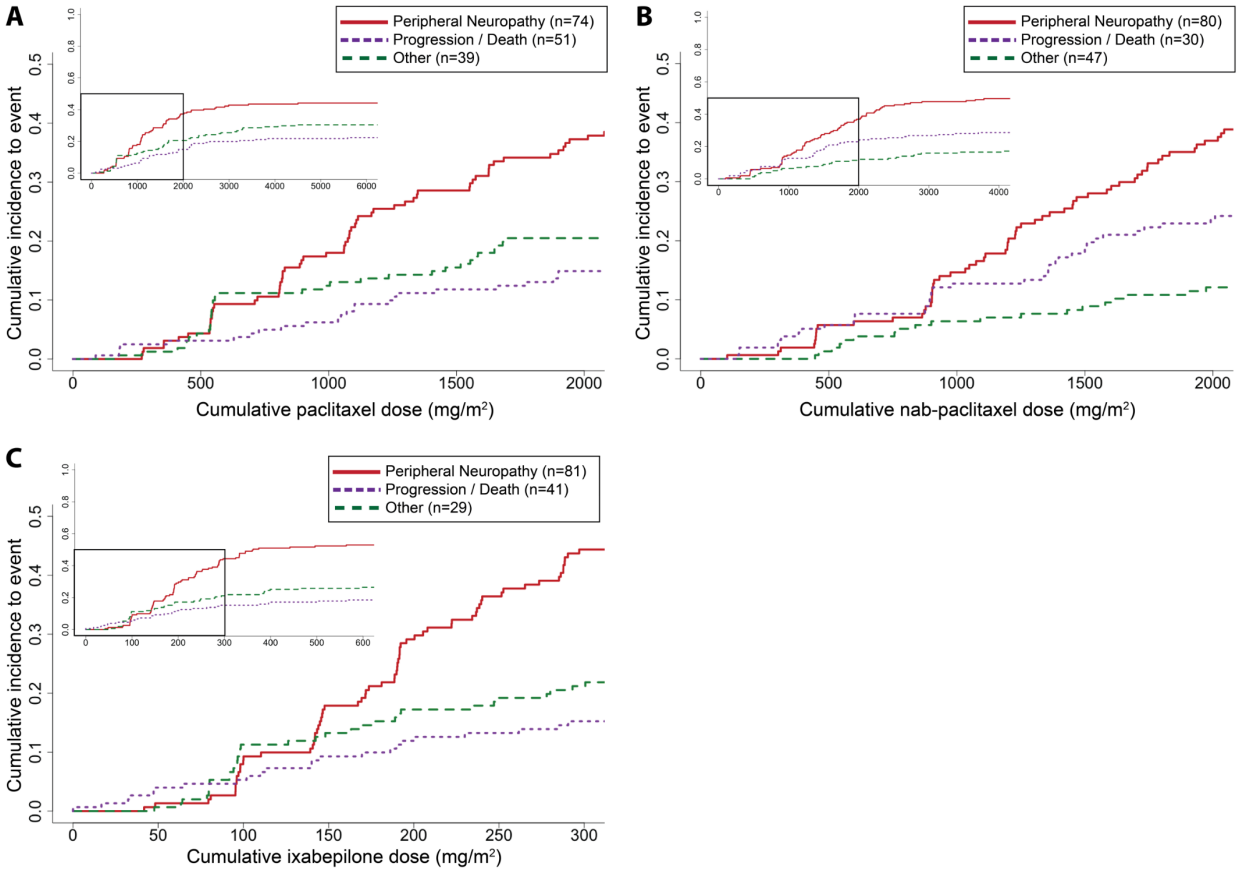

Figure 2.5 Cumulative incidence plot of chemotherapy-induced peripheral neuropathy (A: paclitaxel; B: nab-paclitaxel; C: ixabepilone) and informative competing events as a function of cumulative dose (mg/m^2) to event for all subjects in the pharmacogenetics discovery cohort of CALGB 40502. Top left inset displays the entire range of cumulative doses, where the boxed area denotes where ~75% of the data lies (Figure 2.6) and is represented in the larger plot.

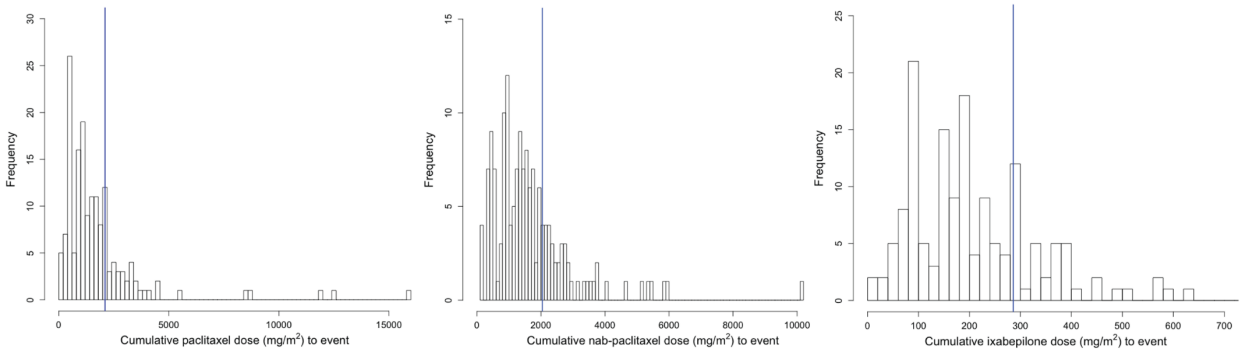

Figure 2.6 Distribution of cumulative dose-to-first instance of grade 2 or higher peripheral neuropathy for each treatment arm in CALGB 40502, where 75% of the distribution lies left of the blue vertical line and represents the cumulative doses used to generate cumulative incidence plots in Figure 2.5.

The meta-analysis of the SNP associations from CALGB 40101 and CALGB 40502 were filtered for SNPs with a minor allele frequency of ≥5% in at least one of the two cohorts. None of the resulting SNPs reached genome-wide significance, although 18 linkage disequilibrium-pruned SNPs ($r^2 \geq 0.7$) had $P < 10^{-5}$ (Table 2.3; Figures 2.7 and 2.8). The 18 SNPs with the lowest *P* values were filtered for further support of association from SNPs in high linkage disequilibrium with the identified SNP and expression in human dorsal root ganglion (DRG)[38]. SNPs in genomic regions annotated to *C9orf106*, *SLITRK1*, *KLHL1*, *ZBBX, LOC100129716, and SEPT5* had limited linkage support from visual inspection of LocusZoom[39] plots (Figures 2.9-2.11) and 11 SNPs were annotated to genes that are not detected in human DRG[38] (*ZFPM2* (three independent SNPs), *C9orf106*, *KLHL1*, *SUGCT* (two independent SNPs), *ZBBX*, *LOC100129716*, *ADGRB3* and *CNGB1*). Based on the expression and linkage support filtering (Figures 2.12-2.17), additional analyses were only considered for the genomic regions around seven SNPs (rs74497159, rs17076837, rs10771973, rs11076190, rs9623812, rs2060717, rs2188156); while there was no support from SNPs in high linkage disequilibrium for a true association within the genomic region surrounding rs17076837 and rs2188156, these SNPs were annotated to the *SLITRK1* and *SEPT5* genes that are highly expressed in the human DRG. Six of the remaining seven SNPs were associated with increased risk of MTA-induced peripheral neuropathy while a single SNP was protective. Cumulative incidence plots for MTA-induced peripheral neuropathy stratified by each of the seven SNPs of interest are shown in Figures 2.18-2.24. Interestingly, the association of rs11076190 and rs2188156 with peripheral neuropathy is driven by the paclitaxel-treated patients.

Table 2.3 Top ranking SNPs for meta-analysis using cumulative dose to first instance of Grade 2 or higher peripheral neuropathy event.

				CALGB 40101			CALGB 40502			META	
SNP*	**Chr**	**Alleles†**	**Gene**	**MAF**	**Effect**	**P**	**MAF**	**Effect**	**P**	**P**	**Direction**
rs74497159	1	T>G	168 kb 3' of *S1PR1*	0.065	0.591	5.96E-04	0.055	0.693	1.59E-04	3.62E-07	++
rs3110366	8	T>A	142 kb 5' of *ZFPM2*	0.204	-0.394	1.20E-03	0.198	-0.446	2.51E-04	1.07E-06	--
rs77526807	9	G>T	39 kb 3' of *C9orf106*	0.053	0.818	4.32E-04	0.059	0.764	1.14E-03	1.66E-06	++
rs17076837	13	C>G	382 kb 3' of *SLITRK1*	0.135	0.578	7.72E-06	0.124	0.304	2.78E-02	1.85E-06	++
rs61963755	13	T>A	intronic region of *KLHL1*	0.050	0.674	3.60E-04	0.055	0.630	1.56E-03	1.88E-06	++
rs2342780	8	T>A	68 kb 5' of *ZFPM2*	0.069	-0.788	8.07E-06	0.064	-0.432	3.81E-02	2.06E-06	--
rs10771973	12	G>A	intronic region of *FGD4*	0.311	0.451	3.91E-06	0.301	0.203	3.65E-02	2.15E-06	++
rs2342791	8	T>C	43 kb 5' of *ZFPM2*	0.164	-0.414	1.03E-03	0.162	-0.430	7.43E-04	2.53E-06	--
rs11076190	16	T>C	8 kb 3' of *CX3CL1*	0.060	0.738	3.18E-05	0.063	0.453	1.38E-02	2.55E-06	++
rs78777495	7	A>T	67 kb 3' of *SUGCT*	0.107	0.602	1.11E-05	0.097	0.328	4E-02	2.99E-06	++
rs9623812	22	A>T	intronic region of *SCUBE1*	0.330	-0.340	3.70E-03	0.335	-0.387	2.60E-04	3.23E-06	--
rs2060717	7	G>A	intronic region of *CALU*	0.069	0.496	4.35E-03	0.066	0.735	1.61E-04	3.48E-06	++
rs6788186	3	T>C	696 kb of 3' *ZBBX*	0.267	0.282	2.11E-02	0.257	0.476	4.11E-05	5.08E-06	++
rs78017515	7	A>G	87 kb 3' of *SUGCT*	0.069	0.621	1.43E-04	0.059	0.488	1.14E-02	5.72E-06	++
rs13168251	5	T>G	718 kb 3' of *LOC100129716*	0.111	0.295	4.18E-02	0.105	0.664	1.13E-05	6.54E-06	++
rs777619	6	T>C	487 kb 5' of *ADGRB3*	0.193	0.416	1.54E-04	0.189	0.315	1.48E-02	8.13E-06	++
rs2188156	22	G>A	65 kb 5' of *SEPT5*	0.051	0.800	1.90E-05	0.052	0.394	5.28E-02	8.23E-06	++
rs57940640	16	G>A	intronic region of *CNGB1*	0.064	0.552	1.65E-03	0.068	0.607	1.64E-03	8.74E-06	++

SNP: single nucleotide polymorphism, Chr: chromosome, MAF: minor allele frequency

*SNPs listed are filtered for $P < 10^{-5}$ and LD-pruned ($r^2 \geq 0.7$) to the top-ranking SNP within each genomic region.

†Alleles are denoted Major>Minor allele

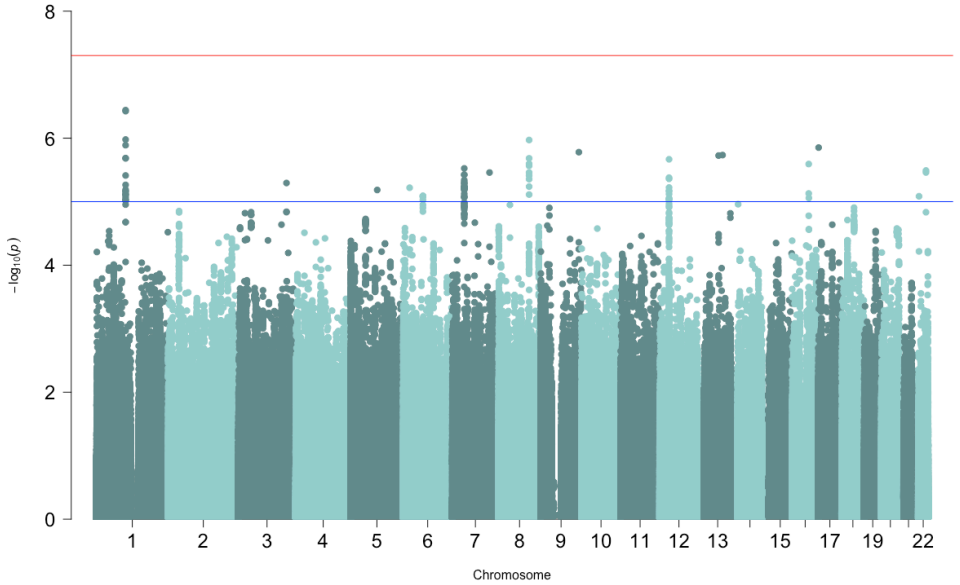

Figure 2.7 Manhattan plot of meta-association analysis in CALGB 40502 and CALGB 40101. Genome-wide association test results are shown as $-\log_{10}$ transformed *P*-values for the Cox proportional hazards analysis indicated on the y-axis. SNPs are plotted by chromosomal location and is displayed on the x-axis. The dark blue horizontal line denotes $P = 10^{-5}$ and the red horizontal line denotes genome-wide significance ($P = 10^{-8}$).

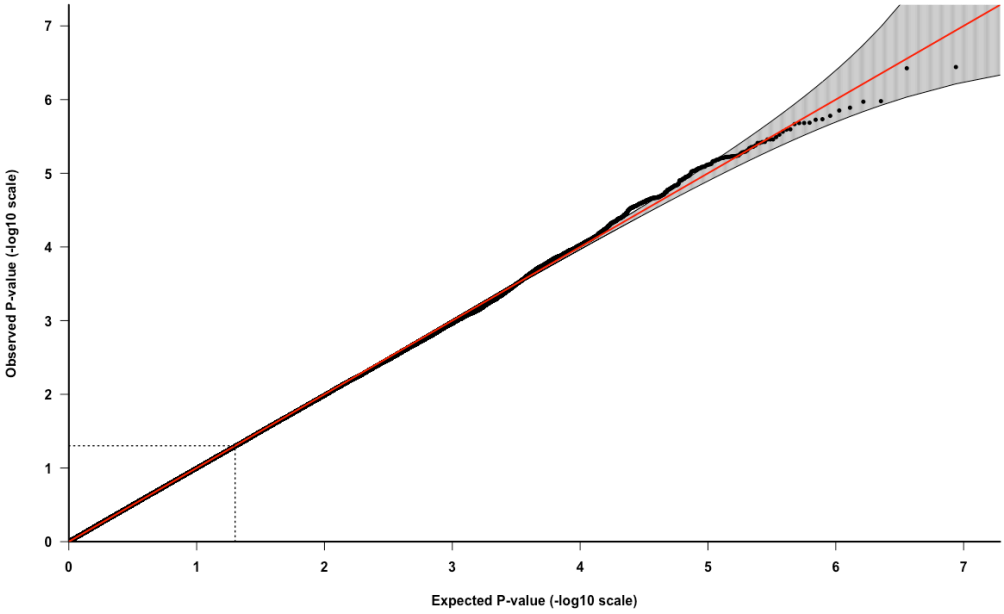

Figure 2.8 Quantile-quantile plot of meta-analysis from genome-wide association tests in CALGB 40502 and CALGB 40101. Observed and predicted *P*-value relationships are plotted for the Cox proportional hazard model. The solid line and shaded area show the expected distribution with 95% CIs assuming no inflation of statistics.

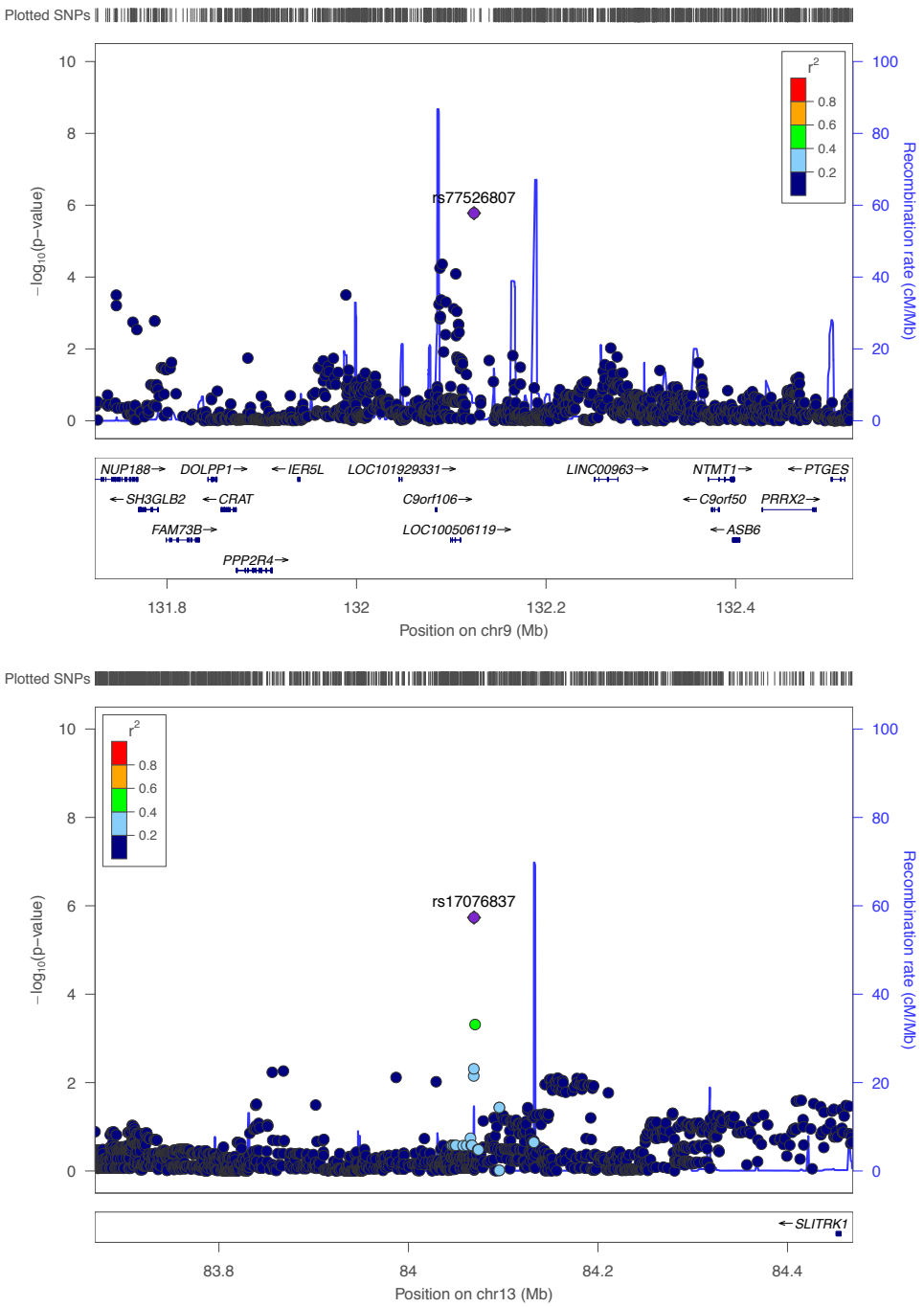

Figure 2.9 LocusZoom plots for genomic regions around rs77526807 located 39 kb 3' of *C9orf106* (top panel) and rs17076837 located 382 kb 3' of *SLITRK1* (bottom panel). Associations with cumulative dose to first instance of grade 2+ peripheral neuropathy for analyzed SNPs are shown on a $-\log_{10}$(P-value) scale. Dot color indicates the strength of linkage disequilibrium (r^2) between the indicated SNP and each SNP in these genomic regions. Plots were produced using LocusZoom (http://locuszoom.sph.umich.edu/).

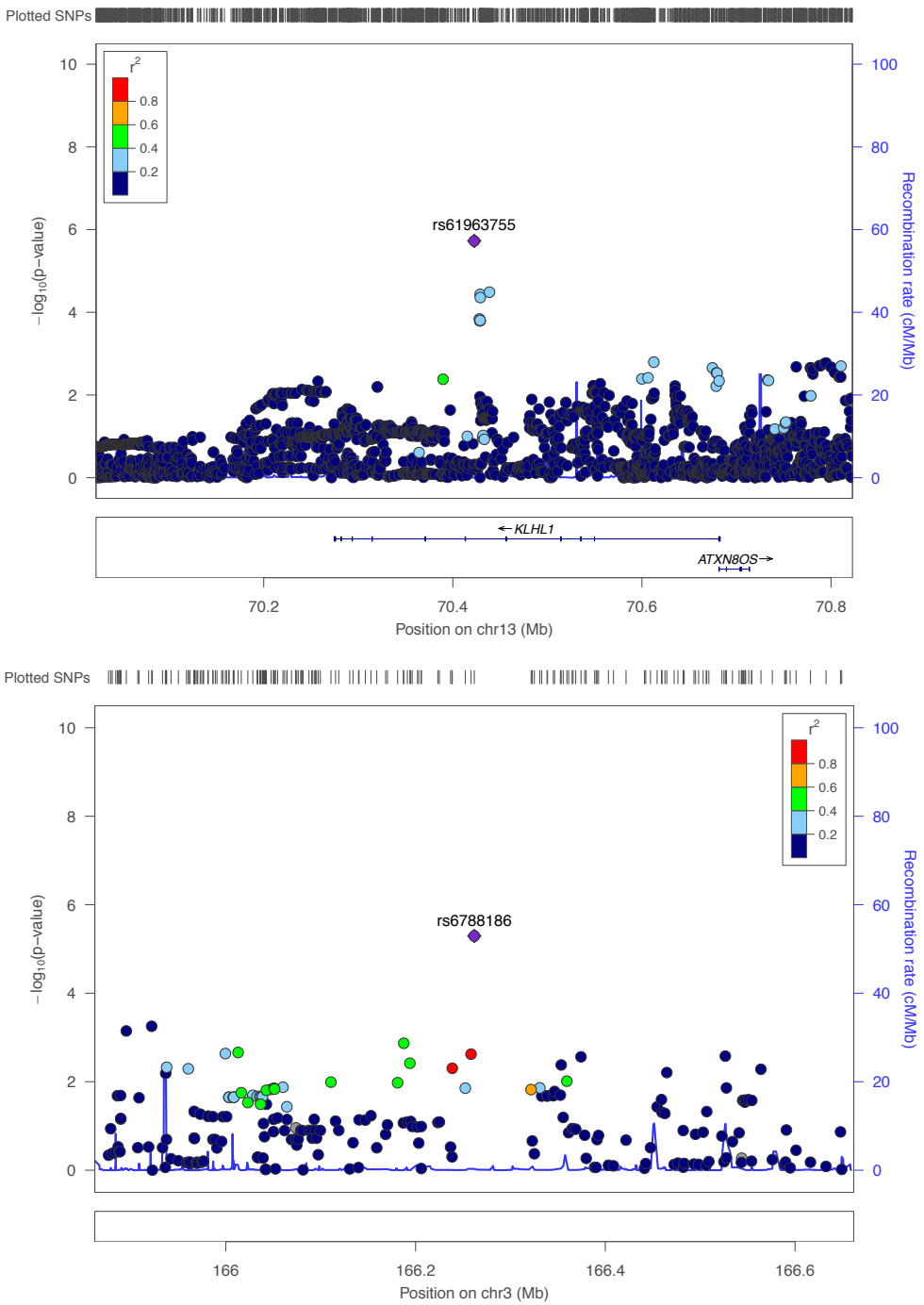

Figure 2.10. LocusZoom plots for associations microtubule targeting agent-induced peripheral neuropathy in the genomic regions around rs61963755 located within an intronic region of *KLHL1* (top panel) and genomic region around rs6788186 located in a gene desert (bottom panel). Associations with cumulative dose to first instance of grade 2+ peripheral neuropathy for analyzed SNPs are shown on a $-\log_{10}$(P-value) scale. Dot color indicates the strength of linkage disequilibrium (r^2) between the indicated SNP and each SNP in this genomic region. Plots were produced using LocusZoom (http://locuszoom.sph.umich.edu/).

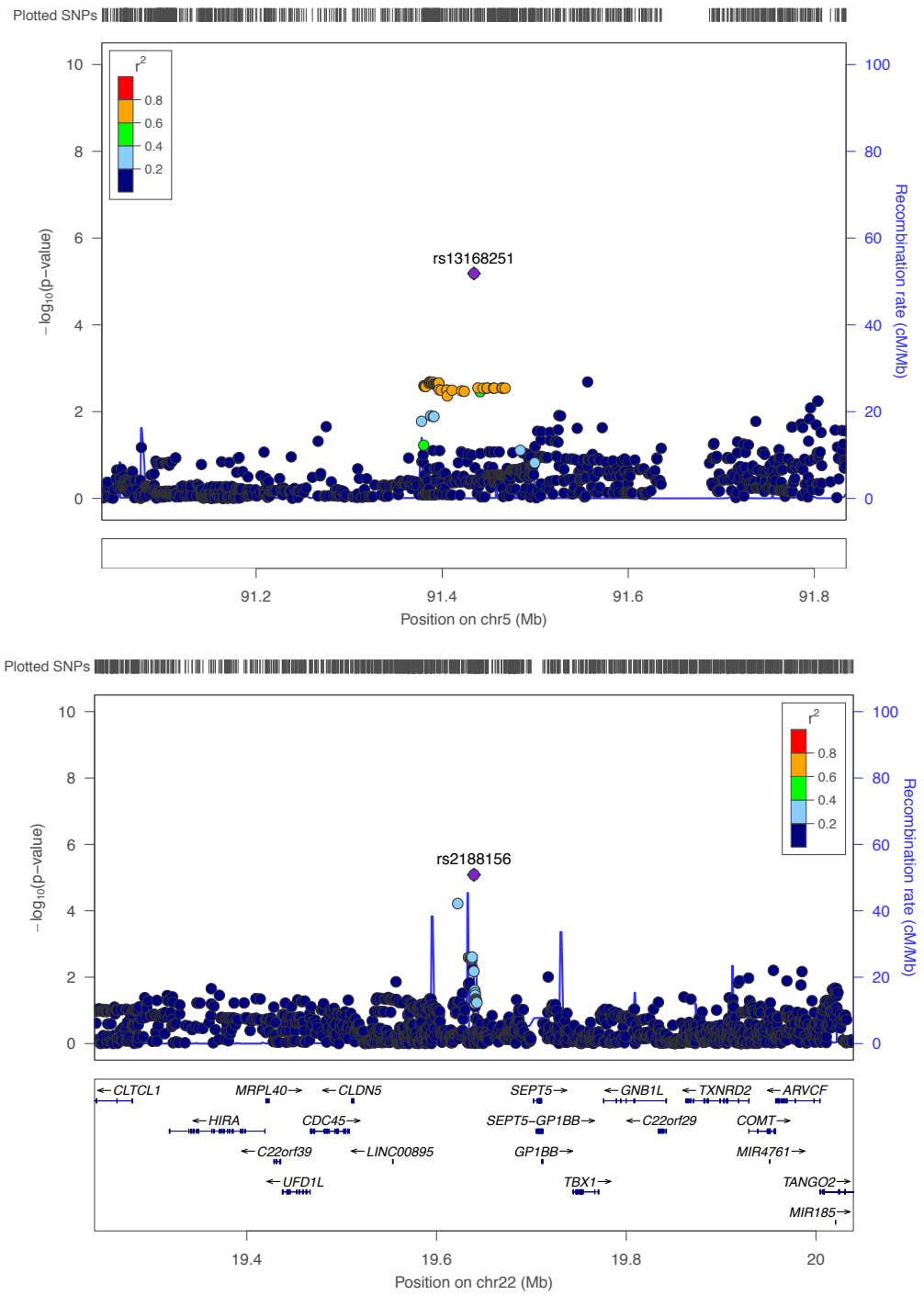

Figure 2.11 LocusZoom plots for associations with microtubule targeting agent-induced peripheral neuropathy in the genomic regions around rs13168251 located in a gene desert (top panel) and rs2188156 located 63 kb 5' of *SEPT5* (bottom panel). Associations with cumulative dose to first instance of grade 2+ peripheral neuropathy for analyzed SNPs are shown on a $-\log_{10}$(P-value) scale. Dot color indicates the strength of linkage disequilibrium (r^2) between the indicated SNP and each SNP in these genomic regions. Plots were produced using LocusZoom (http://locuszoom.sph.umich.edu/).

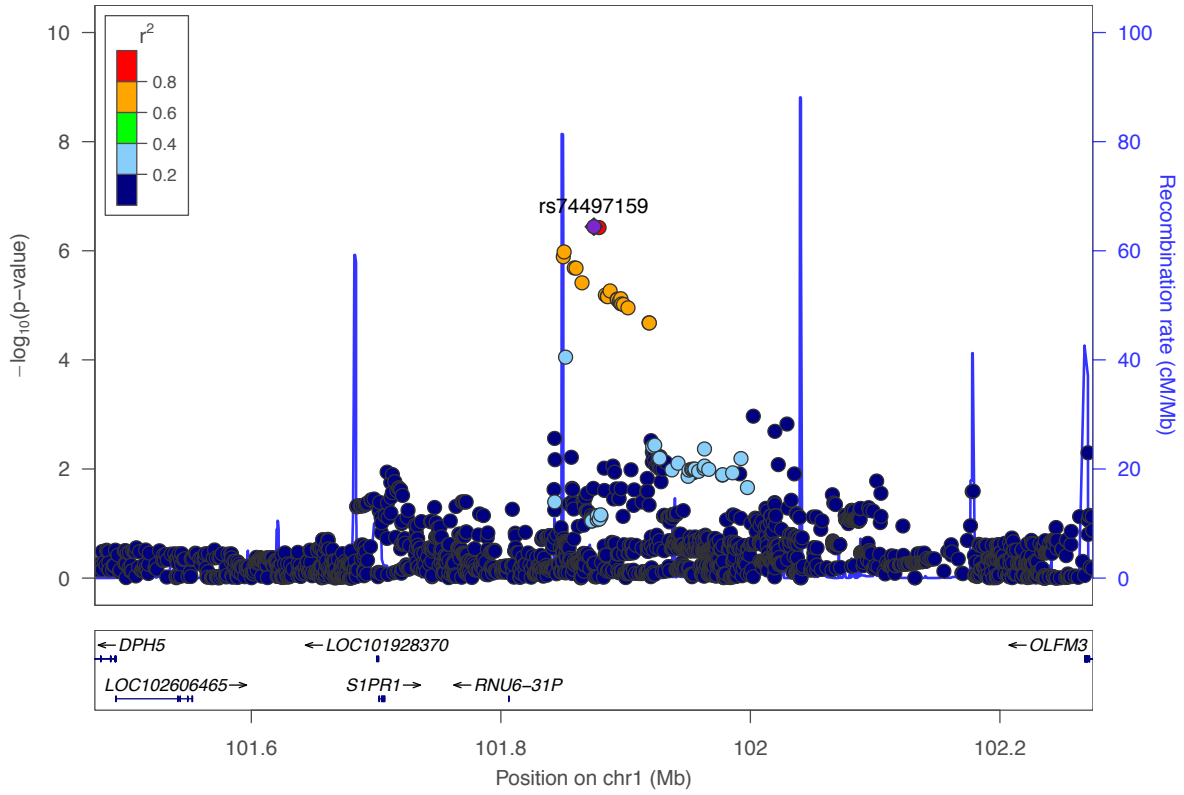

Figure 2.12 LocusZoom plot of the associations with microtubule targeting agent-induced peripheral neuropathy in the genomic region around rs74497159 located downstream of *S1PR1*, a gene which encodes for sphingosine-1-phosphate receptor 1. Associations with cumulative dose to first instance of grade 2+ peripheral neuropathy for analyzed SNPs are shown on a $-\log_{10}$(P-value) scale. Dot color indicates the strength of linkage disequilibrium (r^2) between the indicated SNP and each SNP in this genomic region. Plot was produced using LocusZoom (http://locuszoom.sph.umich.edu/).

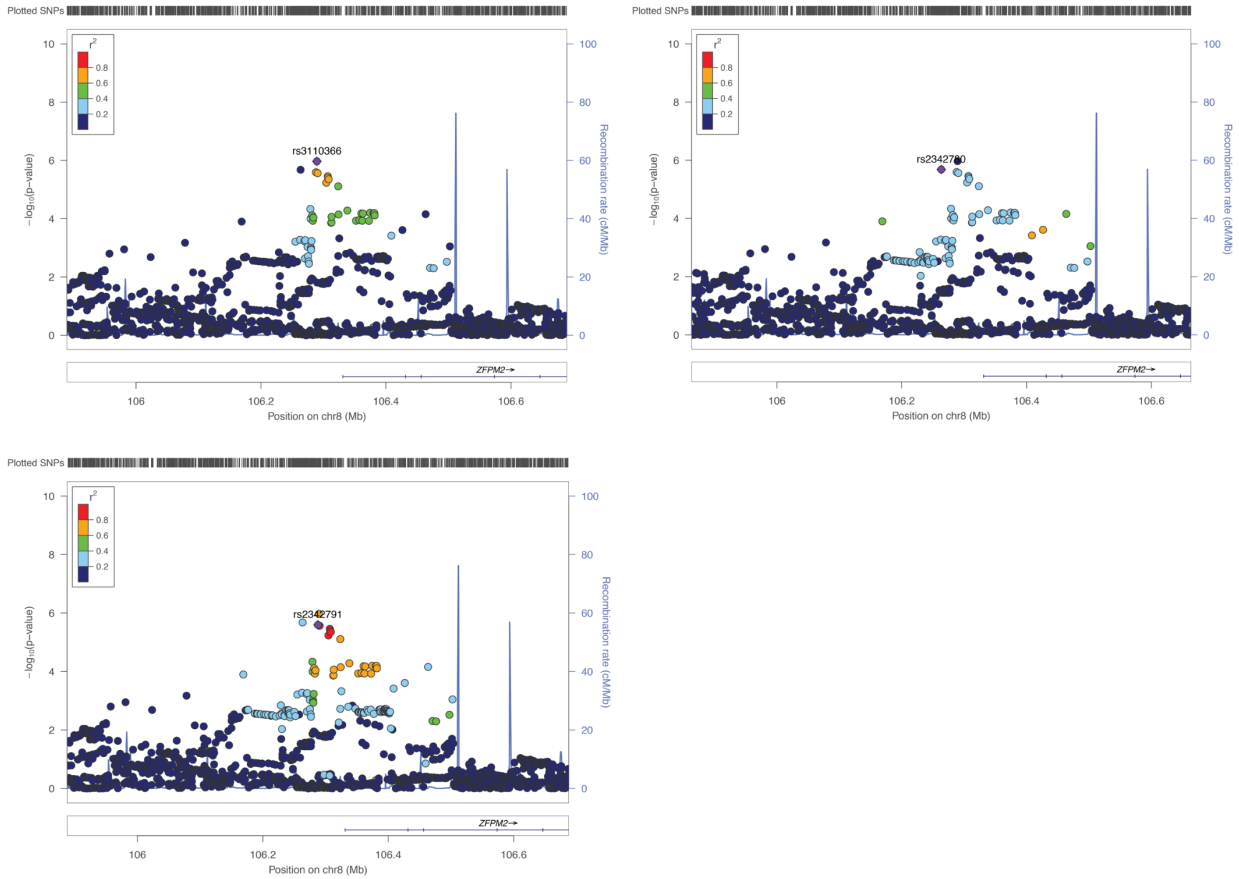

Figure 2.13 LocusZoom plots of the associations with microtubule targeting agent-induced peripheral neuropathy in the genomic region around top-ranking independent SNPs (rs3110266, rs2342780, and rs2342791) annotated to the 5' region of *ZFPM2*. Associations with cumulative dose to first instance of grade 2+ peripheral neuropathy for analyzed SNPs are shown on a $-\log_{10}$(P-value) scale. Dot color indicates the strength of linkage disequilibrium (r^2) between the indicated SNP and each SNP in this genomic region. Plot was produced using LocusZoom (http://locuszoom.sph.umich.edu/).

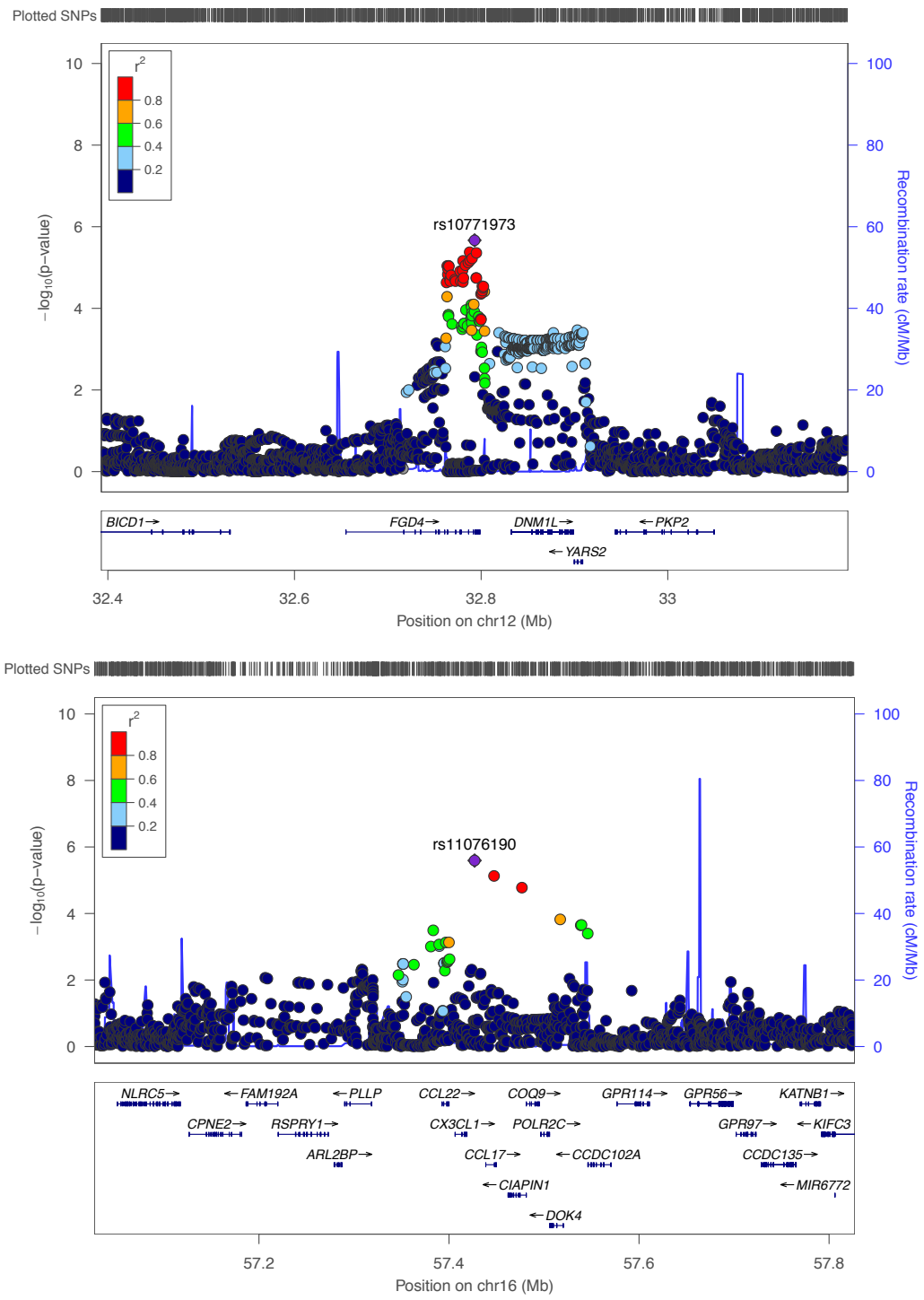

Figure 2.14 LocusZoom plots for the associations with microtubule targeting agent-induced peripheral neuropathy in the genomic region around rs10771973 located within an intronic region of *FGD4* (top panel) and genomic region around rs11076190 located 8 kb from 3' of *CX3CL1* (bottom panel). Associations with cumulative dose to first instance of grade 2+ peripheral neuropathy for analyzed SNPs are shown on a $-\log_{10}$(P-value) scale. Dot color indicates the strength of linkage disequilibrium (r^2) between the indicated SNP and each SNP in this genomic region. Plot was produced using LocusZoom (http://locuszoom.sph.umich.edu/).

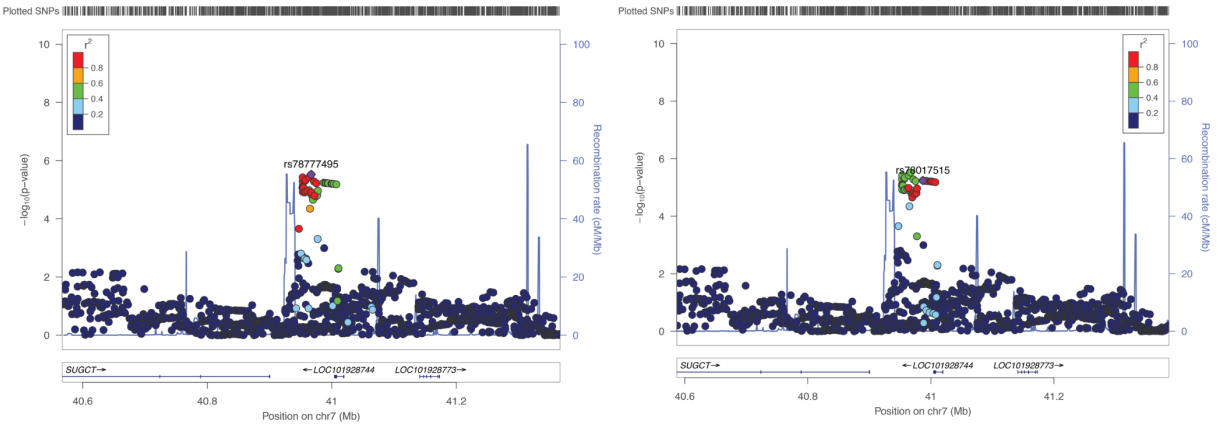

Figure 2.15 LocusZoom plots for the associations with microtubule targeting agent-induced peripheral neuropathy in the genomic region around rs78777495 and rs78017515 located 67 kb and 87 kb from 3' end of *SUGCT*, respectively. Associations with cumulative dose to first instance of grade 2+ peripheral neuropathy for analyzed SNPs are shown on a $-\log_{10}$(P-value) scale. Dot color indicates the strength of linkage disequilibrium (r^2) between the indicated SNP and each SNP in this genomic region. Plot was produced using LocusZoom (http://locuszoom.sph.umich.edu/).

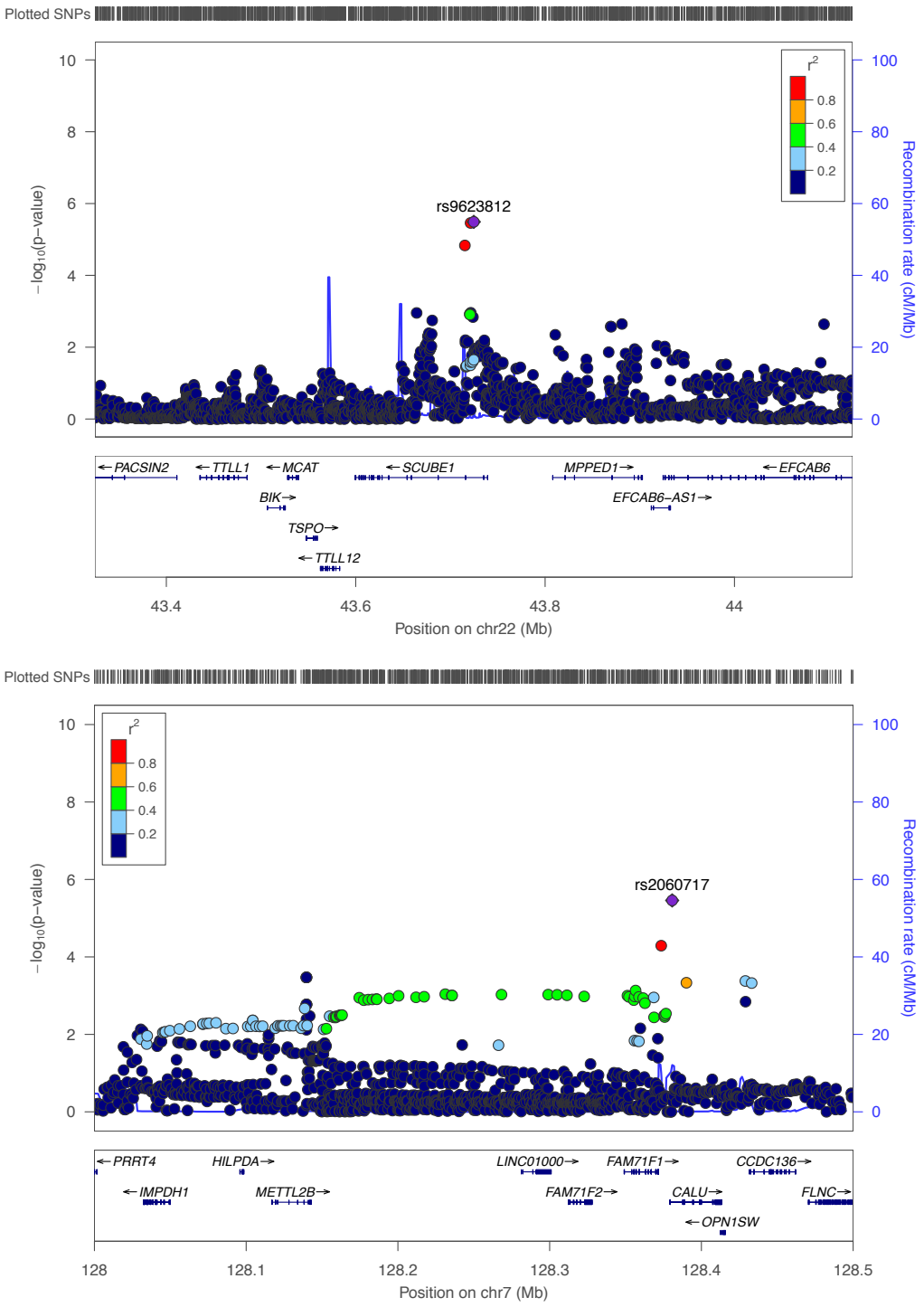

Figure 2.16 LocusZoom plots for the associations with microtubule targeting agent-induced peripheral neuropathy in the genomic region around rs9623812 located within an intronic region of *SCUBE1* (top panel) and around rs2060717 located within an intronic region of *CALU* (bottom panel). Associations with cumulative dose to first instance of grade 2+ peripheral neuropathy for analyzed SNPs are shown on a $-\log_{10}$(P-value) scale. Dot color indicates the strength of linkage disequilibrium (r^2) between the indicated SNP and each SNP in these genomic regions. Plots were produced using LocusZoom (http://locuszoom.sph.umich.edu/).

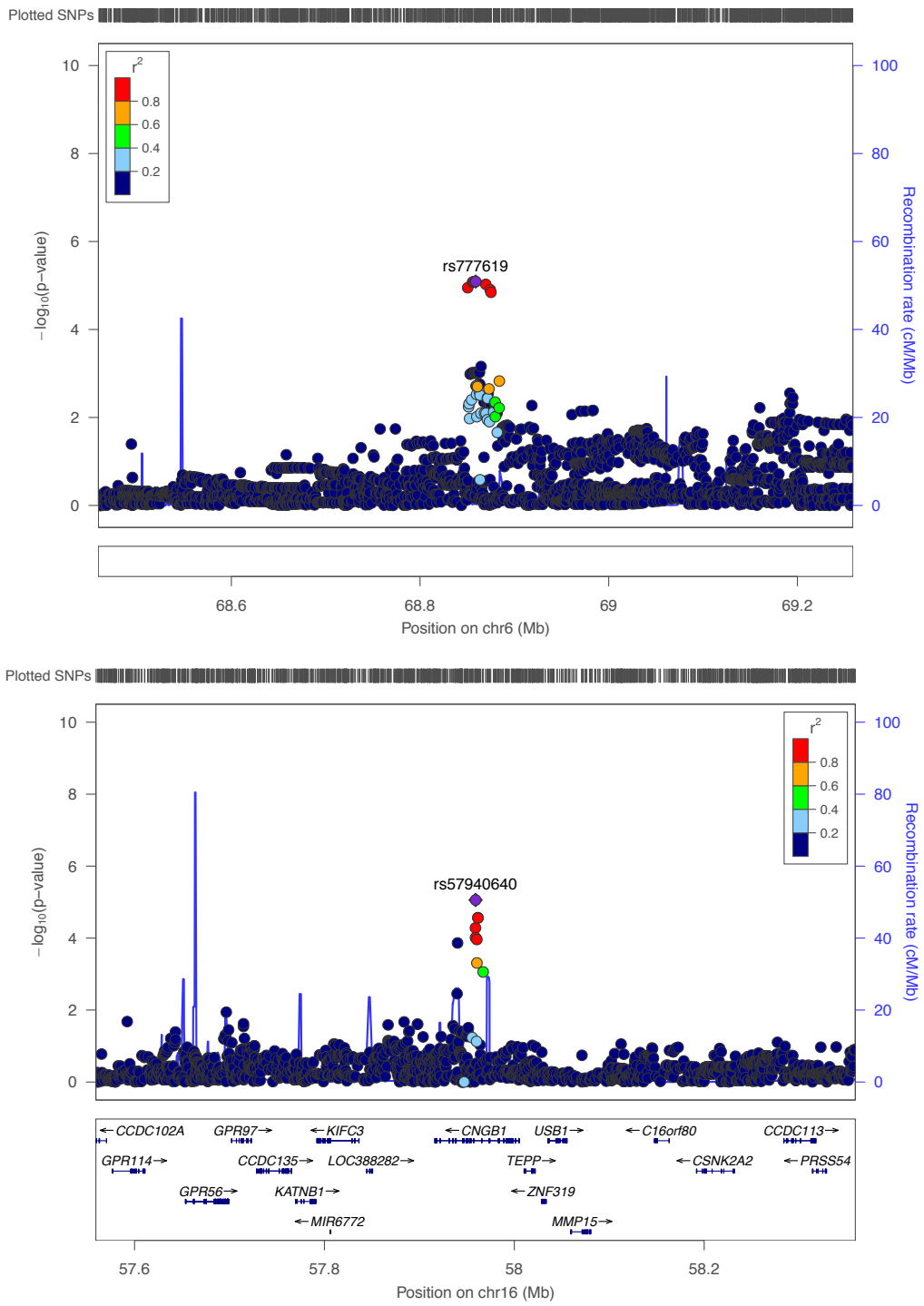

Figure 2.17 LocusZoom plots for the associations with microtubule targeting agent-induced peripheral neuropathy in the genomic region around rs777619 located in a gene desert (top panel) and genomic region around rs57940640 located within an intronic region of *CNGB1* (bottom panel). Associations with cumulative dose to first instance of grade 2+ peripheral neuropathy for analyzed SNPs are shown on a $-\log_{10}$(P-value) scale. Dot color indicates the strength of linkage disequilibrium (r^2) between the indicated SNP and each SNP in this genomic region. Plot was produced using LocusZoom (http://locuszoom.sph.umich.edu/).

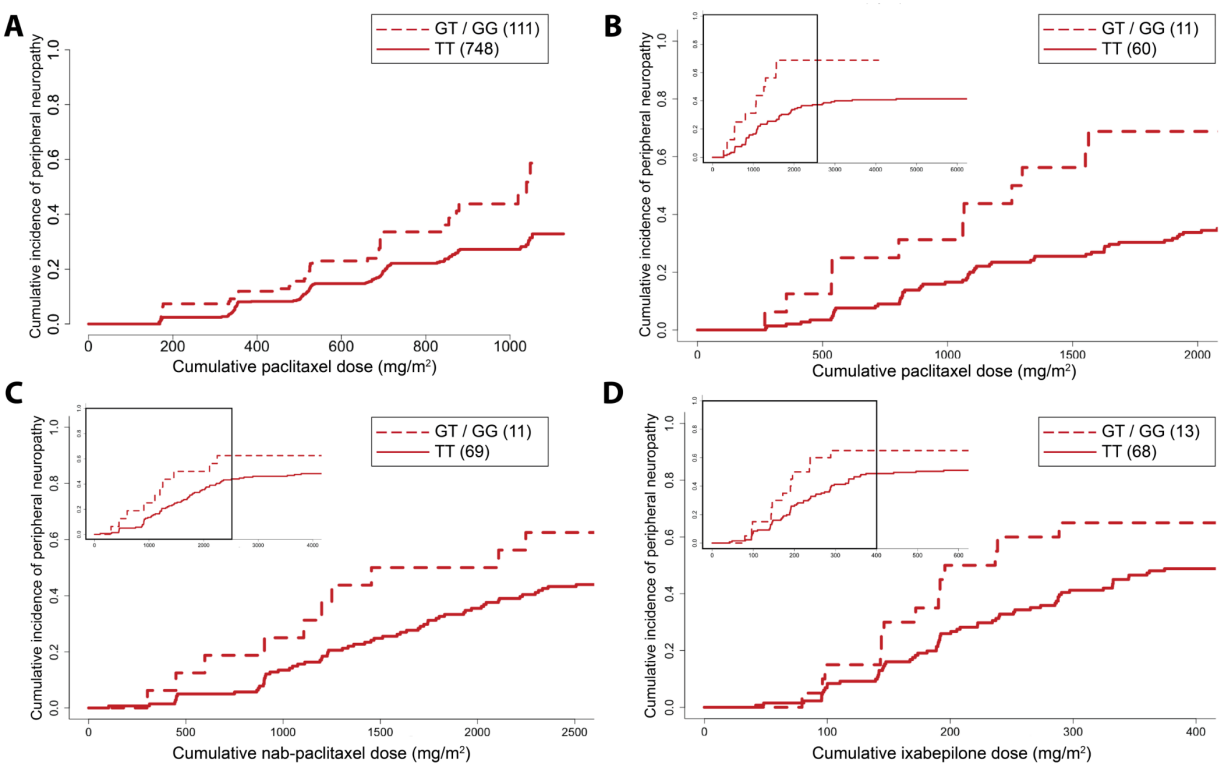

Figure 2.18 Cumulative incidence plot for chemotherapy-induced peripheral neuropathy stratified by rs74497159 genotype in CALGB 40101(A) and CALGB 40502 (B, paclitaxel; C, nab-paclitaxel; D, ixabepilone). Top left insert displays the entire range of cumulative doses, where the boxed area denotes where ~75% of the data lies (Figure 2.5) and is represented in the larger plot. The number of individuals with each genotype is noted in parentheses. The allele risk for peripheral neuropathy events without other competing events are shown in the plots for CALGB 40502 (B-D).

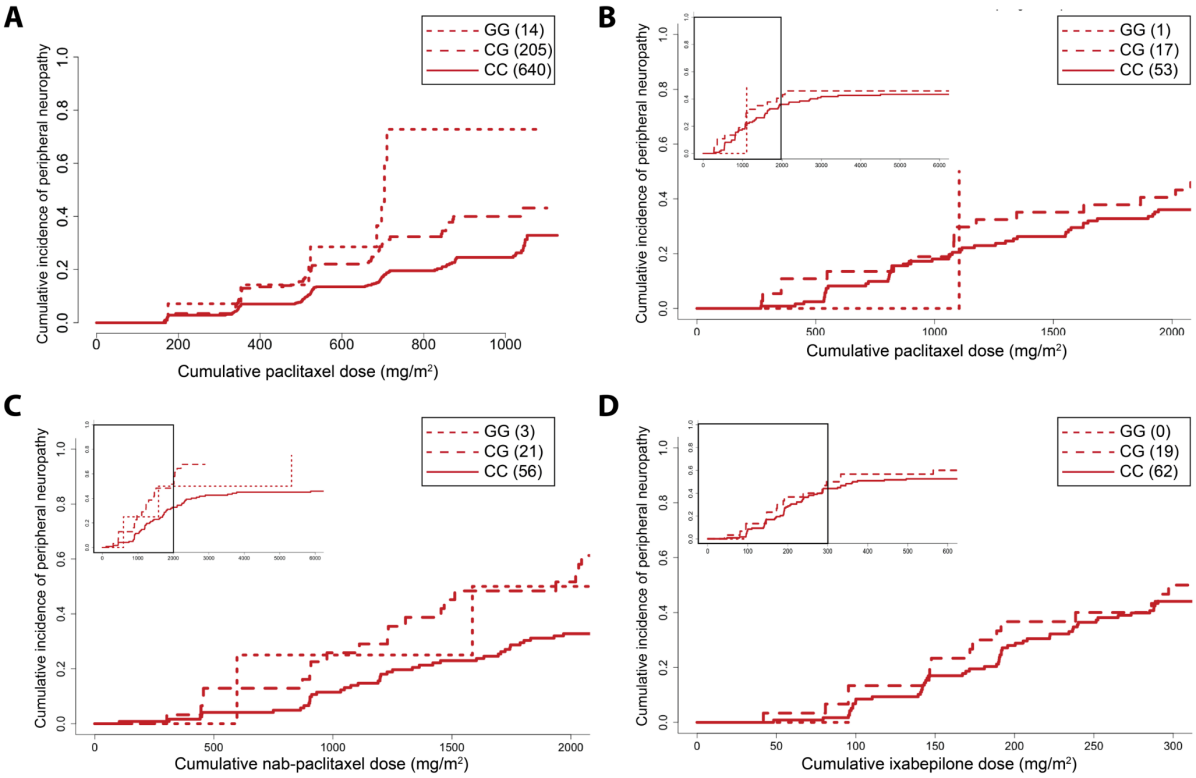

Figure 2.19 Cumulative incidence plot for chemotherapy-induced peripheral neuropathy stratified by rs17076837 (C>G) genotype in CALGB 40101(A) and CALGB 40502 (B, paclitaxel; C, nab-paclitaxel; D, ixabepilone). Top left insert displays the entire range of cumulative doses, where the boxed area denotes where ~75% of the data lies and is represented in the larger plot. The number of individuals with each genotype is noted in parentheses. The allele risk for peripheral neuropathy events without other competing events are shown in the plots for CALGB 40502 (B-D).

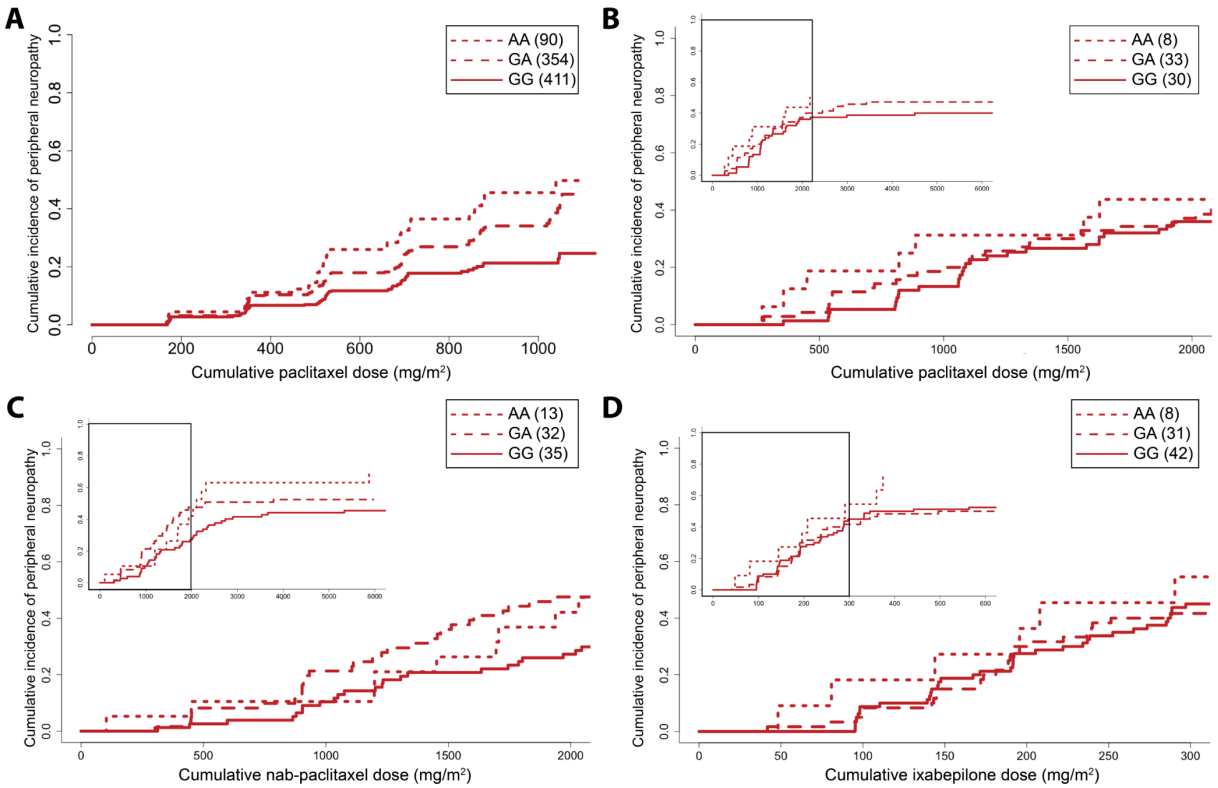

Figure 2.20 Cumulative incidence plot for chemotherapy-induced peripheral neuropathy stratified by rs10771973 (G>A) genotype in CALGB 40101(A) and CALGB 40502 (B, paclitaxel; C, nab-paclitaxel; D, ixabepilone). Top left inset displays the entire range of cumulative doses, where the boxed area denotes where ~75% of the data lies and is represented in the larger plot. The number of individuals with each genotype is noted in parentheses. The allele risk for peripheral neuropathy events without other competing events are shown in the plots for CALGB 40502 (B-D).

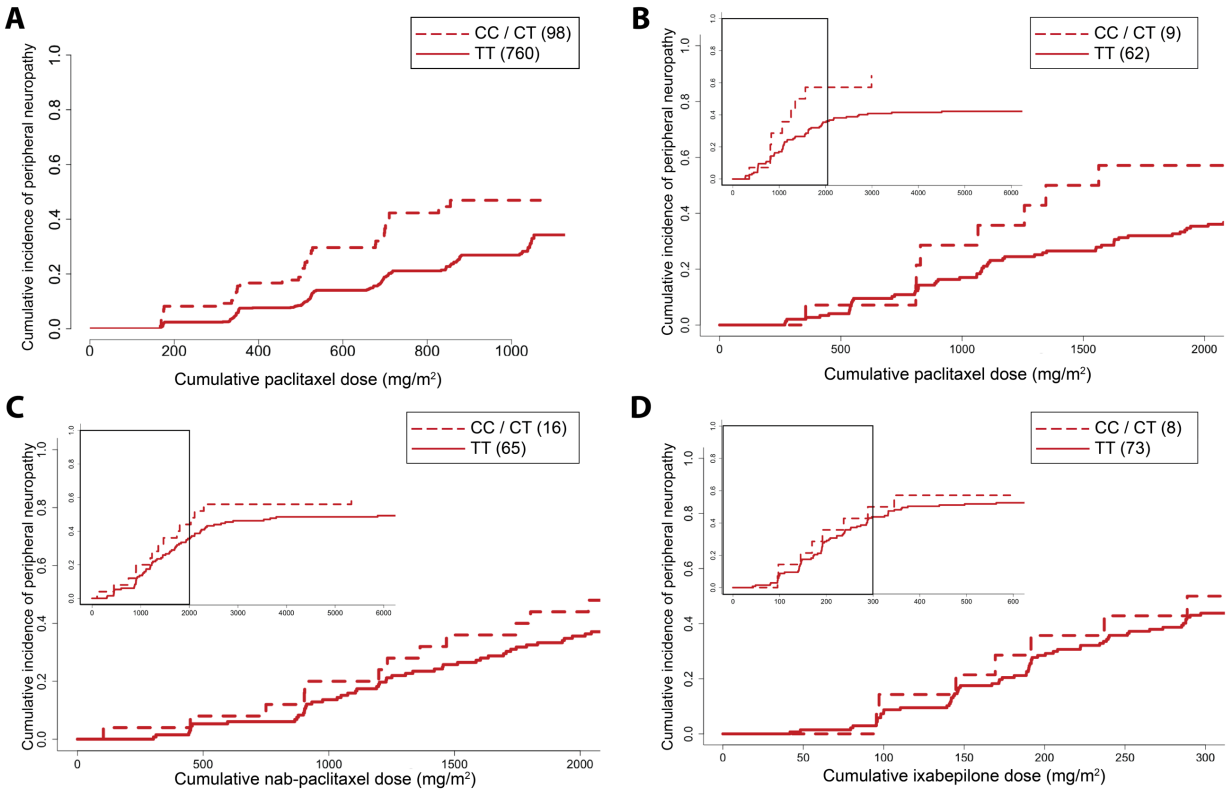

Figure 2.21 Cumulative incidence plot for chemotherapy-induced peripheral neuropathy stratified by rs11076190 (T>C) genotype in CALGB 40101(A) and CALGB 40502 (B, paclitaxel; C, nab-paclitaxel; D, ixabepilone). Top left insert displays the entire range of cumulative doses, where the boxed area denotes where ~75% of the data lies and is represented in the larger plot. The number of individuals with each genotype is noted in parentheses. The allele risk for peripheral neuropathy events without other competing events are shown in the plots for CALGB 40502 (B-D).

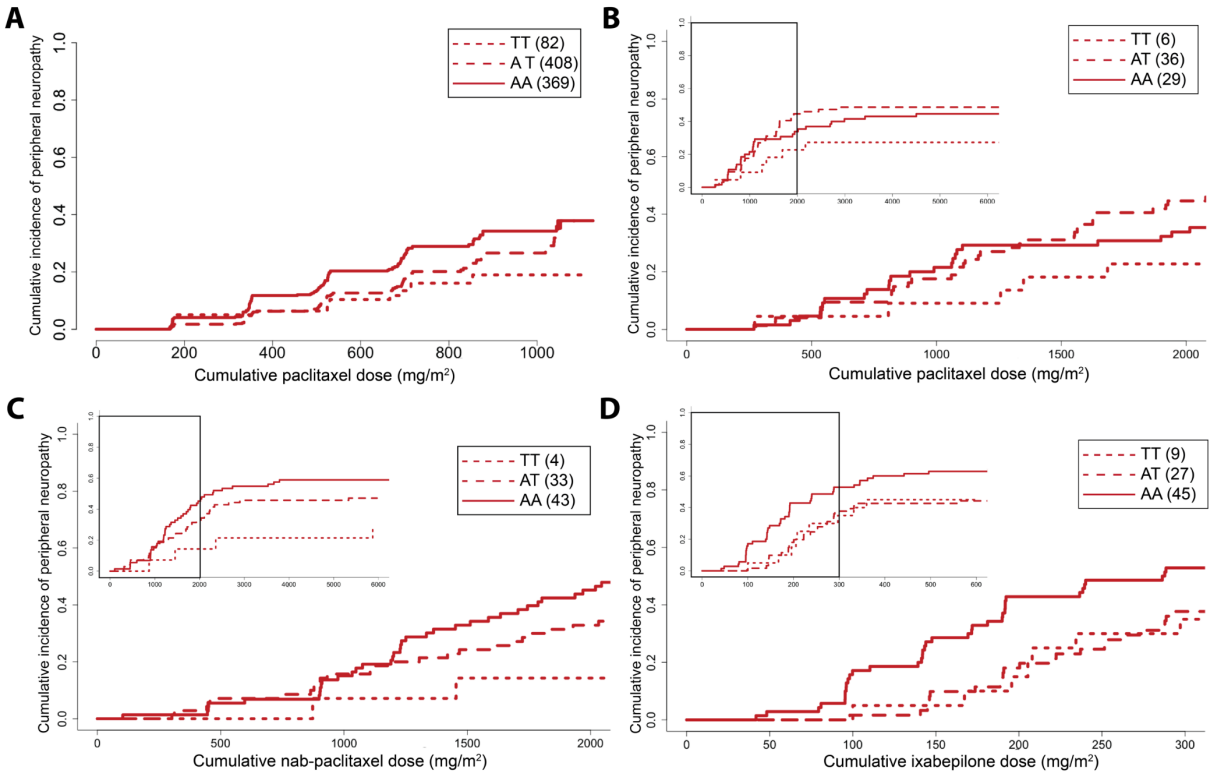

Figure 2.22 Cumulative incidence plot for chemotherapy-induced peripheral neuropathy stratified by rs9623812 (A>T) genotype in CALGB 40101(A) and CALGB 40502 (B, paclitaxel; C, nab-paclitaxel; D, ixabepilone). Top left insert displays the entire range of cumulative doses, where the boxed area denotes where ~75% of the data lies and is represented in the larger plot. The number of individuals with each genotype is noted in parentheses. The allele risk for peripheral neuropathy events without other competing events are shown in the plots for CALGB 40502 (B-D).

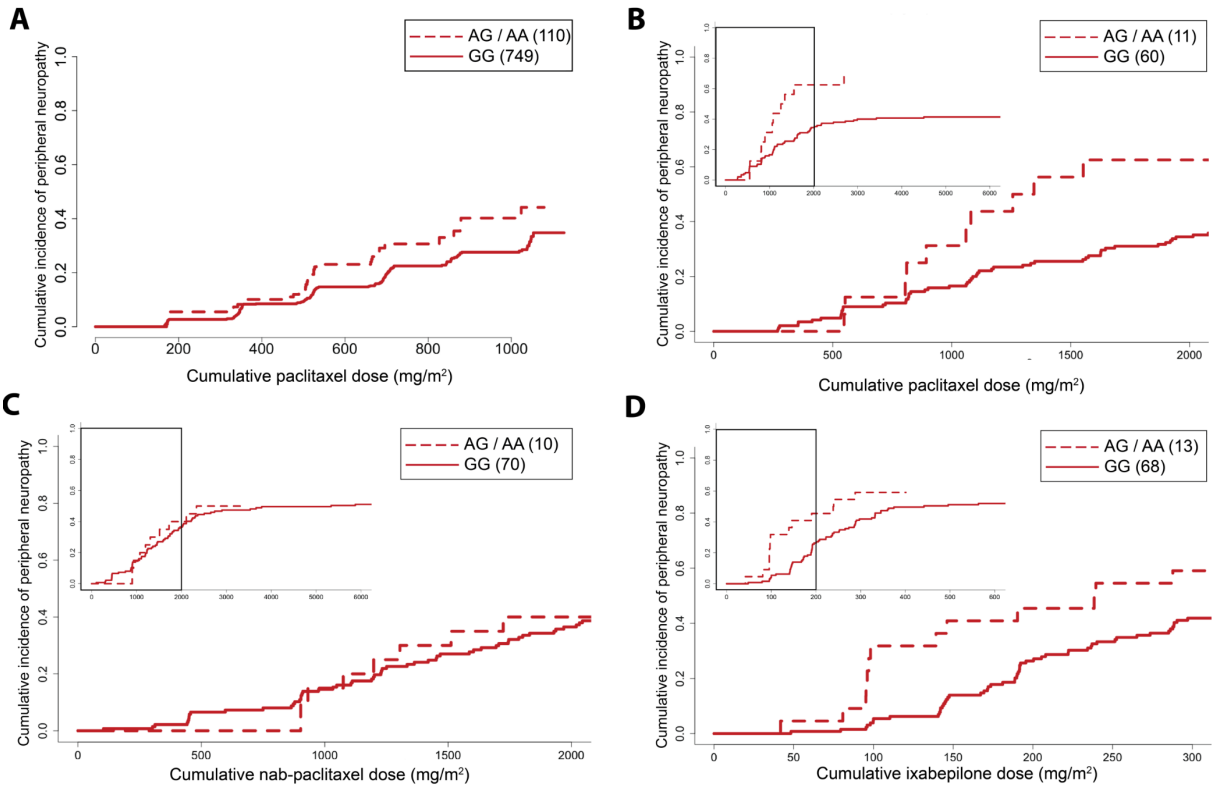

Figure 2.23 Cumulative incidence plot for chemotherapy-induced peripheral neuropathy stratified by rs2060717 (G>A) genotype in CALGB 40101(A) and CALGB 40502 (B, paclitaxel; C, nab-paclitaxel; D, ixabepilone). Top left insert displays the entire range of cumulative doses, where the boxed area denotes where ~75% of the data lies and is represented in the larger plot. The number of individuals with each genotype is noted in parentheses. The allele risk for peripheral neuropathy events without other competing events are shown in the plots for CALGB 40502 (B-D).

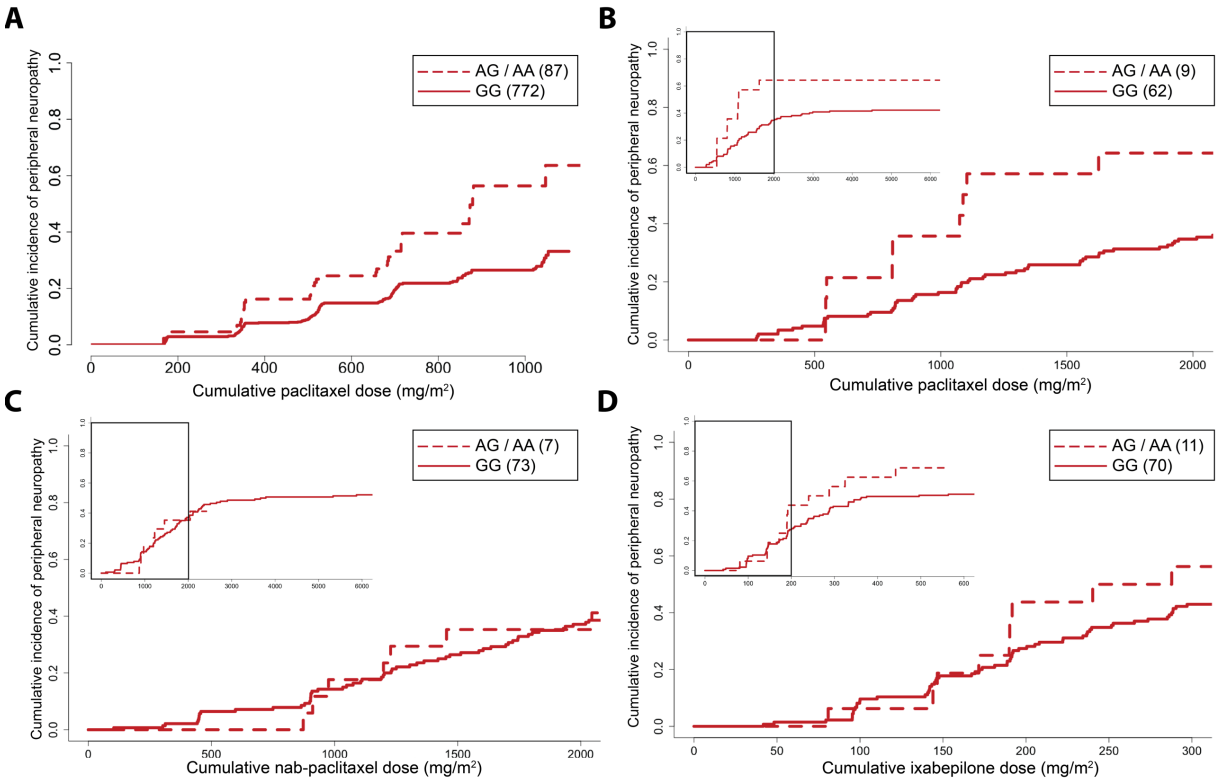

Figure 2.24 Cumulative incidence plot for chemotherapy-induced peripheral neuropathy stratified by rs2188156 (G>A) genotype in CALGB 40101(A) and CALGB 40502 (B, paclitaxel; C, nab-paclitaxel; D, ixabepilone). Top left insert displays the entire range of cumulative doses, where the boxed area denotes where ~75% of the data lies and is represented in the larger plot. The number of individuals with each genotype is noted in parentheses. The allele risk for peripheral neuropathy events without other competing events are shown in the plots for CALGB 40502 (B-D).

Bioinformatic analysis of the genomic regions surrounding the seven SNPs chosen for further analysis was carried out to understand the potential functional effects of genetic variation on gene expression and function; the results from these *in silico* analyses are summarized in Table 2.4. Examination of ENCODE data tracks (UCSC Genome Browser; https://genome.ucsc.edu) identified histone acetylation and methylation marks, DNase peaks, multiple transcription factor binding sites, and predicted functional activity from genome segmentation algorithms within the genomic regions surrounding rs74497159, rs10771973, rs11076190, rs9623812 and rs2060717 (Figures 2.25-2.31). Further evidence that these SNPs are

located in transcriptionally active regions include classification as super-enhancers that interact with multiple genes. In some cases, the predicted enhancer region is expected to directly interact with the annotated gene to control its expression (Table 2.4). For example, a SNP annotated to *S1PR1* (rs74497159) is located downstream of the 3' end of this gene in a super-enhancer region that interacts with *SIPR1*. Similarly, the intronic SNP of *FGD4* (rs10771973) lies adjacent to the last exon within a predicted transcriptional transition or elongation region and interacts directly with *FGD4*.

Figure 2.25 rs74497159 (location denoted by dark red line) lies within a predicted enhancer region 168 kb 3' of *S1PR1* surrounded with multiple active regulatory elements from ENCODE data, including H3K27Ac peaks, multiple transcription factor binding sites, and flanking DNase hypersensitivity/open chromatin peaks.

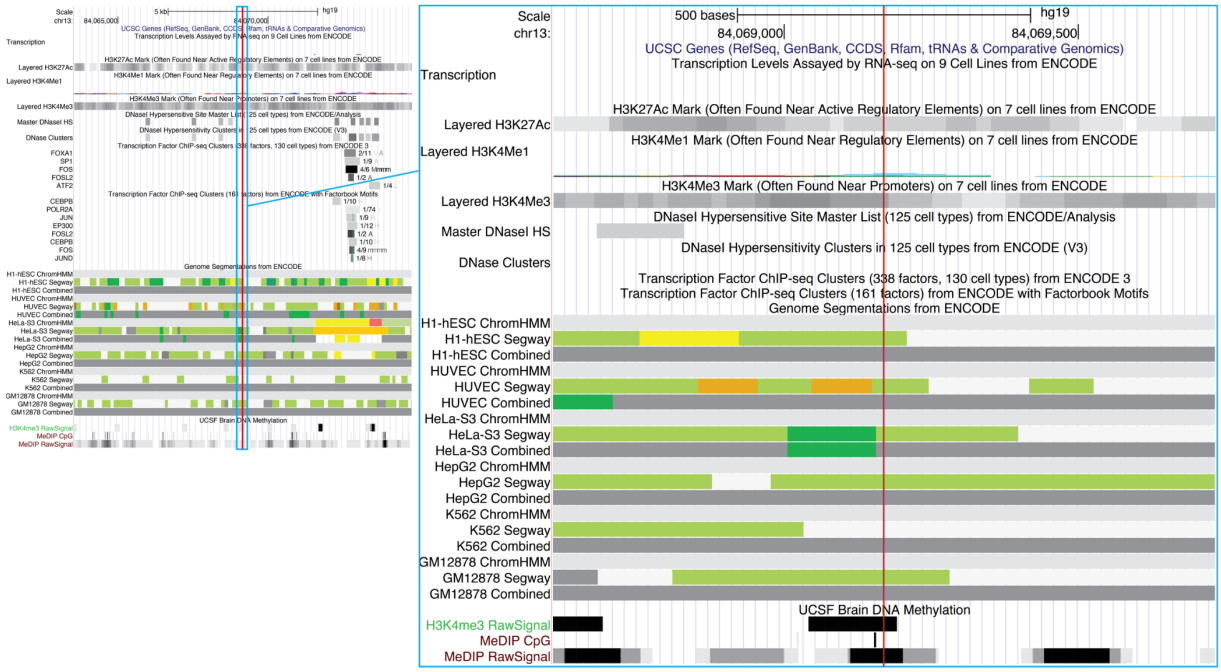

Figure 2.26 rs17076837 (location denoted by dark red line) lies 382 kb 3' of *SLITRK1* within a low activity genomic region based on histone marks, DNase I hypersensitivity and predicted genome segmentations (ChromHMM, Segway, combined algorithms) using ENCODE data.

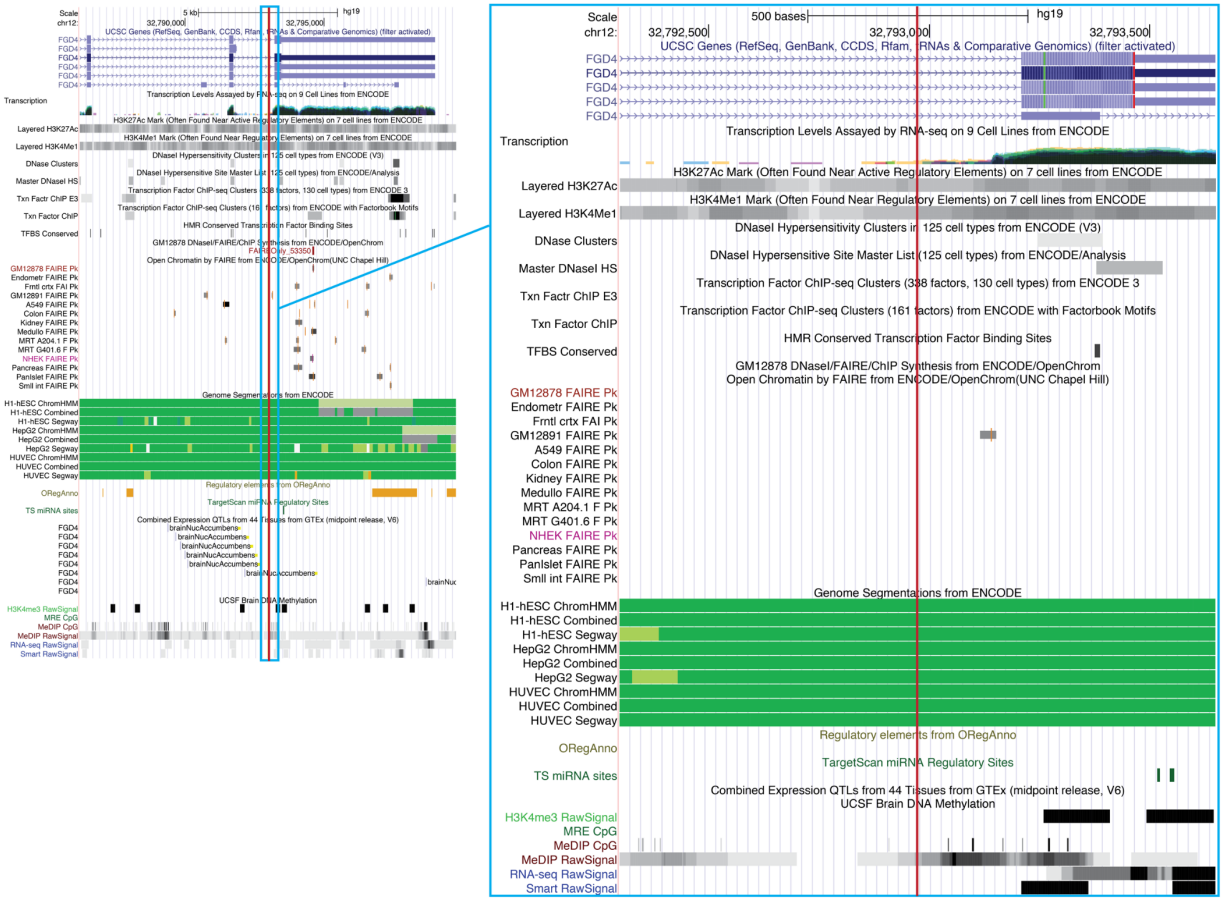

Figure 2.27 Bioinformatic analysis of the genomic region around rs10771973 (location denoted by dark red line) that lies within an intronic region of *FGD4* adjacent to the last exon. This SNP is in a predicted transcriptional elongation region based on ENCODE data.

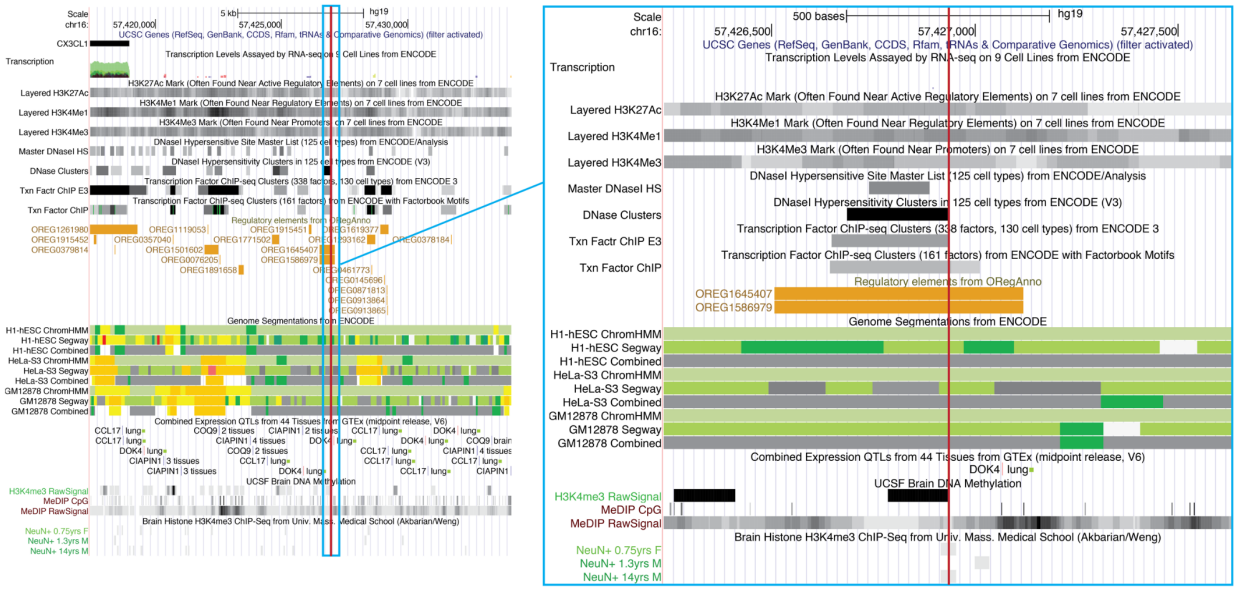

Figure 2.28 rs11076190 (location denoted by dark red line) lies 8 kb 3' of *CX3CL1* within an active transcription factor binding site based on ENCODE data, Open Regulatory Annotation and H3K4me3 peak in young NeuN+ brain samples.

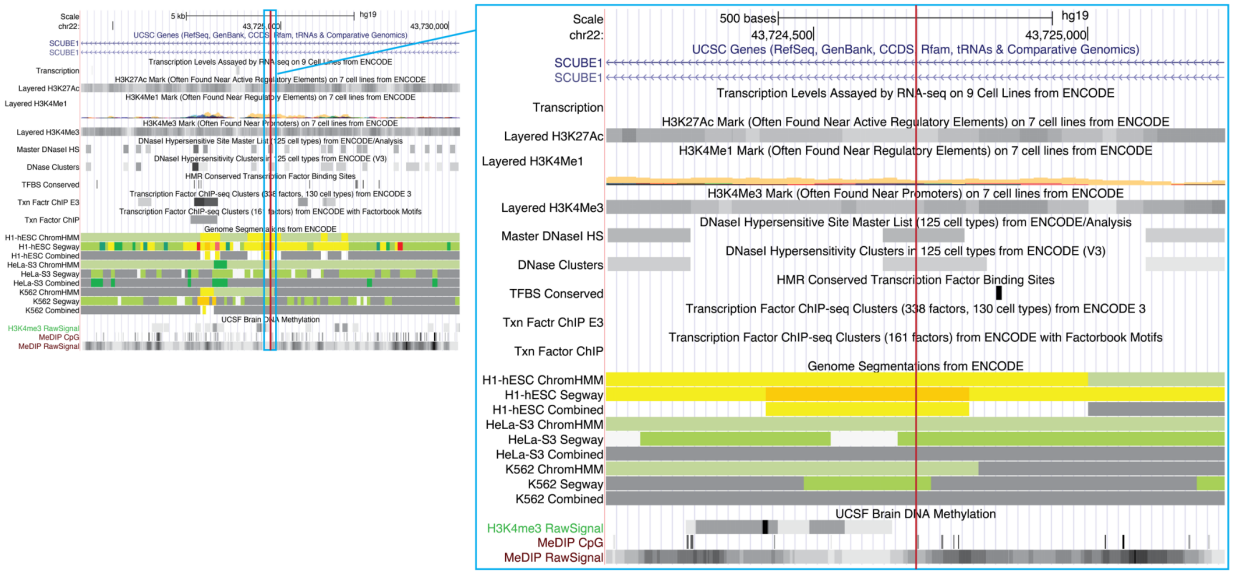

Figure 2.29 rs9623812 (location denoted by dark red line) lies within an intronic region of *SCUBE1* and is predicted to be an active regulatory region based on H3K4 methylation marks, DNAse I hypersensitivity clusters and genome segmentations (ChromHMM, Segway, combined algorithms) using ENCODE data. This regulatory region is predicted to hold enhancer activity in embryonic stem cells (H1-hESC).

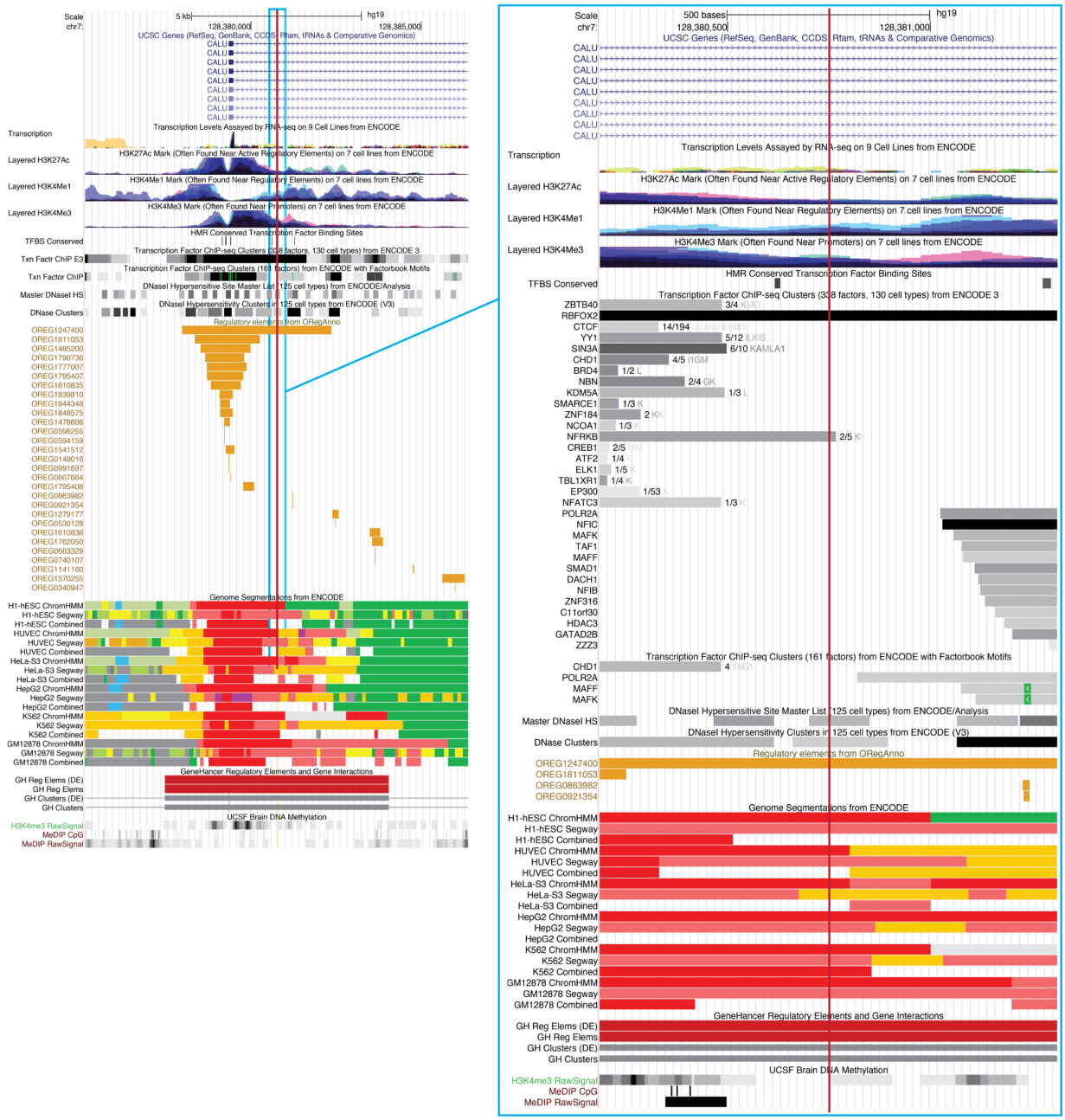

Figure 2.30 rs2060717 (location denoted by dark red line) lies within an intronic region of *CALU* with substantial promoter activity based on H3K27Ac marks, H3K4Me1 marks, H3K4Me3 marks, transcription binding factor sites, DNase I hypersensitivity clusters and genome segmentation predictions (ChromHMM, Segway, combined algorithms) using ENCODE and GeneHancer data.

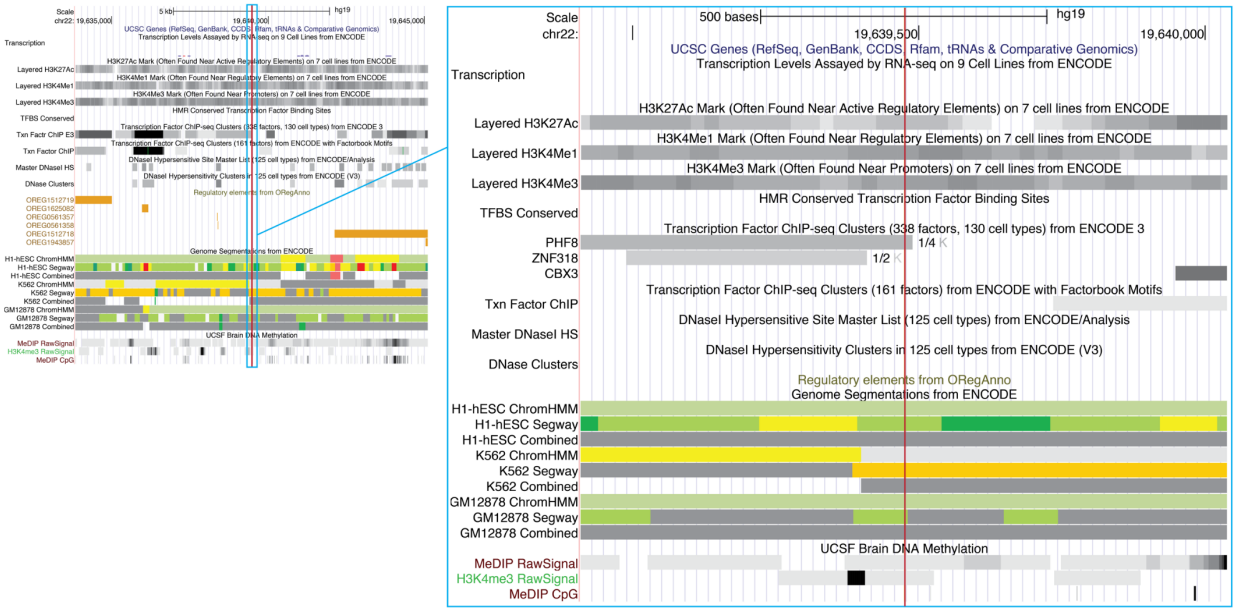

Figure 2.31. rs2188156 (location denoted by dark red line) lies 63 kb 3' of *SEPT5* within a low activity genomic region based on histone marks, DNase I hypersensitivity and predicted genome segmentations (ChromHMM, Segway, combined algorithms) using ENCODE data.

Table 2.4 Summary of *in silico* functional analysis on LD ($r^2 \geq 0.6$) block of rs74497159, rs10771973, rs11076190, rs9623812, and rs2060717

SNP	[a]Gene	[b]SNPs in LD	[#]No. tissues with DNAse peaks	[#]No. tissues with enhancer histone marks		
				H3K27Ac/H3K9Ac	H3K4me1/H3K4me3	ChromHMM 15 core-state
rs74497159	*S1PR1*	21	5	5	14*	6
rs17076837	*SLITRK1*	0	N/A	N/A	N/A	N/A
rs10771973	*FGD4*	42	12	16*	19*	17*
rs11076190	*CX3CL1*	5	6	17*	18*	11
rs9623812	*SCUBE1*	2	2	6	8*	5*
rs2060717	*CALU*	6	6	22*	24*	12*
rs2188156	*SEPT5*	1	N/A	N/A	1	N/A

[#]Promoter and enhancer histone marks, DNAse peaks, and proteins bound are from the Roadmap Epigenomics Consortium 2015 data consolidated and queried from Haploreg v4.1 (https://pubs.broadinstitute.org/mammals/haploreg/haploreg.php). [a]Gene annotated using RefSeq genes. [b]SNPs r^2 with ≥ 0.6. *Includes brain tissue. † Includes tibial nerve.

Table 2.4 (cont.) Summary of *in silico* functional analysis on LD ($r^2 \geq 0.6$) block of rs74497159, rs10771973, rs11076190, rs9623812, and rs2060717

SNP	[a]Gene	[#]No. tissues with promoter histone marks			[#]Proteins bound
		H3K27Ac/H3K9Ac	H3K4me1/H3K4me3	ChromHMM 15 core-state	
rs74497159	*S1PR1*	6	5	1	EBF1, PU1
rs17076837	*SLITRK1*	N/A	N/A	N/A	N/A
rs10771973	*FGD4*	10*	7*	1*	GATA2, CFOS, CJUN
rs11076190	*CX3CL1*	14*	11*	2	P300, EBF1, ELF1, PAX5C20, PAX5N19, TCF12, YY1, NFKB, POL2, ERRA, FOSL2, FOXA1, FOXA2, HDAC2, HNF4A, HNF4G, JUND, RXRA, SP1
rs9623812	*SCUBE1*	6	4*	N/A	N/A
rs2060717	*CALU*	19*	23*	21*	MAFF, MAFK, PU1
rs2188156	*SEPT5*	N/A	1	N/A	N/A

[#]Promoter and enhancer histone marks, DNAse peaks, and proteins bound are from the Roadmap Epigenomics Consortium 2015 data consolidated and queried from Haploreg v4.1 (https://pubs.broadinstitute.org/mammals/haploreg/haploreg.php). [a]Gene annotated using RefSeq genes. *Includes brain tissue. † Includes tibial nerve.

Table 2.4 (cont.) Summary of *in silico* functional analysis on LD ($r^2 \geq 0.6$) block of rs74497159, rs10771973, rs11076190, rs9623812, and rs2060717

SNP	[a]Gene	[‡] eQTL	[‡] sQTL
rs74497159	*S1PR1*	N/A	N/A
rs17076837	*SLITRK1*	N/A	N/A
rs10771973	*FGD4*	*DNM1L*, *FGD4**, *BICD1*, *RP11-278C7.1*	*FGD4*[†] , *DNM1L*
rs11076190	*CX3CL1*	*COQ9* *[†] , *CIAPIN1*, *DOK4*, *FAM192A**	*COQ9*
rs9623812	*SCUBE1*	N/A	N/A
rs2060717	*CALU*	*CICP14*[†] , *FAM71F1*, *RP11-155G14.5*[†] , *RP11-212P7.2**, *RP11-274B21.1*[†] , *RP11-274B21.12*, *RP11-274B21.13*[†] , *RP11-274B21.2*[†] , *RP11-274B21.3*[†] , *RP11-274B21.4 RP11-274B21.2*[†] , *RP11-274B21.9*, *METTL2B*, *CCDC136*	*CCDC136*, *CALU*
rs2188156	*SEPT5*	N/A	N/A

[‡] eQTL and sQTL information was queried from GTEx v8 (https://gtexportal.org/home/). [a]Gene annotated using RefSeq genes. *Includes brain tissue. [†] Includes tibial nerve.

Table 2.4 (cont.) Summary of *in silico* functional analysis on LD ($r^2 \geq 0.6$) block of rs74497159, rs10771973, rs11076190, rs9623812, and rs2060717

SNP	[a]Gene	‡ ‡ Super-enhancer regions detected (tissue)	§ Super-enhancer gene interactions	Previous reports of gene linked to chemotherapy-induced peripheral neuropathy (CIPN)
rs74497159	*S1PR1*	14 (haematopoetic and lymphoid, blood, peripheral blood)	*FRRS1, GPR88, SLC30A7, EXTL2, DPH5, S1PR1, OLFM3, AGL, VCAM1*	Blocking S1PR1 shows reduction in CIPN *in vivo* [40, 41]
rs17076837	*SLITRK1*	N/A	N/A	N/A
rs10771973	*FGD4*	1 (blood)	*METTL20, FGD4, DNM1L*	Variation in *FGD4* have been associated to increased risk of CIPN [9, 14]
rs11076190	*CX3CL1*	27 (pancreas, mammary gland, haematopoetic and lymphoid, oesophagus, embryo, autonomic ganglia, brain, neuroblastoma)	*MT3, HERPUD1, FAM192A, PLLP, ARL2BP, CCL17, CCL22, COQ9, CIAPIN1,*	Anti-CX3CL1 treatments have been shown to reduce macrophage infiltration and initiation of CIPN i*n vivo* [42-44]
rs9623812	*SCUBE1*	4 (esophagus muscularis mucosa, gastroesophageal sphincter, sigmoid colon, neuroblastoma)	*MCAT, EFCAB6, SULT4A1*	N/A
rs2060717	*CALU*	10 (brain and spinal cord, bone, endometrium, ovaries, osteoblastic, skeletal muscle, colon, pectoralis major muscle, other)	*METTL2B, FAM71F2, FAM71F1, CCDC136, OPN1SW, TNPO3*	N/A
rs2188156	*SEPT5*	N/A	N/A	N/A

‡ ‡ Super-enhancer regions are from genetic and epigenetic annotation information analyzed and queried from SEdb v1.03 (http://www.licpathway.net/sedb/). § Super-enhancer gene interactions indicates genes predicted to have interactions with super-enhancer regions. These interactions are derived and queried from HACER (http://bioinfo.vanderbilt.edu/AE/HACER/index.html).
[a]Gene annotated using RefSeq genes. *Includes brain tissue. † Includes tibial nerve.

Interestingly, intronic SNP rs10771973 is significantly associated with splicing quantitative trait loci in tibial nerve tissue (P = 1.2E-11, GTEx[33]), suggesting that this variant may regulate alternative splicing of pre-mRNA levels and affect the overall *FGD4* gene expression. rs11076190 is located in a genomic cluster with several chemokines (Figure 2.28) and is annotated within a FOXA1 transcription factor binding site linked to *CX3CL1* (Open Regulatory Annotation, ORegAnno, track; Figure 2.28). SNPs within linkage disequilibirum with rs10771973 (*FGD4*), rs11076190 (*CX3CL1*) and rs2060717 (*CALU*) are each associated with expression quantitative trait loci and splicing quantitative trait loci, indicating potential relevance for regulation of gene expression. In contrast, there is little evidence that rs17076837 annotated downstream of the 3' end of *SLITRK1* (Figure 2.26) or a SNP (rs2188156) annotated upstream of the 5' end of *SEPT5* (Figure 2.31) lie within regulatory regions.

While the bioinformatic analysis highlights the potential functional activity for five SNPs of interest, the annotated genes from three of the five SNPs (rs74497159/*SIPR1*, rs10771973/*FGD4*, and rs11076190/*CX3CL1*) are linked to CIPN (Table 2.4). For functional validation, we focused on the gene annotated to the genomic region with the highest ranking based on P-value for association to MTA-induced peripheral neuropathy from our genome-wide meta-analysis, *S1PR1*. Since rs74497159 is annotated to the *S1PR1* gene and this SNP and others in linkage disequilibrium are in a super-enhancer region that controls the expression of *S1PR1*, the effect of modulation of $S1PR_1$ functional activity was tested in human iPSC-SNs.

The human iPSC-SNs were generated following a published protocol and yield neurons expressing expected nociceptor markers[37]. Based on paclitaxel dose-response studies, paclitaxel treatment (1 μM) for 48 hours in the iPSC-SNs had no significant effect on caspase-3/7 activity and decreased cellular ATP levels by <30%, indicating limited cytotoxicity under the conditions

used (data not shown). Drug-induced neurotoxicity is phenotypically characterized by a distinctive loss of neurites and a reduction in neurite network complexity without a decrease in total cell count (Figure 2.32-2.34), which was quantified by total neurite area stained for βIII-tubulin and number of DAPI-stained nuclei. There was no significant effect of any treatment on cell numbers, consistent with limited cytotoxicity from paclitaxel and other chemicals. Treatment with 1 μM paclitaxel alone resulted in more than 50% decrease in neurite staining (49-64% reduction, $P < 0.01$; Figure 2.32) compared to vehicle-treated sensory neurons, demonstrating paclitaxel-induced damage to the overall neurite networks. Treatment with 1 μM S1PR functional antagonist FTY720 (0.3-29% reduction) and 1 μM S1PR1 antagonist W146 (0.6-14% reduction) had little to no effect on neurite area (Figures 2.32 and 2.33). Combined treatment of the iPSC-SNs with paclitaxel and FTY720 resulted in partial protection against paclitaxel-induced neuronal damage (33-55% increase in neurite area relative to paclitaxel treatment, $P < 0.05$) (Figures 2.32 and 2.33). The combination of paclitaxel and W146 had minimal effect on the paclitaxel-induced loss of neurite area (4-21% increase in neurite area relative to paclitaxel treatment; Figures 2.32 and 2.33).

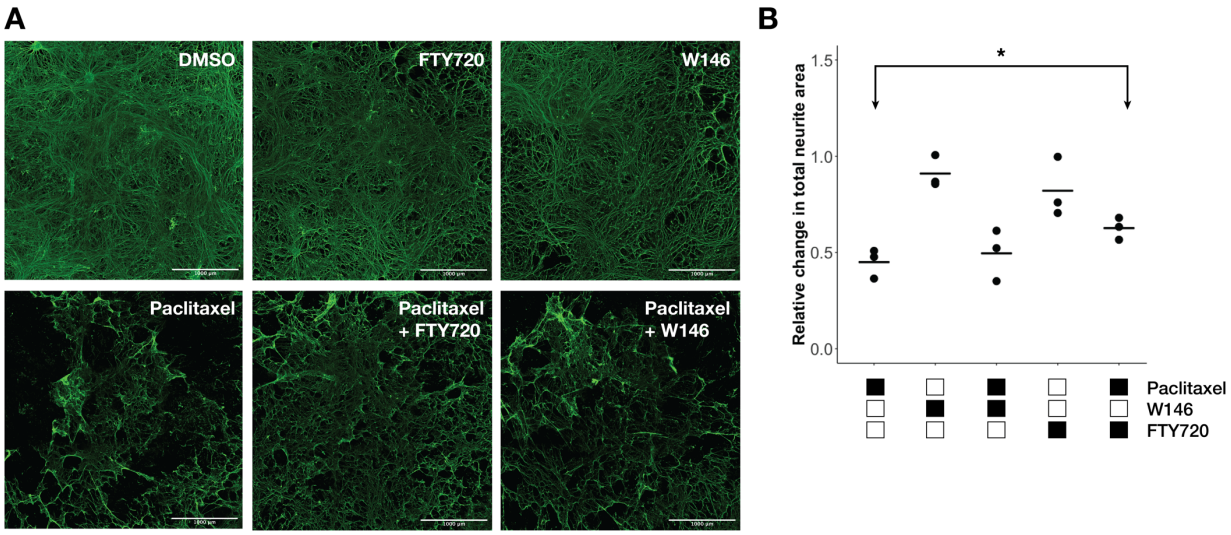

Figure 2.32 Inhibition of S1PR signaling attenuates paclitaxel-induced neuronal damage. (A) Representative per-well images of differentiated sensory neurons (D35+) derived from induced pluripotent stem cells used to investigate S1PR signaling in paclitaxel-induced neuronal damage. Differentiated neurons were treated with 1 μM paclitaxel for 48 hours in the absence and presence of a S1PR1 inhibitor (W146; 1 μM) or a S1PR1 functional antagonist (FTY720; 1 μM). The cells are stained for βIII tubulin and staining was quantified as total neurite area. All images shown are from a single experiment. Scale bar indicates 1 mm. (B) Quantification of mean total neurite area from βIII tubulin staining after drug treatments in three independent differentiations. Each data point represents the mean measurement of 6-8 replicates from a single independent differentiation and is expressed relative to vehicle controls. The coefficient of variation in vehicle-treated neurites ranges from 11-24%. Raw values used to calculate the means are shown in Figure 2.33. Relative mean neurite areas were tested for differences across treatments by one-way ANOVA (P = 6E-05) with post-hoc comparisons using unpaired, two-sided Student's *t* test (*P < 0.05).

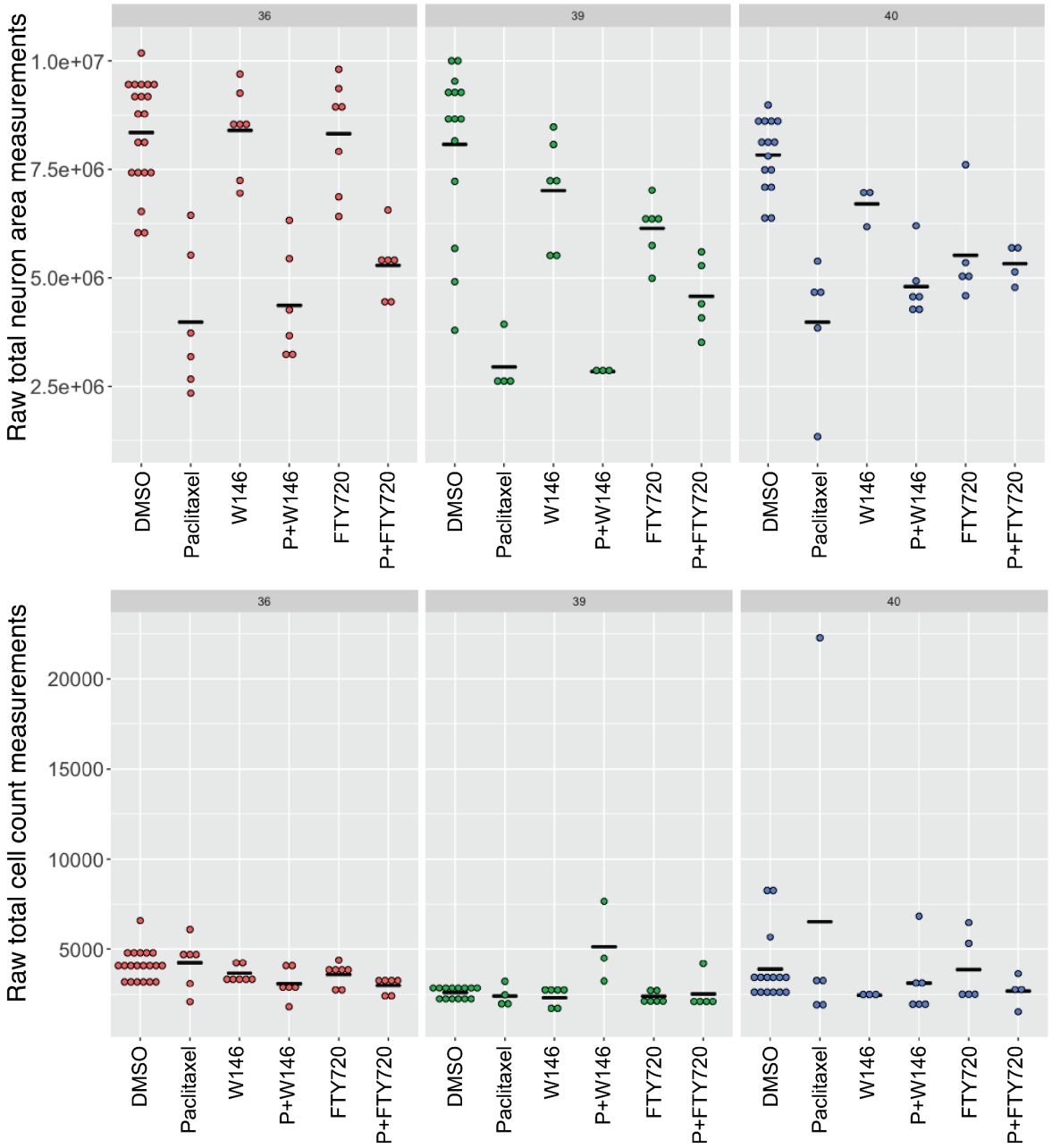

Figure 2.33. Raw measurements of total neurite area (top panel) and total cell count (bottom panel) separated by each independent experiment. Mean measurements for each condition are displayed as the black horizontal lines.

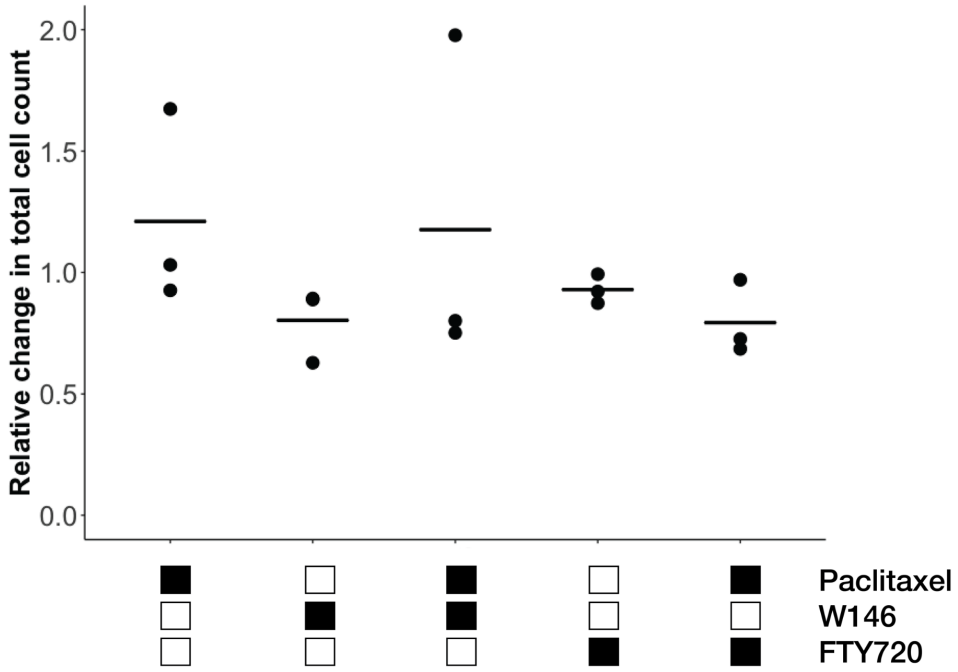

Figure 2.34. Quantification of mean total cell counts from DAPI-staining of nuclei after drug treatments in three independent experiments. Each data point represents the mean measurement of 6-8 replicates from a single independent differentiation and expressed relative to vehicle controls. The coefficient of variation in vehicle-treated cells ranges from 2-9%. Raw values used to calculate the means are shown in Figure 2.33. Relative mean cell counts were tested for differences across drug conditions by one-way ANOVA; no significant differences were seen ($P = 0.552$).

DISCUSSION

We identified multiple SNPs that implicate genes that may be relevant to MTA-induced sensory peripheral neuropathy, even though no SNP associations achieved genome-wide significance. Because the study scope focuses on sensory neuronal mechanisms involved in MTA-induced PN, seven independent SNP associations, whose nearest gene shows expression in human DRG[38], were prioritized for *in silico* functional analysis to determine if the SNP lies in a potential regulatory genomic region. Three of the seven SNPs (rs74497159, rs10771973, rs11076190) had the strongest *in silico* evidence for predicted functional activity with previous reports linking their annotated genes (*S1PR1*[40,41], *FGD4*[9,14] and *CX3CL1*[42–44]) to chemotherapy-induced neurotoxicity.

Among the three genomic regions identified from the primary meta-analysis, the highest-ranking association based on P-values revealed the genomic region in chromosome 1 annotated to *S1PR1,* a gene that encodes for sphingosphine-1-phosphate receptor 1 ($S1PR_1$). $S1PR_1$ is a member of a G-coupled receptor family that is known for its roles in cell proliferation, migration and differentiation[45]. $S1PR_1$ has been shown to be directly involved in mediating inflammatory responses through activation with its signaling ligand sphingosphine-1 phosphate (S1P), which has been targeted for autoimmunity diseases such as multiple sclerosis[46], psoriasis[47], and chronic inflammatory neuropathy[48]. Most notably in peripheral neurons, the S1P-to-$S1PR_1$ axis has been associated with increased neuronal excitability[49], reduction in neuronal growth through Rho GTPase signaling[50], and increased hyperalgesia[51] and other pain-like behaviors[52–55]. The association of $S1PR_1$ G-coupled receptor signaling with Rho GTPase-mediated signaling in peripheral neurons is noteworthy since other genes involved in RhoA signaling have been previously implicated in genome-wide and sequencing studies of MTA-induced PN[9–11,56–58]. In

this study, the leading SNP annotated to *S1PR1* had the highest-ranking association based on P-values with a higher risk of peripheral neuropathy regardless of which MTA was administered. Additionally, this genomic region is encompassed in a functionally predicted enhancer region that may be acting directly on $S1PR_1$ expression. Alongside these results and recent evidence highlighting $S1PR_1$ as a drug target for prevention of chemotherapy-induced neuropathic pain *in vivo*[40,41], functional studies were focused on investigating if modulating $S1PR_1$ function in sensory neurons would protect against MTA-induced damage.

Functional studies were performed using a human iPSC-derived sensory neuronal model that displays paclitaxel-induced neurodegeneration. The addition of the $S1PR_1$ functional antagonist fingolimod (FTY720) to paclitaxel in these sensory neurons attenuates paclitaxel-induced neurotoxicity with similar effect sizes as previous functional validation studies in cellular models of chemotherapy-induced neuronal damage [12,59–61]. Additionally, functional antagonists of $S1PR_1$ have consistently alleviated CIPN and other pain-like symptoms *in vitro* and *in vivo*[40,41,62–64], and have led to recent phase I clinical trials investigating the use of fingolimod to prevent and treat chemotherapy-induced neuropathy (NCT03943498, NCT03941743). While studies have also shown treatment with the $S1PR_1$ antagonist W146 mitigate paclitaxel-induced neuropathic pain[40] and S1P-induced hypersensitivity and thermal sensitivity *in vivo*[40,51], minimal effect is observed with W146 treatment in the current *in vitro* studies. Since previous studies have primarily focused on targeting $S1PR_1$ in the spinal cord and have implicated its role as astrocyte-specific[40,41], it is possible that a decrease in $S1PR_1$ expression from internalization and degradation[65] is essential to mitigate the effects of paclitaxel in peripheral neurons. This need for degradation may explain why only blocking $S1PR_1$[66] does not have the same pronounced protective effect. Interestingly, activation of $S1PR_3$ may also be

involved in sensory neurite retraction, nociceptor excitability, and pain-like symptoms[49,62,67]. FTY720 has also been shown to bind to $S1PR_3$ and other receptors[65], although its functional activity is largely attributed to $S1PR_1$ binding[68]. While expression of both $S1PR_1$ and $S1PR_3$ are known in primary DRG[69] and iPSC-derived sensory neurons used in these studies (Figure 2.35), the exact role of these receptors in sensory peripheral neuropathy is not yet clear. These functional studies are the first step in understanding the role of $S1PR_1$ signaling in peripheral sensory nociceptors under chemotherapy exposure and warrant further investigation to fully elucidate the role of sphingosine signaling in MTA-induced neuropathy.

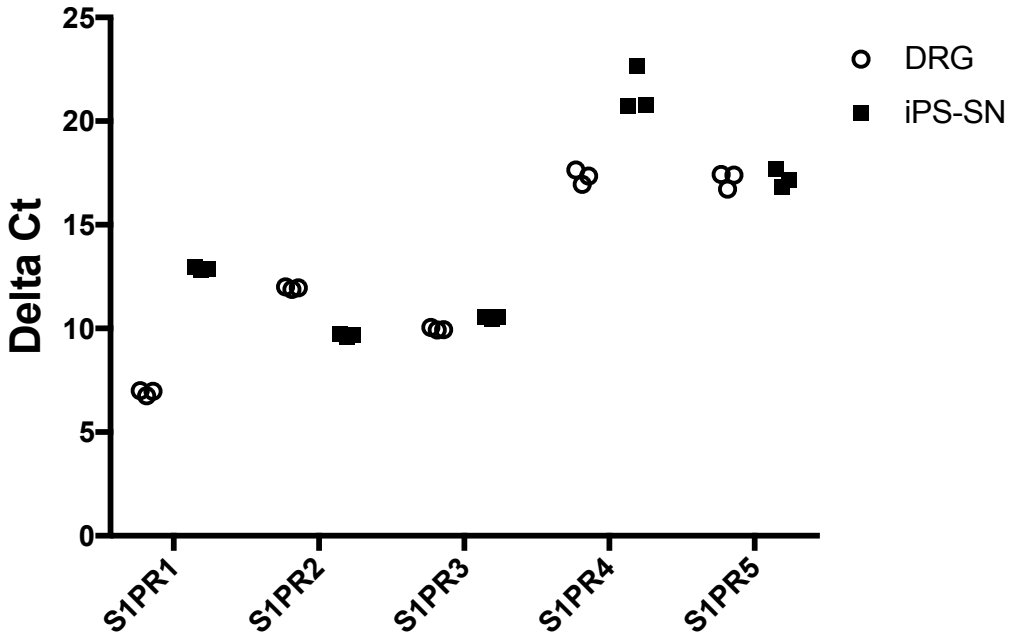

Figure 2.35 Sphingosphine-1-phosphate receptor expression in iPSC-derived sensory neurons compared with human DRG. Each data point represents raw ΔCt value for one experimental replicate. ΔCt values were calculated by normalizing the Ct value of each gene with the Ct value of actin (mean $Ct_{actin,DRG}$ = 15.90, mean $Ct_{actin,iPSC\text{-}SN}$ = 14.24). High ΔCt values correspond to low mRNA expression levels.

This genome-wide association study has also highlighted SNPs in a genomic region near *CX3CL1* and other chemokine genes. The top SNP (rs11076190) in this region lies just downstream of *CX3CL1*, encoding for a small chemokine ligand fractalkine (CX_3CL_1) that

exclusively binds to CX_3CR_1 on lymphocytes. Paclitaxel treatment in pre-clinical models has been shown to increase levels of monocyte infiltration and inflammatory macrophage activation within peripheral nerves through CX_3CL_1-CX_3CR_1 crosstalk, releasing pro-inflammatory cytokines (TNF-α, IL-1β) and initiating peripheral neuropathic pain[70]. However, recent work by Yu et al. has demonstrated that nerve injury signals the local expansion of $CX3CR1^+$ macrophages within the DRG itself and these DRG resident macrophages are responsible for neuropathic pain *in vivo*[71]. Additionally, previous work suggests that increased recruitment of transcription factors (i.e., NF-κB) to the *CX3CL1* promoter region is heightened in *in vivo* models of CIPN[43]. Since rs11076190 is in a predicted transcription factor binding site and potential promoter, it may modulate the contribution of CX_3CL_1 to this toxicity. Interestingly, rs223828 in complete LD with rs11076190 is located within an intronic transcription factor binding-rich region of *CCL17*, a gene that encodes for a small cytokine that has been shown to mediate granulocyte-macrophage-colony stimulating factor-dependent inflammatory pain that causes osteoarthritis[72] and multiple sclerosis[73]. While little is known about the interaction between *CX3CL1* and *S1PR1*, their robust roles in signaling downstream cytokine release (e.g., TNF-α, IL-1β) that results in peripheral neuropathic pain suggests that regulation of neuroimmune interactions is important to the clinical symptoms in the periphery, and further validation may allow for interesting strategies to monitor CIPN.

The intronic SNP rs10771973 of *FGD4* was in the top SNPs from the meta-analysis and was the only variant identified in the previous GWAS in CALGB 40101 that remained in this meta-analysis[9]. Of note, *FGD4* is a critical gene for peripheral nerve development[74] and a known causal gene of Charcot-Marie-Tooth subtype 4H, which is characterized by distal muscle weakness, severe foot deformities, sensory weakness or loss, and gait instability[75]. With this

prior knowledge, it is conceivable that those harboring common genetic variation in *FGD4* may be more susceptible to peripheral neurotoxicity upon drug exposure. Importantly, in another genetic association study in an independent population rs10771973 was linked with increased risk of paclitaxel dose reductions[14]. Investigation of the effects of paclitaxel on *FGD4* function in peripheral sensory neurons warrants further investigation.

While only three of the seven genomic regions associated with MTA-induced peripheral neuropathy have been previously recognized to play a role in CIPN, other genomic regions may also be important for unveiling biological mechanisms underlying this toxicity. rs17076837 and rs2188156 annotate to *SLITRK1* and *SEPT5*, respectively, which are highly expressed in human DRG and are associated with neuronal function. SLITRK1 has been shown to be involved in regulating synaptic formation after axonal growth to its target area in hippocampal neurons[76] while SEPT5 is a member of a highly conserved family of GTP binding proteins that regulates cytoskeletal reorganization in neurons[77]. However, there is limited evidence that these intergenic SNPs are enriched for regulatory activity to these annotated genes. In contrast, rs2060717 lies in a highly predicted promoter site within an intronic region of *CALU*, a gene that encodes for calcium-binding protein calumenin which localizes to the endoplasmic reticulum with potential roles in early neuronal development[78]. Lastly, rs9623812 lies in a potential enhancer site within an intronic region of *SCUBE1*, encoding for a cell surface glycoprotein that is secreted during brain injury[79]. Further studies are needed to understand the roles of these genes in sensory neurons and may lead to novel mechanisms of MTA-induced PN.

While this pharmacogenetic study using human genomic and cellular data has identified potential genes that have a translatable relevance to the CIPN phenotype, there are several limitations. Although a total of 1,324 samples from the discovery cohorts was used in the meta-

analysis, the pharmacogenetic study presented is still insufficiently powered and increasing sample size may provide a more robust analysis. The main limitation is genetic validation of our top-ranking SNPs. None of the top-ranking SNPs ($P < 10^{-5}$) from our meta-analysis were replicated in the taxane-treated ECOG-5103 European cohort[57] or in the UK BioBank (Tables 2.5 and 2.6). In the case of ECOG-5103, paclitaxel treatment is different from both CALGB 40502 and CALGB 40101 and this sample was also limited by size. While the UK BioBank is proving to be a useful resource for replication of genetic associations with common phenotypes, the largest number of drug-induced polyneuropathy cases identified was 122 subjects for two ICD9 codes classified as "polyneuropathy due to drugs" and "polyneuropathy due to toxic agents".

Table 2.5 Results from candidate SNP association analysis in ECOG-5103 replication European cohort (n=1,348)

SNP*	Chr	Alleles[a]	Gene	SNP (r^2)†	MAF	Effect	*P*
rs12402160	1	C>T	178 kb 3' of *S1PR1*	rs74497159 (0.7)	0.100	-0.283	0.0098
rs223828	16	T>C	intronic region of *CCL17*	rs11076190 (1.0)	0.051	-0.216	0.098
rs2060717	7	G>A	intronic region of *CALU*	–	0.059	0.110	0.41
rs1894716	22	G>A	intronic region of *SCUBE1*	rs9623812 (0.97)	0.305	-0.045	0.49
rs11831099	12	C>T	intronic region of *FGD4*	rs10771973 (0.98)	0.316	0.028	0.65

SNP, single nucleotide polymorphism; Chr, chromosome; MAF, minor allele frequency
*SNPs listed are LD-pruned to show the top-ranking SNP by *P* value of replication analysis
[a]Alleles are denoted Ref>Alt
†Linkage disequilibrium r^2 with SNPs from primary meta-analysis (Table 2.3)

Table 2.6 Results from candidate SNP association analysis in UK BioBank replication (n=122)

SNP*	Chr	Alleles[a]	Gene	SNP (r^2)†	MAF	Effect	*P*
rs76464064	7	C>T	107 kb 3' of *SUGCT*	rs78017515 (0.96)	0.074	0.843	0.044
rs74497159	1	T>G	168 kb 3' of *S1PR1*	–	0.072	0.653	0.092
rs57940640	16	G>A	intronic region of *CNGB1*	–	0.069	-0.416	0.094
rs10844261	12	A>G	intronic region of *FGD4*	rs10771973 (0.93)	0.302	0.261	0.130
rs223828	16	C>T	intronic of *CCL17*	rs11076190 (1.0)	0.047	-0.570	0.211
rs2342796	8	T>C	7.5 kb 5' of *ZFPM2*	rs2342791 (0.77)	0.165	-0.180	0.404
rs9623812	22	A>T	intronic region of *SCUBE1*	–	0.329	-0.116	0.454
rs13168251	5	T>G	718 kb 3' of *LOC100129716*	–	0.099	0.200	0.459
rs77526807	9	G>T	39 kb 3' of *C9orf106*	–	0.064	0.252	0.461
rs10281585	7	T>G	75 kb 3' of *SUGCT*	rs78777495 (0.91)	0.115	0.165	0.509
rs2342780	8	A>T	68 kb 5' of *ZFPM2*	–	0.070	-0.197	0.547
rs1083337	6	G>A	490 kb 5' of *ADGRB3*	rs777619 (0.99)	0.201	0.105	0.586
rs2060717	7	G>A	intronic region of *CALU*	–	0.051	0.120	0.741
rs17076837	13	C>G	382 kb 3' of *SLITRK1*	–	0.120	-0.073	0.748
rs6788186	3	C>T	696 kb of 3' *ZBBX*	–	0.268	0.048	0.772

SNP, single nucleotide polymorphism; Chr, chromosome; MAF, minor allele frequency
*SNPs listed are LD-pruned to show the top-ranking SNP by *P* value of replication analysis
[a]Alleles are denoted Ref>Alt
†Linkage disequilibrium r^2 with SNPs from primary meta-analysis (Table 2.3)

The other main limitation is the use of NCI-CTCAE grading for phenotyping peripheral neuropathy events, which has been shown to underestimate the progression of neuropathy symptoms[80,81] and embody inconsistency in scale interpretation[82]. It is likely that phenotyping a combination of patient-reported and physician-reported outcomes will yield more comprehensive

information. Lastly, our functional studies were limited to studying effects of $S1PR_1$ in sensory neurons and did not investigate potential cross-talk between neurons and other cell types in the periphery. As CX_3CL_1 and $S1PR_1$ both play predominant roles in peripheral lymphocytes, it is possible that their effects on paclitaxel-induced damage to peripheral nerves are initiated by external cues from other cell types. This phenomenon is true with *FGD4*, where the interplay of the frabin (*FGD4*)-Cdc42 Rho GTPase axis in Schwann cells causes peripheral nerve demyelination in CMT4H[83]. Additionally, other genes identified by this genome-wide study (e.g., *CALU*, *SCUBE1*) not functionally explored also warrant further studies to investigate their roles in peripheral neurons, which may reveal interesting mechanisms underlying MTA-induced neuropathy.

In conclusion, this genome-wide association meta-analysis has identified potential genetic markers of MTA-induced peripheral neuropathy. This pharmacogenetic study highlights the importance of $S1PR_1$ receptor signaling from a genome-wide discovery analysis using clinical samples and functional validation using human iPSC-derived sensory neurons. Of note, $S1PR_1$ signaling functionally intersects between both Rho-GTPase signaling and neuroinflammation, which have been well-documented to play roles in MTA-induced peripheral neuropathy. Further genomic and functional validation of sphingosine-1-phosphate signaling may lead to a novel and exciting strategy for prevention and/or treatment of chemotherapy-induced neuropathy.

REFERENCES

1. Dumontet, C. & Jordan, M. A. Microtubule-binding agents : a dynamic field of cancer therapeutics. **9**, (2010).
2. Esserman, L. J., Berry, D. A., Cheang, M. C. U., Yau, C., Perou, C. M., Carey, L., De Michele, A., Gray, J. W., Conway-Dorsey, K., Lenburg, M. E., Buxton, M. B., Davis, S. E., Van't Veer, L. J., Hudis, C., Chin, K., Wolf, D., Krontiras, H., Montgomery, L., Tripathy, D., *et al.* Chemotherapy response and recurrence-free survival in Neoadjuvant breast cancer depends on biomarker profiles: Results from the I-SPY 1 TRIAL (CALGB 150007/150012; ACRIN 6657). *Breast Cancer Res. Treat.* **132**, 1049–1062 (2012).
3. Han, Y. & Smith, M. T. Pathobiology of cancer chemotherapy-induced peripheral neuropathy (CIPN). *Front. Pharmacol.* **4 DEC**, 1–16 (2013).
4. Lee, J. J. & Swain, S. M. Peripheral neuropathy induced by microtubule-stabilizing agents. *J. Clin. Oncol.* **24**, 1633–1642 (2006).
5. Cliff, J., Jorgensen, A. L., Lord, R., Azam, F., Cossar, L., Carr, D. F. & Pirmohamed, M. The molecular genetics of chemotherapy–induced peripheral neuropathy: A systematic review and meta-analysis. *Crit. Rev. Oncol. Hematol.* **120**, 127–140 (2017).
6. Hershman, D. L., Weimer, L. H., Wang, A., Kranwinkel, G., Brafman, L., Fuentes, D., Awad, D. & Crew, K. D. Association between patient reported outcomes and quantitative sensory tests for measuring long-term neurotoxicity in breast cancer survivors treated with adjuvant paclitaxel chemotherapy. *Breast Cancer Res. Treat.* **125**, 767–774 (2011).
7. Tanabe, Y., Hashimoto, K., Shimizu, C., Hirakawa, A., Harano, K., Yunokawa, M., Yonemori, K., Katsumata, N., Tamura, K., Ando, M., Kinoshita, T. & Fujiwara, Y. Paclitaxel-induced peripheral neuropathy in patients receiving adjuvant chemotherapy for

breast cancer. *Int. J. Clin. Oncol.* **18**, 132–138 (2013).

8. Hershman, D. L., Lacchetti, C., Dworkin, R. H., Lavoie Smith, E. M., Bleeker, J., Cavaletti, G., Chauhan, C., Gavin, P., Lavino, A., Lustberg, M. B., Paice, J., Schneider, B., Smith, M. Lou, Smith, T., Terstriep, S., Wagner-Johnston, N., Bak, K. & Loprinzi, C. L. Prevention and management of chemotherapy-induced peripheral neuropathy in survivors of adult cancers: American society of clinical oncology clinical practice guideline. *J. Clin. Oncol.* **32**, 1941–1967 (2014).
9. Baldwin, R. M., Owzar, K., Zembutsu, H., Chhibber, A., Kubo, M., Jiang, C., Watson, D., Eclov, R. J., Mefford, J., McLeod, H. L., Friedman, P. N., Hudis, C. A., Winer, E. P., Jorgenson, E. M., Witte, J. S., Shulman, L. N., Nakamura, Y., Ratain, M. J. & Kroetz, D. L. A genome-wide association study identifies novel loci for paclitaxel-induced sensory peripheral neuropathy in CALGB 40101. *Clin. Cancer Res.* **18**, 5099–5109 (2012).
10. Leandro-García, L. J., Inglada-Pérez, L., Pita, G., Hjerpe, E., Leskelä, S., Jara, C., Mielgo, X., González-Neira, A., Robledo, M., Avall-Lundqvist, E., Gréen, H. & Rodríguez-Antona, C. Genome-wide association study identifies ephrin type A receptors implicated in paclitaxel induced peripheral sensory neuropathy. *J. Med. Genet.* **50**, 599–605 (2013).
11. Beutler, A. S., Kulkarni, A. A., Kanwar, R., Klein, C. J., Therneau, T. M., Qin, R., Banck, M. S., Boora, G. K., Ruddy, K. J., Wu, Y., Smalley, R. L., Cunningham, J. M., Le-Lindqwister, N. A., Beyerlein, P., Schroth, G. P., Windebank, A. J., Züchner, S. & Loprinzi, C. L. Sequencing of charcot-marie-tooth disease genes in a toxic polyneuropathy. *Ann. Neurol.* **76**, 727–737 (2014).
12. Hertz, D. L., Owzar, K., Lessans, S., Wing, C., Jiang, C., Kelly, W. K., Patel, J., Halabi, S., Furukawa, Y., Wheeler, H. E., Sibley, A. B., Lassiter, C., Weisman, L., Watson, D.,

Krens, S. D., Mulkey, F., Renn, C. L., Small, E. J., Febbo, P. G., *et al.* Pharmacogenetic discovery in CALGB (alliance) 90401 and mechanistic validation of a VAC14 polymorphism that increases risk of docetaxel-induced neuropathy. *Clin. Cancer Res.* **22**, 4890–4900 (2016).

13. Apellaniz-Ruiz, M., Tejero, H., Inglada-Perez, L., Sanchez-Barroso, L., Gutierrez-Gutierrez, G., Calvo, I., Castelo, B., Redondo, A., García-Donas, J., Romero-Laorden, N., Sereno, M., Merino, M., Curras-Freixes, M., Montero-Conde, C., Mancikova, V., Åvall-Lundqvist, E., Green, H., Al-Shahrour, F., Cascon, A., *et al.* Targeted sequencing reveals low-frequency variants in EPHA genes as markers of paclitaxel-induced peripheral neuropathy. *Clin. Cancer Res.* **23**, 1227–1235 (2017).

14. Lam, S. W., Frederiks, C. N., Van Der Straaten, T., Honkoop, A. H., Guchelaar, H. J. & Boven, E. Genotypes of CYP2C8 and FGD4 and their association with peripheral neuropathy or early dose reduction in paclitaxel-treated breast cancer patients. *Br. J. Cancer* **115**, 1335–1342 (2016).

15. Boora, G. K., Kulkarni, A. A., Kanwar, R., Beyerlein, P., Qin, R., Banck, M. S., Ruddy, K. J., Pleticha, J., Lynch, C. A., Behrens, R. J., Züchner, S., Loprinzi, C. L. & Beutler, A. S. Association of the Charcot–Marie–Tooth disease gene ARHGEF10 with paclitaxel induced peripheral neuropathy in NCCTG N08CA (Alliance). *J. Neurol. Sci.* **357**, 35–40 (2015).

16. Rugo, H. S., Barry, W. T., Moreno-Aspitia, A., Lyss, A. P., Cirrincione, C., Leung, E., Mayer, E. L., Naughton, M., Toppmeyer, D., Carey, L. A., Perez, E. A., Hudis, C. & Winer, E. P. Randomized phase III trial of paclitaxel once per week compared with nanoparticle albumin-bound nab-paclitaxel once per week or ixabepilone with

bevacizumab as first-line chemotherapy for locally recurrent or metastatic breast cancer: CALGB 40502/NCCTG N0. *J. Clin. Oncol.* **33**, 2361–2369 (2015).

17. Shulman, L. N., Berry, D. A., Cirrincione, C. T., Becker, H. P., Perez, E. A., O'Regan, R., Martino, S., Shapiro, C. L., Schneider, C. J., Kimmick, G., Burstein, H. J., Norton, L., Muss, H., Hudis, C. A. & Winer, E. P. Comparison of doxorubicin and cyclophosphamide versus single-agent paclitaxel as adjuvant therapy for breast cancer in women with 0 to 3 positive axillary nodes: CALGB 40101 (alliance). *J. Clin. Oncol.* **32**, 2311–2317 (2014).
18. Das, S., Forer, L., Schönherr, S., Sidore, C., Locke, A. E., Kwong, A., Vrieze, S. I., Chew, E. Y., Levy, S., McGue, M., Schlessinger, D., Stambolian, D., Loh, P. R., Iacono, W. G., Swaroop, A., Scott, L. J., Cucca, F., Kronenberg, F., Boehnke, M., *et al.* Next-generation genotype imputation service and methods. *Nat. Genet.* **48**, 1284–1287 (2016).
19. R Core Team. R: A language and environment for statistical computing. (2016).
20. Aulchenko, Y. S., Ripke, S., Isaacs, A. & van Duijn, C. M. GenABEL: An R library for genome-wide association analysis. *Bioinformatics* **23**, 1294–1296 (2007).
21. Therneau, T. M. A Package for Survival Analysis in S. (2015).
22. Gray, B. cmprsk: Subdistribution Analysis of Competing Risks.
23. Turner, S. D. qqman: an R package for visualizing GWAS results using Q-Q and manhattan plots. *biorXiv* doi:10.1101/005165.
24. Wickham, H. *ggplot2: Elegant Graphics for Data Analysis*. (Springer-Verlag New York, 2016).
25. Willer, C. J., Li, Y. & Abecasis, G. R. METAL: Fast and efficient meta-analysis of genomewide association scans. *Bioinformatics* **26**, 2190–2191 (2010).
26. Lesurf, R., Cotto, K. C., Wang, G., Griffith, M., Kasaian, K., Jones, S. J. M.,

Montgomery, S. B. & Griffith, O. L. ORegAnno 3.0: A community-driven resource for curated regulatory annotation. *Nucleic Acids Res.* **44**, D126–D132 (2016).

27. Fishilevich, S., Nudel, R., Rappaport, N., Hadar, R., Plaschkes, I., Iny Stein, T., Rosen, N., Kohn, A., Twik, M., Safran, M., Lancet, D. & Cohen, D. GeneHancer: genome-wide integration of enhancers and target genes in GeneCards. *Database (Oxford)*. **2017**, 1–17 (2017).

28. Maunakea, A. K., Nagarajan, R. P., Bilenky, M., Ballinger, T. J., Dsouza, C., Fouse, S. D., Johnson, B. E., Hong, C., Nielsen, C., Zhao, Y., Turecki, G., Delaney, A., Varhol, R., Thiessen, N., Shchors, K., Heine, V. M., Rowitch, D. H., Xing, X., Fiore, C., *et al.* Conserved role of intragenic DNA methylation in regulating alternative promoters. *Nature* **466**, 253–257 (2010).

29. Cheung, I., Shulha, H. P., Jiang, Y., Matevossian, A., Wang, J., Weng, Z. & Akbarian, S. Developmental regulation and individual differences of neuronal H3K4me3 epigenomes in the prefrontal cortex. *Proc. Natl. Acad. Sci. U. S. A.* **107**, 8824–8829 (2010).

30. Dunham, I., Kundaje, A., Aldred, S. F., Collins, P. J., Davis, C. A., Doyle, F., Epstein, C. B., Frietze, S., Harrow, J., Kaul, R., Khatun, J., Lajoie, B. R., Landt, S. G., Lee, B. K., Pauli, F., Rosenbloom, K. R., Sabo, P., Safi, A., Sanyal, A., *et al.* An integrated encyclopedia of DNA elements in the human genome. *Nature* **489**, 57–74 (2012).

31. Ward, L. D. & Kellis, M. HaploReg v4: Systematic mining of putative causal variants, cell types, regulators and target genes for human complex traits and disease. *Nucleic Acids Res.* **44**, D877–D881 (2016).

32. Roadmap Epigenomics Consortium, Kundaje, A., Meuleman, W., Ernst, J., Bilenky, M., Yen, A., Heravi-Moussavi, A., Kheradpour, P., Zhang, Z., Wang, J., Ziller, M. J., Amin,

V., Whitaker, J. W., Schultz, M. D., Ward, L. D., Sarkar, A., Quon, G., Sandstrom, R. S., Eaton, M. L., *et al.* Integrative analysis of 111 reference human epigenomes. *Nature* **518**, 317–329 (2015).

33. Lonsdale, J., Thomas, J., Salvatore, M., Phillips, R., Lo, E., Shad, S., Hasz, R., Walters, G., Garcia, F., Young, N., Foster, B., Moser, M., Karasik, E., Gillard, B., Ramsey, K., Sullivan, S., Bridge, J., Magazine, H., Syron, J., *et al.* The Genotype-Tissue Expression (GTEx) project. *Nat. Genet.* **45**, 580–585 (2013).

34. Jiang, Y., Qian, F., Bai, X., Liu, Y., Wang, Q., Ai, B., Han, X., Shi, S., Zhang, J., Li, X., Tang, Z., Pan, Q., Wang, Y., Wang, F. & Li, C. SEdb: A comprehensive human super-enhancer database. *Nucleic Acids Res.* **47**, D235–D243 (2019).

35. Wang, J., Dai, X., Berry, L. D., Cogan, J. D., Liu, Q. & Shyr, Y. HACER: An atlas of human active enhancers to interpret regulatory variants. *Nucleic Acids Res.* **47**, D106–D112 (2019).

36. Miyaoka, Y., Chan, A. H., Judge, L. M., Yoo, J., Huang, M., Nguyen, T. D., Lizarraga, P. P., So, P. L. & Conklin, B. R. Isolation of single-base genome-edited human iPS cells without antibiotic selection. *Nat. Methods* **11**, 291–293 (2014).

37. Chambers, S. M., Qi, Y., Mica, Y., Lee, G., Zhang, X.-J., Niu, L., Bilsland, J., Cao, L., Stevens, E., Whiting, P., Shi, S.-H. & Studer, L. Combined small-molecule inhibition accelerates developmental timing and converts human pluripotent stem cells into nociceptors. *Nat. Biotechnol.* **30**, 715–20 (2012).

38. Flegel, C., Schöbel, N., Altmüller, J., Becker, C., Tannapfel, A., Hatt, H. & Gisselmann, G. RNA-Seq analysis of human trigeminal and dorsal root ganglia with a focus on chemoreceptors. *PLoS One* **10**, 1–30 (2015).

39. Pruim, R. J., Welch, R. P., Sanna, S., Teslovich, T. M., Chines, P. S., Gliedt, T. P., Boehnke, M., Abecasis, G. R., Willer, C. J. & Frishman, D. LocusZoom: Regional visualization of genome-wide association scan results. *Bioinformatics* **27**, 2336–2337 (2011).

40. Janes, K., Little, J. W., Li, C., Bryant, L., Chen, C., Chen, Z., Kamocki, K., Doyle, T., Snider, A., Esposito, E., Cuzzocrea, S., Bieberich, E., Obeid, L., Petrache, I., Nicol, G., Neumann, W. L. & Salvemini, D. The development and maintenance of paclitaxel-induced neuropathic pain require activation of the sphingosine 1-phosphate receptor subtype 1. *J. Biol. Chem.* **289**, 21082–21097 (2014).

41. Stockstill, K., Doyle, T. M., Yan, X., Chen, Z., Janes, K., Little, J. W., Braden, K., Lauro, F., Giancotti, L. A., Harada, C. M., Yadav, R., Xiao, W. H., Lionberger, J. M., Neumann, W. L., Bennett, G. J., Weng, H. R., Spiegel, S. & Salvemini, D. Dysregulation of sphingolipid metabolism contributes to bortezomib-induced neuropathic pain. *J. Exp. Med.* **215**, 1301–1313 (2018).

42. Huang, Z. Z., Li, D., Liu, C. C., Cui, Y., Zhu, H. Q., Zhang, W. W., Li, Y. Y. & Xin, W. J. CX3CL1-mediated macrophage activation contributed to paclitaxel-induced DRG neuronal apoptosis and painful peripheral neuropathy. *Brain. Behav. Immun.* **40**, 155–165 (2014).

43. Wang, J., Zhang, X. S., Tao, R., Zhang, J., Liu, L., Jiang, Y. H., Ma, S. H., Song, L. X. & Xia, L. J. Upregulation of CX3CL1 mediated by NF-κB activation in dorsal root ganglion contributes to peripheral sensitization and chronic pain induced by oxaliplatin administration. *Mol. Pain* **13**, 1–10 (2017).

44. Old, E. A., Nadkarni, S., Grist, J., Gentry, C., Bevan, S., Kim, K. W., Mogg, A. J.,

Perretti, M. & Malcangio, M. Monocytes expressing CX3CR1 orchestrate the development of vincristine-induced pain. *J. Clin. Invest.* **124**, 2023–2036 (2014).

45. Hannun, Y. A. & Obeid, L. M. Principles of bioactive lipid signalling: Lessons from sphingolipids. *Nat. Rev. Mol. Cell Biol.* **9**, 139–150 (2008).

46. Kappos, L., Radue, E.-W., O'Connor, P., Polman, C., Hohlfeld, R., Calabresi, P., Selmaj, K., Agoropoulou, C., Leyk, M., Zhang-Auberson, L., Burtin, P. & FREEDOMS Study Group. A placebo-controlled trial of oral fingolimod in relapsing multiple sclerosis. *N. Engl. J. Med.* **362**, 387–401 (2010).

47. Vaclavkova, A., Chimenti, S., Arenberger, P., Holló, P., Sator, P. G., Burcklen, M., Stefani, M. & D'Ambrosio, D. Oral ponesimod in patients with chronic plaque psoriasis: A randomised, double-blind, placebo-controlled phase 2 trial. *Lancet* **384**, 2036–2045 (2014).

48. Hughes, R., Dalakas, M. C., Merkies, I., Latov, N., Léger, J. M., Nobile-Orazio, E., Sobue, G., Genge, A., Cornblath, D., Merschhemke, M., Ervin, C. M., Agoropoulou, C., Hartung, H. P., Day, T., Spies, J., Roberts, L., Van Damme, P., Van den Bergh, P. Y., Maertens de Noordhout, A., *et al.* Oral fingolimod for chronic inflammatory demyelinating polyradiculoneuropathy (FORCIDP Trial): a double-blind, multicentre, randomised controlled trial. *Lancet Neurol.* **17**, 689–698 (2018).

49. Li, C., Li, J. N., Kays, J., Guerrero, M. & Nicol, G. D. Sphingosine 1-phosphate enhances the excitability of rat sensory neurons through activation of sphingosine 1-phosphate receptors 1 and/or 3. *J. Neuroinflammation* **12**, 1–20 (2015).

50. Postma, F. R., Jalink, K., Hengeveld, T. & Moolenaar, W. H. Sphingosine-1-phosphate rapidly induces Rho-dependent neurite retraction: action through a specific cell surface

receptor. *EMBO J.* **15**, 2388–2392 (1996).

51. Doyle, T., Chen, Z., Obeid, L. M. & Salvemini, D. Sphingosine-1-phosphate acting via the S1P1 receptor is a downstream signaling pathway in ceramide-induced hyperalgesia. *Neurosci. Lett.* **499**, 4–8 (2011).

52. Mair, N., Benetti, C., Andratsch, M., Leitner, M. G., Constantin, C. E., Camprubí-Robles, M., Quarta, S., Biasio, W., Kuner, R., Gibbins, I. L., Kress, M. & Haberberger, R. V. Genetic evidence for involvement of neuronally expressed s1P1 receptor in nociceptor sensitization and inflammatory pain. *PLoS One* **6**, (2011).

53. Chen, Z., Doyle, T. M., Luongo, L., Largent-Milnes, T. M., Giancotti, L. A., Kolar, G., Squillace, S., Boccella, S., Walker, J. K., Pendleton, A., Spiegel, S., Neumann, W. L., Vanderah, T. W. & Salvemini, D. Sphingosine-1-phosphate receptor 1 activation in astrocytes contributes to neuropathic pain. *Proc. Natl. Acad. Sci. U. S. A.* **116**, 10557–10562 (2019).

54. Xie, W., Strong, J. A., Kays, J., Nicol, G. D. & Zhang, J. M. Knockdown of the sphingosine-1-phosphate receptor S1PR1reduces pain behaviors induced by local inflammation of the rat sensory ganglion. *Neurosci. Lett.* **515**, 61–65 (2012).

55. Langeslag, M., Quarta, S., Leitner, M. G., Kress, M. & Mair, N. Sphingosine 1-phosphate to p38 signaling via S1P1 receptor and Gαi/o evokes augmentation of capsaicin-induced ionic currents in mouse sensory neurons. *Mol. Pain* **10**, 74 (2014).

56. Chhibber, A., Mefford, J., Stahl, E. a, Pendergrass, S. a, Baldwin, R. M., Owzar, K., Li, M., Winer, E. P., Hudis, C. a, Zembutsu, H., Kubo, M., Nakamura, Y., McLeod, H. L., Ratain, M. J., Shulman, L. N., Ritchie, M. D., Plenge, R. M., Witte, J. S. & Kroetz, D. L. Polygenic inheritance of paclitaxel-induced sensory peripheral neuropathy driven by axon

outgrowth gene sets in CALGB 40101 (Alliance). *Pharmacogenomics J.* 1–7 (2014) doi:10.1038/tpj.2014.2.

57. Schneider, B. P., Li, L., Radovich, M., Shen, F., Miller, K. D., Flockhart, D. A., Jiang, G., Vance, G., Gardner, L., Vatta, M., Bai, S., Lai, D., Koller, D., Zhao, F., O'Neill, A., Smith, M. Lou, Railey, E., White, C., Partridge, A., *et al.* Genome-Wide Association Studies for Taxane-Induced Peripheral Neuropathy in ECOG-5103 and ECOG-1199. *Clin. Cancer Res.* **21**, 5082–5091 (2015).

58. Schneider, B. P., Lai, D., Shen, F., Jiang, G., Radovich, M., Li, L., Gardner, L., Miller, K. D., O'Neill, A., Sparano, J. A., Xue, G., Foroud, T. & Sledge, G. W. Charcot-Marie-Tooth gene, SBF2, associated with taxaneinduced peripheral neuropathy in African Americans. *Oncotarget* **7**, 82244–82253 (2016).

59. Wheeler, H. E., Wing, C., Delaney, S. M., Komatsu, M. & Dolan, M. E. Modeling chemotherapeutic neurotoxicity with human induced pluripotent stem cell-derived neuronal cells. *PLoS One* **10**, e0118020 (2015).

60. Diouf, B., Crews, K. R., Lew, G., Pei, D., Cheng, C., Bao, J., Zheng, J. J., Yang, W., Fan, Y., Wheeler, H. E., Wing, C., Delaney, S. M., Komatsu, M., Paugh, S. W., McCorkle, J. R., Lu, X., Winick, N. J., Carroll, W. L., Loh, M. L., *et al.* Association of an Inherited Genetic Variant With Vincristine-Related Peripheral Neuropathy in Children With Acute Lymphoblastic Leukemia. *JAMA* **313**, 815 (2015).

61. Komatsu, M., Wheeler, H. E., Chung, S., Low, S. K., Wing, C., Delaney, S. M., Gorsic, L. K., Takahashi, A., Kubo, M., Kroetz, D. L., Zhang, W., Nakamura, Y. & Dolan, M. E. Pharmacoethnicity in paclitaxel-induced sensory peripheral neuropathy. *Clin. Cancer Res.* **21**, 4337–4346 (2015).

62. Quarta, S., Camprubí-Robles, M., Schweigreiter, R., Matusica, D., Haberberger, R. V., Proia, R. L., Bandtlow, C. E., Ferrer-Montiel, A. & Kress, M. Sphingosine-1-phosphate and the S1P3 receptor initiate neuronal retraction via RhoA/ROCK associated with CRMP2 phosphorylation. *Front. Mol. Neurosci.* **10**, 1–13 (2017).

63. Zhang, D. D., Linke, B., Suo, J., Zivkovic, A., Schreiber, Y., Ferreirós, N., Henke, M., Geisslinger, G., Stark, H. & Scholich, K. Antinociceptive effects of FTY720 during trauma-induced neuropathic pain are mediated by spinal S1P receptors. *Biol. Chem.* **396**, 783–794 (2015).

64. Doolen, S., Iannitti, T., Donahue, R. R., Shaw, B. C., Grachen, C. M. & Taylor, B. K. Fingolimod reduces neuropathic pain behaviors in a mouse model of multiple sclerosis by a sphingosine-1 phosphate receptor 1-dependent inhibition of central sensitization in the dorsal horn. *Pain* **159**, 224–238 (2018).

65. Brinkmann, V., Davis, M. D., Heise, C. E., Albert, R., Cottens, S., Hof, R., Bruns, C., Prieschl, E., Baumruker, T., Hiestand, P., Foster, C. A., Zollinger, M. & Lynch, K. R. The immune modulator FTY720 targets sphingosine 1-phosphate receptors. *J. Biol. Chem.* **277**, 21453–21457 (2002).

66. Tarrasón, G., Aulí, M., Mustafa, S., Dolgachev, V., Domènech, M. T., Prats, N., Domínguez, M., López, R., Aguilar, N., Calbet, M., Pont, M., Milligan, G., Kunkel, S. L. & Godessart, N. The sphingosine-1-phosphate receptor-1 antagonist, W146, causes early and short-lasting peripheral blood lymphopenia in mice. *Int. Immunopharmacol.* **11**, 1773–1779 (2011).

67. Hill, R. Z., Morita, T., Brem, R. B. & Bautista, D. M. S1PR3 mediates itch and pain via distinct TRP channel-dependent pathways. *J. Neurosci.* **38**, 7833–7843 (2018).

68. Sykes, D. A., Riddy, D. M., Stamp, C., Bradley, M. E., McGuiness, N., Sattikar, A., Guerini, D., Rodrigues, I., Glaenzel, A., Dowling, M. R., Mullershausen, F. & Charlton, S. J. Investigating the molecular mechanisms through which FTY720-P causes persistent S1P1 receptor internalization. *Br. J. Pharmacol.* **171**, 4797–4807 (2014).

69. Kays, J. S., Li, C. & Nicol, G. D. Expression of sphingosine 1-phosphate receptors in the rat dorsal root ganglia and defined single isolated sensory neurons. *Physiol. Genomics* **44**, 889–901 (2012).

70. Huang, Z. Z., Li, D., Liu, C. C., Cui, Y., Zhu, H. Q., Zhang, W. W., Li, Y. Y. & Xin, W. J. CX3CL1-mediated macrophage activation contributed to paclitaxel-induced DRG neuronal apoptosis and painful peripheral neuropathy. *Brain. Behav. Immun.* **40**, 155–165 (2014).

71. Yu, X., Liu, H., Hamel, K. A., Morvan, M. G., Yu, S., Leff, J., Guan, Z., Braz, J. M. & Basbaum, A. I. Dorsal root ganglion macrophages contribute to both the initiation and persistence of neuropathic pain. *Nat. Commun.* **11**, 264 (2020).

72. Conaghan, P. G., Cook, A. D., Hamilton, J. A. & Tak, P. P. Therapeutic options for targeting inflammatory osteoarthritis pain. *Nat. Rev. Rheumatol.* **15**, 355–363 (2019).

73. Scheu, S., Ali, S., Ruland, C., Arolt, V. & Alferink, J. The C-C chemokines CCL17 and CCL22 and their receptor CCR4 in CNS autoimmunity. *Int. J. Mol. Sci.* **18**, (2017).

74. Stendel, C., Roos, A., Deconinck, T., Pereira, J., Castagner, F., Niemann, A., Kirschner, J., Korinthenberg, R., Ketelsen, U. P., Battaloglu, E., Parman, Y., Nicholson, G., Ouvrier, R., Seeger, J., De Jonghe, P., Weis, J., Krüttgen, A., Rudnik-Schöneborn, S., Bergmann, C., *et al.* Peripheral nerve demyelination caused by a mutant Rho GTPase guanine nucleotide exchange factor, frabin/FGD4. *Am. J. Hum. Genet.* **81**, 158–164 (2007).

75. Delague, V., Jacquier, A., Hamadouche, T., Poitelon, Y., Baudot, C., Boccaccio, I., Chouery, E., Chaouch, M., Kassouri, N., Jabbour, R., Grid, D., Mégarbané, A., Haase, G. & Lévy, N. Mutations in FGD4 encoding the Rho GDP/GTP exchange factor FRABIN cause autosomal recessive Charcot-Marie-Tooth type 4H. *Am. J. Hum. Genet.* **81**, 1–16 (2007).

76. Beaubien, F., Raja, R., Kennedy, T. E., Fournier, A. E. & Cloutier, J. F. Slitrk1 is localized to excitatory synapses and promotes their development. *Sci. Rep.* **6**, 1–10 (2016).

77. Marquardt, J., Chen, X. & Bi, E. Architecture, remodeling, and functions of the septin cytoskeleton. *Cytoskeleton* **76**, 7–14 (2019).

78. Vasiljevic, M., Heisler, F. F., Hausrat, T. J., Fehr, S., Milenkovic, I., Kneussel, M. & Sieghart, W. Spatio-temporal expression analysis of the calcium-binding protein calumenin in the rodent brain. *Neuroscience* **202**, 29–41 (2012).

79. Turkmen, S., Eryigit, U., Karaca, Y., Mentese, A., Sumer, U. A., Yulug, E., Aksut, N., Gazioglu, S. & Gunduz, A. Diagnostic value of plasma signal peptide-Cub-Egf domain-containing protein-1 (SCUBE-1) in an experimental model of acute ischemic stroke. *Am. J. Emerg. Med.* **33**, 262–265 (2015).

80. Nyrop, K. A., Deal, A. M., Reeder-Hayes, K. E., Shachar, S. S., Reeve, B. B., Basch, E., Choi, S. K., Lee, J. T., Wood, W. A., Anders, C. K., Carey, L. A., Dees, E. C., Jolly, T. A., Kimmick, G. G., Karuturi, M. S., Reinbolt, R. E., Speca, J. E. C. & Muss, H. B. Patient-reported and clinician-reported chemotherapy-induced peripheral neuropathy in patients with early breast cancer: Current clinical practice. *Cancer* **125**, 2945–2954 (2019).

81. Shimozuma, K., Ohashi, Y., Takeuchi, A., Aranishi, T., Morita, S., Kuroi, K., Ohsumi, S.,

Makino, H., Katsumata, N., Kuranami, M., Suemasu, K., Watanabe, T. & Hausheer, F. H. Taxane-induced peripheral neuropathy and health-related quality of life in postoperative breast cancer patients undergoing adjuvant chemotherapy: N-SAS BC 02, a randomized clinical trial. *Support. Care Cancer* **20**, 3355–3364 (2012).

82. Postma, T. J., Heimans, J. J., Muller, M. J., Ossenkoppele, G. J., Vermorken, J. B. & Aaronson, N. K. Pitfalls in grading severity of chemotherapy-induced peripheral neuropathy. *Ann. Oncol.* **9**, 739–744 (1998).

83. Horn, M., Baumann, R., Pereira, J. A., Sidiropoulos, P. N. M., Somandin, C., Welzl, H., Stendel, C., Lühmann, T., Wessig, C., Toyka, K. V., Relvas, J. B., Senderek, J. & Suter, U. Myelin is dependent on the Charcot-Marie-Tooth Type 4H disease culprit protein FRABIN/FGD4 in Schwann cells. *Brain* **135**, 3567–3583 (2012).

Chapter 3: Exome Sequencing in CALGB 40502 Reveals Genes in Actin Dynamics Associated with Microtubule Targeting Agent-Induced Sensory Peripheral Neuropathy

INTRODUCTION

The main dose-limiting non-hematological toxicity for patients undergoing microtubule targeting chemotherapy is sensory peripheral neuropathy (PN). Understanding patient susceptibility to developing drug-induced SPN has the potential to guide selection of chemotherapies, optimize dose, manage neurotoxicity, and improve overall quality of life. Previous genome-wide studies on microtubule targeting agent (MTA)-induced peripheral neuropathy have been primarily focused on identifying associations of the neurotoxicity with common genetic variants due to the high incidence rate, where such studies are statistically powered to discover common variants with modest effect sizes (Chapter 1, Table 1.3).

Human genetic studies in this field have not yet fully explored the importance of multiple rare variants involved in this common complex phenotype, although it is recognized that the majority of functional variability with large effects in complex traits lie within rare variation[1,2]. Collectively, the known clinical factors and identified common genetic variants associated with MTA-induced SPN have not accounted for the high incidence rate, suggesting there are still undiscovered predictors contributing to the development of the toxicity. A previous polygenic heritability analysis on common SNPs suggests genes critical to axon outgrowth processes are important drivers of paclitaxel-induced sensory peripheral neuropathy (PN)[3]; however these gene have not been fully captured with conventional GWAS and may lie within rare variation. Fortunately, recent genomic technological advances have allowed the opportunity to interrogate these rare variants with large effect sizes, which are likely to have more clinical utility and lead to novel insights on the underlying mechanism behind the development of MTA-induced toxicity. A few targeted sequencing studies on MTA-induced PN have supported involvement of

gene pathways previously implicated in GWA studies. The Beutler et al. 2014[4] study identified patients with genetic variations in *ARHGEF10*, a Charcot-Marie-Tooth (CMT) disease gene essential for Rho GTPase activity during neuronal extension and morphogenesis, were more susceptible to chemotherapy-induced peripheral neuropathy (CIPN); a finding replicated in an independent cohort[5]. Consistent with some initial candidate gene studies, Apellániz-Ruiz et al. demonstrated patients with rare variants in drug metabolizing gene *CYP3A4* had reduced enzyme activity and higher probability of paclitaxel modifications due to severe neuropathy events[6]. However, another study[7] focusing on targeted sequencing in coding regions in *EPHA* genes, paclitaxel pharmacokinetic genes, and CMT genes found only low-frequency variants in *EPHA5/6/8* contribute to paclitaxel-induced neuropathy.

While targeted sequencing corroborates gene associations previously implicated in GWAS, whole exome sequencing provides an unbiased approach to discovering novel genes associated with MTA-induced PN. However, only a few sequencing studies have utilized this exome-wide approach. The first whole exome sequencing study on MTA-induced PN further underscored the connection with rare congenital peripheral neuropathies, discovering association of rare deleterious variants in CMT gene *SBF2* to taxane-induced peripheral neuropathy[8]. The second exome sequencing study on vincristine-induced peripheral neuropathy implicated genes related to mitochondrial protein synthesis, neuronal migration, and transcriptional regulation (*i.e.*, *MRPL47*, *SYNE2*, *BAHD1*)[9].

Building on these exome-wide studies, our study is motivated to further extend the discovery from common variants to include low-frequency and rare variants that may influence susceptibility to MTA-induced SPN. More specifically, our study uses a gene-based approach to identify novel genes that may influence the underlying mechanisms involved in sensory neuronal

damage under MTA exposure, manifesting in risk of chemotherapy-induced peripheral neuropathy.

MATERIALS AND METHODS

Participants

All study participants were enrolled in Cancer and Leukemia Group B (CALGB) 40502, a randomized three-arm phase III trial conducted to determine whether nanoparticle albumin-bound (nab) paclitaxel or ixabepilone is superior to paclitaxel as first-line therapy for patients with advanced breast cancer. CALGB 40502 was open from October 2008 through November 2011, enrolling a total of 799 subjects. Eligibility criteria for enrollment has been previously described[10]. CALGB is now part of the Alliance for Clinical Trials in Oncology. All patients provided written informed consent for both the treatment and companion protocols that met state, federal, and institutional guidelines. Patient characteristics of entire CALGB 40502 cohort and those consented into the pharmacogenetic study have been previously described (Chapter 2, Results Table 2.2).

Definition of peripheral neuropathy phenotype

Adverse events, including chemotherapy-induced peripheral neuropathy (PN), are graded according to the NCI Common Terminology Criteria for Adverse Event (NCI-CTCAE), defining the range of severity of neuropathy cases as Grade 0-5. Because the incidence of the toxicity is dependent on cumulative drug exposure, sensory peripheral neuropathy was assessed with a dose-to-event phenotype. A microtubule-targeting agent (MTA)-induced sensory peripheral neuropathy event was defined as the cumulative MTA dose (mg/m^2) to first instance of grade II or higher PN event and used as the primary endpoint in analyses. For patients who experience no

neuropathy event, the cumulative chemotherapy dose was censored at the time of removal from study, accounting for competing risks to developing a neuropathy event. Characteristics of cumulative dose-to-first instance of grade 2 or higher PN phenotype was previously described (Chapter 2, Results).

Whole Exome Sequencing

From those enrolled in CALGB 40502, a total of 635 consented patients with DNA samples were available for whole-exome sequencing. Genomic DNA extracted from blood samples was provided by the Alliance Pathology Coordinating Office, and sequencing was performed at the UCSF Genomics Core Facility. Probes were designed to target the whole exome and additional intronic regions from selected candidate genes for a total target size of 90 Mb (64 Mb standard exome with 26 Mb custom regions). Candidate genes were chosen based on existing mechanistic information on sensory peripheral neuropathy, including genes involved in taxane metabolism and transport, genes associated with inherited peripheral neuropathies, genes previously identified in Gene Ontology (GO) terms related to axon outgrowth, and additional genes curated from a review of literature on chemotherapy-induced peripheral neuropathy; a total of 242 unique genes were selected (Table 3.1). Variants annotated to 3' and 5' untranslated regions (UTRs), downstream and upstream regions, intergenic regions, and intronic regions of the candidate genes were additionally captured along with those captured from the standard exome.

Sequencing libraries were generated using the KAPA HyperPrep Kits (Illumina) and captured enrichment of custom target regions using SeqCap EZ Exome Plus Kit (Roche NimbleGen). Enriched libraries were sequenced on the HiSeq4000 System (Illumina) using paired-end 150 bp runs. For a random set of 150 sequenced samples, a mean target coverage of

83X (range: 4.52-176.80X) was achieved, where 99% of samples exhibited at least 20X coverage over 80% of the target.

Table 3.1 Candidate genes in targeted custom capture

Genes	Description	Count
ABCB1, ABCC1, ABCC2, ABCG2, CYP1B1, CYP2C8, CYP3A4, CYP3A5, MAP2, MAP4, MAPT, NR1I2, SLCO1B3	Paclitaxel PKPD pathway	13
SETX, ARHGEF10, ATL1, BSCL2, CCT5, CTDP1, DCTN1, EGR2, DNM2, FAM134B, FGD4, FIG4, GAN, GARS, GDAP1, GJB1, HSPB1, HSPB8, IGHMBP2, IKBKAP, KIF1B, LITAF, LMNA, MFN2, MPZ, MTMR2, NDRG1, NEFL, NGF, NTRK1, PLEKHG5, PMP22, PRPS1, PRX, RAB7A, SBF2, SEPT9, SH3TC2, SLC12A6, SOX10, SPTLC1, SPTLC2, YARS, WNK1	Inherited peripheral neuropathy genes	44
NRP2, SEMA3F, SEMA3B, PLXNC1, DSCAM, RTN4, SEMA4B, RTN4R, ALCAM, SEMA5A, GOLGA4, RYK, SEMA6C, ULK2, TPBGL, MT3, PLXND1, SHTN1, SEMA3D, SEMA4F, NTN1, L1CAM, SLIT2, SEMA6D, TWF2, SEMA3E, SEMA4D, SLC9A6, PLXNA4, SEMA6A, SEMA4A, SEMA6B, VEGFA, PPP3CB, RNF6, ULK1, SEMA7A, MACF1, SLIT3, SLIT1, PLXNA2, PLXNA1, CDKL5, SEMA3C, MEGF8, MAPT, BCL11A, PLXNB1, SEMA4G, SEMA3G, SEMA3A, CDK5, NLGN3, USP9X, SEMA4C, RUFY3, LIMK1, ISLR2, NRP1, SEMA5B, PLXNA3, CYFIP1, DPYSL2, MGLL, TTL, AMIGO1, METRN, EPHA4, EPHB3, GDI1, BDNF, OMG, ROBO1, MARK2, LINGO1, PLXNB2, ARHGEF1, NRCAM, ROBO2, LRRC4C, CHN1, CLASP2, MAG, LRP4, NGFR, SKIL, SSH1, OLFM1, THY1, PLXNB3, SSH3, APOE, PTPRO, NTRK2, CTTN, SIPA1L1, SSH2, ABL1, KIF13B, NGF, RHOA, FGF13, PTEN, FEZF2, ARHGDIA, DNM2, DCC	Genes from Gene Ontology Axonogenesis pathway	107

Table 3.1 (cont.) Candidate genes in targeted custom capture

Genes	Description	Count
TRPA1, TRPV1, TRPV4, CCR2, CCL2, SIGMAR1, MORN4, SLC1A3, SLC1A1, SLC1A2, GSK3B, MTOR, AKT1, CX3CR1, PRKCB, PRKCD, PRKCE, CCL3, P2X7R, TNF, ROCK1, KCNB2, TRPM8, CNR2, TLR4, MYD88, ADORA3, CACNA2D1, CAPN1	Literature on animal peripheral neuropathy studies	29
SCN4A, PRX, ARHGEF10, IKBKAP, NEFL, NGFR, CTSS, CTLA4, PSMB1, DYNC1I1, TCF4, SERPINE1, ADRB2, ID3, CYP2C9, CAMKK1, SLC10A2, NFATC2, TAC1, FOXC1, ITGA1, CYP2C8, TUBB2A, RFX2, EPHA4, EPHA5, EPHA6, LIMK2, XKR4, ACTG1, CAPG, ABCB1, CCNH, ABCG2, ABCG1, GPX7, ABCC4, TUBB2A, ARHGEF10, CEP72,VAC14, FZD3, EPHA5, FGD4, DNM1L, ERCC1, ERCC2, ABCA1, FANCD2, RWDD3, TECTA, FZD3, NDRG1, FGD4, PITPNA, CAND1, CACNB2, XKR4, BCL6, CYP2C8, ABCB1, ABCC2, CYP1B1, ERBB4, LIMK2, MISP, SHROOM3, GPX7, ABCC4, BCR, AIPL1, FCAMR, WLS, DPP6, DIDO1, ATP1A2	Literature on human peripheral neuropathy studies	75

Quality Control

Sequencing reads were processed on an internal pipeline in accordance to GATK Best Practices Workflows on germline short variant discovery (version 2018Jan07). In brief, sequencing reads were mapped to hg38 reference genome using Burrows-Wheeler Aligner (BWA-MEM v0.7.15). Aligned reads were marked for duplications using Picard (version 2.18.27-1-g21ad30b-SNAPSHOT) and recalibration of base quality scores were performed using GATK (v4.0.12.0). Variant discovery was conducted on all samples using GATK v4.0.12.0 HaplotypeCaller in GVCF mode to allow for efficient joint genotyping of all samples (GATK v4.0.12.0 GenotypeGVCFs) and resulted in a single variant call format (VCF) file. Variants were initially filtered for high quality calls, excluding variants with VQSLOD score corresponding to the truth

sensitivity threshold of 99.90% for indels and 99.80% for SNPs (GATK v4.0 0.12.0 VQSR) and variant calls were set to null if read depth (DP) < 10 and genotype quality (GQ) < 20. Only variants with a single nucleotide reference allele were considered in the discovery analysis.

Concordance checks between sequencing variants that overlapped with genotyped variants on OmniExpressExome array (Illumina) were conducted; samples were confirmed to have concordance rates > 90%. Samples with low mean read depth (<10X; n = 4), per-sample call rate < 90% (n = 3), heterozygosity estimation beyond three standard deviations (n = 2), and high degree of relatedness due to plating errors (n = 2) were excluded. Sex check was performed on genotyped data and excluded three additional samples. Principal component analysis (PCA) was performed on these samples using genotyped data, and the first 3 PC vectors were used to adjust for population stratification in the discovery analysis. Among these subjects that passed sample quality control, a total of 612 subjects had both genotype and phenotype information, which were further used as the discovery cohort in this analysis. After sample exclusion, variants were excluded if > 10% missing data among the discovery cohort, significant deviation from Hardy-Weinburg equilibrium ($P < 10^{-6}$), and monomorphic in those with reported PN events within each stratum. A summary of sample and variant quality control is displayed in Figure 3.1, and sample metrics of the discovery cohort are tabulated in Table 3.2.

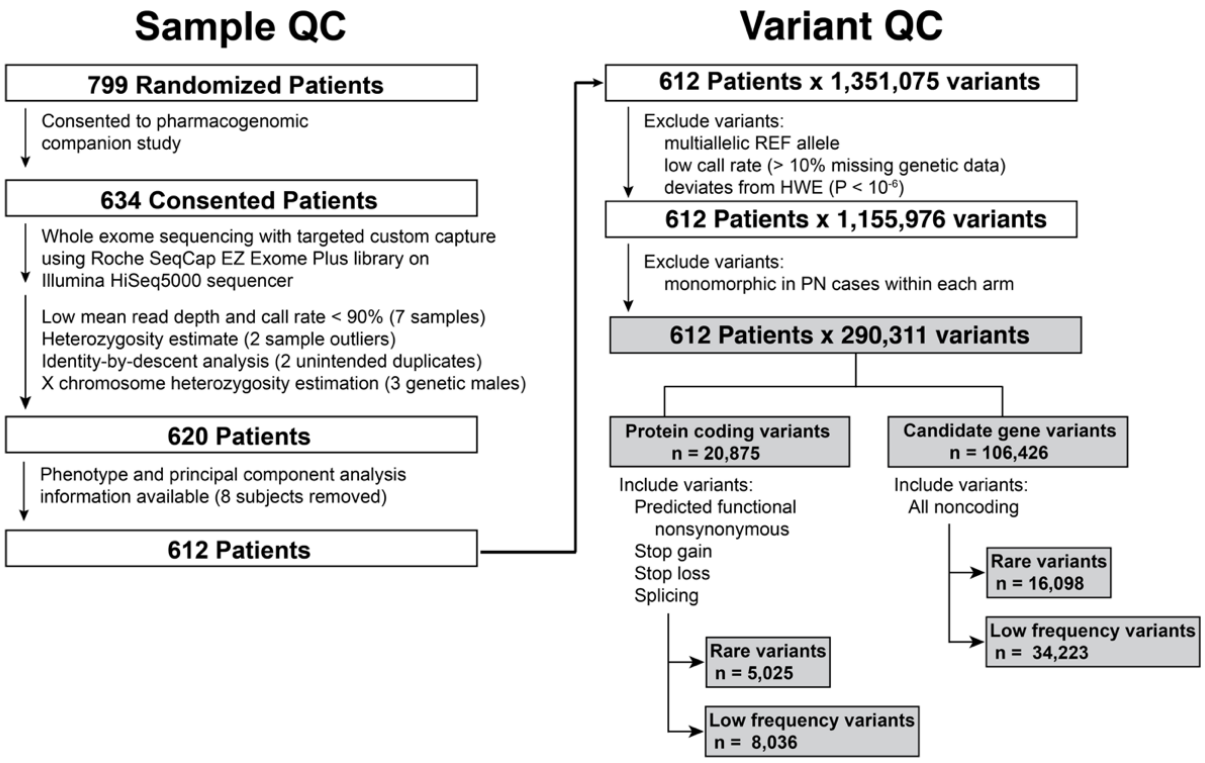

Figure 3.1 Summary of sample and variant quality control pipeline.

Table 3.2 Summary of sample quality on discovery cohort (N = 612).

	Mean	Range	Total
Call rate†	95.09	0.901-0.975	–
Read depth†	66.13	32.737-156.206	–
Heterozygosity†	0.0384	-0.273-0.192	–
Ti/Tv ratio	2.13	1.93-2.25	2.32
Nonsynonymous/synonymous ratio	0.947	0.911-0.978	1.4
All variants	4,608,106	1,858,968-12,431,101	1,351,075
Novel variants (absent from dbSNP 150)	105,725	99,367-126,219	191,129
Singletons	144,661	121,811-175,517	634,352

†Estimated on samples after filtering variant calls with DP > 10 and GQ > 20

The remaining variants were annotated with Ensembl gene names and functional consequences using ANNOVAR (v2018APR16). Predictions of functional impact for variants were obtained from bioinformatic databases, including SIFT, PolyPhen2-HDIV, Mutation Assessor, REVEL, CADD, and GERP++. Protein coding variants were defined as "exonic", "exonic;splicing", or "splicing" variants by Ensembl annotation. Nonsynonymous variants with

predicted deleterious state in at least two (out of six) databases (Table 3.3), frameshift deletions, stop gain variants, stop loss variants, and all splicing variants were considered in the genome-wide gene-based analysis (Table 3.4). All noncoding variants annotated to the candidate genes were used in the candidate gene-based analysis.

Sequence kernel association tests (SKAT) were used to evaluate the aggregated effects of two variants types: 1) rare (MAF ≤ 1%) and 2) low frequency variants (MAF 1-5%) in each gene. Candidate gene analyses only included variants annotated to any of the 242 candidate genes (Table 3.1). Each association test was performed with a Cox regression analysis using the cumulative dose-to-first instance of grade 2 or higher PN event as the phenotype. All tests were stratified by treatment arm and adjusted for age. Associations with Bonferroni-adjusted *P* values < 0.05 were considered statistically significant. All *P* values reported are unadjusted.

Statistical analyses

Gene-based SKAT analyses were performed using the seqMeta[11] and survival[12] packages within the *R* (v3.5.3)[13] statistical environment.

Table 3.3 Bioinformatic databases used for functional prediction and corresponding outcomes of predicted variant function

Functional prediction database	Possible prediction outcomes	Deleterious definition
SIFT	Tolerated (T), deleterious (D)	D
Polyphen2-HDIV	Unknown (U), benign (B), probably damaging (D), possibly damaging (P)	D, P
Mutation Assessor	Neutral (N), low (L), medium (M), high (H)	M, H
REVEL score†	0 – 0.996	> 0.5 (score at which 75% variants deleterious and 10% neutral)
CADD phred score†	0.001 - 72	≥ 10 (predicted in top 10% deleterious variants)
GERP++ score†	-12.30 – 6.17	> 0 (positive scores are considered highly-conserved positions)

†Range of scores observed from annotation of all variants

Table 3.4 Summary of gene-based association tests performed

Analysis type	Variant type	Criteria
Genome-wide, exonic regions	Rare variant*	Coding variants: • At least 2/6 databases with deleterious label • Stop gain and stop loss variants • Frameshift mutations • Splicing variants
	Low-frequency variant†	Coding variants: • At least 2/6 databases with deleterious label • Stop gain and stop loss variants • Frameshift mutations • Splicing variants
Candidate gene regions	Rare variant*	Noncoding variants
	Low-frequency variant†	Noncoding variants

*Rare variants defined by minor allele frequency ≤ 1% in discovery cohort, which included singletons (alternate variant allele count = 1)

†Low-frequency variants defined by minor allele frequency of 1-5% in discovery cohort

Gene-based association analysis

RESULTS

Among the 799 individuals randomized to CALGB 40502, 635 subjects were sequenced on the Illumina HiSeq4000 using the Roche SeqCap EZ Exome Plus library, targeting whole exomes with additional custom candidate gene regions. Patient characteristics of the pharmacogenetics and clinical trial population of CALGB 40502 have been previously described (Chapter 2, Results Table 2.2). In brief, the pharmacogenetic discovery cohort used in this analysis is proportional to the entire clinical trial cohort in regards to patient characteristics, including age, self-reported race/ethnicity, prior taxane status, and tumor subtype. After sample quality control, a total of 612 subjects and 1,155,976 variants were isolated for the discovery analyses (Figure 3.1). The cumulative incidence of PN in each treatment arm of CALGB 40502 was previously described (Chapter 2, Results Figure 2.5). From the discovery cohort, a total of 312 patients had a reported grade 2 or higher PN event, and cumulative doses were defined at time of event. The remaining 300 patients were censored at the time they were removed from the trial for progression/death, other adverse events, other complicating disease, patient withdrawal, and other reasons. Only four of the 300 completed treatment per protocol and were censored at therapy completion.

To investigate gene-based effects on cumulative risk of chemotherapy-induced peripheral neuropathy in this cohort, a Cox regression model incorporated into the SKAT tests was performed to calculate the aggregated contribution of rare or low frequency deleterious coding variants from each gene (Table 3.4). None of the gene associations reached genome-wide significance in either the low-frequency or rare variant analysis, although there are some top-ranking genes based on *P* value that were further investigated. Because the goal of these discovery analyses is focused on understanding the biology of the underlying sensory neuron

toxicity, we further filtered for genes with $P < 10^{-4}$, an expression level of at least 3 FPKM in human dorsal root ganglion (DRG)[14] and a previously described function in neurogenesis or associations to neuropathy (Table 3.5); only two genes met these criteria, *PRDM16* and *SHC4*. Since the role of *IFT46* is primarily characterized in ciliated sensory neurons in *C. elegans* without a clear translation to human neurons, it was not considered further. While *PEAR1* and *TRIOBP* did not reach the same association *P* value threshold, these genes are highly expressed in human DRG with evidence for involvement in sensory neuron excitability and axonal extension. All variants aggregated from these four genes were missense exonic variants with minor allele count (MAC) ranging from 4-50 (Table 3.6).

Among the identified genes in the rare variant analysis, *PRDM16* was explored for further support of association with PN. The rare variant rs371654192, which lies in exon 9 of *PRDM16,* is predicted to be deleterious in five of six *in silico* prediction databases (Table 3.6). In CALGB 40502, there was a trend toward a higher proportion of reported PN events for patients harboring rs371654192 compared to those with reference allele (paclitaxel: 0.47 vs. 1, nab-paclitaxel: 0.54 vs. 0.67, ixabepilone: 0.51 vs. 0.50) (Figure 3.2), although these estimates are interpreted with caution considering the small number of subjects harboring this rare variant. Additional bioinformatic analysis using ENCODE data (UCSC Genome Browser) revealed this SNP lies within a regulatory element for early growth response 1 (EGR-1), a binding site for transcription factor enhancer of zeste homolog 2 (EZH2), and a DNaseI hypersensitivity site. Subjects with the variant had 40-50% of the median cumulative MTA dose to first instance of PN when compared to those without the variant.

Table 3.5 Top gene associations ranked by *P* value from genome-wide tests aggregating effects across rare and low-freqency variants

Analysis	Gene	Gene Description	*P*	Cumulative MAF	No. SNPs	Human DRG†	Literature PMID
Rare variants	*OR8B2*	Olfactory Receptor 8B2	6.12E-05	0.0090	1	0.00	–
	PRDM16	PR Domain Containing 16	1.74E-04	0.0065	1	6.17	29779941, 22197833, 19050759
	PARP15	Poly(ADP-Ribose) Polymerase Family Member 15	6.99E-04	0.0075	1	0.41	–
	IFT46	Intraflagellar Transport 46	9.08E-04	0.0033	1	11.13	24339792
	MGAT4B	Alpha-1,3-Mannosyl-Glycoprotein 4-Beta-N-Acetylglucosaminyl transferase B	0.00107	0.0098	2	28.70	–
Low frequency variants	*USP6*	Ubiquitin specific peptidase 6	3.57E-04	0.026	1	1.62	31841517
	SHC4	Src Homology 2 Doman-Containing-Transforming Protein C4	2.67E-04	0.015	1	12.80	21117147, 28213521, 31823725
	C7orf50	Chromosome 7 Open Reading Frame 50	0.00120	0.014	1	28.36	–
	PEAR1	Platelet Endothelial Aggregation Receptor 1	0.00174	0.085	4	20.94	31992767
	TRIOBP	TRIO And F-actin Binding Protein	0.00182	0.12	5	15.87	25065758, 28832620, 25333879

†Human DRG RNA-Seq expression levels from Flegel et al.[14]

Table 3.6 Characterization of deleterious variants aggregated in genes of interest from genome-wide analysis

Variant Name	Gene	Ref>Alt	MAC	Variant type	Functional consequence*	Deleterious labels
rs371654192	*PPRDM16*	G>C	8	missense	Exon 9, R824P	S, P, M, C, G
rs16961728	*SHC4*	T>G	18	missense	Exon 8, Q400H	MA, C
rs147639000	*PEAR1*	G>A	28	missense	Exon 10, D343N	C, G
rs1952294	*PEAR1*	C>T	13	missense	Exon 8, S234P	C, G
rs41299597	*PEAR1*	C>G	26	missense	Exon 19, S802C	P, C, G
rs77795865	*PEAR1*	C>T	37	missense	Exon 11, S381F	S, P, MA, C, G
rs142024473	*TRIOBP*	C>T	44	missense	Exon 7, A660V	MA, C, G
rs150690007	*TRIOBP*	G>A	13	missense	Exon 7, R745K	S, G
rs193043234	*TRIOBP*	C>G	21	missense	Exon 7, P1030R	S, P, MA, C, G
rs41296243	*TRIOBP*	C>T	24	missense	Exon 7, S826L	S, C, G
rs41302575	*TRIOBP*	C>G	50	missense	Exon 7, T817S	P, C, G

MAC: minor allele count, MA: MutationAssessor, P: PolyPhen2, S: SIFT, C: CADD, G: GERP++
*Based on longest transcript in Ensembl annotation

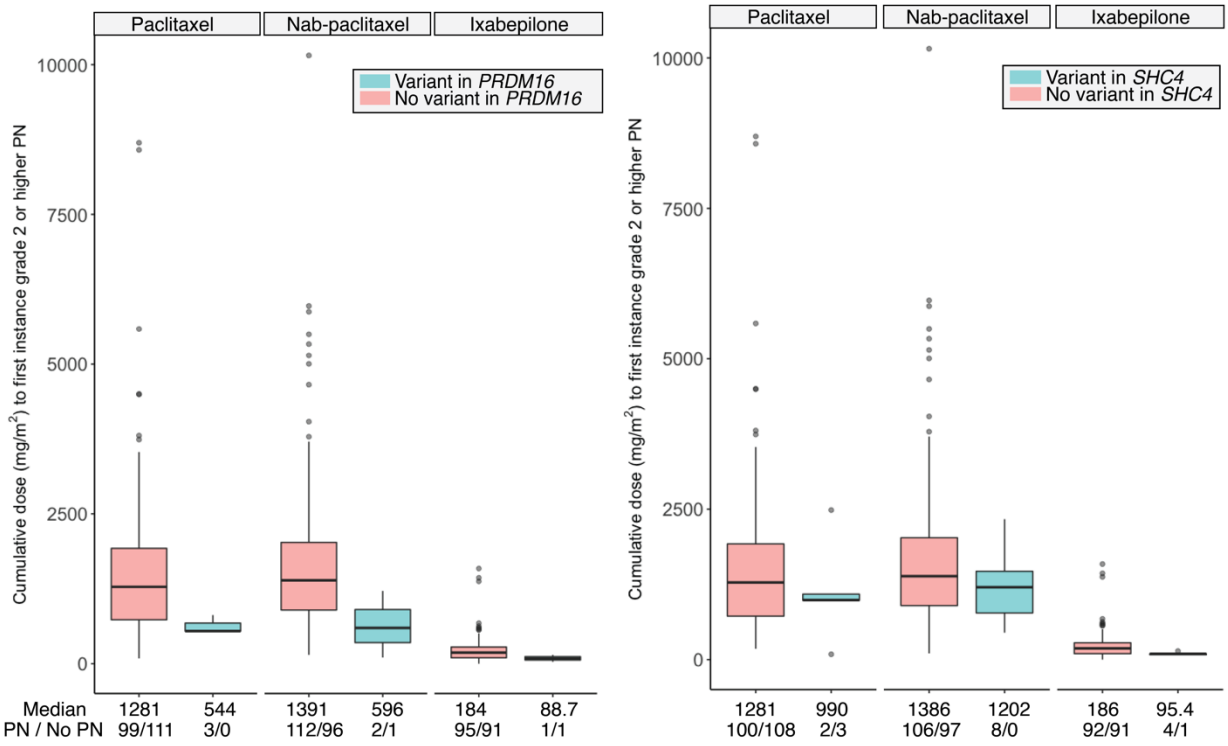

Figure 3.2 Cumulative dose to first instance of PN event for those with and without alternate alleles in rare variants rs371654192/*PRDM16* and rs16961728/*SHC4*. The median cumulative doses to first instance of grade 2 or higher PN event and number of patients with and without a reported grade 2 or higher PN event in each category are displayed below the boxplots.

From the low-frequency variant analysis, a similar increase in PN event rate was observed in those harboring the SNP rs16961728 in exon 8 of *SHC4* (Figure 3.2) in both the nab-paclitaxel and ixabepilone arms but not in the paclitaxel arm; the median doses to grade 2 PN were largely unchanged between carriers and non-carriers of rs16961728. Bioinformatic analysis on rs16961728 shows predicted disruption in the regulatory motif for autoimmune regulator (AIRE) with regulatory histone promoter, histone enhancer, and DNase marks in various tissues (HaploReg v4.1). Four missense exonic SNPs (rs147639000, rs1952294, rs41299597, rs77795865) were evaluated in the gene association test for *PEAR1*. Subjects with at least one low-frequency variant in *PEAR1* have a higher incidence of grade 2 or higher PN events (paclitaxel: 0.44 vs 0.71, nab-paclitaxel: 0.52 vs 0.69, ixabepilone: 0.48 vs 0.63) with no significant difference in median cumulative MTA exposure between carriers and non-carriers of a *PEAR1* variant (Figure 3.3). rs147639000 was found to be in high linkage disequilibrium with intronic SNPs of *ARHGEF11* (HaploReg v4.1). One of these SNPs, rs41299597, is significantly associated with expression quantitative trait loci for multiple genes, suggesting this variant may regulate expression of *PEAR1* (whole blood tissue), *ARHGEF11* (thyroid tissue), and *SLC25A44* (tibial nerve) (GTEx). The other SNPs are also annotated with histone enhancer and promoter marks in various tissues and predicted to disrupt regulatory motifs for important neuron transcriptional factors including neuron-restrictive silencer factor (NRSF) (HaploReg v4.1). For *TRIOBP*, five missense SNPs (rs142024473, rs150690007, rs193043234, rs41296243, rs41302575) were considered in the gene association test. Patients in the ixabepilone arm and to a lesser extent in the nab-paclitaxel arm harboring at least one low-frequency variant in *TRIOBP* tolerated higher median cumulative doses with similar rates of PN events (Figure 3.3). Bioinformatic analysis supports disruption of protein regulatory motifs important for

neurogenesis, including early growth response protein 1 (EGR-1) and glucocorticoid receptor (GR), by the rs150690007, rs41296243, and rs193043234 variants. The SNPs rs41296243 and rs41302575 are also associated with expression quantitative trait loci for multiple genes including *SLC16A8* in tibial nerve tissue (GTEx).

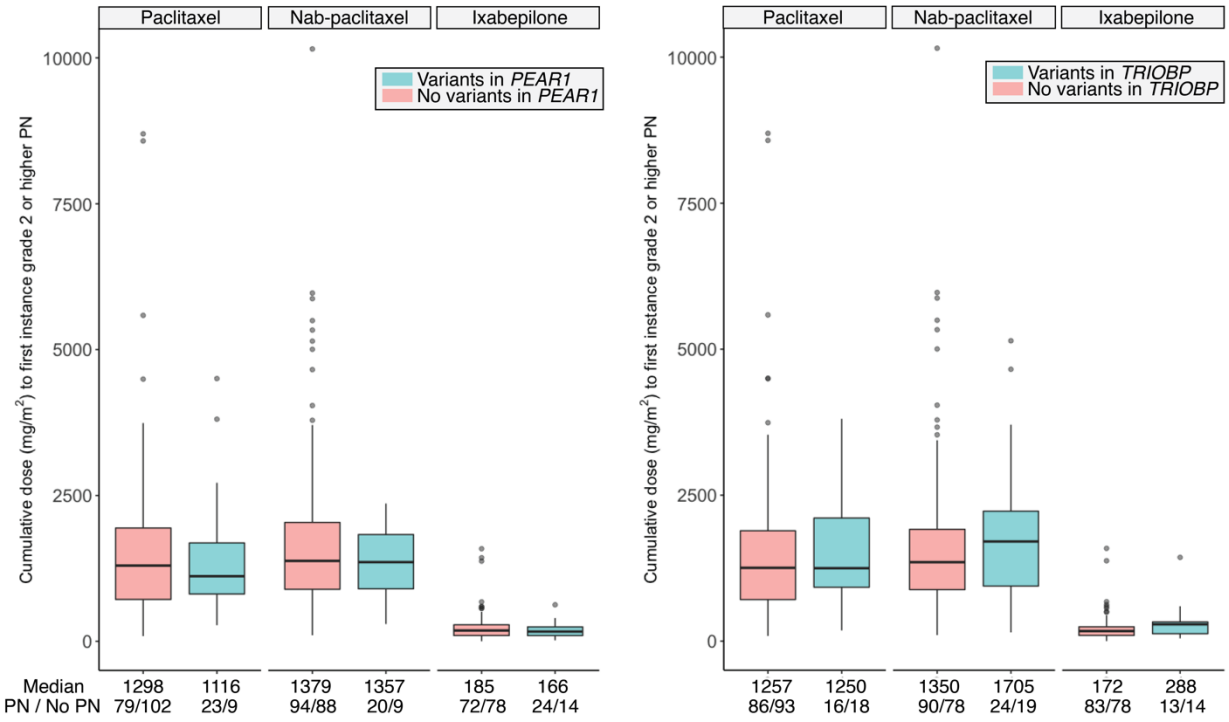

Figure 3.3 Cumulative dose to first instance of grade 2 or higher PN event in each treatment arm for those with and without deleterious low-frequency variants in *PEAR1* (left) and *TRIOBP* (right). The median cumulative doses to first instance of grade 2 or higher PN event and number of patients with and without a reported grade 2 or higher PN event in each category are displayed below the boxplots.

For candidate gene analysis, none of the gene-based associations reached statistical significance (unadjusted threshold, $P < 10^{-4}$) (Table 3.7). Among the top-ranking genes in both low frequency and rare variant candidate gene analyses, only one gene (*ACTG1*) reached a threshold of P value < 0.01 and has the highest expression in human DRG. Of the 10 SNPs, one SNP (rs1140892) is a splicing variant, three SNPs (rs117809695, rs75355043, rs76770927) are

intronic variants, five SNPs (rs1139408, rs1139414, rs11549167, rs55902924, rs55978907) are located in the 3'UTR, and one SNP (rs1139403) is located in the 5'UTR (Figure 3.4). Subjects in the nab-paclitaxel arm harboring at least one low-frequency variant in *ACTG1* trended towards a higher median cumulative MTA doses, but this was not consistent in the other two treatment arms. The proportion of patients developing PN was also similar in carriers and non-carriers in each study arm. However, SNPs in *ACTG1* (rs76770927, rs1139408) have been linked to disruption in regulatory binding motifs of NRSF and GR, similarly to those in *PEAR1* and *TRIOBP*, respectively.

Table 3.7 Top-ranking gene associations ($P < 0.05$) from candidate gene-based association tests using rare and low-frequency variants.

Analysis	Gene	Gene Description	*P*	Cumulative MAF	No. SNPs	Human DRG†
Rare variant	*LMNA*	Lamin A/C	0.012	0.11	15	124.04
	PRX	Periaxin	0.016	0.069	8	263.49
	ADORA3	Adenosine A3 Receptor	0.019	0.0065	2	6.84
	NR1I2	Pregnane X Receptor	0.046	0.169	23	0.02
	NGFR	Nerve Growth Factor Receptor	0.047	0.033	6	325.76
	EPHA4	Ephrin Type-A Receptor 4	0.047	0.84	134	0.84
Low-frequency variant	*ACTG1*	Actin Gamma 1	0.0065	0.26	10	1426.86
	SLC1A3	Excitatory Amino Acid Transporter 1	0.018	1.03	41	5.66
	CCT5	Chaperonin Containing TCP1 Subunit 5	0.027	0.26	13	36.34
	CYP3A4	Cytochrome P450 3A4	0.028	0.45	19	0.04
	SEMA6D	Semaphorin 6D	0.034	13.67	611	10.86
	SHTN1	Shootin 1	0.034	5.35	243	5.85

†Human DRG RNAseq expression levels from Flegel et al.[14]

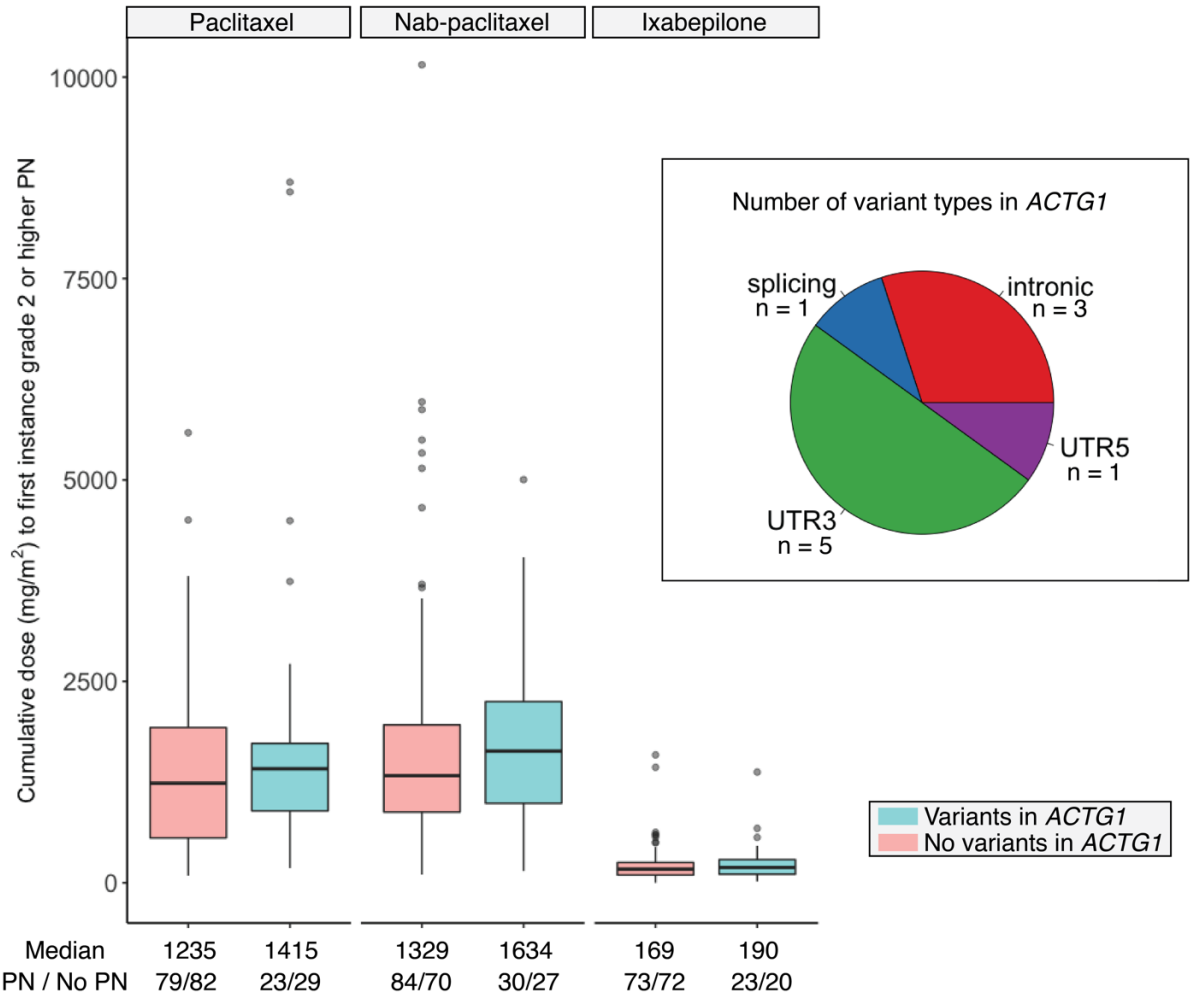

Figure 3.4 Cumulative dose to first instance of grade 2 or higher PN event in each treatment arm for those with and without low-frequency noncoding variants in *ACTG1* (left). The median cumulative doses to first instance of grade 2 or higher PN event and number of patients with and without a reported grade 2 or higher PN event in each category are displayed below the boxplots. Annotation of low-frequency variant types aggregated in *ACTG1* from the candidate gene-based analysis is shown in the inset (right).

From the top-ranking candidate gene associations, our results also highlight *CYP3A4* and *PRX*, which have been previously implicated with CIPN in whole exome sequencing studies. Among the 19 low-frequency variants evaluated in *CYP3A4*, 17 SNPs are intronic variants, and two SNPs (rs28371763, rs28988604) are located in the 3'UTR (Figure 3.5). Carriers of CYP3A4 low-frequency variants had similar median cumulative doses to first instance of grade 2 or higher PN and a similar proportion of PN events compared to non-carriers (Figure 3.5). For *PRX*, a total

of 8 intronic rare variants (rs117182727, rs117780513, rs117952516, rs142805539, rs145046254, rs1981957, rs3947852, rs78458775) were analyzed in the gene-based association test (Figure 3.6). Patients with at least one rare genetic variant in *PRX* have higher incidence of reported grade 2 or higher PN events than those without *PRX* variants.

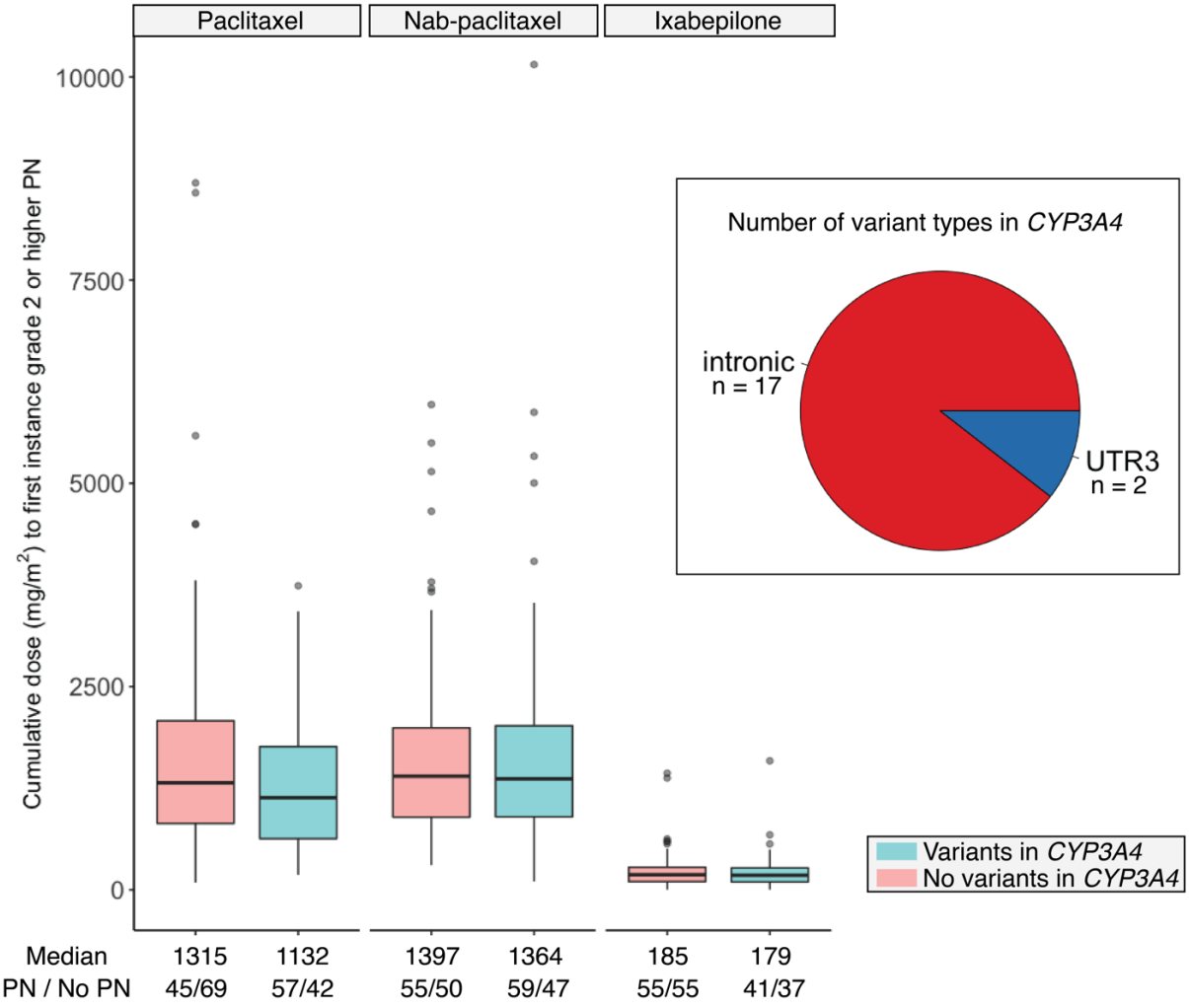

Figure 3.5 Cumulative dose to first instance of grade 2 or higher PN event in each treatment arm for those with and without low-frequency noncoding variants in *CYP3A4* (left). The median cumulative doses to first instance of grade 2 or higher PN event and number of patients with and without a reported grade 2 or higher PN event in each category are displayed below the boxplots. Annotation of low-frequency variant types aggregated in *CYP3A4* from the candidate gene-based analysis is shown in the inset (right).

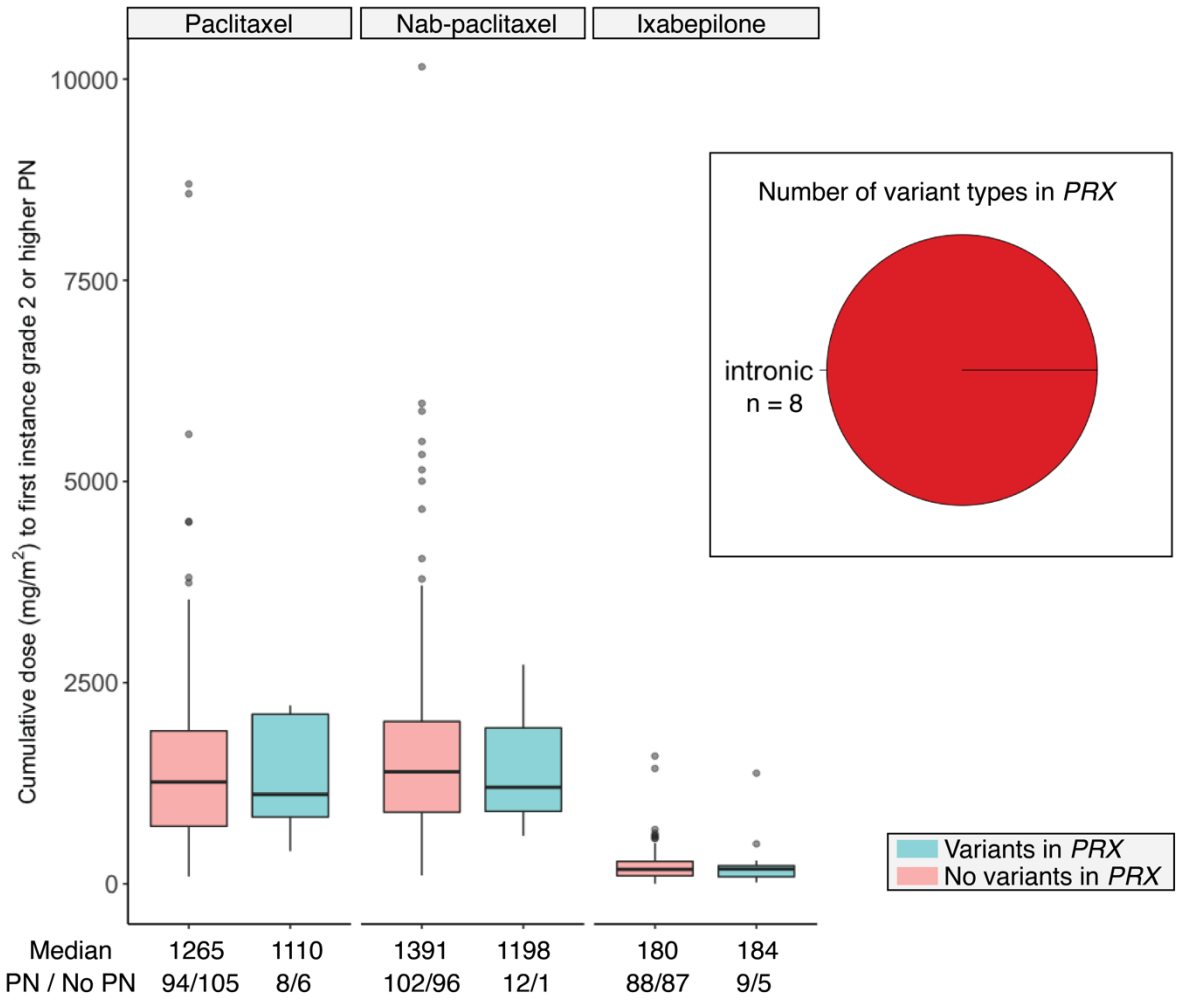

Figure 3.6 Cumulative dose to first instance of grade 2 or higher PN event in each treatment arm for those with and without rare variants in *PRX* (left). The median cumulative doses to first instance of grade 2 or higher PN event and number of patients with and without a reported grade 2 or higher PN event in each category are displayed below the boxplots. Annotation of low-frequency variant types aggregated in *PRX* from the candidate gene-based analysis is shown in the inset (right).

DISCUSSION

In these discovery genome-wide analyses, we identified several genes with rare and low-frequency variation that may contribute to the risk of grade 2 or higher peripheral neuropathy, albeit no gene-based associations achieved unadjusted *P* value thresholds. Among the genes with lowest association *P* value, four genes (*PRDM16, SHC4, PEAR1* and *TRIOBP*) were further prioritized based on expression levels in human DRG and/or previously described biologically-relevant functional activity in neurons.

In the exome-wide discovery analysis, the most significant gene association with grade 2 or higher MTA-induced peripheral neuropathy was *PRDM16,* a gene that encodes for zinc finger transcriptional coregulator PRDM16 and is mostly known for its activity in development of brown adipose tissue[15] However, a recent study investigated its role in regulating epigenetic state of transcriptional enhancers for neurogenesis and neuronal migration in cortical neurons[16]. Interestingly, the missense exonic variant rs371654192 identified in *PRDM16* may disrupt binding of early growth response-1 (EGR-1), an overall marker for neuronal activity and an important nerve growth factor (NGF)-stimulated transcription factor that mediates inflammatory responses to tissue damage[17]. Since its activity could be related to neuronal response to chemotherapy exposure, imbalance in *PRDM16* activity may impair nerve repair mechanisms needed to combat chemotherapy-induced damage and thus increase patient susceptibility to MTA-induced peripheral neuropathy.

From the low-frequency variant analysis, we further prioritized *SHC4,* which encodes for a member of the Shc family of adaptor proteins that functions as a platform to recruit and transduce extracellular signaling events primarily through MAPK and PI3K activation[18]. Alongside many CIPN studies that focused on the inflammatory response due to increased PI3K

signaling[19], there is also evidence that nerve growth factor (NGF)-mediated phosphorylation of Shc proteins can signal its translocation to the cytoskeleton and directly bind F-actin in neurons[20]. NGF-mediated Shc activity was also shown to initiate RhoA activation via Ras and initiate cytoskeletal organization[21,22]. Although the functional role of Shc proteins in sensory neurons are still unknown, it is plausible to suggest that improper Shc function may lead to the inability to signal appropriate inflammatory signals and cytoskeletal rearrangements after nerve injury.

The gene *PEAR1* (platelet endothelial aggregation receptor 1) encodes for a protein that is primarily known for its role in platelet activation[23]. However, recent studies in peripheral nerves implicated its function in satellite glia of DRG[24] and showed mutations in *PEAR1* cause increased sensory excitability via crosstalk between sensory neurons and non-neuronal supporting cells[25]. This notion is in accordance with the observed increased incidence in grade 2 or higher PN in patients who carry deleterious variation in *PEAR1*. The SNP rs41299597 observed in *PEAR1* is also an eQTL for *SLC25A44,* a member of solute carrier transporters within the inner mitochondrial membrane[26], in tibial nerve tissue, supporting the idea that mitochondrial function contributes to altered excitability of peripheral neurons[27]. Furthermore, it is notable that one exonic SNP (rs147639000) identified in *PEAR1* is linked to intronic variants of *ARHGEF11*, a member of guanine nucleotide exchange factors (GEFs) for RhoA GTPase. Beutler et al. [4] previously associated common variation in CMT genes *ARHGEF10 and PRX* with susceptibility of chemotherapy-induced neuropathy. Intriguingly, patients harboring variation in *ARHGEF10* were more likely to experience peripheral neuropathy symptoms induced by chemotherapy. This connection between variation in congenital neuropathy genes

and susceptibility to drug-induced neuropathies has also been highlighted in other genome-wide association studies[8,28].

TRIOBP encodes for a protein that functions primarily to control neural development and actin cytoskeleton organization via stabilization of F-actin structures. Mutations in exons 6-9 are associated with inherited sensorineural hearing impairment[29]. While the bioinformatic analysis on *TRIOBP* low-frequency variants predicted disruption in binding of transcription factors (*i.e.*, EGR-1 and GR) essential to promote neuronal growth, we observed a potential protective effect against occurrence of developing grade 2 or higher peripheral neuropathy in those with *TRIOBP* low-frequency variants within CALGB 40502. All the "deleterious" mutations observed lie within exon 7, suggesting some functional consequence to TRIOBP. Nonetheless, considering little is understood about the role of *TRIOBP* in sensory nociceptive peripheral neurons additional mechanistic investigation is warranted to clarify its role.

None of the 242 candidate genes in the exome-wide discovery analysis using only "deleterious" coding variants met the criteria for further investigation. The lowest P value for gene association was observed for *CACNB 2* (P = 3.95E-03) encoding for a voltage-dependent calcium channel with low human DRG expression (FPKRM = 1.32) and thus, was not further explored. To explore the role of noncoding regulatory variation in these candidate genes, we performed a candidate gene-based analysis using solely noncoding variants. The most significant association was observed with Actin Gamma 1 or *ACTG1,* which was also highly expressed in DRGs. By virtue of the candidate-gene selection (Table 3.1), common variant rs1135989 in *ACTG1* has previously been implicated in increased risk to vincristine-induced peripheral neuropathy[9,30]. It will be important to examine genetic variation in ACTG1 in larger populations

of patients treated with both microtubule stabilizing and destabilizing drugs to resolve its role in risk of PN.

It should be noted that our candidate gene study also features *CYP3A4* and *PRX* among the genes with most significant association, which have been previously implicated in other whole exome sequencing CIPN studies. *PRX*, encodes for periaxin protein that is responsible for maintenance of peripheral nerve myelin with roles in remyelination after nerve injury. Mutations in *PRX* are causal to CMT neuropathy type 4F and are characterized by significant demyelination of peripheral nerves as a result of impaired myelin peripheral sheaths[31]. Following the same direction of effect observed in a previous study[4], low-frequency SNPs in the noncoding regions of *PRX* are associated with increasing rate of PN in CALGB 40502 and less tolerance to cumulative MTA exposure. This further emphasizes the notion that CMT mutation carriers are predisposed to development of peripheral neuropathy when exposed to microtubule-targeting agent chemotherapy. Noncoding variation in *CYP3A4* was not associated with increased risk of MTA-induced PN events, in contrast to coding variants reported by others[6]. It is plausible that noncoding variation does not reduce the drug metabolizing activity enough to increase the overall drug exposure, although this should be examined in larger populations. Future work will be focused on exploring these genetic effects in risk of developing MTA dose modifications, which may be a more reflective and sensitive to genetic variation in the genes identified above to CIPN.

Although more functional sensory neuron studies and genetic validation studies in independent cohorts are needed to corroborate the contributions of these genes to MTA-induced PN, these discovery analyses highlight the importance of Rho GTPase signaling in drug-induced peripheral neuropathies. A number of genome-wide association studies have identified other

genes (*FGD4*, *EPHA4/5/6/8*, *ARHGEF10*, *S1PR1*, *SEPT5*)[32] that have converged on the Rho GTPase signaling pathway, suggesting that susceptibility to CIPN may be related to dysregulation in actin cytoskeleton reorganization. It remains unclear whether dysregulation is directly triggered by MTA accumulation within the sensory neurons or during the critical process to reinnervate the epidermis and restore sensory function after chemotherapy-induced nerve damage.

While our study discovered some relevant genes, this study has several caveats. As the majority of pharmacogenetic studies, these findings are limited by low study sample size and further restricted by stratification of each treatment arm. As a result, the study is largely underpowered to identify significant associations with direct clinical utility. However, our study still discovered some biologically-relevant genes among those with the lowest *P* value for association that support previous mechanistic investigations into how chemotherapy-induced neuropathy develops. Future work will include a closer examination of rare and low-frequency variants among extreme phenotypes (i.e., those treated with large amount of MTA doses without any reported neuropathy events compared to those with immediate PN events after low MTA doses). An extreme responder-like analysis might reveal important variation that may be directly actionable and provide interesting additional mechanistic insights critical in toxicity progression.

While our additional custom capture focused on identifying novel variants in genes with known biological function in axon guidance, MTA pharmacokinetics, and peripheral neuropathies, an important limitation in our study is the inability to capture flanking regions, which are more likely to contribute to regulatory activity of genes[33]. To address this, future work will include the imputation of these genomic regions using the sequencing information, which might highlight candidate genes that were not identified in the analyses presented here.

Another limitation in the analyses is that MTA-induced PN was defined using the NCI-CTCAE grading scale, which may not completely encompass the progression of neuropathy symptoms[34–36]. Future work will also investigate the use of patient-reported outcomes to yield a phenotype that embodies a more comprehensive perspective on neuropathy progression, which may reveal additional genes associated with development of drug-induced neuropathy. In fact, an earlier whole exome sequencing study utilized patient-reported outcomes to define severe peripheral neuropathy cases, which revealed the fruitful associations of CMT mutations with risk of developing CIPN[4].

Lastly, another important next step is to explore these gene regions in independent cohorts and perform functional validation. Due to the limited number of sequencing studies investigating CIPN, it may be necessary to attempt genetic validation in cohorts with genome-wide imputed data (e.g. CALGB 40101 from Chapter 2). Although genetic imputation cannot infer genotype calls for rare variants, there may be some sensitivity in exploring low-frequency variation in these genomic regions to validate our findings. Mechanistic validation of any genomic findings will also be essential in future work. The use of human sensory neurons derived from induced pluripotent stem cells would also be a crucial next step to further implicate the relevance of these identified genes to sensitize or mitigate chemotherapy-stimulated sensory neuronal damage.

Overall, our study highlighted novel genes involved in Rho GTPase signaling that may influence the mechanisms underlying sensory neuropathy caused by MTA therapy. As more genes are discovered from human genetic and functional genomic studies focused on CIPN, we will further uncover the exact molecular mechanisms that drive the development of this complex toxicity and reveal a clearer understanding of how the neuropathic symptoms manifest.

REFERENCES

1. Kryukov, G. V., Shpunt, A., Stamatoyannopoulos, J. A. & Sunyaev, S. R. Power of deep, all-exon resequencing for discovery of human trait genes. *Proc. Natl. Acad. Sci. U. S. A.* **106**, 3871–3876 (2009).
2. Walter, K., Min, J. L., Huang, J., Crooks, L., Memari, Y., McCarthy, S., Perry, J. R. B., Xu, C., Futema, M., Lawson, D., Iotchkova, V., Schiffels, S., Hendricks, A. E., Danecek, P., Li, R., Floyd, J., Wain, L. V., Barroso, I., Humphries, S. E., *et al.* The UK10K project identifies rare variants in health and disease. *Nature* **526**, 82–89 (2015).
3. Chhibber, A., Mefford, J., Stahl, E. a, Pendergrass, S. a, Baldwin, R. M., Owzar, K., Li, M., Winer, E. P., Hudis, C. a, Zembutsu, H., Kubo, M., Nakamura, Y., McLeod, H. L., Ratain, M. J., Shulman, L. N., Ritchie, M. D., Plenge, R. M., Witte, J. S. & Kroetz, D. L. Polygenic inheritance of paclitaxel-induced sensory peripheral neuropathy driven by axon outgrowth gene sets in CALGB 40101 (Alliance). *Pharmacogenomics J.* 1–7 (2014) doi:10.1038/tpj.2014.2.
4. Beutler, A. S., Kulkarni, A. a, Kanwar, R., Klein, C. J., Therneau, T. M., Qin, R., Banck, M. S., Boora, G. K., Ruddy, K. J., Wu, Y., Smalley, R. L., Cunningham, J. M., Le-Lindqwister, N. A., Beyerlein, P., Schroth, G. P., Windebank, A. J., Züchner, S. & Loprinzi, C. L. Sequencing of Charcot-Marie-Tooth disease genes in a toxic polyneuropathy. *Ann. Neurol.* **76**, 727–37 (2014).
5. Boora, G. K., Kulkarni, A. A., Kanwar, R., Beyerlein, P., Qin, R., Banck, M. S., Ruddy, K. J., Pleticha, J., Lynch, C. A., Behrens, R. J., Züchner, S., Loprinzi, C. L. & Beutler, A. S. Association of the Charcot–Marie–Tooth disease gene ARHGEF10 with paclitaxel induced peripheral neuropathy in NCCTG N08CA (Alliance). *J. Neurol. Sci.* **357**, 35–40

(2015).

6. Apellániz-Ruiz, M., Lee, M. Y., Sánchez-Barroso, L., Gutiérrez-Gutiérrez, G., Calvo, I., García-Estévez, L., Sereno, M., García-Donás, J., Castelo, B., Guerra, E., Leandro-García, L. J., Cascón, A., Johansson, I., Robledo, M., Ingelman-Sundberg, M. & Rodríguez-Antona, C. Whole-exome sequencing reveals defective CYP3A4 variants predictive of paclitaxel dose-limiting neuropathy. *Clin. Cancer Res.* **21**, 322–328 (2015).
7. Apellaniz-Ruiz, M., Tejero, H., Inglada-Perez, L., Sanchez-Barroso, L., Gutierrez-Gutierrez, G., Calvo, I., Castelo, B., Redondo, A., García-Donas, J., Romero-Laorden, N., Sereno, M., Merino, M., Curras-Freixes, M., Montero-Conde, C., Mancikova, V., Åvall-Lundqvist, E., Green, H., Al-Shahrour, F., Cascon, A., *et al.* Targeted sequencing reveals low-frequency variants in EPHA genes as markers of paclitaxel-induced peripheral neuropathy. *Clin. Cancer Res.* **23**, 1227–1235 (2017).
8. Schneider, B. P., Lai, D., Shen, F., Jiang, G., Radovich, M., Li, L., Gardner, L., Miller, K. D., O'Neill, A., Sparano, J. A., Xue, G., Foroud, T. & Sledge, G. W. Charcot-Marie-Tooth gene, SBF2, associated with taxaneinduced peripheral neuropathy in African Americans. *Oncotarget* **7**, 82244–82253 (2016).
9. Abaji, R., Ceppi, F., Patel, S., Gagné, V., Xu, C. J., Spinella, J. F., Colombini, A., Parasole, R., Buldini, B., Basso, G., Conter, V., Cazzaniga, G., Leclerc, J. M., Laverdière, C., Sinnett, D. & Krajinovic, M. Genetic risk factors for VIPN in childhood acute lymphoblastic leukemia patients identified using whole-exome sequencing. *Pharmacogenomics* **19**, 1181–1193 (2018).
10. Rugo, H. S., Barry, W. T., Moreno-Aspitia, A., Lyss, A. P., Cirrincione, C., Leung, E., Mayer, E. L., Naughton, M., Toppmeyer, D., Carey, L. A., Perez, E. A., Hudis, C. &

Winer, E. P. Randomized phase III trial of paclitaxel once per week compared with nanoparticle albumin-bound nab-paclitaxel once per week or ixabepilone with bevacizumab as first-line chemotherapy for locally recurrent or metastatic breast cancer: CALGB 40502/NCCTG N0. *J. Clin. Oncol.* **33**, 2361–2369 (2015).

11. Voorman, A., Brody, J., Chen, H., Lumley, T. & Davis, B. seqMeta : an R Package for meta-analyzing region-based tests of rare DNA variants. 1–17 (2017).
12. Therneau, T. M. A Package for Survival Analysis in S. (2015).
13. R Core Team. R: A language and environment for statistical computing. (2016).
14. Flegel, C., Schöbel, N., Altmüller, J., Becker, C., Tannapfel, A., Hatt, H. & Gisselmann, G. RNA-Seq analysis of human trigeminal and dorsal root ganglia with a focus on chemoreceptors. *PLoS One* **10**, 1–30 (2015).
15. Chi, J. & Cohen, P. The multifaceted roles of PRDM16: Adipose biology and beyond. *Trends Endocrinol. Metab.* **27**, 11–23 (2016).
16. Baizabal, J. M., Mistry, M., García, M. T., Gómez, N., Olukoya, O., Tran, D., Johnson, M. B., Walsh, C. A. & Harwell, C. C. The Epigenetic State of PRDM16-Regulated Enhancers in Radial Glia Controls Cortical Neuron Position. *Neuron* **98**, 945-962.e8 (2018).
17. Kendall, G., Ensor, E., Brar-Rai, A., Winter, J. & Latchman, D. S. Nerve growth factor induces expression of immediate-early genes NGFI-A (Egr-1) and NGFI-B (nur 77) in adult rat dorsal root ganglion neurons. *Mol. Brain Res.* **25**, 73–79 (1994).
18. Ahmed, S. B. M. & Prigent, S. A. Insights into the Shc family of adaptor proteins. *J. Mol. Signal.* **12**, 1–17 (2017).
19. Gu, H., Wang, C., Li, J., Yang, Y., Sun, W., Jiang, C., Li, Y., Ni, M., Liu, W. T., Cheng, Z. & Hu, L. High mobility group box-1-toll-like receptor 4-phosphatidylinositol 3-

kinase/protein kinase B-mediated generation of matrix metalloproteinase-9 in the dorsal root ganglion promotes chemotherapy-induced peripheral neuropathy. *Int. J. Cancer* **1**, 1–13 (2019).

20. Thomas, D., Patterson, S. D. & Bradshaw, R. A. Src homologous and collagen (Shc) protein binds to F-actin and translocates to the cytoskeleton upon nerve growth factor stimulation in PC12 cells. *J. Biol. Chem.* **270**, 28924–28931 (1995).
21. Faisal, A., Kleiner, S. & Nagamine, Y. Non-redundant Role of Shc in Erk Activation by Cytoskeletal Reorganization. *J. Biol. Chem.* **279**, 3202–3211 (2004).
22. Ma, Z., Myers, D. P., Ru, F. W., Nwariaku, F. E. & Terada, L. S. p66Shc mediates anoikis through RhoA. *J. Cell Biol.* **179**, 23–31 (2007).
23. Kauskot, A., Michele, M. Di, Loyen, S., Freson, K., Verhamme, P. & Hoylaerts, M. F. A novel mechanism of sustained platelet alpha-II-beta-3 activation via PEAR1. **119**, 4056–4066 (2018).
24. Wu, H. H., Bellmunt, E., Scheib, J. L., Venegas, V., Burkert, C., Reichardt, L. F., Zhou, Z., Farĩas, I. & Carter, B. D. Glial precursors clear sensory neuron corpses during development via Jedi-1, an engulfment receptor. *Nat. Neurosci.* **12**, 1534–1541 (2009).
25. Trevisan, A. J., Bauer, M. B., Brindley, R. L., Currie, K. P. M. & Carter, B. D. Jedi-1 deficiency increases sensory neuron excitability through a non-cell autonomous mechanism. *Sci. Rep.* **10**, 1–15 (2020).
26. Haitina, T., Lindblom, J., Renström, T. & Fredriksson, R. Fourteen novel human members of mitochondrial solute carrier family 25 (SLC25) widely expressed in the central nervous system. *Genomics* **88**, 779–790 (2006).
27. Zajaczkowską, R., Kocot-Kępska, M., Leppert, W., Wrzosek, A., Mika, J. & Wordliczek,

J. Mechanisms of chemotherapy-induced peripheral neuropathy. *Int. J. Mol. Sci.* **20**, (2019).

28. Baldwin, R. M., Owzar, K., Zembutsu, H., Chhibber, A., Kubo, M., Jiang, C., Watson, D., Eclov, R. J., Mefford, J., McLeod, H. L., Friedman, P. N., Hudis, C. A., Winer, E. P., Jorgenson, E. M., Witte, J. S., Shulman, L. N., Nakamura, Y., Ratain, M. J. & Kroetz, D. L. A genome-wide association study identifies novel loci for paclitaxel-induced sensory peripheral neuropathy in CALGB 40101. *Clin. Cancer Res.* **18**, 5099–5109 (2012).
29. Park, S., Lee, H., Kim, M., Park, J., Kim, S. H. & Park, J. Emerging roles of TRIO and F-actin-binding protein in human diseases. *Cell Commun. Signal.* **16**, 2–6 (2018).
30. Ceppi, F., Langlois-Pelletier, C., Gagné, V., Rousseau, J., Ciolino, C., Lorenzo, S. De, Kevin, K. M., Cijov, D., Sallan, S. E., Silverman, L. B., Neuberg, D., Kutok, J. L., Sinnett, D., Laverdière, C. & Krajinovic, M. Polymorphisms of the vincristine pathway and response to treatment in children with childhood acute lymphoblastic leukemia. *Pharmacogenomics* **15**, 1105–1116 (2014).
31. Gillespie, C. S., Sherman, D. L., Fleetwood-Walker, S. M., Cottrell, D. F., Tait, S., Garry, E. M., Wallace, V. C. J., Ure, J., Griffiths, I. R., Smith, A. & Brophy, P. J. Peripheral demyelination and neuropathic pain behavior in periaxin-deficient mice. *Neuron* **26**, 523–531 (2000).
32. Cliff, J., Jorgensen, A. L., Lord, R., Azam, F., Cossar, L., Carr, D. F. & Pirmohamed, M. The molecular genetics of chemotherapy–induced peripheral neuropathy: A systematic review and meta-analysis. *Crit. Rev. Oncol. Hematol.* **120**, 127–140 (2017).
33. Epstein, D. J. Cis-regulatory mutations in human disease. *Briefings Funct. Genomics Proteomics* **8**, 310–316 (2009).

34. Nyrop, K. A., Deal, A. M., Reeder-Hayes, K. E., Shachar, S. S., Reeve, B. B., Basch, E., Choi, S. K., Lee, J. T., Wood, W. A., Anders, C. K., Carey, L. A., Dees, E. C., Jolly, T. A., Kimmick, G. G., Karuturi, M. S., Reinbolt, R. E., Speca, J. E. C. & Muss, H. B. Patient-reported and clinician-reported chemotherapy-induced peripheral neuropathy in patients with early breast cancer: Current clinical practice. *Cancer* **125**, 2945–2954 (2019).

35. Shimozuma, K., Ohashi, Y., Takeuchi, A., Aranishi, T., Morita, S., Kuroi, K., Ohsumi, S., Makino, H., Katsumata, N., Kuranami, M., Suemasu, K., Watanabe, T. & Hausheer, F. H. Taxane-induced peripheral neuropathy and health-related quality of life in postoperative breast cancer patients undergoing adjuvant chemotherapy: N-SAS BC 02, a randomized clinical trial. *Support. Care Cancer* **20**, 3355–3364 (2012).

36. Postma, T. J., Heimans, J. J., Muller, M. J., Ossenkoppele, G. J., Vermorken, J. B. & Aaronson, N. K. Pitfalls in grading severity of chemotherapy-induced peripheral neuropathy. *Ann. Oncol.* **9**, 739–744 (1998).

CHAPTER 4: Predicting Dose-Limiting Chemotherapy-Induced Peripheral Neuropathy Using Early Patient-Reported Outcomes and Genome-Wide Data from Breast Cancer Patients in CALGB 40502

INTRODUCTION

Chemotherapy-induced neuropathy is one of the main adverse events that contribute to dose reductions and therapy discontinuation, potentially diminishing overall chemotherapy benefit[1]. In addition, cancer survivors who experience severe chemotherapy-induced sensory peripheral neuropathy (CIPN) suffer from long-term neurological effects that hinder daily functions[2,3]. Due to these complications, there is an increasing need to appropriately monitor and manage CIPN symptoms during chemotherapy to minimize lasting impairments to health-related quality of life.

Although CIPN is frequently described as tingling/numbness or abnormal sensations that initiate at the fingertips and toes, it is still challenging to quantifiably capture the onset and severity of this neurotoxicity, in part due to interindividual differences in patient experience. Common approaches to survey CIPN symptoms include clinician-based assessments (e.g., NCI-CTCAE), patient-reported outcomes (e.g., CIPN20, EORTC, FACT/GOG-Ntx), and objective diagnostic tests (e.g., nerve conduction studies)[4,5]. While a combination of these approaches is likely most suitable to fully describe CIPN symptoms, clinician-based criteria and patient-reported questionnaires are the most commonly used in clinical trials and clinical practice[4,6].

Previous studies comparing these two types of assessments have shown that clinician-based criteria tend to underreport the severity of sensory neuropathy symptoms[7] and miss early signs of neurological impairment[8–10]. Because of these findings, there has been increasing recognition of patient-reported outcomes as a means to collect a more comprehensive view of CIPN progression over the course of treatment and/or to prospectively monitor, evaluate, and manage CIPN symptoms. Human genetic association studies have even started to use patient-

reported data to discover novel genetic markers that may help identify at-risk patients[6,11]. However, there is still a gap in understanding how to implement patient-reported outcomes and genetics as tools to predict risk for dose-limiting neuropathy events.

In this study, we investigated whether early patient-reported outcomes and genome-wide data can be used to predict dose reductions, dose delays, or therapy discontinuations (RDD) due to sensory peripheral neuropathy. Our study is motivated by the need to develop an effective and simple strategy for prevention of dose-limiting neuropathy events, which requires early prediction of patient susceptibility to developing severe neuropathy. Validation of the findings presented here will provide the first step to achieving this clinical application and lead to future studies of the proactive utilization of large-scale patient-reported outcomes to monitor and control CIPN.

MATERIALS AND METHODS

Participants

All study participants were enrolled in Cancer and Leukemia Group B (CALGB) 40502, a randomized three-arm phase III trial conducted to determine whether nanoparticle albumin-bound (nab) paclitaxel or ixabepilone is superior to paclitaxel as first-line therapy for patients with advanced breast cancer. CALGB 40502 was open from October 2008 through November 2011, enrolling a total of 799 subjects. Eligibility criteria for enrollment has been previously described[12]. All patients provided written informed consent for both the treatment and pharmacogenomic protocols that met state, federal, and institutional guidelines. Patient characteristics for the entire clinical trial cohort were previously described[12,13] (Chapter 2, Results).

Curation of FACT-GOG/Ntx scores

Patient-reported neurotoxicity assessment in CALGB 40502 was performed using the FACT/GOG-Ntx subscale (C-669 v5). The FACT/GOG-Ntx subscale is a validated 11-item questionnaire that uses a 5-pt Likert-like scale ("Not at all"; "A little bit"; "Somewhat"; "Quite a bit"; "Very much") to evaluate symptoms associated with chemotherapy-induced neuropathy. Patients were asked to answer the questionnaire every treatment cycle, considering their experiences and symptoms for the last week. From the entire subscale, four items capturing experiences of sensory peripheral neuropathy and two items focusing on dysfunctional neuropathy (Table 4.1) were considered, and each item response was converted to scores 0-4. For each assessment, the four sensory neuropathy scores (fgsum4) and all six scores (fgsum6) were summed to quantitate the cumulative peripheral neuropathy symptoms experienced. A total of 6,207 FACT/GOG-Ntx assessments across the 799 randomized patients were curated. Assessments were matched with treatment cycle times using FACT/GOG-Ntx assessment week period, where a match was only implemented if the assessment week period lies within four days of a treatment cycle start and end dates (Figure 4.1). Baseline assessment entries were subsequently included for those patients with available matched data. After this process, a total of 5,998 FACT/GOG-Ntx assessments across 719 patients (PRO cohort) were used for further analysis.

Table 4.1 FACT/GOG-Ntx questionnaire items capturing experiences of chemotherapy-induced neuropathy.

	FACT/GOG-Ntx subscale items	Summed scores	
Sensory neuropathy	I have numbness and tingling in my hands. I have numbness and tingling in my feet. I feel discomfort in my hands. I feel discomfort in my feet.	fgsum4	fgsum6
Dysfunctional neuropathy	I have trouble buttoning buttons. I have trouble feeling the shape of small objects when they are in my hand.		

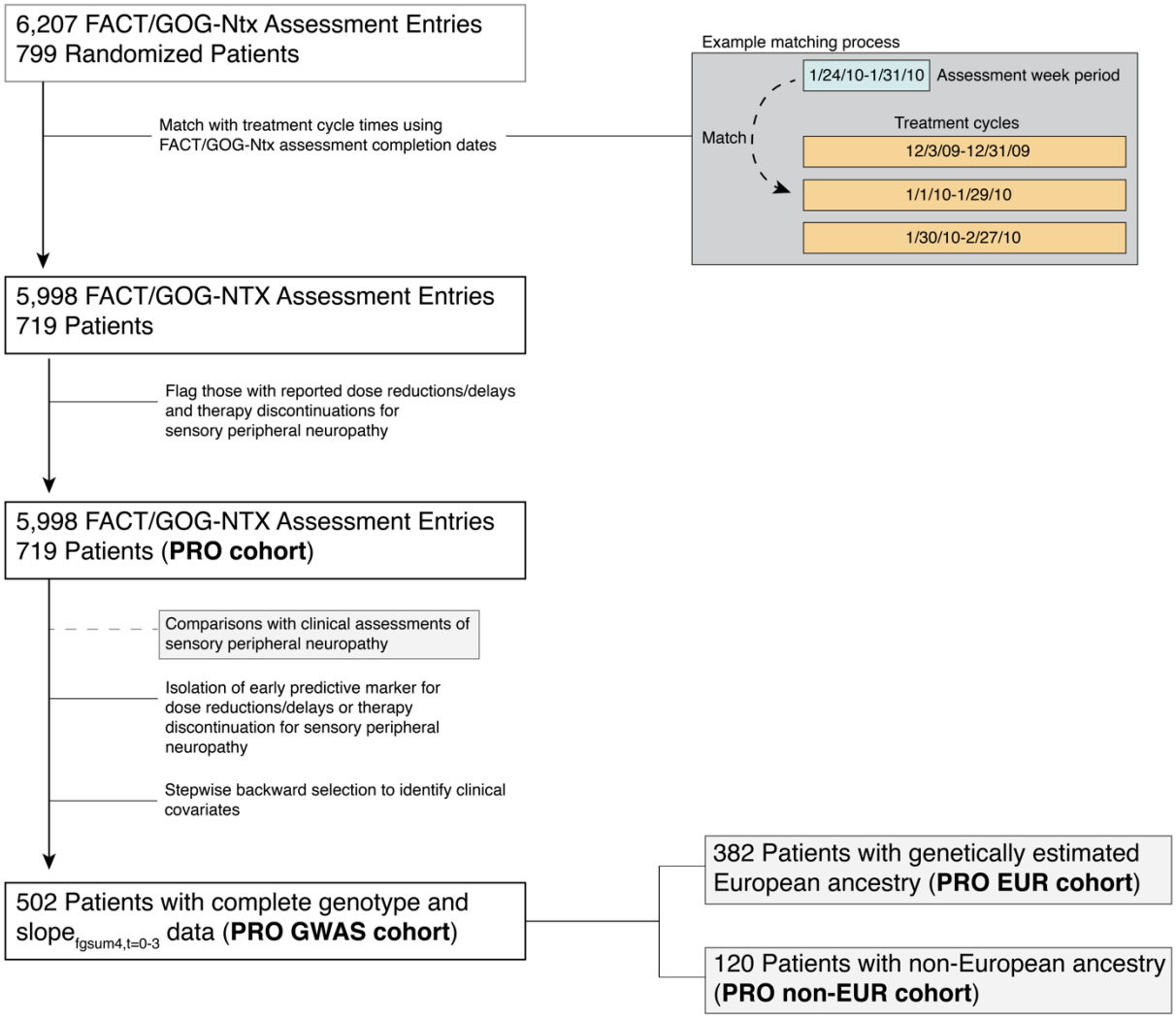

Figure 4.1 Schematic workflow of FACT/GOG-Ntx score curation and definition of PRO cohort.

Identifying an early predictor for sensory neuropathy

To investigate if patient-reported outcomes data can be used as a predictive marker for neuropathy, we considered six different constructs of fgsum4 and fgsum6 scores: fgsum4 or fgsum6 score at treatment cycle 3 ($fgsum4_{t=3}$, $fgsum6_{t=3}$), slope of fgsum4 or fgsum6 scores until treatment cycle 3 ($slope_{fgsum4,t=0-3,}$ $slope_{fgsum6,t=0-3}$), and area under the curve (AUC) of fgsum4 or fgsum6 scores until treatment cycle 3 ($AUC_{fgsum4,t=0-3}$, $AUC_{fgsum6,t=0-3}$). Each construct was tested as a predictor in a logistic regression for severe neuropathy events in the PRO cohort (n = 719), where each model was trained on 75% of data and a model AUC_{ROC} was calculated on the remaining 25% of the data to determine the best early predictor of sensory neuropathy. Severe neuropathy events were defined by dose reductions or delays and therapy discontinuations specifically denoted for sensory peripheral neuropathy. The construct with the largest model AUC_{ROC} was chosen for further prediction analyses. For the $fgsum4_{t=3}$ and $fgsum6_{t=3}$, the closest fgsum4 or fgsum6 score to treatment cycle 3 is used for those who do not have scores at cycle 3 (n=159), where a mean score is used when the closest scores are equidistant in time or two scores are captured for a given treatment cycle time. Patients with scores more than two cycles away from cycle 3 were excluded (n = 3). Patients who experienced RDD for sensory peripheral neuropathy before cycle 3 were also excluded, leaving 703 $fgsum4_{t=3}$ and $fgsum6_{t=3}$ measurements. For slope predictors, only those with at least three scores through cycle 3 were included (n=629), and slopes were calculated using a linear regression with fgsum4 or fgsum6 scores and treatment cycle time. For $AUC_{fgsum4,t=0-3}$ or $AUC_{fgsum4,t=0-3}$, all scores until cycle 3, regardless of the number of scores, were used to calculate score AUCs using the trapezoid rule. No patients were excluded, leaving 719 $AUC_{fgsum4,t=0-3}$ and $AUC_{fgsum6,t=0-3}$ measurements.

Genotype Data

A similar quality control workflow was used to isolate genotype data and has been described in a previous chapter (Chapter 2, Methods). Briefly, from those enrolled in CALGB 40502, a total of 633 consented patients with DNA samples were genotyped using the Illumina HumanOmniExpressExome-8 BeadChip, interrogating 964,055 SNPs with coverage of common variants and additional exonic content. Genotyping data were filtered using a standard quality control (QC) pipeline. All samples were filtered for low call rate (< 0.99) or low genotyping performance; none were excluded. Identity-by-descent (IBD) analysis identified the presence of two closely related individuals, which were excluded and found later to be a plating error. An X chromosome heterozygosity estimation identified three genetic males that were removed, leaving 628 subjects for further analysis. Principal component analysis (PCA) was performed using directly genotyped single nucleotide polymorphisms (SNPs) of all 628 study subjects to determine genetic ancestry with the GenABEL R package. A total of 478 subjects of European genetic ancestry were identified by using the mean values for the first 3 PC vectors with self-declaring "White" race and "Non-Hispanic" / "Unknown" ethnicity. SNPs were excluded using the following quality control filters: minor allele frequency (MAF) < 0.05, deviation from Hardy-Weinberg equilibrium with *P* value < 1E-08, call rate < 0.99, and non-autosomal SNPs, leaving 593,989 SNPs for genome-wide analysis. Among the 478 genetically estimated Europeans with genotyped data, a total of 382 patients with FACT/GOG-Ntx information (PRO EUR cohort) was used in the prediction analysis. From the remaining 150 study subjects of non-European genetic ancestry, a total of 120 with FACT/GOG-Ntx information were used as the validation set (PRO non-EUR cohort).

Statistical analysis for comparisons between patient-reported and clinician-based assessments

All comparisons of fgsum4 and fgsum6 scores between those who experience grade 2 or higher neuropathy events (defined by NCI NCI-CTCAE v3.0) and those who had no reported neuropathy events were evaluated using the Mann-Whitney-Wilcoxon test. Differences in all constructs of fgsum4 and fgsum6 scores between those who experience RDD and those who had no reported RDD events for sensory peripheral neuropathy were also similarly tested using the Mann-Whitney-Wilcoxon test. All tests were conducted using the function *wilcox.test* under the *R* v3.5.3 statistical environment.

Prediction analysis

The final prediction model was determined using the PRO EUR cohort with dose reductions or delays and therapy discontinuations (RDD) specific for sensory peripheral neuropathy as the primary outcome. To identify any clinical covariates, a stepwise backward selection of clinical characteristics on the PRO cohort, including self-reported race/ethnicity, age, hormone receptor status, bevacizumab therapy, visceral metastases, diabetic status, prior taxane status, and body surface area, was performed using a conditional logistic regression stratifying for treatment arm; no clinical features remained. After identifying the best early predictor for sensory neuropathy, a final PRO prediction model for RDD was generated on PRO EUR cohort (n = 382) using $\text{slope}_{\text{fgsum6,t=0-3}}$ as the primary predictor within the framework of a conditional logistic regression, stratifying for treatment arm. The final PRO model was validated on the PRO non-EUR cohort (n = 120).

To investigate whether genome-wide association data would improve the final PRO prediction model, a 10-fold cross-validation was performed to generate a prediction model with

slope$_{fgsum6,t=0-3}$ and genetics using the PRO EUR cohort (Figure 4.2). First, samples were subdivided into 10 groups of approximately equal sizes, where one group was reserved as the test set and each individual was only used once in a single test set. GWAS was performed on each training set to identify SNPs associated with RDD status (*P* value threshold < 1E-04). To generate ten initial models, a stepwise backwards regression was performed with slope$_{fgsum6,t=0-3}$ and the identified SNPs using a conditional logistic regression, stratifying for treatment arm, on each training set. The final PRO genetic model included slope$_{fgsum6,t=0-3}$ and SNPs that remained in at least 50% of the initial models, and a model AUC$_{ROC}$ was calculated on the PRO non-EUR cohort. This analysis was conducted under the *R* v3.5.3 statistical environment[14].

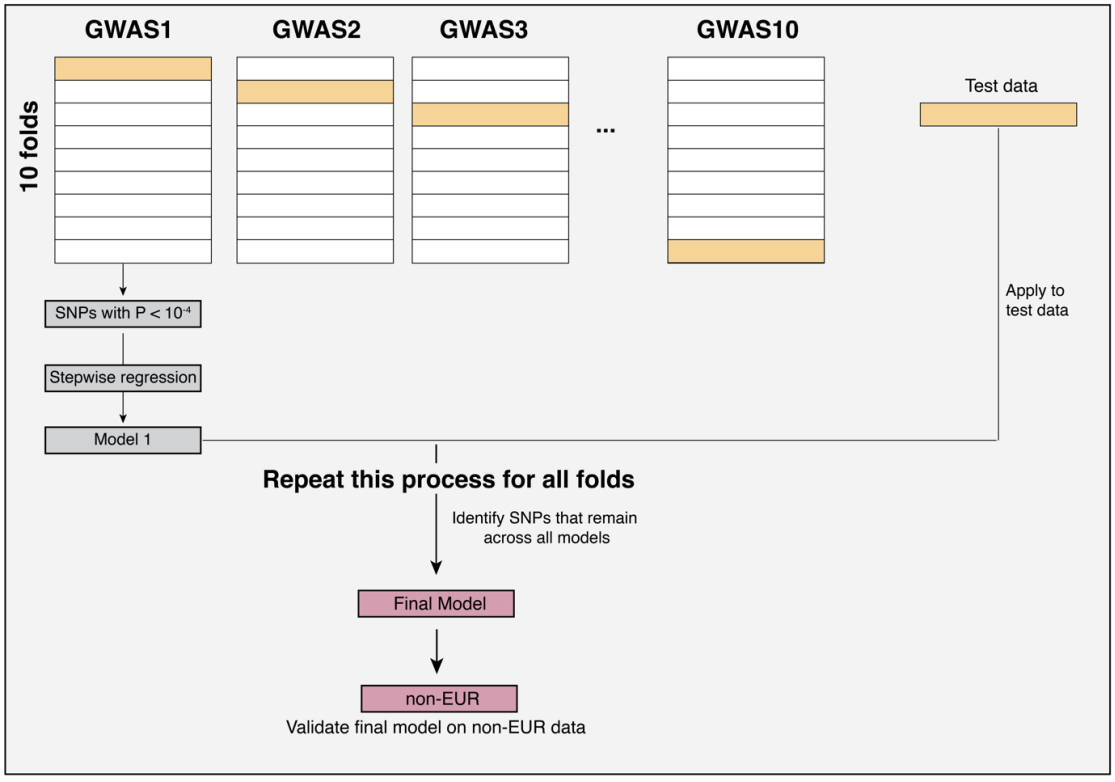

Figure 4.2 Overview of the PRO genetic prediction model. A 10-fold cross-validation in PRO EUR (n = 382) cohort was performed to build a prediction model using slope$_{fgsum6,t=0-3}$ with SNPs. Ten GWAS were performed to identify SNPs associated with RDD specific for neuropathy. A stepwise backwards regression with SNPs with association of P < 1E-04 was performed to build ten initial PRO genetic models. A final PRO genetic prediction model was created using slope$_{fgsum6,t=0-3}$ and SNPs that remained in at least 50% of the ten initial models, and a model AUC$_{ROC}$ was generated using the PRO non-EUR cohort.

RESULTS

Among the 799 patients randomized in CALGB 40502, a total of 6,207 FACT/GOG-Ntx assessment entries were collected during the clinical trial and were used as patient-reported outcomes of sensory peripheral neuropathy. Assessments were matched with treatment cycle and dosing information using completion dates with treatment cycle start and end dates. Patients with no recorded FACT/GOG-Ntx and treatment cycle data (n = 17), patients with either no recorded treatment cycle data (n = 6) or FACT/GOG-Ntx data (n = 14), patients with no matching FACT/GOG-Ntx entries (n = 9), and patients with only baseline FACT/GOG-Ntx entries (n = 34) were excluded. After this matching process, a total of 5,998 FACT/GOG-Ntx assessments across 719 patients (PRO cohort) were used for further analysis, where 75% of patients have one to 10 assessments and the median number of assessments per patient is six (Figure 4.3). We focused on characterizing the sum of the four sensory peripheral neuropathy items (fgsum4) and sum of these four items in addition to two dysfunctional neuropathy items (fgsum6) as the primary patient-reported measurements for chemotherapy-induced neuropathy. (Table 4.1).

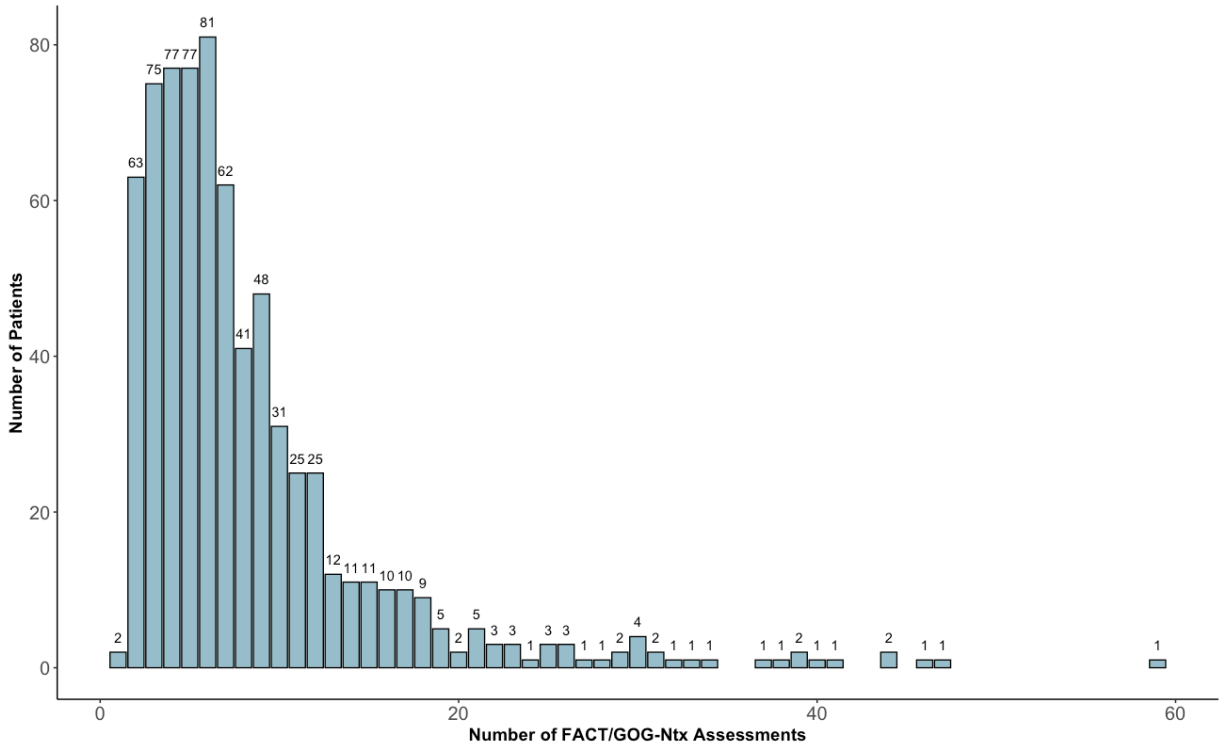

Figure 4.3 Distribution of FACT/GOG-Ntx assessments captured for patients in CALGB 40502. The numbers at the top of each bar represents the number of patients with *x* amount of FACT/GOG-Ntx assessments. The median number of FACT/GOG-Ntx assessments per patient is six.

Patient-reported scores capture neuropathy events in CALGB 40502

Before assessing whether patient-reported outcomes can be used as an early predictor of significant neuropathy, we assessed whether fgsum4 and fgsum6 scores capture clinician-reported sensory peripheral neuropathy events. In CALGB 40502, neurotoxicity adverse events were assessed using the NCI-CTCAE grading scale, where any significant grade 2 or higher peripheral neuropathy events were required to be reported. Patients with reported grade 2 or higher peripheral neuropathy events generally had higher fgsum4 and fgsum6 scores compared to those without any reported events, regardless of treatment arm (Figure 4.4). The score differences between these two groups are observed as early as treatment cycle 1 in the paclitaxel (P_{fgsum4} = 7.92E-04, P_{fgsum6} = 1.76E-03, Mann-Whitney-Wilcoxon test) and nab-paclitaxel

(P_{fgsum4} = 0.048; P_{fgsum6} = 0.059; Mann-Whitney-Wilcoxon test) arms and treatment cycle 2 in the ixabepilone arm (P_{fgsum4} = 1.64E-05; P_{fgsum6} = 4.25E-05; Mann-Whitney-Wilcoxon test) (Figure 4.4). On an individual level, fgsum4 and fgsum6 scores captured the time at which peripheral neuropathy events occur (Figure 4.5). Furthermore, to determine if the summed scores are sensitive in distinguishing patients with and without neuropathy, fgsum4 and fgsum6 scores at time of reported NCI-CTCAE grade 2 or higher neuropathy event were compared with those at time of last assessment for patients without any reported neuropathy events. All item scores and the cumulative fgsum4 and fgsum6 scores are statistically different between patients with and without grade 2 or higher neuropathy (Figure 4.6; P < 2E-16, Mann-Whitney-Wilcoxon test).

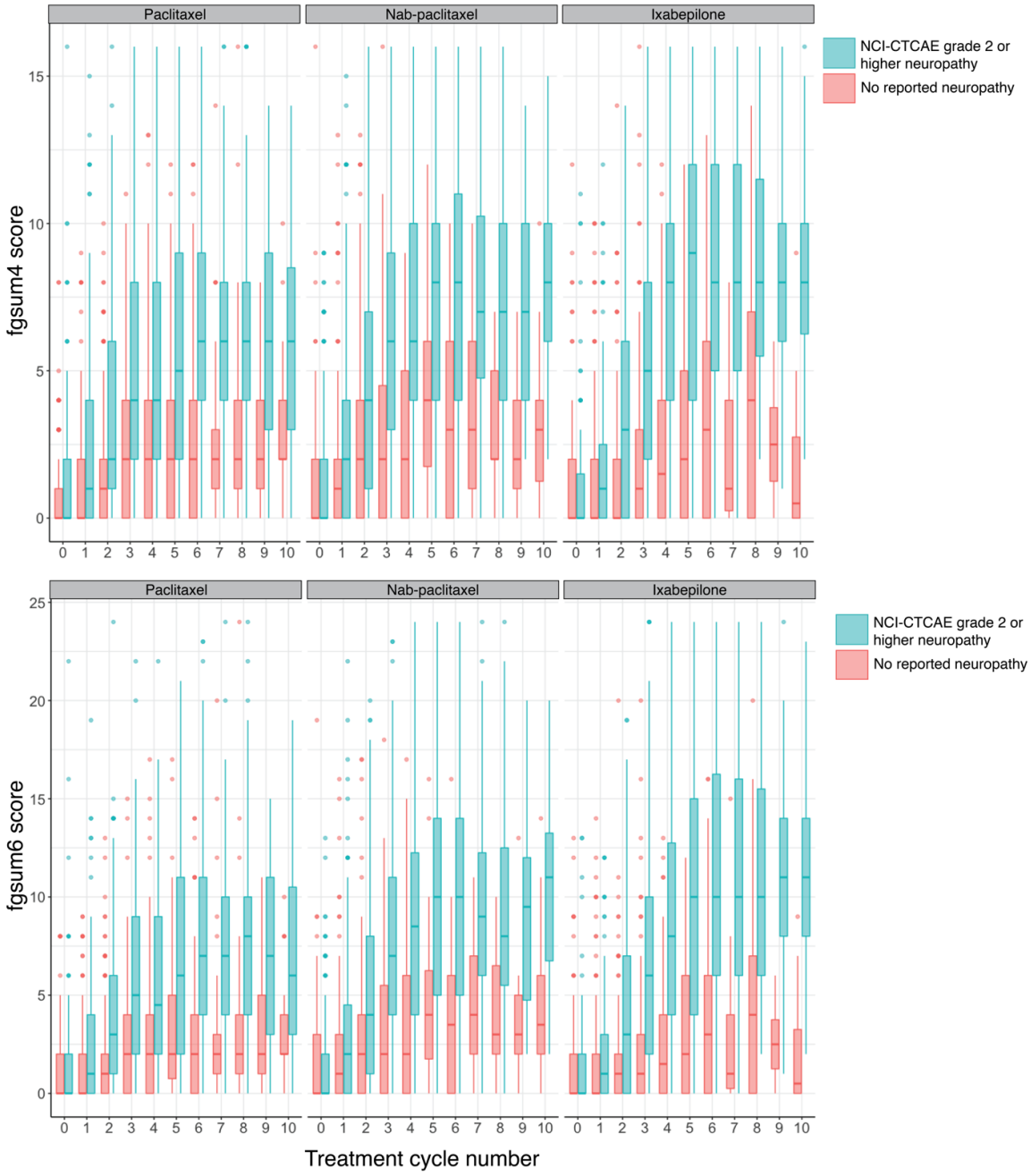

Figure 4.4 Box plots of fgsum4 and fgsum6 scores at baseline and for the first ten treatment cycles. Score distributions are binned by those with reported NCI-CTCAE grade 2 or higher neuropathy events (blue) and those with no reported neuropathy events (pink). Each panel represents the three treatment arms in CALGB 40502. Score differences between two patient groups are statistically significant as early as cycle 1 for paclitaxel (P_{fgsum4} = 7.92E-04, P_{fgsum6} = 1.76E-03) and nab-paclitaxel (P_{fgsum4} = 0.048; P_{fgsum6} = 0.059), and treatment cycle 2 in the ixabepilone arm (P_{fgsum4} = 1.64E-05; P_{fgsum6} = 4.25E-05). Differences in scores at each cycle are tested using the Mann-Whitney-Wilcoxon test.

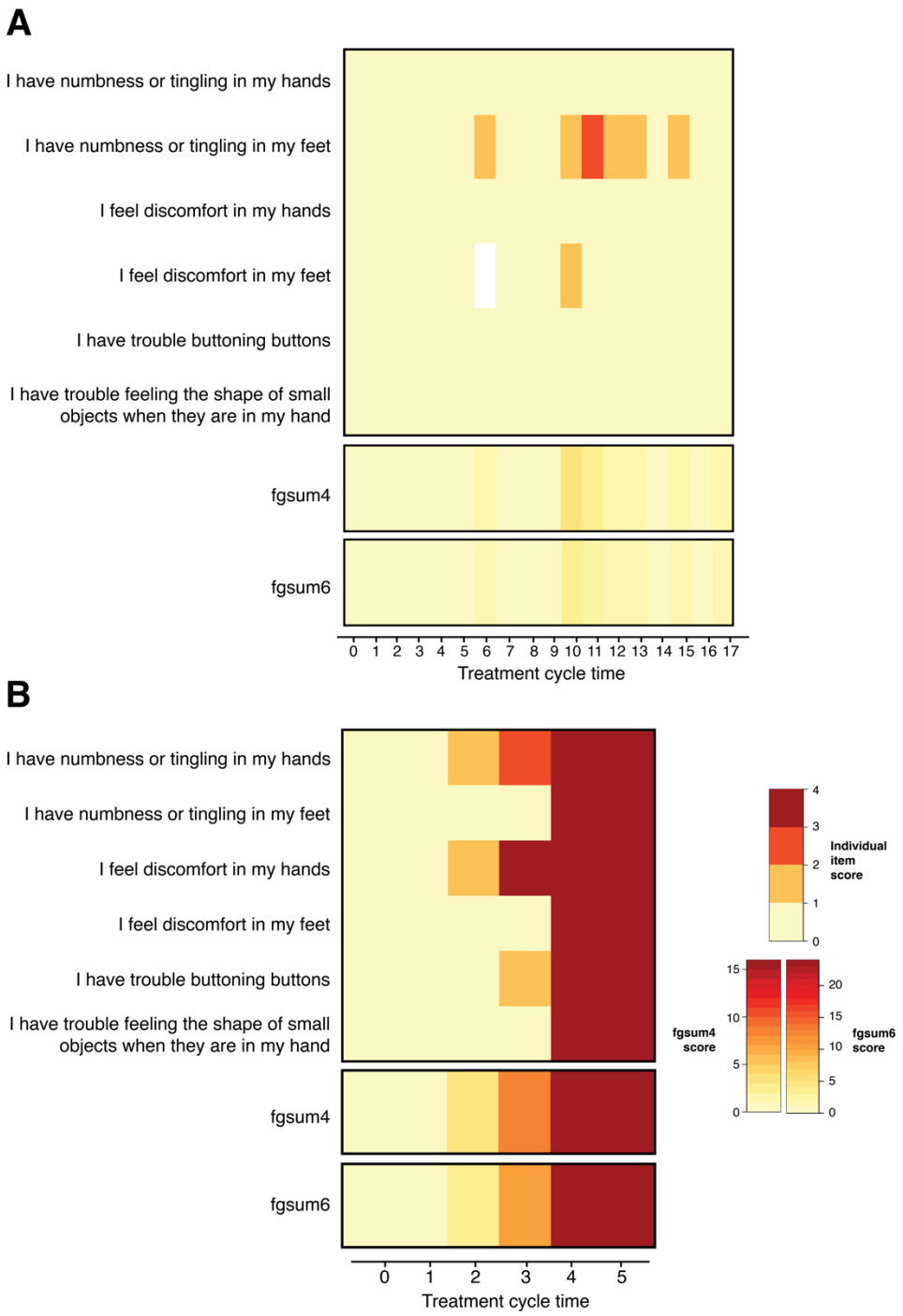

Figure 4.5 Heatmap of scores for two example patients, one without any reported peripheral neuropathy events (A) and one with a reported NCI-CTCAE grade 2 or higher peripheral neuropathy event at treatment cycle 4 (B). Each box represents a score for each sensory neuropathy item (rows) at each treatment cycle time point captured (columns). A response of "not at all" corresponds to a score of 0 while a response of "very much" corresponds to a score of 4.

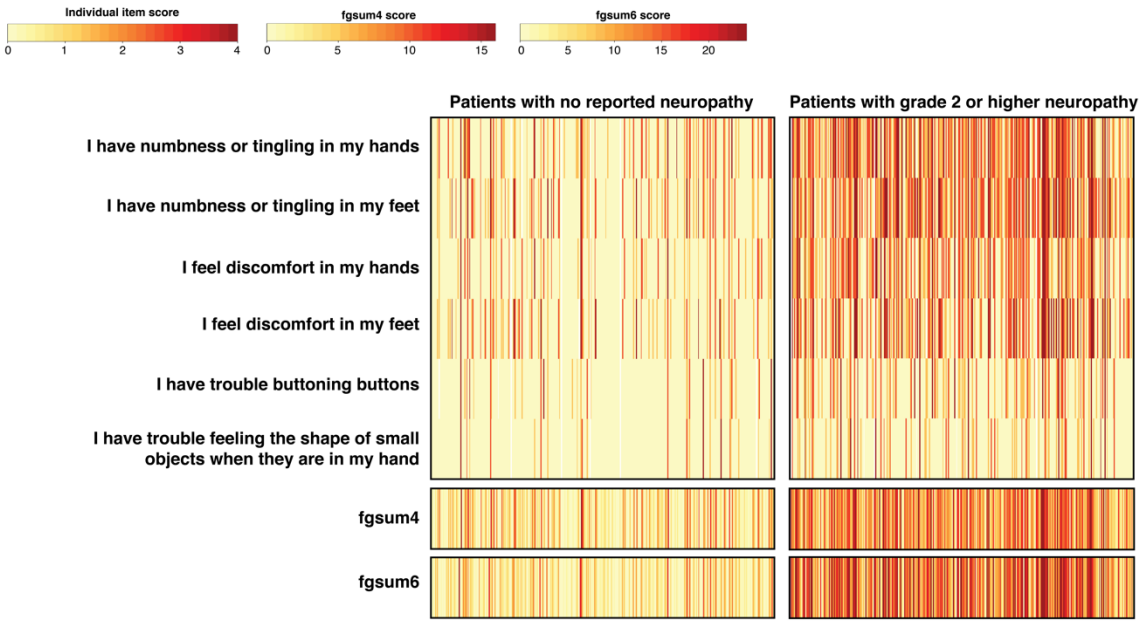

Figure 4.6 Heatmaps of sensory neuropathy items, fgsum4 and fgsum6 for all patients. Each box in each panel represents a score for each sensory neuropathy item and fgsum4 and fgsum6 (rows) for each individual (columns). A response of "not at all" corresponds to a score of 0 while a response of "very much" corresponds to a score of 4. Scores displayed for patients with no reported neuropathy (left panel, n = 348) were taken at the last assessment. Scores displayed for those with neuropathy (right panel, n = 326) were taken at the time of reported NCI-CTCAE grade 2 or higher neuropathy event. Each item score or summed score was statistically significant between patients with no reported neuropathy and those with grade 2 or higher neuropathy (P < 2E-16, Mann-Whitney-Wilcoxon test).

In the clinical trial setting, peripheral neuropathy adverse events are often reported using the NCI-CTCAE grading scale; however, in standard clinical practice, these events are often reported as dose reductions and delays due to peripheral neuropathy or as the reason for therapy discontinuation. In CALGB 40502, the median cycle time to first dose reduction/delay or therapy discontinuation for peripheral neuropathy is cycle six, five, and five in the paclitaxel, nab-paclitaxel, and ixabepilone arms, respectively (Figure 4.7). Patients with reported dose reductions/delays or therapy discontinuations for peripheral neuropathy generally had higher fgsum4 and fgsum6 scores compared to those without any reported events as early as treatment cycle 2, regardless of treatment arm (Figure 4.8; paclitaxel, P_{fgsum4} = 0.0277, P_{fgsum6} = 0.0205; nab-paclitaxel, P_{fgsum4} = 4.74E-03, P_{fgsum6} = 4.09E-03; ixabepilone, P_{fgsum4} = 1.91E-05, P_{fgsum6} =

7.13E-05; Mann-Whitney-Wilcoxon test). Similar to sensitivity in distinguishing patients with grade 2 or higher peripheral neuropathy, fgsum4 and fgsum6 scores at time of first dose reduction/delay or therapy discontinuation for peripheral neuropathy were significantly different to those at time of last assessment for the remaining patients (Figure 4.9; P_{fgsum4}, P_{fgsum6} < 2.2E-16, Mann-Whitney-Wilcoxon test). Overall, both fgsum4 and fgsum6 scores can distinguish between those who experience peripheral neuropathy (e.g. grade 2 or higher neuropathy and dose reductions/delays or therapy discontinuation) and those who did not, regardless of treatment arm. Because dose reductions/delays or therapy discontinuations are significant dose-limiting events that may reduce overall chemotherapy benefit, they were defined as our main phenotype for predicting sensory neuropathy using either fgsum4 or fgsum6 scores in subsequent analyses.

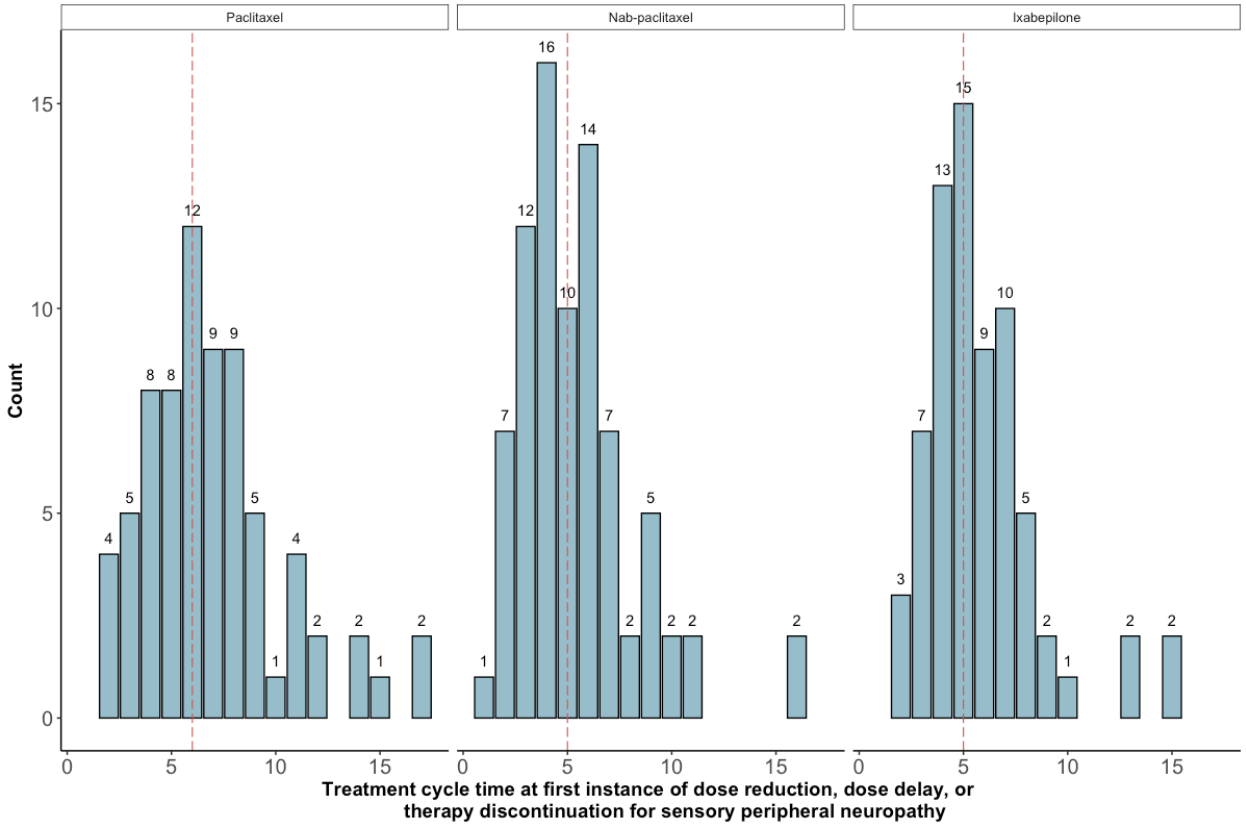

Figure 4.7 Time of dose reductions/delays or therapy discontinuation for sensory neuropathy observed in each treatment arm of CALGB 40502. The numbers above the bars represent the number of patients with the first dose reduction/delay or therapy discontinuation at the given treatment cycle time. Median treatment cycle time to first dose reduction/delay or therapy discontinuation for sensory neuropathy for each treatment arm is shown as the vertical red dashed line. Total number of patients with dose reductions/delays or therapy discontinuation for sensory neuropathy is 72, 80, and 69 in the paclitaxel, nab-paclitaxel, and ixabepilone arms, respectively.

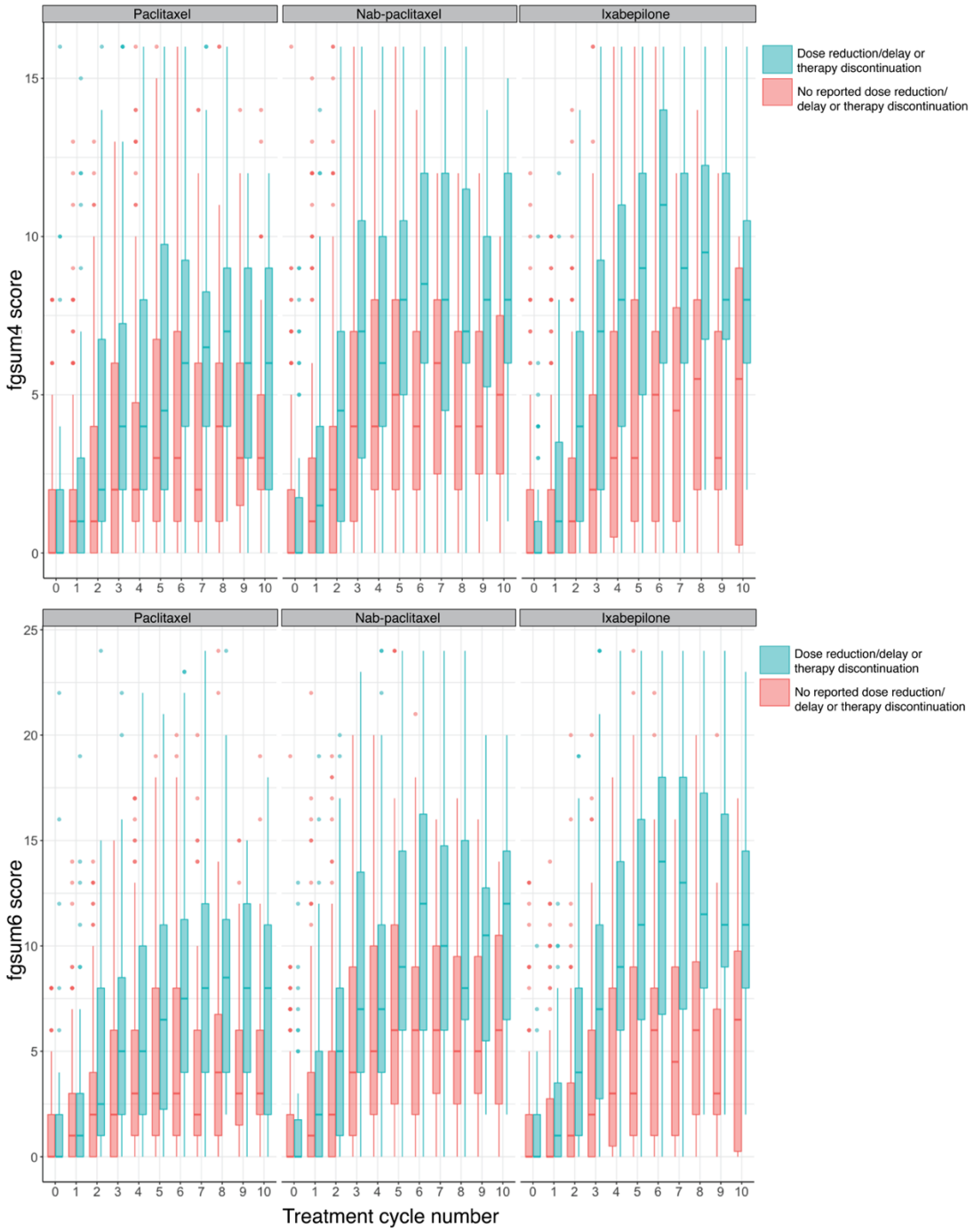

Figure 4.8 Box plots of fgsum4 and fgsum6 scores at baseline and for the first ten treatment cycles. Score distributions are binned by those with reported dose reductions/delays or therapy discontinuation for neuropathy (blue) and those without reported events (pink). Each panel represents one of the three treatment arms in CALGB 40502. Score differences between the two patient groups are statistically significant as early as cycle 2 for all treatment arms (paclitaxel, P_{fgsum4} = 0.0277, P_{fgsum6} = 0.0205; nab-paclitaxel, P_{fgsum4} = 4.74E-03, P_{fgsum6} = 4.09E-03; ixabepilone, P_{fgsum4} = 1.91E-05, P_{fgsum6} = 7.13E-05). Differences in scores at each cycle are tested using the Mann-Whitney-Wilcoxon test.

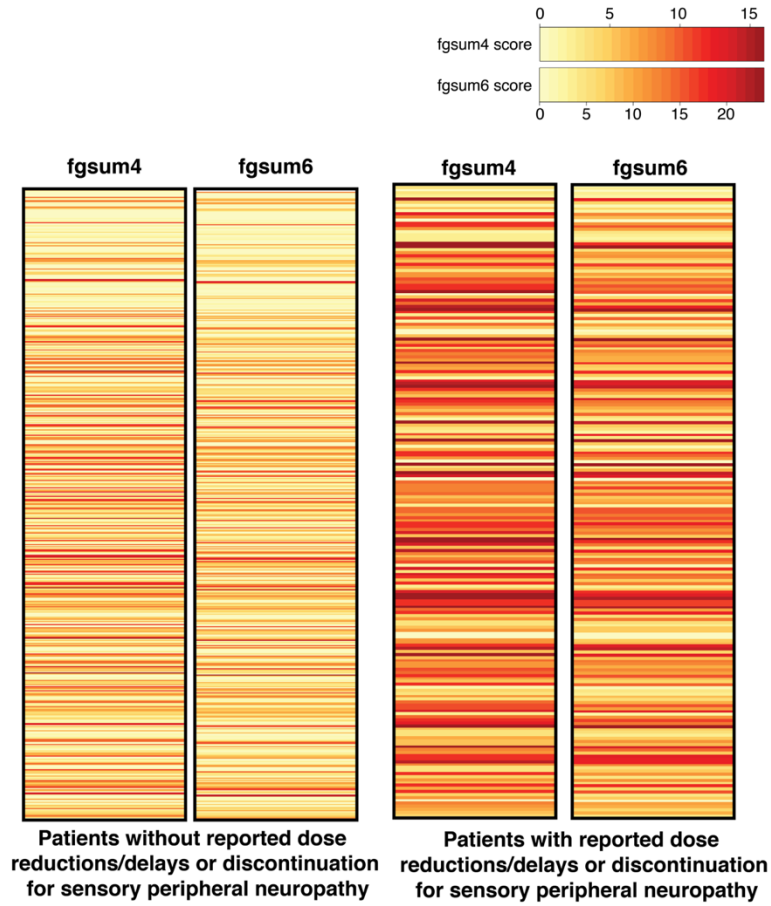

Figure 4.9 Heatmaps of fgsum4 and fgsum6 scores at time of first dose reduction/delay or therapy discontinuation. Each box in each panel represents the fgsum4 and fgsum6 score for each patient. Scores displayed for patients with no reported dose reduction/delay or discontinuation (RDD) (left panel, n = 504) were taken at the last assessment. Scores displayed for those with reported dose reduction/delay or discontinuation (right panel, n = 212) were taken at the time of reported event. Patients with fgsum4/fgsum6 scores that could not be captured within two cycles of reported RRD or last assessment time were excluded from the plot (n = 3). Differences in all scores between patients with no reported neuropathy and those with dose reductions/delays or therapy discontinuation for peripheral neuropathy are significant (P_{fgsum6}, P_{fgsum4} < 2.2E-16, Mann-Whitney-Wilcoxon test).

Characteristics of early predictors for RDD using patient-reported outcomes

To investigate if patient-reported outcomes data can be used as an early predictive marker for neuropathy, we considered six different constructs of fgsum4 and fgsum6 scores: fgsum4 or fgsum6 score at treatment cycle 3 ($fgsum4_{t=3}$, $fgsum6_{t=3}$), slope of fgsum4 or fgsum6 scores until treatment cycle 3 ($slope_{fgsum4,t=0-3}$, $slope_{fgsum6,t=0-3}$), and area under the curve of fgsum4 or fgsum6

scores until treatment cycle 3 ($AUC_{fgsum4,t=0-3}$, $AUC_{fgsum6,t=0-3}$). Treatment cycle 3 was chosen as the last considered time point since most dose reductions/delays or therapy discontinuations for peripheral neuropathy occur around treatment cycle 5 (Figure 4.7). Figure 10 shows the distribution of the $AUC_{fgsum4,t=0-3}$ measurements in each treatment arm, where the median $AUC_{fgsum4,t=0-3}$ values were 4, 6, and 3 for paclitaxel, nab-paclitaxel, and ixabepilone, respectively. Differences in $AUC_{fgsum4,t=0-3}$ between patients with reported dose reductions/delays or therapy discontinuations for peripheral neuropathy are significant in all three treatment arms (Figure 4.10). A similar distribution of $AUC_{fgsum6,t=0-3}$ measurements is shown in Figure 4.11, where the median $AUC_{fgsum6,t=0-3}$ values were 4.5, 6.5, and 3 for paclitaxel, nab-paclitaxel, and ixabepilone, respectively. Similarly to $AUC_{fgsum4,t=0-3}$, patients with RDD had significantly higher $AUC_{fgsum6,t=0-3}$ than those without RDD for peripheral neuropathy (Figure 4.11).

For scores at cycle 3, the median $fgsum4_{t=3}$ scores were 2, 4, and 2 while the median $fgsum6_{t=3}$ scores were 3, 5, and 2 for paclitaxel, nab-paclitaxel, and ixabepilone, respectively (Figures 4.12-4.13). Patients with reported dose reductions/delays or therapy discontinuations for peripheral neuropathy scored higher than those without these events in all three treatment arms (Figures 4.12-4.13). Similar to $fgsum4_{t=3}$ scores, $fgsum6_{t=3}$ scores are also higher in patients with RDD than those who do not experience RDD for sensory peripheral neuropathy (Figure 4.13).

Figures 4.14-4.15 show the distribution of the $slope_{fgsum4,t=0-3}$ and $slope_{fgsum6,t=0-3}$ measurements in each treatment arm. The mean $slope_{fgsum4,t=0-3}$ values were 0.889, 1.320, and 0.969 while the mean $slope_{fgsum6,t=0-3}$ values were 1.04, 1.60, and 1.15 for paclitaxel, nab-paclitaxel, and ixabepilone, respectively. Slopes using both fgsum4 and fgsum6 calculated from patients with reported dose reductions/delays or therapy discontinuations for peripheral neuropathy are significantly higher than those without RDD (Figures 4.14-4.15).

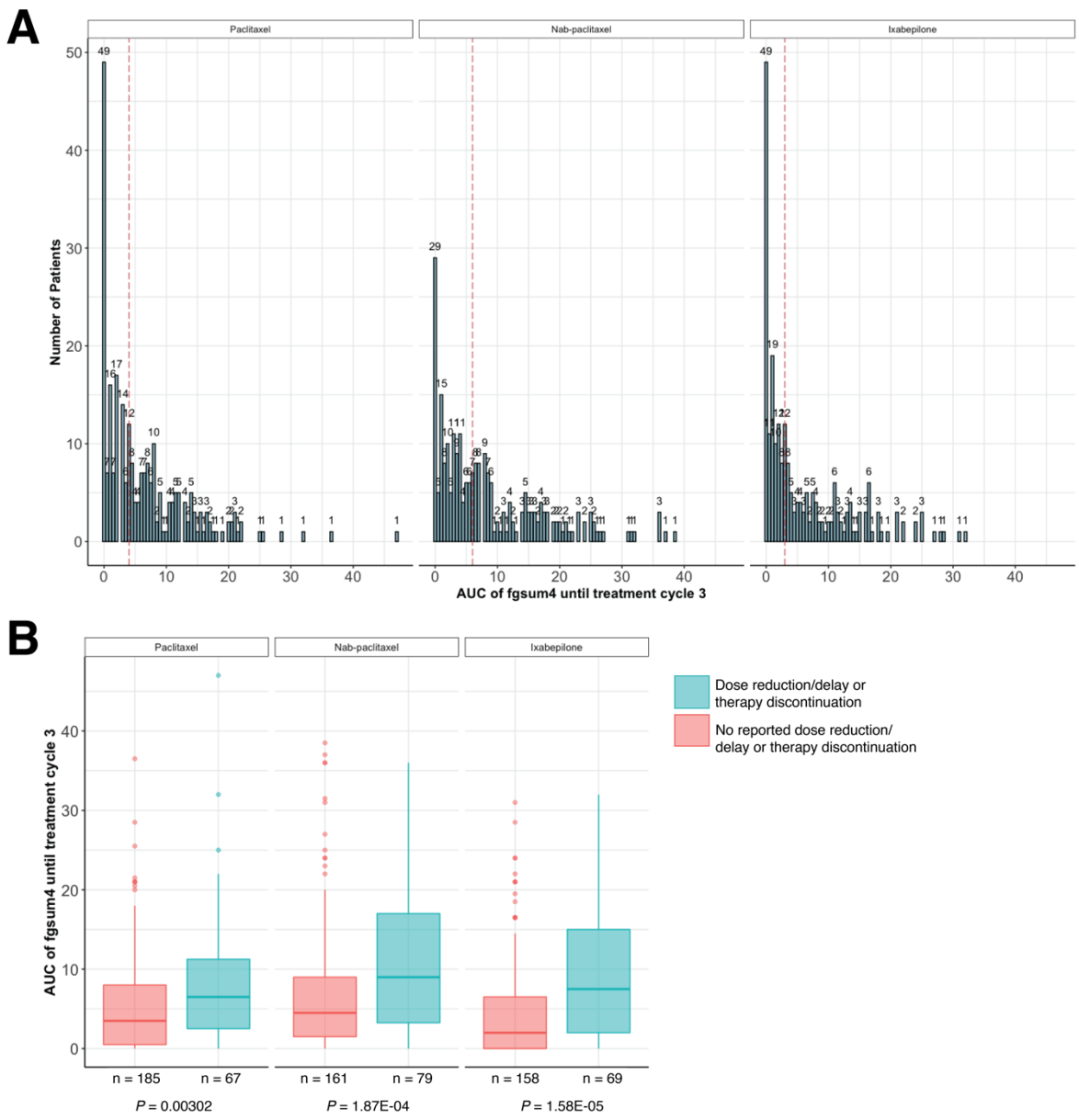

Figure 4.10 Distribution of $AUC_{fgsum4,t=0-3}$ and relationship to dose reductions/delays or therapy discontinuation. (A) Distribution of $AUC_{fgsum4,t=0-3}$ measurements observed in each treatment arm of CALGB 40502, where the numbers above the bars represent the number of patients with a given $AUC_{fgsum4,t=0-3}$ measurement. Median $AUC_{fgsum4,t=0-3}$ measurements are shown as red dotted vertical lines. (B) Comparison of $AUC_{fgsum4,t=0-3}$ measurements between those who experience dose reduction/delay or discontinuation for sensory peripheral neuropathy (blue) and those who do not have any reported events (pink). The number of measurements in each boxplot are denoted on the x-axis. Differences between the two groups are significant in all three treatment arms and *P* values are shown in below plot (Mann-Whitney-Wilcoxon test).

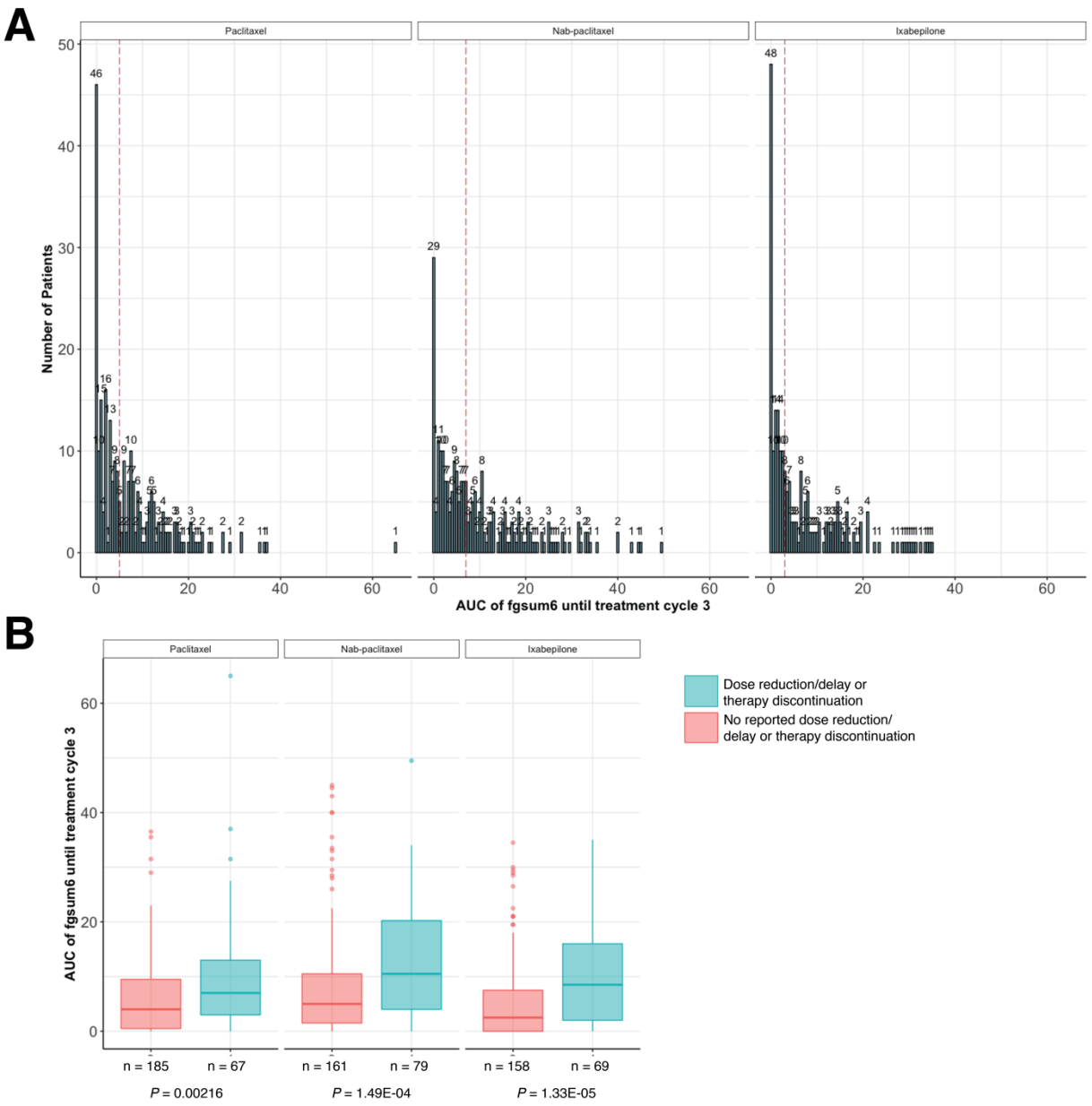

Figure 4.11 Distribution of $AUC_{fgsum6,t=0-3}$ and relationship to dose reductions/delays or therapy discontinuation. (A) Distribution of $AUC_{fgsum6,t=0-3}$ measurements observed in each treatment arm of CALGB 40502, where the numbers above the bars represent the number of patients with a given $AUC_{fgsum6,t=0-3}$ measurement. Median $AUC_{fgsum6,t=0-3}$ measurements are shown as red dotted vertical lines. (B) Comparison of $AUC_{fgsum6,t=0-3}$ measurements between those who experience dose reduction/delay or discontinuation for sensory peripheral neuropathy (blue) and those who do not have any reported events (pink). The number of measurements in each boxplot are denoted on the x-axis. Differences between the two groups are significant in all three treatment arms and *P* values are shown in below plot (Mann-Whitney-Wilcoxon test).

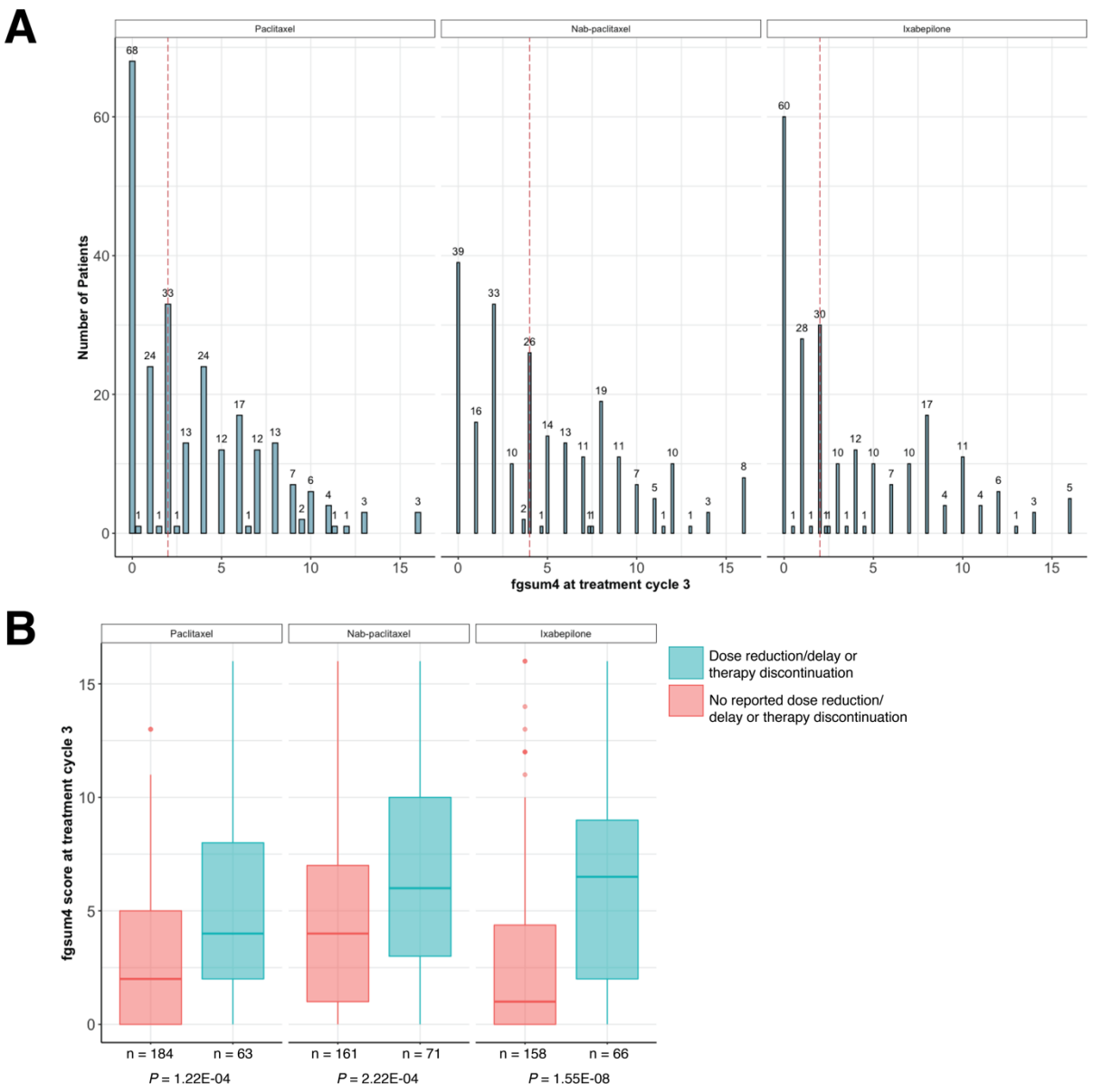

Figure 4.12 Distribution of fgsum4$_{t=3}$ and relationship to dose reductions/delays and therapy discontinuation. (A) Distribution of fgsum4$_{t=3}$ measurements observed in each treatment arm of CALGB 40502, where the numbers above the bars represent the number of patients with a given fgsum4$_{t=3}$ measurement. Median fgsum4$_{t=3}$ measurements are shown as red dotted vertical lines. (B) Comparison of fgsum4$_{t=3}$ measurements between those who experience dose reduction/delay or discontinuation for sensory peripheral neuropathy (blue) and those who do not have any reported events (pink). The number of measurements in each boxplot are denoted on the x-axis. Differences between the two groups are significant in all three treatment arms and *P* values are shown in below plot (Mann-Whitney-Wilcoxon test).

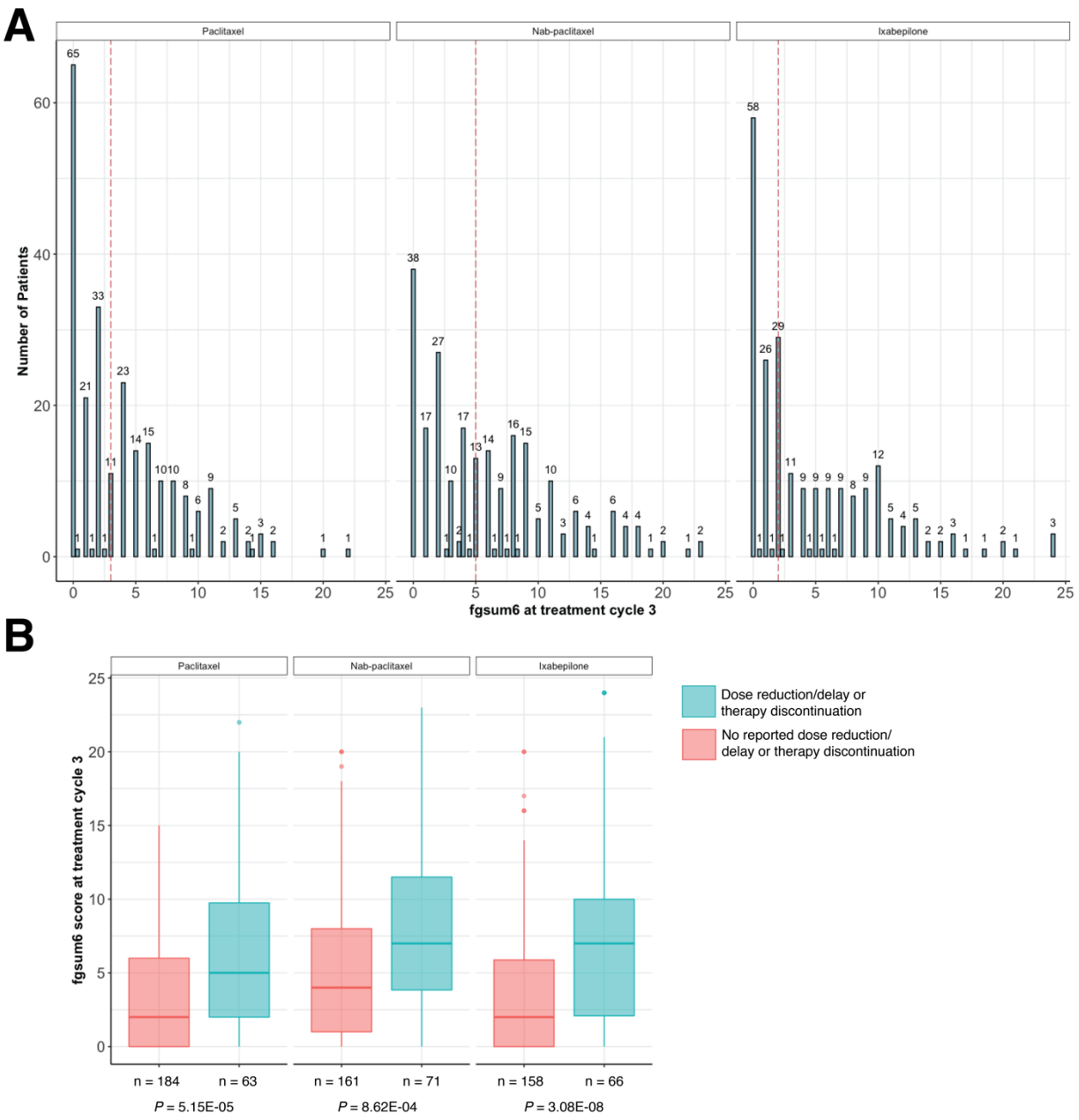

Figure 4.13 Distribution of fgsum6$_{t=3}$ and relationship with dose reductions/delays or therapy discontinuation. (A) Distribution of fgsum6$_{t=3}$ measurements observed in each treatment arm of CALGB 40502, where the numbers above the bars represent the number of patients with a given fgsum6$_{t=3}$ measurement. Median fgsum6$_{t=3}$ measurements are shown as red dotted vertical lines. (B) Comparison of fgsum6$_{t=3}$ measurements between those who experience dose reduction/delay or discontinuation for sensory peripheral neuropathy (blue) and those who do not have any reported events (pink). The number of measurements in each boxplot are denoted on the x-axis. Differences between the two groups are significant in all three treatment arms and *P* values are shown in below plot (Mann-Whitney-Wilcoxon test).

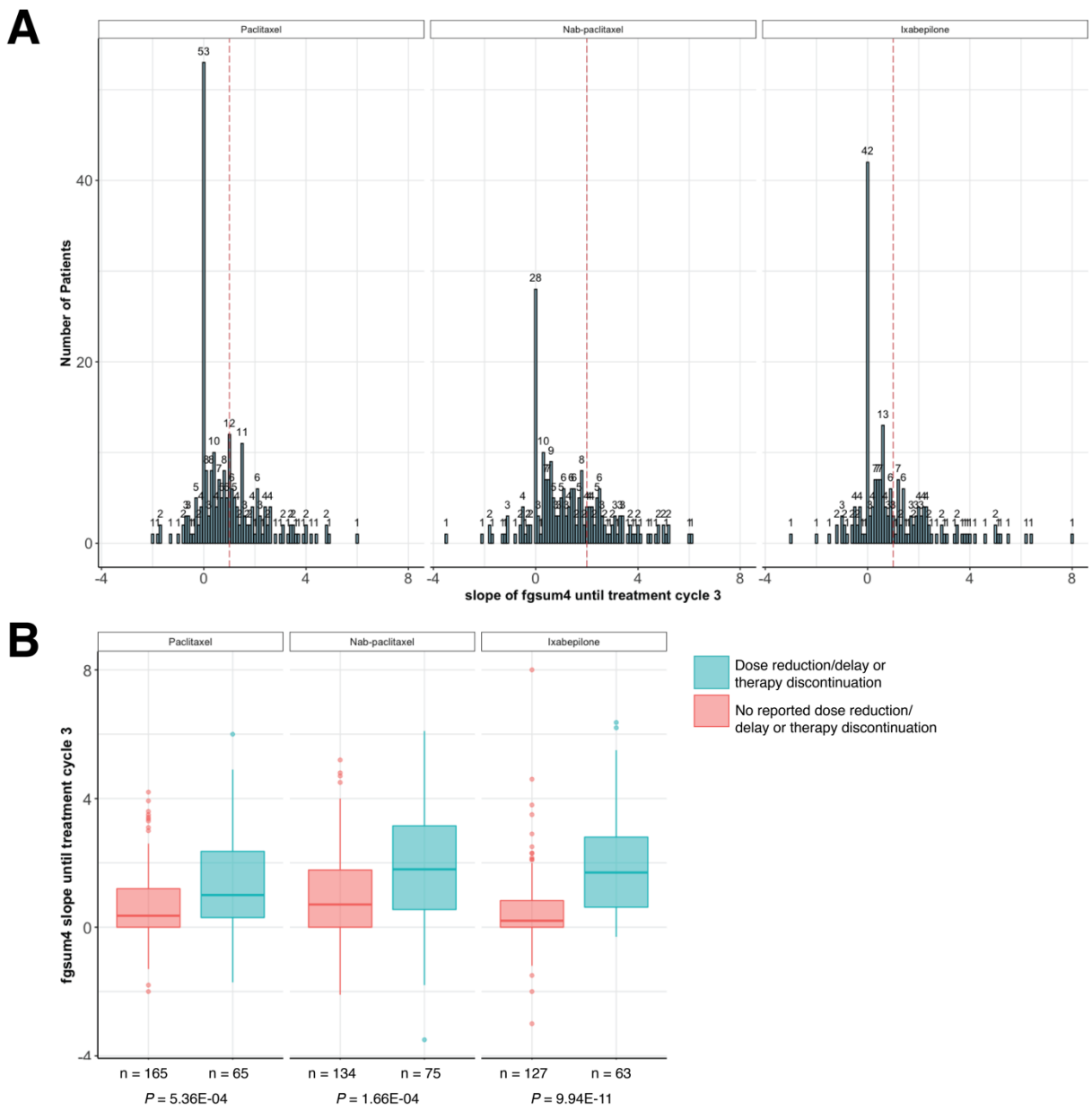

Figure 4.14 Distribution of $slope_{fgsum4,t=0-3}$ and relationship to dose reductions/delays and therapy discontinuation. (A) Distribution of $slope_{fgsum4,t=0-3}$ measurements observed in each treatment arm of CALGB 40502, where the numbers above the bars represent the number of patients with a given $slope_{fgsum4,t=0-3}$ measurement. Median $slope_{fgsum4,t=0-3}$ measurements are shown as red dotted vertical lines. (B) Comparison of $slope_{fgsum4,t=0-3}$ measurements between those who experience dose reduction/delay or discontinuation for sensory peripheral neuropathy (blue) and those who do not have any reported events (pink). The number of measurements in each boxplot are denoted on the x-axis. Differences between the two groups are significant in all three treatment arms and *P* values are shown in below plot (Mann-Whitney-Wilcoxon test).

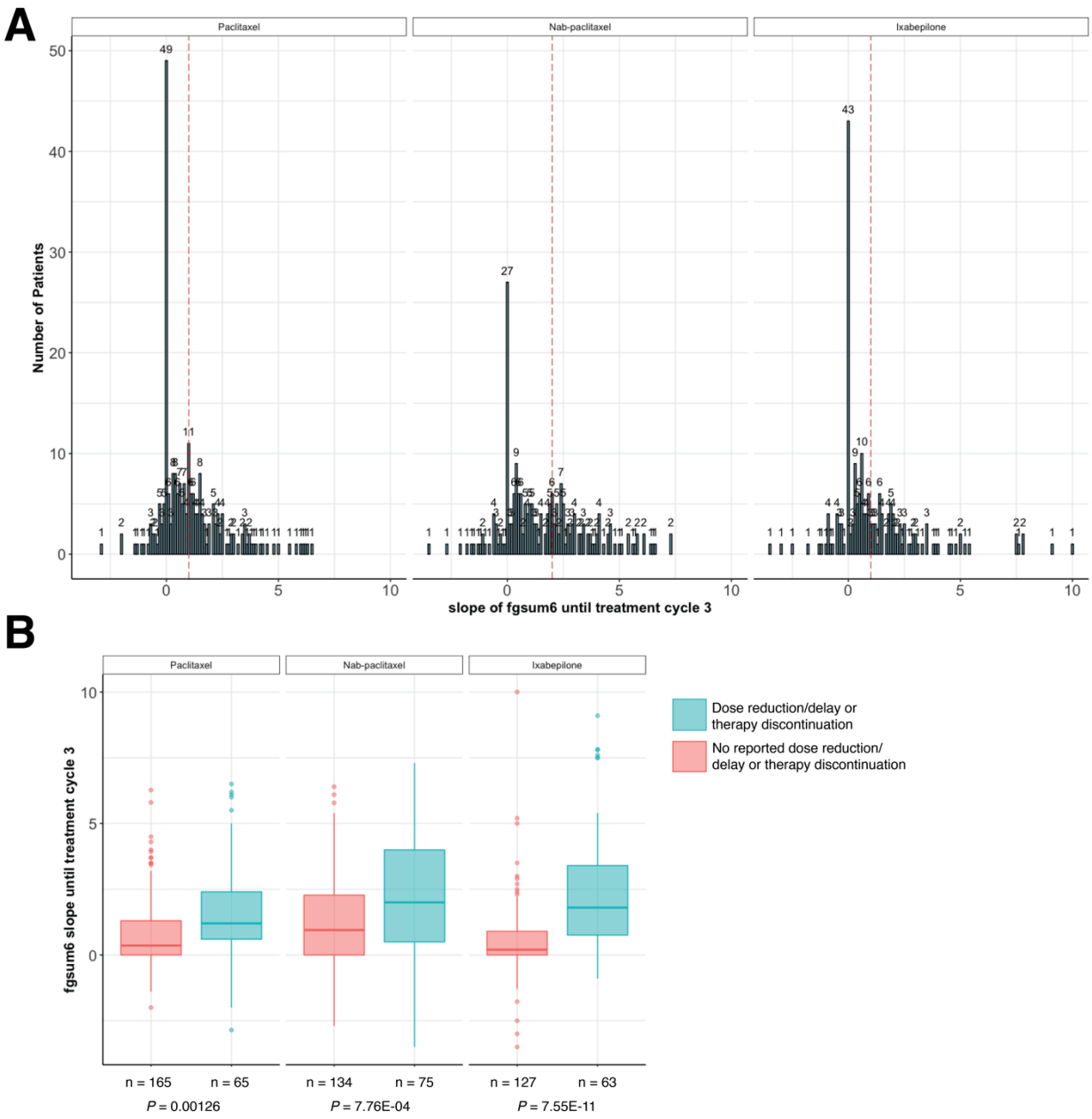

Figure 4.15 Distribution of slope$_{fgsum6,t=0-3}$ and relationship to dose reductions/delays and therapy discontinuation. (A) Distribution of slope$_{fgsum6,t=0-3}$ measurements observed in each treatment arm of CALGB 40502, where the numbers above the bars represent the number of patients with a given slope$_{fgsum6,t=0-3}$ measurement. Median slope$_{fgsum6,t=0-3}$ measurements are shown as red dotted vertical lines. (B) Comparison of slope$_{fgsum6,t=0-3}$ measurements between those who experience dose reduction/delay or discontinuation for sensory peripheral neuropathy (blue) and those who do not have any reported events (pink). The number of measurements in each boxplot are denoted on the x-axis. Differences between the two groups are significant in all three treatment arms and *P* values are shown in below plot (Mann-Whitney-Wilcoxon test).

$Slope_{fgsum6,t=0-3}$ identified as early predictor for dose-limiting neuropathy

Since each construct of fgsum4 and fgsum6 scores were able to distinguish between patients with RDD for peripheral neuropathy, each were tested as a predictor in a conditional logistic regression stratified by treatment arm prediction of RDD status. For each construct, a model was trained with 75% of the data from the PRO cohort with complete information and subsequently a model AUC_{ROC} was calculated on the remaining 25%. Among the six constructs, $slope_{fgsum6,t=0-3}$ had the largest model AUC_{ROC} (0.675) and a prediction accuracy of 71.3% to predict RDD for sensory peripheral neuropathy (Table 4.2, Figure 4.16). Except for the slope constructs, using fgsum6 scores did not further improve the prediction compared with the corresponding variables using fgsum4 scores alone (Table 4.2). Since the slope construct using fgsum6 had a marginal improvement over slope construct using fgsum4, $slope_{fgsum6,t=0-3}$ was selected as the best early predictor for the final PRO model.

Table 4.2 Model AUC_{ROC} and prediction accuracy for each predictor analyzed for prediction of RDD using PRO cohort.

Predictor	No. Subjects[†]	Test set	AUC_{ROC} (95% CI)	Accuracy (95% CI)
$AUC_{fgsum4,t=0-3}$	719	179	0.655 (0.555-0.755)	0.743 (0.673-0.805)
$AUC_{fgsum6,t=0-3}$	719	179	0.653 (0.554-0.753)	0.760 (0.690-0.820)
$slope_{fgsum4,t=0-3}$	703	175	0.667 (0.568-0.765)	0.713 (0.636-0.783)
$slope_{fgsum6,t=0-3}$	703	175	0.675 (0.578-0.772)	0.720 (0.643-0.788)
$fgsum4_{t=3}$	629	156	0.592 (0.484-0.699)	0.737 (0.665-0.801)
$fgsum6_{t=3}$	629	156	0.584 (0.477-0.692)	0.737 (0.665-0.801)

[†]Total number of subjects in PRO cohort with available predictor information

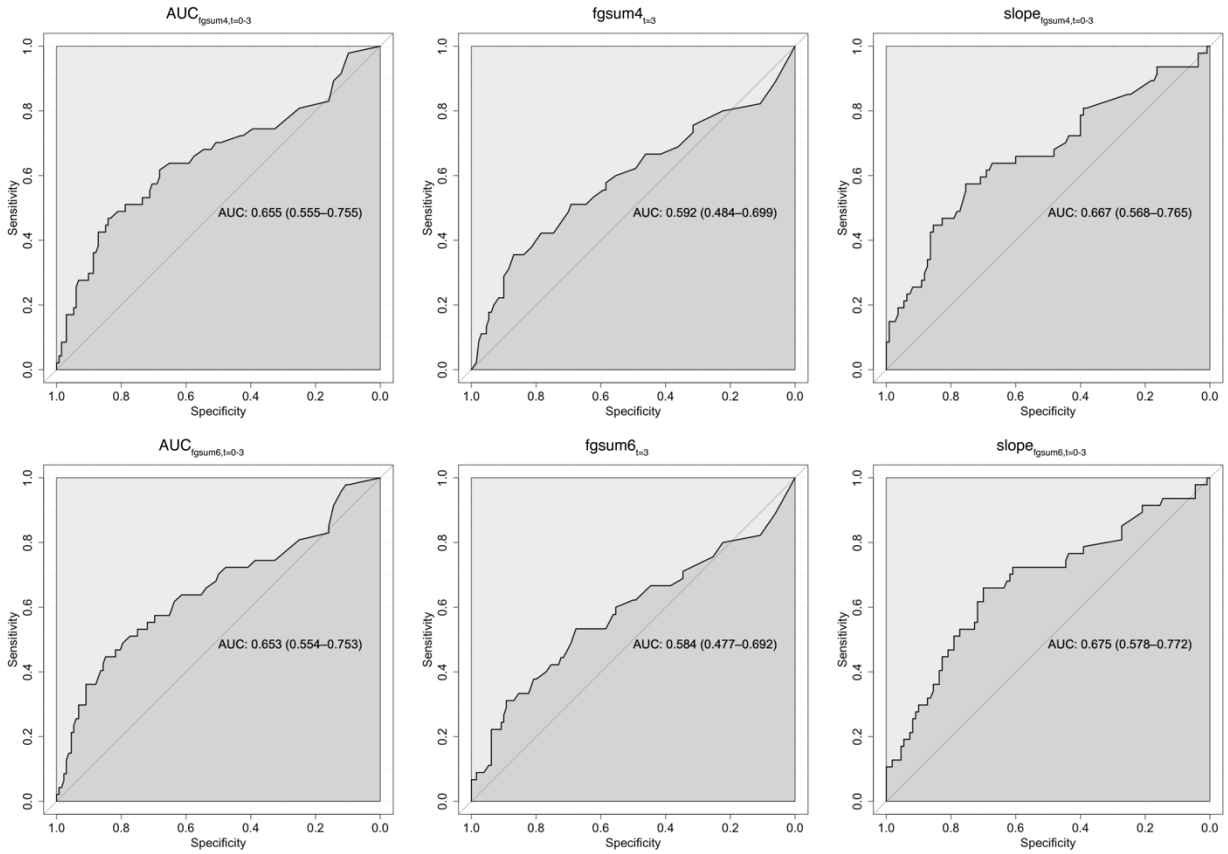

Figure 4.16 Receiver operating characteristic (ROC) curves for each construct using the PRO cohort. ROC curve illustrates the performance ability of the models with each construct to distinguish between RDD status for peripheral neuropathy. The model AUC_{ROC} for each model is shown with 95% confidence intervals. $Slope_{fgsum6,t=0-3}$ has the largest model AUC_{ROC} (0.675) to predict RDDs for sensory peripheral neuropathy.

Prediction analysis

A final PRO prediction model for RDD was generated on PRO EUR cohort (n = 382) using $slope_{fgsum6,t=0-3}$ as the primary predictor within the framework of a conditional logistic regression, stratifying for treatment arm. To evaluate if any patient characteristics are critical to dose reductions/delays or therapy discontinuations for sensory peripheral neuropathy, a stepwise backwards regression was performed on clinical features, including self-reported race/ethnicity, age, hormone receptor status, bevacizumab therapy, visceral metastases, diabetic status, prior taxane status, and body surface area; no clinical features remained in the model. The final PRO

prediction model was validated on the PRO non-EUR cohort with a model AUC_{ROC} of 0.652 (95% CI: 0.550-0.753) (Figure 4.17).

To assess if the addition of SNPs would improve the prediction model, a 10-fold cross-validation was performed to generate a prediction model with $slope_{fgsum6,t=0-3}$ and SNPs using the PRO EUR cohort (Figure 4.2). Ten GWAS were performed on each training set to identify SNPs that associate with RDD for sensory neuropathy. Among the ten analyses, no SNP association reached genome-wide significance (P < 5E-08). However, a total of 103 unique SNPs reached P < 1E-04 across all GWAS; four SNPs (rs686865, rs12751148, rs7953698, rs8134611) remained in at least 50% of initial models after stepwise backwards regression with training set (Figure 4.18). These SNPs were added into the final PRO genetic model and applied to the PRO non-EUR cohort. The resulting model AUC_{ROC} which included both $slope_{fgsum6,t=0-3}$ and SNP features is 0.607 (95% CI: 0.502-0.711), showing no improvement compared to PRO prediction model (Figure 4.17).

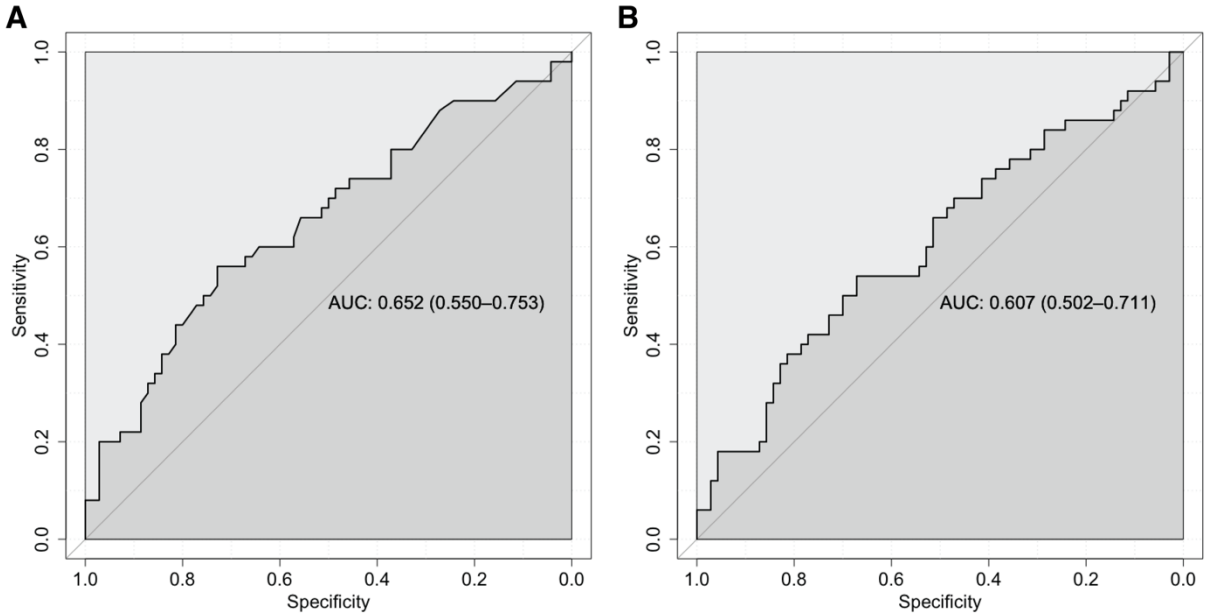

Figure 4.17 ROC curve for prediction analysis using PRO non-EUR cohort with final PRO prediction models with and without genetics. ROC curve illustrates the performance ability of model PRO information alone (A) and with the addition of four SNPs (rs686865, rs12751148, rs7953698, rs8134611) (B) to predict RDD status for peripheral neuropathy.

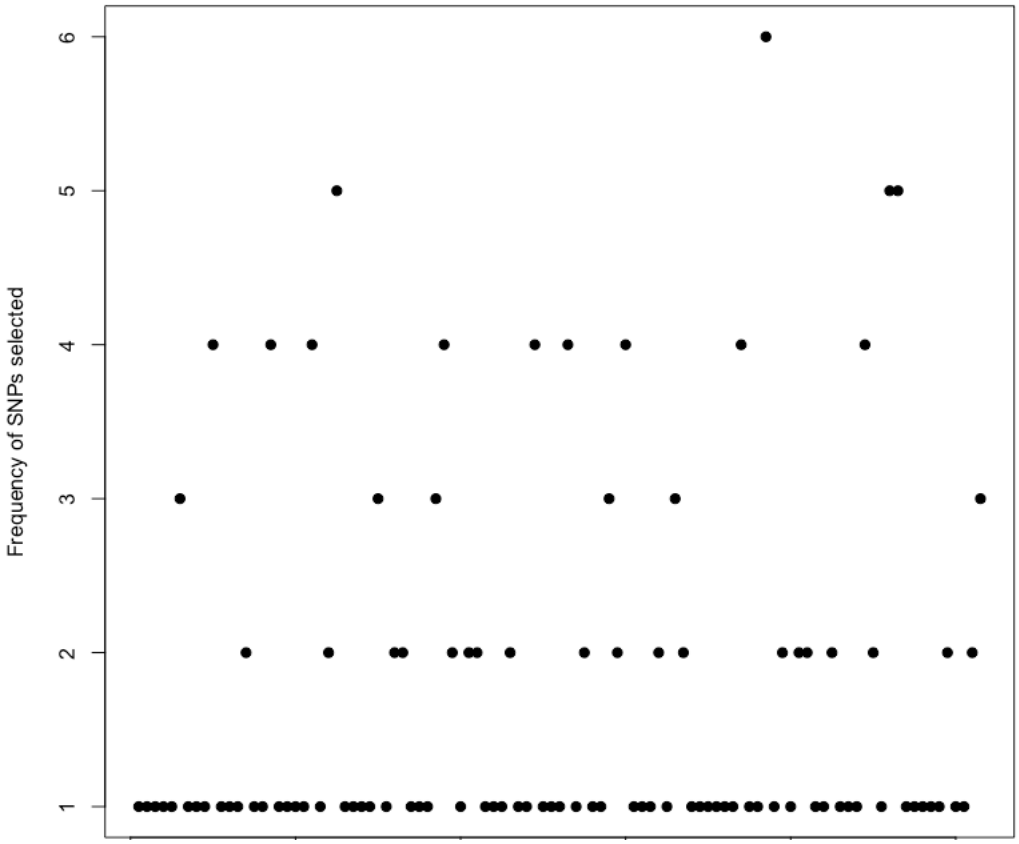

Figure 4.18 Number of times SNPs selected from stepwise backward regression. Each dot represents a SNP from the 115 unique SNPs with association of $P < 10^{-4}$ across ten GWAS. Only four SNPs (rs686865, rs12751148, rs7953698, rs8134611) were selected at least 50% of the models.

DISCUSSION

Patient-reported outcomes of CIPN are an increasingly recognized tool to comprehensively monitor, evaluate, and manage CIPN progression during treatment. However, there is no current standard to implement the use of PRO into clinical decisions and there remains a need to develop an effective and simple strategy for prevention of dose-limiting neuropathy events. Previous studies have shown the specific reliability and validity of the sensory subscale of FACT/GOG-Ntx to assess neuropathy symptoms[15–20]. In this study, we validate that patient-reported scores from the FACT/GOG-Ntx subscale (fgsum4 and fgsum6) distinguished between those who experience clinician-reported sensory neuropathy events and those who had no reported events regardless of chemotherapy regimen as early as the first treatment cycle. Furthermore, we also validate the ability of FACT/GOG-Ntx subscale to capture patient neurotoxicity profiles over time, where CIPN cases often report increases in fgsum4 and fgsum6 scores prior to the time of a clinician-reported neuropathy event. Because of this, six different constructs of fgsum4 and fgsum6 scores were created to investigate if CIPN symptoms at the latest time considered (score at cycle 3), cumulative symptom exposure (score AUC until cycle 3), or symptom progression (slope of scores until cycle 3) were predictors for dose reductions/delays or therapy discontinuation. All six constructs were able to show differences between patients with and without reported RDD for sensory peripheral neuropathy (Table 4.2), where higher scores, score AUCs, and slopes were observed in the group with reported RDD for sensory neuropathy regardless of treatment arm. Among the six constructs, slopes using both fgsum4 and fgsum6 scores predicted RDD status with the highest AUC_{ROC} values (0.667 and 0.675, respectively). Interestingly, although $slope_{fgsum6,t=0-3}$ showed the highest predictive ability among all six constructs, the addition of the two dysfunctional items to summed scores did not drastically

improve the predictive accuracy, which is in accordance with Huang et al. 2007[15] who reported that the four-item sensory scale alone efficiently captures clinically relevant neuropathy. It is possible that the PRO prediction model may perform similarly with only the four-item sensory scale, which can be further investigated with additional independent validation cohorts.

While the PRO prediction model using $slope_{fgsum4,t=0-3}$ showed some predictive value (AUC_{ROC}: 0.652 (0.550-0.753)), we also asked whether the addition of genome-wide data improves the prediction of RDD for sensory neuropathy. A 10-fold cross validated analysis (Figure 4.2) was performed in the PRO EUR cohort to build a PRO genetic prediction model using $slope_{fgsum6,t=0-3}$ and four selected SNPs (rs686865, rs12751148, rs7953698, rs8134611). In comparison to the model with PRO information alone, there was no improvement with the addition of genetic covariates to the model (AUC_{ROC}: 0.607 (0.502-0.711)). Due to sample size constraints, it is possible these SNPs are not predictive in a multi-ethnic population as they were initially discovered in a genetically estimated European population. Future work focused on the inclusion of more appropriately sized multi-ethnic populations will likely identify SNPs that may improve the prediction model. Alternatively, the use of other regression methods aimed at incorporating genome-wide data without a high risk of overfitting may also warrant better prediction models. Rashkin et al. 2019[13] applied the elastic net regularization in development of a prediction model for progression-free survival using both clinical features and SNPs in CALGB 40502. While this study employed a similar 10-fold cross validated analysis, the elastic net regression or other penalized regression methods can be applied to improve SNP selection and reduce overfitting.

While the focus of the study was to develop a predictive model with multiple SNPs that collectively show predictive ability, the analysis revealed some potentially biologically relevant

genes (Table 4.3) annotated to the selected SNPs. rs8134611 is a SNP located 27 kb 5' of *DSCAM*, a gene encoding a cell adhesion molecule and netrin-1 receptor shown to play a critical role in regulating axonal growth and guidance during neural development[21] that may be regulated directly by sphingolipid signaling[22]. Mutations in *DSCAM in vivo* have shown to impair peripheral signals to spinal circuits and result in sensorimotor controls[23,24]. The SNP rs7953698 which lies 61 kb 5' of *C12orf67* has been shown to be an eQTL for expression of *BCAT1*[25], a gene encoding an isoform for BCAT enzyme that functions in glutamate metabolism. Interestingly, gabapentin, a commonly prescribed anticonvulsant drug for diabetic neuropathy and CIPN, competitively inhibits BCAT1/2 to slow glutamate production and reduce neuropathic pain. This notion may suggest that the protective effect of the SNP may be acting similarly to reduce glutamate levels. The SNP rs12751148 lies within the intronic region of *TGFBR3*, encoding betaglycan or formerly known as transforming growth factor (TGF)-β type III receptor. Betaglycan is an accessory receptor that lacks a TGF-β signaling domain but functions primarily to regulate TGFβ signaling via binding and reserving ligands for TGFβ type I/II receptors[26]. Interestingly, stimulating TGFβ signaling has been shown to attenuate chronic nerve injury and neuropathic pain[27–29]. Although *TGFBR3* may be an interesting genetic target, it is unclear how variations in betaglycan might affect TGF-β signaling under chemotherapy exposure and warrants further investigation. Lastly, the SNP rs686865 is located in a gene desert with the nearest gene 605 kb away from the 3' end of *PLOD2*, a gene encoding a member of a protein family responsible for stabilizing collagen molecules in the extracellular matrix[30] that has been implicated in RhoA-mediated axonal cytoskeletal arrangements in primary dorsal root ganglia[31]. Functional investigation of these genes may point to novel mechanisms of CIPN and aid in understanding the genetic factors involved in development of CIPN symptoms.

Table 4.3 Effect of clinical and genetic features for risk of dose reductions/delays and therapy discontinuation using the PRO GWAS cohort (N=502).

Variable	Chr	Gene†	MAF‡	β	SE	*P*
$Slope_{fgsum6,t=0-3}$	–	–	–	0.368	0.060	1.05E-09
rs8134611	21	*DSCAM*	0.46 / 0.25	0.431	0.145	4.86E-06
rs7953698	12	*C12orf67*	0.16 / 0.06	-0.889	0.226	8.22E-05
rs12751148	1	*TGFBR3*	0.35 / 0.10	-0.767	0.168	0.00302
rs686865	3	*PLOD2*	0.41 / 0.54	-0.433	0.150	0.00395

†Nearest gene using refGene annotation
‡MAF denoted in PRO EUR / Non-EUR cohorts

While other items in the FACT/GOG-Ntx subscale were not investigated in this study, motor and hearing neuropathy items may improve predictive ability when incorporating a wider cohort set treated with other chemotherapy regimens. For example, platinum-containing chemotherapy regimens often cause tinnitus and/or hearing loss while vincristine-treated patients can often present with gait issues. Furthermore, our study focused primarily on describing patient-reported neuropathic experiences as an alternative to NCI-CTCAE reporting, although a multi-component assessment based on both clinician-based criteria and patient-reported questionnaires may be more suitable to fully describe and predict CIPN symptoms. As more comprehensive studies incorporate the collection of PRO information to monitor CIPN, we will begin to more extensively investigate which early PRO information is most informative and how they can be appropriately used to predict dose-limiting neuropathy events across chemotherapy regimens.

Overall in this study, we have identified $slope_{fgsum6,t=0-3}$ as an early predictor of dose modifications or therapy discontinuation for sensory peripheral neuropathy in both PRO EUR and non-EUR cohorts, where increasing $slope_{fgsum6,t=0-3}$ result in higher risk of dose-limiting neuropathy events. Consistent with our findings, a recent study[32] using early patient-reported outcomes from CALGB 40502 data also demonstrated the predictive accuracy for high neuropathy scores at treatment cycle 6, which may be useful for preventative dose-adjustments.

While more complex phenotyping with early patient-reported outcomes may result in better prediction, our study focused on the need to phenotype and test simple constructs of early PRO measures that require minimal training and use for easy adoption into the clinical trial and clinical practice[33]. Validation in independent multi-ethnic cohorts of $slope_{fgsum6,t=0-3}$ is critical to translate our findings into clinical settings and identify a more comprehensive predictive signature that include germline variations. With the growing advances of technology in healthcare, there will be more opportunities and innovative techniques to continually monitor cancer survivorship enriched with large-scale data directly from patients. One recent study has demonstrated the use of wearable technologies to quantify balance and gait difficulties after chemotherapy, showing cancer patients with CIPN suffered from issues with ankle stability and slower stride velocity[34], which likely contribute to increased risk of secondary mobility complications post-treatment. Future studies aimed at the use of innovative technologies and methods to appropriately monitor and control CIPN early holds promise for clinical application of patient-reported alongside clinician-based data, novel preventative strategies against CIPN including early screening methods for patient susceptibility to severe neuropathy, and improved clinical decisions that maximize chemotherapy benefit while limiting development of CIPN.

REFERENCES

1. Hershman, D. L., Lacchetti, C., Dworkin, R. H., Lavoie Smith, E. M., Bleeker, J., Cavaletti, G., Chauhan, C., Gavin, P., Lavino, A., Lustberg, M. B., Paice, J., Schneider, B., Smith, M. Lou, Smith, T., Terstriep, S., Wagner-Johnston, N., Bak, K. & Loprinzi, C. L. Prevention and management of chemotherapy-induced peripheral neuropathy in survivors of adult cancers: American society of clinical oncology clinical practice guideline. *J. Clin. Oncol.* **32**, 1941–1967 (2014).
2. Zanville, N. R., Nudelman, K. N. H., Smith, D. J., Von Ah, D., McDonald, B. C., Champion, V. L. & Saykin, A. J. Evaluating the impact of chemotherapy-induced peripheral neuropathy symptoms (CIPN-sx) on perceived ability to work in breast cancer survivors during the first year post-treatment. *Support. Care Cancer* **24**, 4779–4789 (2016).
3. Shah, A., Hoffman, E. M., Mauermann, M. L., Loprinzi, C. L., Windebank, A. J., Klein, C. J. & Staff, N. P. Incidence and disease burden of chemotherapy-induced peripheral neuropathy in a population-based cohort. *J. Neurol. Neurosurg. Psychiatry* **89**, 636–641 (2018).
4. Nyrop, K. A., Deal, A. M., Reeder-Hayes, K. E., Shachar, S. S., Reeve, B. B., Basch, E., Choi, S. K., Lee, J. T., Wood, W. A., Anders, C. K., Carey, L. A., Dees, E. C., Jolly, T. A., Kimmick, G. G., Karuturi, M. S., Reinbolt, R. E., Speca, J. E. C. & Muss, H. B. Patient-reported and clinician-reported chemotherapy-induced peripheral neuropathy in patients with early breast cancer: Current clinical practice. *Cancer* **125**, 2945–2954 (2019).
5. Zhi, W. I., Chen, P., Kwon, A., Chen, C., Harte, S. E., Piulson, L., Li, S., Patil, S., Mao, J.

J. & Bao, T. Chemotherapy-induced peripheral neuropathy (CIPN) in breast cancer survivors: a comparison of patient-reported outcomes and quantitative sensory testing. *Breast Cancer Res. Treat.* **178**, 587–595 (2019).

6. Park, S. B., Kwok, J. B., Asher, R., Lee, C. K., Beale, P., Selle, F. & Friedlander, M. Clinical and genetic predictors of paclitaxel neurotoxicity based on patient- versus clinicianreported incidence and severity of neurotoxicity in the ICON7 trial. *Ann. Oncol.* **28**, 2733–2740 (2017).
7. Molassiotis, A., Cheng, H. L., Lopez, V., Au, J. S. K., Chan, A., Bandla, A., Leung, K. T., Li, Y. C., Wong, K. H., Suen, L. K. P., Chan, C. W., Yorke, J., Farrell, C. & Sundar, R. Are we mis-estimating chemotherapy-induced peripheral neuropathy? Analysis of assessment methodologies from a prospective, multinational, longitudinal cohort study of patients receiving neurotoxic chemotherapy. *BMC Cancer* **19**, 1–19 (2019).
8. Cavaletti, G., Frigeni, B., Lanzani, F., Mattavelli, L., Susani, E., Alberti, P., Cortinovis, D. & Bidoli, P. Chemotherapy-Induced Peripheral Neurotoxicity assessment: A critical revision of the currently available tools. *Eur. J. Cancer* **46**, 479–494 (2010).
9. Le-Rademacher, J., Kanwar, R., Seisler, D., Pachman, D. R., Qin, R., Abyzov, A., Ruddy, K. J., Banck, M. S., Lavoie Smith, E. M., Dorsey, S. G., Aaronson, N. K., Sloan, J., Loprinzi, C. L. & Beutler, A. S. Patient-reported (EORTC QLQ-CIPN20) versus physician-reported (CTCAE) quantification of oxaliplatin- and paclitaxel/carboplatin-induced peripheral neuropathy in NCCTG/Alliance clinical trials. *Support. Care Cancer* **25**, 3537–3544 (2017).
10. Alberti, P., Rossi, E., Cornblath, D. R., Merkies, I. S. J., Postma, T. J., Frigeni, B., Bruna, J., Velasco, R., Argyriou, A. A., Kalofonos, H. P., Psimaras, D., Ricard, D., Pace, A.,

Galiè, E., Briani, C., Dalla Torre, C., Faber, C. G., Lalisang, R. I., Boogerd, W., *et al.* Physician-assessed and patient-reported outcome measures in chemotherapy-induced sensory peripheral neurotoxicity: Two sides of the same coin. *Ann. Oncol.* **25**, 257–264 (2014).

11. Boora, G. K., Kulkarni, A. A., Kanwar, R., Beyerlein, P., Qin, R., Banck, M. S., Ruddy, K. J., Pleticha, J., Lynch, C. A., Behrens, R. J., Züchner, S., Loprinzi, C. L. & Beutler, A. S. Association of the Charcot-Marie-Tooth disease gene ARHGEF10 with paclitaxel induced peripheral neuropathy in NCCTG N08CA (Alliance). *J. Neurol. Sci.* **357**, 35–40 (2015).

12. Rugo, H. S., Barry, W. T., Moreno-Aspitia, A., Lyss, A. P., Cirrincione, C., Leung, E., Mayer, E. L., Naughton, M., Toppmeyer, D., Carey, L. A., Perez, E. A., Hudis, C. & Winer, E. P. Randomized phase III trial of paclitaxel once per week compared with nanoparticle albumin-bound nab-paclitaxel once per week or ixabepilone with bevacizumab as first-line chemotherapy for locally recurrent or metastatic breast cancer: CALGB 40502/NCCTG N0. *J. Clin. Oncol.* **33**, 2361–2369 (2015).

13. Rashkin, S. R., Chua, K. C., Ho, C., Mulkey, F., Jiang, C., Mushiroda, T., Kubo, M., Friedman, P. N., Rugo, H. S., McLeod, H. L., Ratain, M. J., Castillos, F., Naughton, M., Overmoyer, B., Toppmeyer, D., Witte, J. S., Owzar, K. & Kroetz, D. L. A Pharmacogenetic Prediction Model of Progression-Free Survival in Breast Cancer using Genome-Wide Genotyping Data from CALGB 40502 (Alliance). *Clin. Pharmacol. Ther.* **105**, 738–745 (2019).

14. Therneau, T. M. A Package for Survival Analysis in S. (2015).

15. Huang, H. Q., Brady, M. F., Cella, D., Fleming, G. & Mackey, D. Validation and

reduction of FACT/GOG-Ntx subscale for platinum/paclitaxel- induced neurologic symptoms: A gynecologic oncology group study. *Int. J. Gynecol. Cancer* **17**, 387–393 (2007).

16. Hershman, D. L., Weimer, L. H., Wang, A., Kranwinkel, G., Brafman, L., Fuentes, D., Awad, D. & Crew, K. D. Association between patient reported outcomes and quantitative sensory tests for measuring long-term neurotoxicity in breast cancer survivors treated with adjuvant paclitaxel chemotherapy. *Breast Cancer Res. Treat.* **125**, 767–774 (2011).
17. Driessen, C. M. L., de Kleine-Bolt, K. M. E., Vingerhoets, a J. J. M., Mols, F. & Vreugdenhil, G. Assessing the impact of chemotherapy-induced peripheral neurotoxicity on the quality of life of cancer patients: the introduction of a new measure. *Support. Care Cancer* **20**, 877–81 (2012).
18. Beijers, A. J. M., Mols, F., Driessen, C. M. L., Dercksen, M. & Vreugdenhil, G. Chemotherapy-induced peripheral neuropathy and impact on quality of life six months after treatment with taxanes and platinum derivatives. *J. Community Support. Oncol.* **12**, 401–406 (2014).
19. Cho, J., Kang, D., Lee, J. Y., Kim, K. & Kim, S. J. Impact of dose modification on intravenous Bortezomib-induced peripheral neuropathy in multiple myeloma patients. *Support. Care Cancer* **22**, 2669–2675 (2014).
20. Ajewole, V. B., Cox, J. E., Swan, J. T., Chikermane, S. G., Lamoth, B., Iso, T., Okolo, L. O., Ford, C. L., Schneider, A. M., Hobaugh, E. C. & Baker, K. R. Incidence of chemotherapy-induced peripheral neuropathy within 12 weeks of starting neurotoxic chemotherapy for multiple myeloma or lymphoma: a prospective, single-center, observational study. *Support. Care Cancer* (2019) doi:10.1007/s00520-019-05006-6.

21. Jain, S. & Welshhans, K. Netrin-1 induces local translation of down syndrome cell adhesion molecule in axonal growth cones. *Dev. Neurobiol.* **76**, 799–816 (2016).

22. Goyal, G., Zheng, J., Adam, E., Steffes, G., Jain, M., Klavins, K. & Hummel, T. Sphingolipid-dependent Dscam sorting regulates axon segregation. *Nat. Commun.* **10**, (2019).

23. Thiry, L., Lemieux, M., D Laflamme, O. & Bretzner, F. Role of DSCAM in the development of the spinal locomotor and sensorimotor circuits. *J. Neurophysiol.* **115**, 1338–1354 (2016).

24. Lemieux, M., Laflamme, O. D., Thiry, L., Boulanger-Piette, A., Frenette, J. & Bretzner, F. Motor hypertonia and lack of locomotor coordination in mutant mice lacking DSCAM. *J. Neurophysiol.* **115**, 1355–1371 (2016).

25. Westra, H. J., Peters, M. J., Esko, T., Yaghootkar, H., Schurmann, C., Kettunen, J., Christiansen, M. W., Fairfax, B. P., Schramm, K., Powell, J. E., Zhernakova, A., Zhernakova, D. V., Veldink, J. H., Van Den Berg, L. H., Karjalainen, J., Withoff, S., Uitterlinden, A. G., Hofman, A., Rivadeneira, F., *et al.* Systematic identification of trans eQTLs as putative drivers of known disease associations. *Nat. Genet.* **45**, 1238–1243 (2013).

26. Bilandzic, M. & Stenvers, K. L. Betaglycan: A multifunctional accessory. *Mol. Cell. Endocrinol.* **339**, 180–189 (2011).

27. Chen, N. F., Huang, S. Y., Chen, W. F., Chen, C. H., Lu, C. H., Chen, C. L., Yang, S. N., Wang, H. M. & Wen, Z. H. TGF-β1 attenuates spinal neuroinflammation and the excitatory amino acid system in rats with neuropathic pain. *J. Pain* **14**, 1671–1685 (2013).

28. Sulaiman, W. & Nguyen, D. H. Transforming growth factor beta 1, a cytokine with

regenerative functions. *Neural Regen. Res.* **11**, 1549–1552 (2016).

29. Echeverry, S., Shi, X. Q., Haw, A., Liu, H., Zhang, Z. W. & Zhang, J. Transforming growth factor-β1 impairs neuropathic pain through pleiotropic effects. *Mol. Pain* **5**, 1–18 (2009).

30. Du, H., Chen, Y., Hou, X., Huang, Y., Wei, X., Yu, X., Feng, S., Wu, Y., Zhan, M., Shi, X., Lin, S., Lu, L., Yuan, S. & Sun, L. PLOD2 regulated by transcription factor FOXA1 promotes metastasis in NSCLC. *Cell Death Dis.* **8**, e3143 (2017).

31. Read, M. L., Mir, S., Spice, R., Seabright, R. J., Suggate, E. L., Ahmed, Z., Berry, M. & Logan, A. Profiling RNA interference (RNAi)-mediated toxicity in neural cultures for effective short interfering RNA design. *J. Gene Med.* **11**, 523–534 (2009).

32. Sharma, M. R., Mehrotra, S., Gray, E., Wu, K., Barry, W. T., Hudis, C., Winer, E. P., Lyss, A. P., Toppmeyer, D. L., Moreno-Aspitia, A., Lad, T. E., Velasco, M., Overmoyer, B., Rugo, H. S., Ratain, M. J. & Gobburu, J. V. Personalized Management of Chemotherapy-Induced Peripheral Neuropathy Based on a Patient Reported Outcome: CALGB 40502 (Alliance). *J. Clin. Pharmacol.* **40502**, (2019).

33. Colvin, L. A. Chemotherapy-induced peripheral neuropathy: Where are we now? *Pain* **160**, S1–S10 (2019).

34. Zahiri, M., Chen, K. M., Zhou, H., Nguyen, H., Workeneh, B. T., Yellapragada, S. V., Sada, Y. H., Schwenk, M. & Najafi, B. Using wearables to screen motor performance deterioration because of cancer and chemotherapy-induced peripheral neuropathy (CIPN) in adults - Toward an early diagnosis of CIPN. *J. Geriatr. Oncol.* **10**, 960–967 (2019).

CHAPTER 5: Conclusions and Perspectives

Summary

Cytotoxic chemotherapies are commonly prescribed first-line treatments for various solid tumors that target and eradicate rapidly dividing cells. While clinically efficacious, these drugs are often accompanied by significant toxicities. One common dose-limiting toxicity of antineoplastic drugs is sensory peripheral neuropathy (PN), which can cause debilitating pain and abnormal sensory perception that persist for years[1–4]. Although there are known clinical features for risk of developing chemotherapy-induced peripheral neuropathy (CIPN), these factors still do not account for the observed interindividual variation in onset and severity of CIPN[5]. From functional mechanistic investigations in animal and *in vitro* models of CIPN, there is evidence to suggest that key genetic drivers may explain the initiation and development of CIPN[6]. Recent reverse translational studies are aimed at identifying these genetic networks underlying CIPN by investigating significant genetic variation among patients with and without reported CIPN and mechanistically studying how these drivers elicit chemotherapy-stimulated peripheral nerve degeneration. The research described in this dissertation explores the application of pharmacogenetic approaches to understand patient susceptibility and the underlying mechanisms contributing to microtubule-targeting agent (MTA)-induced PN. Alongside revealing novel insights to the pathophysiology of this complex dose-limiting toxicity, these efforts using human-level data are aimed at identifying actionable genomic targets that can directly translate into development of effective therapeutic strategies to prevent and treat CIPN.

A meta-analysis of genome-wide association studies (GWAS) using genotyping array data in breast cancer patients treated with microtubule-targeting agents (CALGB 40101 and CALGB 40502) was conducted to identify novel genes associated with risk of developing MTA-

induced PN (Chapter 2). SNP associations of cumulative dose to first instance of grade 2 or higher MTA-induced PN were tested. Among the associations based on *P* values, SNPs within a predicted regulatory region near *S1PR1* were the highest-ranked associations. Patients harboring genetic variants in a predicted regulatory region downstream of *S1PR1* were observed with higher cumulative incidence of peripheral neuropathy events during chemotherapy. Using human sensory neurons derived from induced pluripotent stem cells, we show that pharmacologically inhibiting sphingosine-1-phosphate receptor signaling attenuated paclitaxel-induced neuronal damage. This work provides further evidence to support previous implications of sphingosine-1-phosphate receptor signaling in animal models of CIPN. Other top associations in the meta-analysis further validated intronic SNPs of *FGD4,* a causal Charcot-Marie-Tooth disease gene that was initially highlighted in a previous GWAS of CALGB 40101, and implicated SNPs near *CX3CL1*, an inflammatory signaling gene suggested to be involved in paclitaxel-stimulated neuroinflammatory responses. Together, these findings warrant additional studies to investigate their exact mechanistic functions in the pathogenesis of CIPN.

Alongside the meta-analysis, a discovery-based sequencing study was performed to determine whether rare or less common variation plays a significant role in MTA-induced PN (Chapter 3). Whole exomes and candidate gene regulatory regions were sequenced in MTA-treated breast cancer patients of CALGB 40502. Gene-based associations of cumulative dose to first instance of grade 2 or higher MTA-induced PN were completed, aggregating effects of rare or low-frequency variants either in exomes across the genome or in targeted regulatory regions of candidate genes. Although there were no significant gene associations, our exploratory analyses did reveal additional genes involved in actin cytoskeletal reorganization (*SHC4*, *TRIOBP*, *ACTG1*) and impairment in sensory neuronal excitability (*PEAR1*). Additional

genome-wide association and functional studies on these genes are critical to validate their role in patient susceptibility of significant MTA-induced PN, and may lead to novel drug targets against CIPN.

Collectively with other genome-wide studies on CIPN, there is emerging evidence that dysregulation of the actin cytoskeleton is a critical event in mechanistic development of chemotherapy-induced peripheral nerve degeneration. While the distinct role of the cytoskeleton to maintain cell shape and initiate cell migration is shared among most non-neuronal cells, the cytoskeletal structure and function in peripheral neurons are distinct, largely in part due to their length and constant reinnervation into the epidermis. The axon of peripheral afferent neurons is mainly comprised of microtubule and intermediate filaments that span the sensory connection from the spinal cord to the dermis. Along the terminal ends, actin structures regulate a specialized region called the growth cone, which is responsible to initiate growth, guidance, and extension of axons. During the normal process of axon generation and extension, a balanced coordination among actin, intermediate filaments, and microtubules allow for proper microtubule- and actin-polymerization cued by internal and external signals[7]. The main biological switches that regulate actin dynamics within the cytoskeleton are Rho GTPases (Cdc42, Rac1, and RhoA)[8], which function to signal the formation of specific actin structures. Many genome-wide studies on CIPN have implicated genetic variations in molecular regulators of Rho GTPase activity (Figure 5.1), and warrant further functional studies to understand how this imbalance is elicited by chemotherapy exposure and how it propagates into CIPN symptoms.

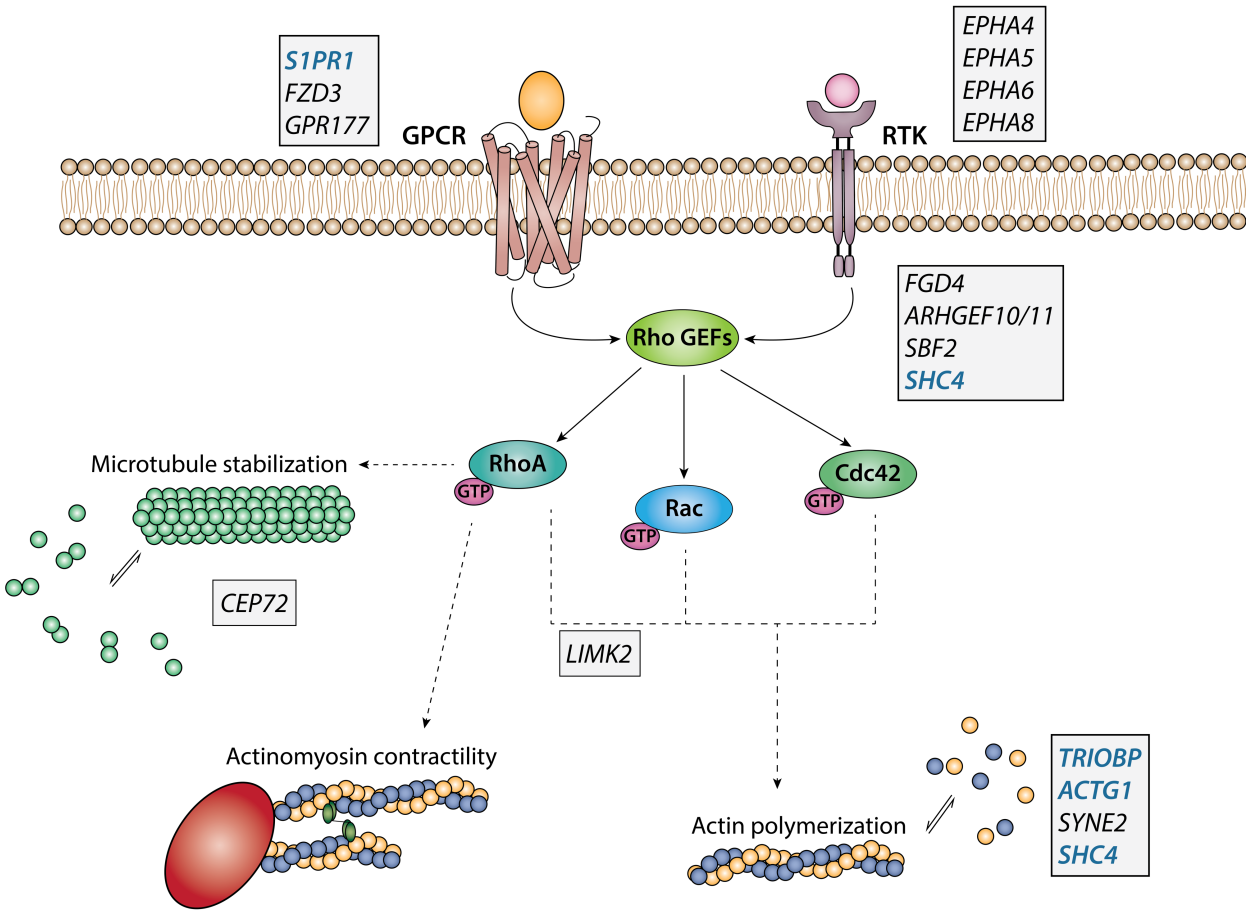

Figure 5.1 Proposed mechanisms of actin cytoskeletal genes implicated in CIPN. Genes identified from the analyses described in this dissertation are denoted in blue.

While genome-wide studies are continually providing insight into the mechanisms of CIPN, there is still a need to utilize this information for early screening of at-risk patients for severe neuropathy events. Although NCI-CTCAE reporting for sensory peripheral neuropathy is the most commonly used assessment in clinical settings, patient-reported outcomes have been shown to be more sensitive to characterize onset and progression of CIPN[9]; however, there are no current standardized means of implementing patient-reported outcomes (PRO) into clinical decisions. The use of early patient-reported outcomes and genotyping array data was explored as a tool to predict dose modifications/delays or therapy cessation due to sensory neuropathy (Chapter 4). Patient-reported scores of sensory and dysfunctional neuropathy items in the

FACT/GOG-Ntx questionnaire reported were used to define and test early predictors of dose-limiting neuropathy. All defined early PRO predictors ($AUC_{fgsum4,t=0-3}$, $AUC_{fgsum6,t=0-3}$, $slope_{fgsum4,t=0-3,}$ $slope_{fgsum6,t=0-3}$, $fgsum4_{t=3}$, $fgsum6_{t=3}$) were validated to distinguish between patients with and without clinician-reported sensory neuropathy events as early as the first cycle across MTA treatment, where the $slope_{fgsum6,t=0-3}$ showed the best predictive ability. Although the addition of genetics did not show an improvement in the prediction model using $slope_{fgsum6,t=0-3}$, this study has set a foundation for future investigations into the use of patient-reported outcomes and genome-wide data to predict clinically significant toxicity events. Additional work is required to incorporate the use of genome-wide data into an actionable prediction model of CIPN, which will be aimed at innovating novel strategies to improve patient outcomes and post-treatment quality of life.

Challenges, perspectives and future directions

The research described within this dissertation highlights a persistent challenge in pharmacogenetic studies of adverse drug reactions. Even with growing interest in genetic studies, it remains a challenge to collect large, appropriately-powered studies for discovery and replication genetic studies. Large-scale publicly accessible sources of genome-wide data (e.g. UK Biobank) are often limited by the lack of information captured on drug response and toxicity, especially when phenotype curation involves multiple layers of clinical information. As growing efforts to standardize tracking and sharing of 'big data' are ongoing, we will begin to expect larger numbers in pharmacogenetic studies and gain even more insights into genetic influences on drug response and toxicity.

As most clinical settings will consistently use the NCI-CTCAE grading scale, the primary peripheral neuropathy phenotype used in these genetic studies stem from this reporting criteria; however, these criteria are known to encompass variation in interindividual grade interpretation[10] and can be reported differently among various protocols. A more comprehensive avenue to collect neuropathy data should focus on the incorporation of patient-reported outcomes (PROs) and clinician-based assessments. While CALGB 40502 captured both patient-reported and clinician-reported neuropathy data, the collection of both set of data types are not common practice and rarely continue to follow patients after therapy is completed. With the new wave of app-based technology, these outcomes will be more readily collected before, during, and after treatments and accessible for clinical and research implementation. The PRO characterization and prediction study was motivated to start these investigations and create simple and effective ways to utilize these data for early prevention strategies.

The studies presented here focus on the impact of DNA sequence variation in individual risk of developing CIPN; however, there are other genetic mechanisms that may also affect CIPN risk not explored here. While we can infer regulatory genetic mechanisms based on prediction algorithms, it is critical to also consider chemotherapy-induced changes in epigenome, transcriptome, and proteome that can reveal novel insights on mechanisms underlying CIPN. Recent studies have shown roles in epigenetic modifications in peripheral nerve injury[11–14] and transcriptomic changes associated with chemotherapy-induced neuropathy[15–20]. With the genetic advances in technology, future studies should use a multi-omics approach to study CIPN, which would lead to a better understanding of the overall drug-induced genomic changes that may be imperative to CIPN initiation and development.

Novel functional *in vitro* models of CIPN are emerging that more closely resemble that of human sensory neurons. These functional studies are crucial to validate the consequences of identified genetic variation within target tissues and translate them back to patient predisposition. While the mechanistic investigation using human iPSC-derived sensory neurons presented in Chapter 2 was focused on neuron-specific responses to chemotherapy exposure, we did not investigate the cross talk between neurons and non-neuronal supporting cells. There has been increasing evidence that satellite glial cells[21–23] and Schwann cells[24] may be contributing to CIPN similarly to the neuron itself, although it is not yet clear which are primary responses to direct chemotherapy stimulation or secondary responses to repair neuron damage initially present from chemotherapy exposure. Future studies on these newer *in vitro* model systems should focus on incorporating co-culture systems to investigate these potential mechanisms of CIPN. While these systems are imperative for mechanistic studies, other future work should also place attention on utilization of patient iPSC-derived sensory neurons as a means to directly interrogate how patient-specific genomic variations cause CIPN predisposition and translate these findings into tailored treatments to mitigate patient CIPN symptoms.

Conclusion

This dissertation explores the use of a pharmacogenetic approach to identify novel genetic variations that potentially influence susceptibility of developing MTA-induced sensory peripheral neuropathy and further advance our understanding of the mechanisms underlying this toxicity. The findings presented support the hypothesis that the primary mechanism to chemotherapy-induced peripheral nerve damage may involve disruption of the actin cytoskeleton. Functional studies to investigate Rho GTPase signaling pathways are critical to

uncovering actionable genetic drivers, which will inform the development of novel drug strategies against CIPN. Additionally, this dissertation sets the foundation for the use of patient genetics and early symptom monitoring to predict severe neuropathy and inform clinical decisions to balance maximum chemotherapy benefit and mitigate drug adverse risk. The application of prediction modeling in CIPN contributes new methods to enable the translation of validated genomic targets into strategies to screen, predict, manage, and treat at-risk patients genetically susceptible to CIPN.

REFERENCES

1. Flatters, S. J. L., Dougherty, P. M. & Colvin, L. A. Clinical and preclinical perspectives on Chemotherapy-Induced Peripheral Neuropathy (CIPN): A narrative review. *Br. J. Anaesth.* **119**, 737–749 (2017).
2. Shah, A., Hoffman, E. M., Mauermann, M. L., Loprinzi, C. L., Klein, C. J., Staff, N. P., Clinic, M. & Clinic, M. Peripheral neuropathy in a population-based cohort. **89**, 636–641 (2018).
3. Brouwers, E. E. M., Huitema, A. D. R., Boogerd, W., Beijnen, J. H. & Schellens, J. H. M. Persistent neuropathy after treatment with cisplatin and oxaliplatin. *Acta Oncol. (Madr).* **48**, 832–841 (2009).
4. Ewertz, M., Qvortrup, C. & Eckhoff, L. Chemotherapy-induced peripheral neuropathy in patients treated with taxanes and platinum derivatives. *Acta Oncol. (Madr).* **54**, 587–591 (2015).
5. Hershman, D. L., Lacchetti, C., Dworkin, R. H., Smith, E. M. L., Bleeker, J., Cavaletti, G., Chauhan, C., Gavin, P., Lavino, A., Lustberg, M. B., Paice, J., Schneider, B., Smith, M. Lou, Smith, T., Terstriep, S., Wagner-johnston, N., Bak, K. & Loprinzi, C. L. Prevention and Management of Chemotherapy-Induced Peripheral Neuropathy in Survivors of Adult Cancers : American Society of Clinical Oncology Clinical Practice Guideline. (2014) doi:10.1200/JCO.2013.54.0914.
6. Park, S. B., Goldstein, D., Krishnan, A. V., Lin, C. S. Y., Friedlander, M. L., Cassidy, J., Koltzenburg, M. & Kiernan, M. C. Chemotherapy-induced peripheral neurotoxicity: A critical analysis. *CA Cancer J. Clin.* **63**, 419–437 (2013).
7. Fletcher, D. A. & Mullins, R. D. Cell mechanics and the cytoskeleton. *Nature* **463**, 485–

492 (2010).

8. Kalpachidou, T., Spiecker, L., Kress, M. & Quarta, S. Rho GTPases in the Physiology and Pathophysiology of Peripheral Sensory Neurons. *Cells* **8**, 591 (2019).

9. Cavaletti, G., Frigeni, B., Lanzani, F., Mattavelli, L., Susani, E., Alberti, P., Cortinovis, D. & Bidoli, P. Chemotherapy-Induced Peripheral Neurotoxicity assessment: A critical revision of the currently available tools. *Eur. J. Cancer* **46**, 479–494 (2010).

10. Molassiotis, A., Cheng, H. L., Lopez, V., Au, J. S. K., Chan, A., Bandla, A., Leung, K. T., Li, Y. C., Wong, K. H., Suen, L. K. P., Chan, C. W., Yorke, J., Farrell, C. & Sundar, R. Are we mis-estimating chemotherapy-induced peripheral neuropathy? Analysis of assessment methodologies from a prospective, multinational, longitudinal cohort study of patients receiving neurotoxic chemotherapy. *BMC Cancer* **19**, 1–19 (2019).

11. Wang, Y., Liu, C., Guo, Q. L., Yan, J. Q., Zhu, X. Y., Huang, C. S. & Zou, W. Y. Intrathecal 5-azacytidine inhibits global DNA methylation and methyl- CpG-binding protein 2 expression and alleviates neuropathic pain in rats following chronic constriction injury. *Brain Res* **1418**, 64–69 (2011).

12. Palmisano, I., Danzi, M. C., Hutson, T. H., Zhou, L., McLachlan, E., Serger, E., Shkura, K., Srivastava, P. K., Hervera, A., Neill, N. O., Liu, T., Dhrif, H., Wang, Z., Kubat, M., Wuchty, S., Merkenschlager, M., Levi, L., Elliott, E., Bixby, J. L., *et al.* Epigenomic signatures underpin the axonal regenerative ability of dorsal root ganglia sensory neurons. *Nat. Neurosci.* **22**, 1913–1924 (2019).

13. Mo, K., Xu, H., Gong, H., Lei, H., Wang, Y., Guo, W., Xu, S. & Tu, W. Dorsal Root Ganglia Coactivator-associated Arginine Methyltransferase 1 Contributes to Peripheral Nerve Injury-induced Pain Hypersensitivities. *Neuroscience* **394**, 232–242 (2018).

14. Uchida, H., Matsushita, Y. & Ueda, H. Epigenetic regulation of BDNF expression in the primary sensory neurons after peripheral nerve injury: Implications in the development of neuropathic pain. *Neuroscience* **240**, 147–154 (2013).

15. Sivanesan, E., Stephens, K. E., Huang, Q., Chen, Z., Ford, N. C., Duan, W., He, S.-Q., Gao, X., Linderoth, B., Raja, S. N. & Guan, Y. Spinal cord stimulation prevents paclitaxel-induced mechanical and cold hypersensitivity and modulates spinal gene expression in rats. *PAIN Reports* **4**, e785 (2019).

16. Zhao, X., Du, W., Zhang, M., Atiq, Z. O. & Xia, F. Sirt2-associated transcriptome modifications in cisplatin-induced neuronal injury. 1–9 (2020).

17. Miaskowski, C., Topp, K., Conley, Y. P., Paul, S. M., Melisko, M., Schumacher, M., Chesney, M., Abrams, G., Levine, J. D. & Kober, K. M. Perturbations in neuroinflammatory pathways are associated with paclitaxel-induced peripheral neuropathy in breast cancer survivors. *J. Neuroimmunol.* **335**, 577019 (2019).

18. Starobova, H., Mueller, A., Deuis, J. R., Carter, D. A. & Vetter, I. Inflammatory and Neuropathic Gene Expression Signatures of Chemotherapy-Induced Neuropathy Induced by Vincristine, Cisplatin, and Oxaliplatin in C57BL/6J Mice. *J. Pain* (2019) doi:10.1016/j.jpain.2019.06.008.

19. Lessans, S., Lassiter, C. B., Carozzi, V., Heindel, P., Semperboni, S., Oggioni, N., Chiorazzi, A., Thompson, C., Wagner, M., Holden, J., Rahn, E., Sweatt, J. D., Cavaletti, G., Renn, C. L. & Dorsey, S. G. Global transcriptomic profile of dorsal root ganglion and physiological correlates of cisplatin-induced peripheral neuropathy. *Nurs. Res.* **68**, 145–155 (2019).

20. Kober, K. M., Olshen, A., Conley, Y. P., Schumacher, M., Topp, K., Smoot, B., Mazor,

M., Chesney, M., Hammer, M., Paul, S. M., Levine, J. D. & Miaskowski, C. Expression of mitochondrial dysfunction-related genes and pathways in paclitaxel-induced peripheral neuropathy in breast cancer survivors. *Mol. Pain* **14**, (2018).

21. Boyette-Davis, J. A., Hou, S., Abdi, S. & Dougherty, P. M. An updated understanding of the mechanisms involved in chemotherapy-induced neuropathy. *Pain Manag.* **8**, 363–375 (2018).
22. Brandolini, L., D'Angelo, M., Antonosante, A., Allegretti, M. & Cimini, A. Chemokine signaling in chemotherapy-induced neuropathic pain. *Int. J. Mol. Sci.* **20**, 1–13 (2019).
23. Lees, J. G., Makker, P. G. S., Tonkin, R. S., Abdulla, M., Park, S. B., Goldstein, D. & Moalem-Taylor, G. Immune-mediated processes implicated in chemotherapy-induced peripheral neuropathy. *Eur. J. Cancer* **73**, 22–29 (2017).
24. Imai, S., Koyanagi, M., Azimi, Z., Nakazato, Y., Matsumoto, M., Ogihara, T., Yonezawa, A., Omura, T., Nakagawa, S., Wakatsuki, S., Araki, T., Kaneko, S., Nakagawa, T. & Matsubara, K. Taxanes and platinum derivatives impair Schwann cells via distinct mechanisms. *Sci. Rep.* **7**, 1–14 (2017).

Publishing Agreement

It is the policy of the University to encourage open access and broad distribution of all theses, dissertations, and manuscripts. The Graduate Division will facilitate the distribution of UCSF theses, dissertations, and manuscripts to the UCSF Library for open access and distribution. UCSF will make such theses, dissertations, and manuscripts accessible to the public and will take reasonable steps to preserve these works in perpetuity.

I hereby grant the non-exclusive, perpetual right to The Regents of the University of California to reproduce, publicly display, distribute, preserve, and publish copies of my thesis, dissertation, or manuscript in any form or media, now existing or later derived, including access online for teaching, research, and public service purposes.

DocuSigned by:
Katherina Chua
4420EBA5903B418...
Author Signature

3/17/2020
Date